INTERNATIONAL CENTER FOR AGGREGATES RESEARCH

ICAR

DETERMINATION OF AGGREGATE SHAPE PROPERTIES USING X-RAY TOMOGRAPHIC METHODS AND THE EFFECT OF SHAPE ON CONCRETE RHEOLOGY

RESEARCH REPORT ICAR 106-1

Sponsored by the
Aggregates Foundation
for Technology, Research and Education

Technical Report Documentation Page

1. Report No.	2. Government Accession No.	3. Recipient's Catalog No.
ICAR 106-1		

4. Title and Subtitle	5. Report Date
Determination of Aggregate Shape Properties Using X-ray Tomographic Methods and the Effect of Shape on Concrete Rheology	August 2005
	6. Performing Organization Code

7. Author(s)	8. Performing Organization Report No.
Sinan Turhan Erdoğan and Dr. David W. Fowler	Research Report 106-1

9. Performing Organization Name and Address	10. Work Unit No. (TRAIS)
International Center for Aggregates Research The University of Texas at Austin 4030 W Braker Lane, Bldg 200, Ste 252 Austin, Texas 78759-5329	11. Contract or Grant No. Project No. ICAR 106

12. Sponsoring Agency Name and Address	13. Type of Report and Period Covered
Aggregates Foundation for Technology, Research, and Education 1605 King Street Alexandria, VA 22314	September 2002-August 2005
	14. Sponsoring Agency Code

15. Supplementary Notes

16. Abstract

The shape of aggregate particles can significantly influence certain properties of concrete, both in its fresh and hardened states. Therefore, there is a need to be able to completely characterize the shape of aggregate particles, in three dimensions, in order to develop computational models that accurately predict properties. In the past, numerous methods have been suggested for this task. However, these methods are often only applicable to two-dimensional images of particles, they output a single or a few values, and fail to characterize the true shape of the particle.

X-ray tomographic techniques allow the capturing of the true shape of particles and have been applied to concrete aggregates. Computed tomography has been used to characterize coarse and fine aggregate particles, while X-ray microtomography has been used to characterize particles passing the 75∝m sieve. Sample preparation methods and scanning parameters applicable to concrete aggregates have been developed. The spherical harmonic method was used to efficiently store shape information, and to calculate useful parameters for individual particles, such as volume and surface area. Comparisons of the results to properties determined using other techniques were made and it was determined that the results of indirect or two-dimensional shape and size characterization methods can be misleading.

The shapes of aggregate particles particularly influence the rheological properties of concrete mixtures. However, it is not clear to what degree different-scale shape properties (the overall shape, angularity and texture) influence flow separately. Artificial aggregates were prepared in the laboratory and simplified test cases were chosen to independently investigate the effect of overall shape and surface texture on the yield stress and plastic viscosity of mixtures and to obtain a set of results that could be used to calibrate computational models. These tests revealed that the overall shape of coarse aggregate particles significantly influences the plastic viscosity of a mixture, but does not affect the yield stress visibly. Particle surface texture does not seem to noticeably influence either viscosity or yield stress for the cases tested. The results were also used to verify the "Dissipative Particle Dynamics" model and showed good correlation with the predictions.

17. Key Words	18. Distribution Statement
X-ray tomography, X-ray mictotomography, concrete aggregates, artificial aggregates, particle surface, spherical harmonic, aggregate particles	No restrictions.

19. Security Classif.(of this report)	20. Security Classif.(of this page)	21. No. of Pages	22. Price
Unclassified	Unclassified		

Form DOT F 1700.7 (8-72) **Reproduction of completed page authorized**

Determination of Aggregate Shape Properties Using X-ray Tomographic Methods and the Effect of Shape on Concrete Rheology

Sinan Turhan Erdoğan
The University of Texas at Austin
Austin, TX

and

David W. Fowler
The University of Texas at Austin
Austin, TX

ICAR Report 106-1

ICAR 106: Adapting the Virtual Cement and Concrete Testing Laboratory to Optimizing the Selection of Aggregates for Concrete

Sponsored by:
International Center for Aggregates Research
The University of Texas at Austin

Aggregates Foundation for Technology, Research, and Education (AFTRE)

August 2005

ACKNOWLEDGEMENTS

Research findings presented in this report are a result of a project carried out at the Construction Materials Research Group at The University of Texas at Austin. The authors gratefully acknowledge the funding provided by the Aggregates Foundation for Technology, Research, and Education. The authors also wish to thank Dr. Edward J. Garboczi of the National Institute of Standards and Technology, for serving as a co-supervisor for the project, and the staff of the International Center for Aggregates Research for their assistance and support throughout this project.

ABSTRACT

The shape of aggregate particles can significantly influence certain properties of concrete, both in its fresh and hardened states. Therefore, there is a need to be able to completely characterize the shape of aggregate particles, in three dimensions, in order to develop computational models that accurately predict properties. In the past, numerous methods have been suggested for this task. However, these methods are often only applicable to two-dimensional images of particles, they output a single or a few values, and fail to characterize the true shape of the particle.

X-ray tomographic techniques allow the capturing of the true shape of particles and have been applied to concrete aggregates. Computed tomography has been used to characterize coarse and fine aggregate particles, while X-ray microtomography has been used to characterize particles passing the 75∝m sieve. Sample preparation methods and scanning parameters applicable to concrete aggregates have been developed. The spherical harmonic method was used to efficiently store shape information, and to calculate useful parameters for individual particles, such as volume and surface area. Comparisons of the results to properties determined using other techniques were made and it was determined that the results of indirect or two-dimensional shape and size characterization methods can be misleading.

The shapes of aggregate particles particularly influence the rheological properties of concrete mixtures. However, it is not clear to what degree different-scale shape properties (the overall shape, angularity and texture) influence flow separately. Artificial aggregates were prepared in the laboratory and simplified test cases were chosen to independently investigate the effect of overall shape and surface texture on the yield stress and plastic viscosity of mixtures and to obtain a set of results that could be used to calibrate computational models. These tests revealed that the overall shape of coarse aggregate particles significantly influences the plastic viscosity of a mixture, but does not affect the yield stress visibly. Particle surface texture does not seem to noticeably influence either viscosity or yield stress for the cases tested. The results were also used to verify the “Dissipative Particle Dynamics” model and showed good correlation with the predictions.

TABLE OF CONTENTS

LIST OF FIGURES

LIST OF TABLES

CHAPTER 1 INTRODUCTION

1.1 Background

Aggregates make up a substantial part of the total volume of concrete (70 to 80%), and naturally significantly affect its properties in both the fresh and hardened states. In addition, aggregates have an impact on the cost effectiveness of concrete, as they are the cheapest component besides water. Aggregate shape properties (overall shape, and surface texture) and size distribution influence the workability, pumpability, and segregation resistance of fresh concrete, and strength, stiffness, creep, density, permeability, and durability of hardened concrete. In addition to being an inexpensive "filler", use of large amounts of aggregates is also beneficial to concrete by reducing the amount of cement paste required, since the paste component is responsible for heat generation, shrinkage and many durability problems. For these reasons, it is important to optimize the aggregates used in concrete mixtures, using an amount as large as feasible while maintaining good flow properties. It is clear that too high an aggregate content will result in a harsh, unworkable mixture and too low a content will result in an uneconomical mixture with problems.

Finding the ideal aggregate content for a specific application relies on a good knowledge of aggregate size distribution (grading) and aggregate shape. Grading can be controlled to some extent through sieving individual aggregate sources and blending aggregates of different sizes (and types) if needed. A good grading helps minimize the voids between particles, which in turn minimizes the amount of cement paste required to fill the voids to provide adequate workability. However, aggregate grading alone does not suffice to minimize voids and optimize the packing of aggregates, and the shapes of the particles need to be known. Flat or elongated and angular particles for example, can result in higher voids contents than cubical, rounded particles.

Without sufficient knowledge about aggregate shape, researchers have previously assumed regular shapes such as spherical particles and only taken into account the effects of grading in modeling, or have calculated an average shape factor (visually or using digital techniques) for a set of particles and attempted to relate it to the properties of concrete. Attempts have been made also to relate shape factors to aggregate particle packing. These techniques, while useful, have certain drawbacks such as being non-mathematical/arbitrary or mathematical but incomplete (such as a two-dimensional technique). Due to a lack of sufficient knowledge of aggregate shape and an efficient means of obtaining shape information, mixture proportioning methods generally do not incorporate the effects of aggregate shape. ACI 211, one of the most widely used proportioning methods, takes into account aggregate shape through indirectly considering packing ability by means of the fineness modulus of fine aggregates and dry rodded unit weight of coarse aggregates. Some others minimize the void content and maximize packing density of solids in the mixture.

A method of measuring shape properties of particles, which is applicable to the complete range of sizes of concrete aggregates (several micrometers to several tens of millimeters) used in concrete, is required. The depletion of natural aggregate sources has resulted in the increased use of manufactured aggregates in recent years. Manufactured sand production often results in the generation of a high amount, typically 10 to 20 % by mass, of material passing the No.200 (75 μm) sieve (microfines). ASTM C 33 was developed based on the use of natural sands and limits the amount of microfines which can be used to 3 to 5 %, for natural sands, and 5 to 7% for manufactured fine aggregate. Research around the world has shown that good quality concrete can be made using higher amounts of microfines, with up to 20% having been suggested (Quiroga, 2003). Characterization of the shape of microfine particles is essential to developing a better understanding of the effect of microfines on concrete properties and to possibly increasing the ASTM limit. Microfines, because their size is comparable to cement particles, could also have an effect on hydration of the cement paste, by providing nucleation sites for the hydration products.

The results of a shape characterization method should be mathematically sound, should completely describe a particle in three-dimensions, should allow the comparison of aggregate particles of different shapes; should allow the relation of aggregate shape to performance; and should permit the incorporation of actual aggregate shape into computational models. A collection of such concrete property prediction models that could benefit from aggregate shape characterization is the Virtual Cement and Concrete Testing Laboratory (VCCTL).

1.2 The Virtual Cement and Concrete Testing Laboratory

The "Virtual Cement and Concrete testing Laboratory" (VCCTL) is a National Institute of Standards and Technology (NIST) / industry consortium established in 2001, with the goal of developing a virtual testing system for designing and testing cement-based materials, which can accurately predict durability and service life based on detailed knowledge of starting materials, curing conditions, and environmental factors (Garboczi et al., 2004). An updated software package of models to predict various concrete properties is released annually. It includes programs for: simulating cement hydration and building three-dimensional cement paste microstructures; assembling three-dimensional concrete microstructures using model aggregates; analyzing microstructures using percolation concepts; and computing physical (thermal, electrical, diffusional, and mechanical) properties using finite difference, finite element, and random walker algorithms (Bullard et al., 2004). In addition, research is ongoing in the areas of comprehensive characterization of materials and the experimental measurement and computer modeling of rheological properties. Several of the properties that the VCCTL attempts to predict are influenced by the amount, size distribution, and shape of aggregate particles. In particular, the elastic properties model and the rheology model are significantly affected by the aggregate component of a mixture.

Prior to the study presented here, the models in VCCTL used spheres and ellipsoids as model aggregate particles, because of the mathematical simplicity of defining these shapes and mainly due to the lack of a sound method for determining the complete three-dimensional (real) shape of particles. Complete characterization of aggregate shape allows the models to use real aggregate particles. This is particularly important because it allows a very controlled comparison of the different aggregate shapes and size distributions, and the study of concrete flow. The characterization of aggregate shape could also be an important step towards the development of accurate particle packing models which would otherwise not be possible.

The addition of real aggregate shapes, from coarse aggregate down to microfine aggregates, into the VCCTL will greatly increase the accuracy of the models in predicting concrete behavior. Once the models are able to correctly and rapidly predict properties for given materials and proportions, rapid, virtual mixture proportioning will be possible. This will allow the testing and optimization of mixtures incorporating high amounts of coarse and fine, and particularly microfine aggregates, resulting in important savings and the use of an otherwise waste material. Aggregate producers will be able to see how their aggregates perform in concrete mixtures without having to perform intensive physical testing and will be able to compare the effects of different crushing processes.

It is important to note that the shape characterization techniques presented here can be used to input real-shaped aggregates into models developed for asphaltic concrete as well. Aggregate shape is even more important in the case of asphaltic concrete because flat and elongated particles complicate pavement constructability and require thicker lifts to avoid breakdown of the aggregate during compaction, and because many properties such as rutting are dependent on aggregate shape. The ratio of aggregate to binder has a profound effect on hot mix asphalt mixtures. Thus, when computer models are developed to model asphaltic concrete, the existence of a method to completely characterize aggregate shape will be of great value.

1.3 Objectives and Plan

The main objectives of this research were the following:

1. Investigate the state of the art regarding the influence of aggregate shape and size characteristics on the performance of fresh and hardened concrete.
2. Investigate the state of the art regarding methods of measuring shape properties of aggregates, for coarse, fine and microfine particles.
3. Investigate the technique of high-resolution x-ray computed tomography (CT) and improve the application of the technique to concrete aggregate shape determination.
4. Investigate the technique of x-ray microtomography (μCT) using synchrotron radiation and develop the application of the technique to concrete microfine aggregate shape determination.
5. Perform CT and μCT tests on several aggregates, evaluate the results, and suggest practical uses.
6. Investigate the separate effects of particle shape and particle surface texture on concrete rheology and workability, and establish empirical results for simplified cases which can be used to calibrate computer models.
7. Investigate the effect of particle size and size distribution on concrete rheology and workability, and establish empirical results for simplified cases which can be used to calibrate computer models.
8. Develop general guidelines for measuring aggregate shape properties and to consider the effect of aggregate shape on rheology of concrete mixtures.

This dissertation is divided into nine chapters, including the introduction. The results of the literature survey on aggregate shape properties, shape characterization methods and a background on concrete rheology are presented in Chapter 2. Chapter 3 introduces the techniques of x-ray tomography and microtomography and explains the image analysis techniques employed and the mathematical methods used to analyze the results. Chapters 4 and 5 introduce the tomography experiments and the rheology experiments conducted to evaluate the effect of overall shape, and surface texture, on concrete flow, respectively. The results of the tomography tests, analysis of the results, and potential practical uses are given in Chapter 6. The results of the rheology tests and analysis of the results are given in Chapter 7. Chapter 8 describes the role of aggregates in the VCCTL and lists potential benefits of the VCCTL to the aggregates industry. Finally, Chapter 9 presents the summary and conclusions for the research project and lists recommendations for future work.

CHAPTER 2 LITERATURE REVIEW

2.1 Introduction

A review of the literature on the definition of aggregate shape properties, qualitative and quantitative shape characterization methods, and the effects of aggregate shape on properties of fresh and hardened portland cement concrete is presented in this chapter. As there are a multitude of techniques to measure aggregate shape, only types of techniques and a few representative techniques of each type are introduced. In addition, a background on rheology and its use in evaluating the flow and deformation of concrete mixtures is provided to make it easier for the reader to understand the motivation for performing the tests presented in the following chapters and to interpret the results.

2.2 Aggregate Shape Properties

In 1978, Ozol wrote:

The increasing use of crushed stone for both coarse and fine aggregate, along with perhaps recycled concrete and other recycled materials, forecasts that the effects and significance of shape, texture and surface area will be prominent considerations in the future.

Today, the need to characterize the shape of aggregate particles is greater than ever because of this reason and because shape characterization is an important step towards having accurate concrete property prediction tools such as the rheological or mechanical property models in the VCCTL. Aggregate shape has been defined in many different ways, by many researchers, and consequently attempts to characterize it are based on what one considers as aggregate shape. A good starting point is to look at various descriptions or definitions of particle shape.

2.2.1 Definitions of Aggregate Shape Properties

There are a couple of general notions which can be used to classify various definitions of shape properties or parameters invented to define aggregate shape which serve as a good introduction to the subject. The first is that the shape of an aggregate particle can be defined, classified, or measured on different scales. For example, a visual examination of a particle will yield a coarse scale set of observations such as being equi-dimensional or elongated, flat, etc. A fine scale set of observations could be having a smooth (visually or to the touch) or rough surface, or a combination of these, as possible in the case of a partially crushed particle. One or more scales between these two extremes are possible and an intermediate one has been used by many researchers. The second notion is that shape of a particle can be defined using a term which gives a crude idea about true particle shape, such as the area of an arbitrary projection (two-dimensional) of the particle, or is exact, such as true volume, or true surface area (measured in three-dimensions).

Barrett (1980) suggested that the shape of a rock particle can be expressed in terms of form (overall shape), roundness (large scale smoothness) and surface texture (fine scale smoothness). These are geometrically independent although there may be a natural correlation between them in that a process which affects one may promote or inhibit the development of others. Parameters further describing properties at each of these three different scales have been defined. While older definitions are often qualitative, more recent definitions are quantitative. One of the older definitions of aggregate particle shape, a qualitative one based on morphological observations, is shown in Figure 2.1.

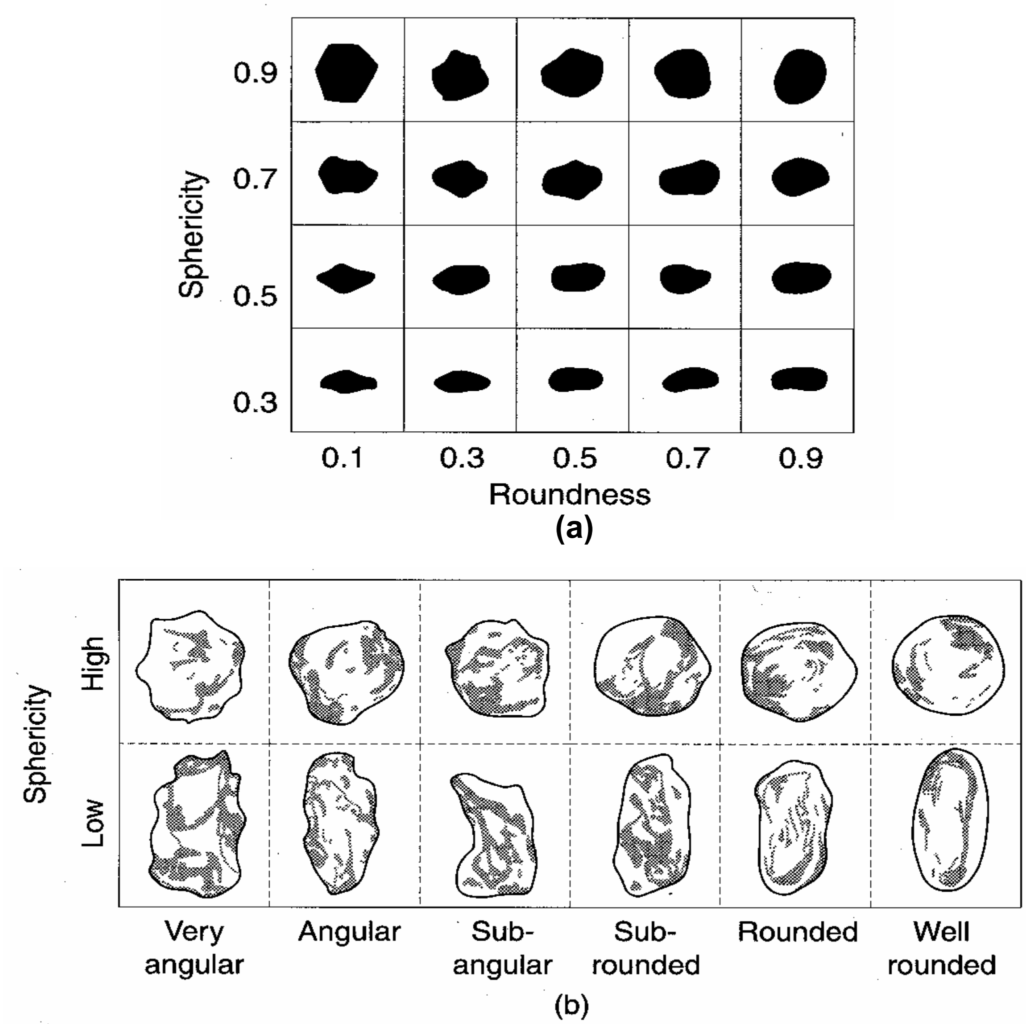

Figure 2.1 Visual assessment of particle shape (a) Derived from Measurements of sphericity and roundness, (b) Based upon morphological observations (Ahn, 2000)

These are coarse and intermediate scale definitions; therefore they do not indicate fine surface characteristics of the particles and only give an idea about particle shape. They put forth some terms that require explanation, such as sphericity and roundness, and use rounded and angular as opposite terms to crudely define surface characteristics. The following are some shape parameters/indices frequently mentioned in the literature: sphericity, roundness, angularity, shape factor, fullness ratio, flatness (flakiness) ratio, elongation ratio, convexity ratio etc. Such terms are introduced in the following sections, grouped by the scale at which they are defined.

2.2.1.1 Coarse and Intermediate Scale Parameters

Rao et al. (2002) proposed the following as properties that an angularity index parameter should have. The parameter should:

be independent of the size of the particle

not be sensitive to orientation

have physical meaning for possibly correlating with material strength properties

be sensitive to changes in particle contour.

These are in fact applicable to all shape parameters, and should be remembered when evaluating parameters which have been proposed.

The term ***form*** is used to describe the overall shape of an aggregate particle. ***Shape factor*** is often used as a parameter that describes form (Hudson, 1999) and is sometimes used synonymously. Folk (1968) defined form, and Aschenbrenner (1956) defined shape factor as measures of the relation between the three dimensions of a particle based on ratios between the proportions of the long, medium, and short axes of the particle, or of the smallest circumscribing ellipsoid. Figure 2.2 explains what is meant by the principal dimensions of a particle.

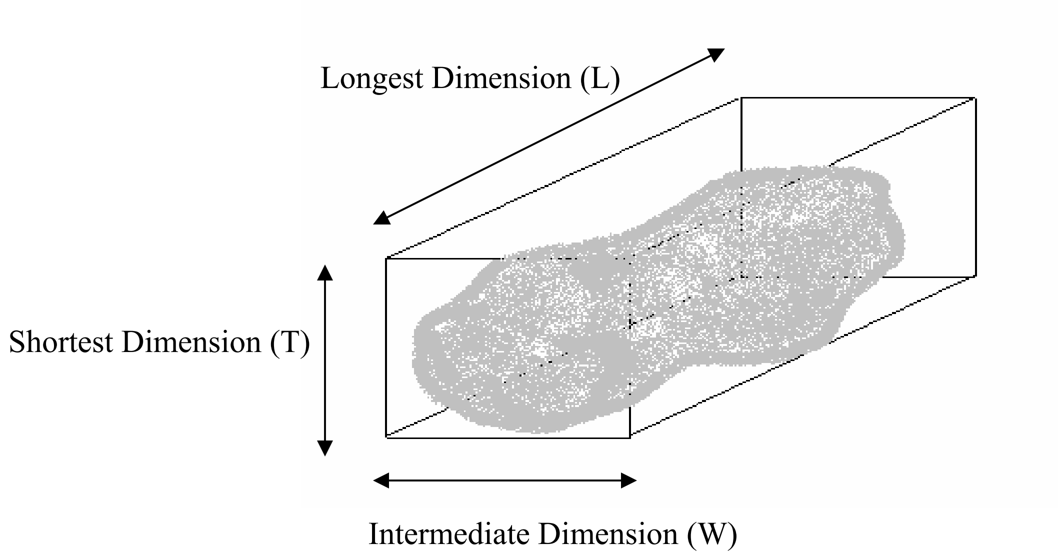

Figure 2.2 The principal dimensions of an aggregate particle (Erdoğan, 2003)

Sphericity is a measure of form and is sometimes called "form factor" (Rao et al., 2002). It is the property that measures, or varies with the ratio of the surface area of the particle to its volume, the relative lengths of its principal axes or those of the circumscribing rectangular prism, or the relative settling velocity (Mather, 1966). As can be understood by this definition, this term is rather vague. Sphericity has also been defined as a measure of how nearly equal the three axes or dimensions of a particle are, based on the degree to which the volume of a particle fills the volume of a circumscribed sphere whose diameter is the maximum dimension of the particle (Ozol, 1978). By this definition, the sphericity of a sphere will be 1.0; the cube will be about 0.37; and any other rectangular prism, lower.

Various mathematical definitions have been proposed for sphericity. If s is the surface area of a hypothetical sphere of the same volume as a particle, and S is the actual surface area of the particle itself, then, since a sphere has the least surface for a given volume, the ratio s/S is the sphericity (Wadell, 1932). By this definition, the sphericity of a sphere will be 1.0 and that of a cube will be 0.806. Since proportions of a particle are determined more easily than surface areas, a more practical expression for sphericity (.) is:

$$. = \frac{D_n}{D_{cs}} \qquad (2.1)$$

where; D_n is the diameter of the sphere of the same volume as the particle (nominal diameter) and D_{cs} is the diameter of the circumscribing sphere (Wadell, 1935). This relation derives from the expression, developed by Wadell (1932), and taken as the fundamental equation,

$$S(.) = \left(\frac{V_p}{V_{cs}}\right)^{1/3} = \frac{\left(\frac{\pi}{6D_n}\right)^{1/3}}{\left(\frac{\pi}{6D_{cs}}\right)^{1/3}} = \frac{D_n}{D_{cs}} \qquad (2.2)$$

where V_p is the volume of the particle and V_{cs} is the volume of the circumscribing sphere.

Krumbein (1941) used the product of the principal dimensions (as if the particle were enclosed in a circumscribing triaxial ellipsoid rather than a sphere) to approximate $D_n^{\ 3}$ and to define sphericity as:

$$S(.) = \frac{\left(\frac{\pi}{6}LWT\right)^{1/3}}{\left(\frac{\pi}{6}L^3\right)^{1/3}} = \left(\frac{WT}{L^2}\right)^{1/3} \qquad (2.3)$$

where L, W, and T are the principal dimensions, as described in Figure 2.2.

Sneed and Folk (1958) defined sphericity based on the settling velocity of a particle in a fluid. The settling velocity of a particle is supposed to increase with increasing sphericity but they pointed out that a rod will settle faster than a disk, even though the Wadell sphericity values might indicate the opposite. Since particles tend to orient, in hydrodynamic behavior, with the maximum projected area (the plane with the L and W axes perpendicular to the direction of the motion of the fluid), they defined sphericity as:

$$\left(\frac{T^2}{LW}\right)^{1/3} \tag{2.4}$$

This formula compares the maximum projection of a particle with the maximum projection of a sphere of the same volume.

Riley (1941) defined sphericity based on a projection of a particle, as in a petrographic thin section, as:

$$\text{Riley Sphericity} = \left(\frac{D_i}{D_c}\right)^{1/2} \tag{2.5}$$

where D_i is the diameter of the largest inscribed circle, and D_c is the diameter of the smallest circumscribing circle.

A flat/oblate particle can have the same numerical sphericity as a long/prolate particle. Distinction between these forms is possible by means of manipulations of the axial lengths of the particle, which, when used in conjunction with Wadell sphericity, can uniquely define the particle geometry (Ozol, 1978). Sneed and Folk (1958) used a triangular diagram to plot T / L versus (L-W) / (L-T), producing a scheme for the combined specification of form and sphericity. Figure 2.3 shows this diagram (The notation I is used instead of W, and S is used inplace of T, in the figure).

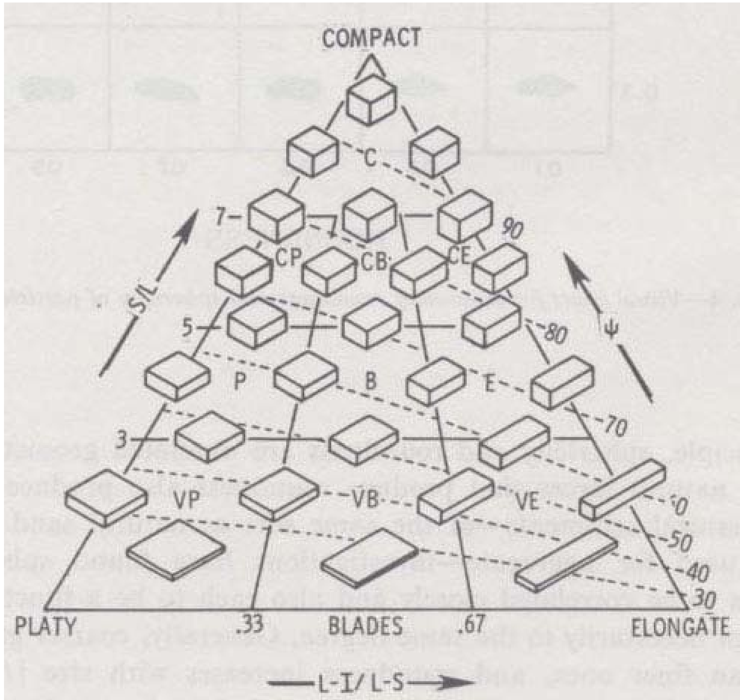

Figure 2.3 Form triangle of Sneed and Folk (Ozol, 1978)

All blocks in the diagram have the same volume. The independence of form and sphericity can be demonstrated by following an isosphericity contour from the left to the right.

Aschenbrenner (1956) designed the shape factor as:

$$F = (W/L)/(T/W) = \frac{LT}{W^2} \tag{2.6}$$

Values of F > 1 represent prolate (rod-like) forms with W approaching T, and values of F < 1 represent oblate (disk-like) forms with W approaching L. This additional idea permits the gross particle geometry to be completely specified by Wadell sphericity and Aschenbrenner shape factor, as seen in Figure 2.4.

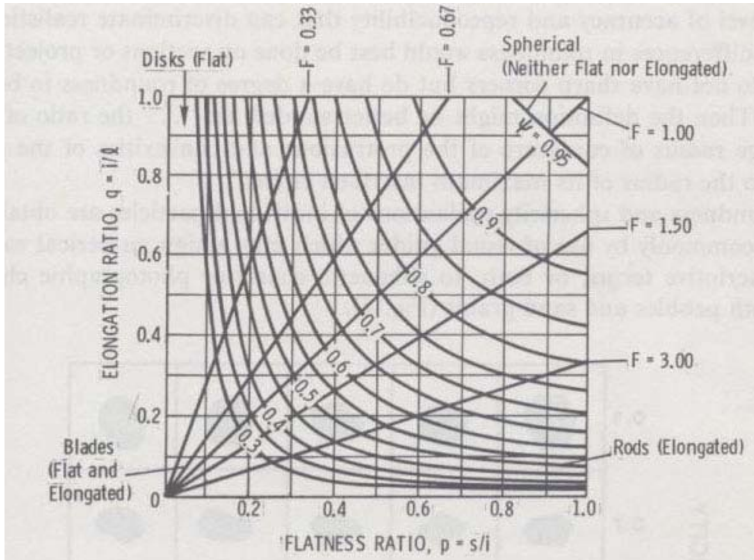

Figure 2.4 Particle Shape as defined by Wadell sphericity (ψ) and Aschenbrenner shape factor (F) (Ozol, 1978)

Sphericity increases with increasing size and this relationship is more pronounced in naturally occurring materials than with crushed materials (Ozol, 1978). The design and operation of crushing equipment influence the sphericity of crushed particles; generally the greater the reduction ratio, the lower the sphericity (Mather, 1966).

Two other parameters suggested to describe overall particle shape are ***elongation***, which relates the longest dimension of the particle to the intermediate dimension and ***flatness***, which relates the intermediate dimension to the shortest dimension. These terms are explained in equation form below, where L, W and T represent the longest, intermediate and shortest dimension of a particle.

$$\text{Elongation Ratio} = \frac{W}{L} \tag{2.7}$$

$$\text{Flatness Ratio} = \frac{T}{W} \tag{2.8}$$

Flatness and elongation have also been called flakiness and slenderness, respectively. Some researchers have used the inverse of Equations (2.7) and (2.8) as elongation and flatness parameters. A particle is said to be flat and/or elongated if the width to thickness and length to width ratios exceed a specified value such as 3 or 5. Different specifications use different limiting values.

The shape of the particles of an aggregate material is not the same for all size fractions. As the reduction ratio during crushing increases, particles tend to become more flat and elongated. This is slightly more so if the machine is of the compression type (jaw, gyratory, or cone crusher type) and less with impact type machines. With impact type crushers, the particles tend to be more cubical or equi-dimensional. The speed of the crusher also influences particle shape (Ozol, 1978).

Roundness is an intermediate scale property and is independent of sphericity and form. It is the opposite of angularity. Pettijohn (1949) describes roundness as the ratio of the average radius of curvature of corners and edges of the particle to the radius of the maximum inscribed circle. Roundness can be divided into the roundness of corners (opposite of the sharpness of corners, more important for abrasive properties of particles), and the roundness of the outline of the particle (overall roundness, generally measured in terms of convexity and more important when considering interlocking ability of aggregate particles and packing density). It has also been defined as the degree to which the contour of a particle fits the curvature of the largest sphere that can be contained within the particle (Ozol, 1978). It is easier to measure roundness on two-dimensional projections or cross-sections of a particle. Wadell (1932) defines roundness as the average radius of curvature of all the corners divided by the radius of the largest inscribed circle:

$$. = \sum \frac{(r_i/R)}{N} \qquad (2.9)$$

By this definition, a sphere has a roundness of 1.0. A cylinder capped with two hemi-spheres also has a roundness of 1.0, and shapes with right-angled corners have a roundness of 0, because of their infinitely small radius of curvature (at the corners).

Roundness and sphericity evaluations are often obtained by using visual guides such as the one shown in Figure 2.1. Roundness is primarily a function of strength and abrasion resistance of the material and the amount of wear to which the particle has been subjected (Mather, 1966). The roundability of mineral rock fragments depends directly on their hardness, and toughness and inversely on the presence of cleavage or cracks. Roundness generally increases with size. Sphericity and roundness are correlated but not to the same degree. A small increase in sphericity might coincide with a large change in roundness.

Angularity is a measure of the sharpness of the edges and corners of a particle. It is the opposite of roundness and affects particle packing and concrete workability. Mora and Kwan (2000) mention two aspects related to roundness and angularity, one related to the sharpness of the edges and corners and the other to the roundness of the outline of the particle, which may be measured in terms of convexity. Angularity can be defined numerically as the ratio of the average radius of curvature of corners and edges of the particle to the radius of the maximum inscribed circle, but descriptive terms, such as the following, are commonly used (Pettijohn, 1949):

Angular: little evidence of wear on the particle surfaces

Subangular: evidence of some wear but faces untouched

Rounded: faces almost gone

Subrounded: considerable wear, faces reduced in area

Well rounded: no original faces left

Several terms have been defined to further describe angularity. The convexity of a particle is related to its angularity and is often defined in two-dimensions using the ***convexity ratio*** (Mora and Kwan, 2000):

Convexity Ratio (CR) = Area / Convex Area (2.10) where the area and convex area are as described in Figure 2.5:

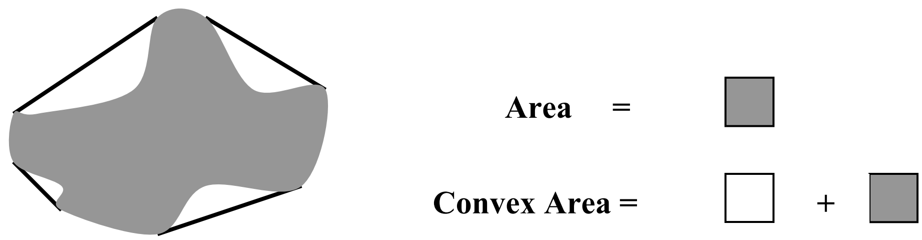

Figure 2.5 Description of the area and the convex area of a projection or cross-section of a particle

In reality, all aggregate particles are non-convex but some can be assumed to be convex when observed at a coarse scale. ***Fullness ratio*** is another parameter which has been proposed as a measure of angularity and is described by:

$$\text{Fullness Ratio} = (\text{Area} / \text{Convex Area})^{1/2} \tag{2.11}$$

Convexity ratio and fullness ratio are indices of concavity and are related to roundness and angularity. However, since they do not involve the sharpness of corners, they are not complete measures of angularity.

2.2.1.2 Surface Texture

Surface texture is a measure of the roughness of the particle boundary and is independent of form and roundness. It may be measured in terms of the magnitude and sharpness of the protrusions and indentations on the particle boundary (Mora and Kwan, 2000). Two independent geometric properties are the basic components of surface texture: 1) the degree of surface relief, also called roughness or rugosity, 2) the amount of surface area per unit of dimensional or projected area. The latter property, although it is the ratio of areas, has been defined by Wenzel (1949), as the roughness factor:

$$R = \frac{A}{a} \tag{2.12}$$

where A is the true/real surface area and a is the apparent/projected surface area. In addition to quantitative measurement of roughness, the types of roughness may be of importance. Blanks (1950) differentiated the relative significance of undulatory (smooth, wavelike) and abrupt rugosity. Surface texture depends on hardness, grain size, pore structure and texture of the rock and the degree to which the forces acting on the particle have roughened or smoothened it. Hard, dense, fine-grained material will generally have smooth surfaces.

2.2.1.3 Grading and Fineness Modulus

Grading is simply the frequency distribution of the particle sizes of a given aggregate. This distribution is given in certain ranges for each sieve size. Grading changes are perhaps more prevalent than shape and surface texture, in the case of coarse and fine aggregates, because of their natural tendency to segregate during stockpiling and transporting. In addition, unlike particle shape, grading is often within the control of the user.

The ideal grading for fine aggregate is often calculated by Talbot's formula:

$$P = \left(\frac{d}{D}\right)^{n} \qquad (2.13)$$

where P is the cumulative percentage passing sieve size d, the specific sieve size (in mm); D, the maximum aggregate size (in mm) and n, an exponent related to particle shape. Mather (1966) reported that an n value of 0.30 to 0.38 is approximate for angular crushed fine aggregate and a value of 0.50 is appropriate for spherical natural sands. Angular aggregates with an n value from 0.30 to 0.40 result in a greater proportion of fine particles to reduce voids. A well-manufactured sand will likely have an exponent of about 0.40 (Hudson, 1998).

The basic method for determining grading is ASTM C 136, method for sieve analysis for fine and coarse aggregate, done basically by separating the material on a nest of sieves and determining the mass percentage of each sieve size present. Each successive size is approximately one-half the opening of its predecessor. The percentage of material on each sieve can be plotted equally spaced on a log-scale and the grading curve can be plotted. ASTM C 33 gives a wide mass percentage range for each sieve to accumulate and to allow for economical production considerations.

Fineness modulus (FM) of fine or coarse aggregates according to ASTM C 125 is calculated by adding the cumulative percentage retained on sieves from size 150 mm to No.100 and dividing by 100. It is an index of the fineness of an aggregate; the higher the FM, the coarser the aggregate. Different aggregate gradings may have identical FM.

2.2.2 Methods of Aggregate Shape Characterization

Numerous methods have been proposed to characterize one or more aspects of the shape of aggregate particles. Some are direct, and some indirect, some are simple and some involve sophisticated mathematics, some yield a single value for a particle (or for a set of many particles) and some yield multiple values. It is important to note that most visual or manual assessment methods can be used only for coarse aggregate particles and large fine aggregate; however, it is generally accepted that the shape properties of fine aggregates and microfines affect overall concrete properties more significantly, in many cases due to their high surface area.

2.2.2.1 Direct / Non-digital Techniques

Several direct tests have been suggested to measure form. These often involve visual assessment of the particle shape. One such method is the Corps of Engineers Method CRD-C120-55, Method of Test for Flat and Elongated Particles in Fine Aggregates. In this test, particle shape is evaluated by observation with a microscope. An aggregate sample is divided into five sizes. The number of particles for which $L / W > 3$ in each size is counted and reported as a percentage. This test evaluates only shape and not texture (Kandhal et al., 1991).

Methods have also been proposed to measure intermediate scale shape properties such as roundness and angularity. Several researchers worked with two-dimensional images of particles. In the Laughlin method (1960), developed for fine aggregate, photographs of particles retained on various sieves are taken, radii of curvature and the radius of an inscribing circle are measured and roundness is calculated. Yudhbir and Abedinzadeh (1991) quantify angularity by the number of tangents on the particle boundary (a measure of the total number of protrusions). Palasamudram and Bahadur (1997) measure angularity as a function of the sharpness of corners (taken as inversely proportional to the angle of the corner) and the probabilities of the corners being connected by other bodies.

Devices and methods to measure surface texture have also been proposed. Orchard (1970) proposed that surface profiles for analysis of roughness can be generated using the electromechanical stylus device, which is used for investigation of metal surfaces and determines the profile length per unit of center line length. Jones (1952) suggested that a device such as the replica surface analyzer can be of value in the study of surface texture. Scrivener and Hudson (1963) used a device with spring loaded probes to determine profile length. Adsorption methods such as the BET nitrogen adsorption method have also been used to determine the surface area of the particles. Patat (1961) developed a method based on weighing the amount of adsorbed substance directly on the surface using the Gibbs adsorption isotherm.

If the principal dimensions of a particle are measured, the formula by Chamberlin (1966) may be used to calculate the specific surface, although not exactly:

$$cm^2 / cm^3 = \frac{2}{\mathrm{I}}\left(\frac{\mathrm{W}}{\mathrm{L}} + \frac{\mathrm{W}}{\mathrm{T}} + 1\right) \qquad (2.14)$$

If sphericity (.) is known, specific surface can be estimated from sieve analysis using the following formula (Ozol, 1978):

$$cm^2 / cm^3 = \left(\frac{558}{.}\right)\left(P_1 + \frac{1}{2}P_2 + \frac{1}{4}P_3 + \frac{1}{8}P_4 + \ldots\right) \quad (2.15)$$

where P_1, P_2, … are the solid volume fractions or the weight fractions if the specific gravity is the same for all sizes, and 558 is the specific surface area of spheres for group 1 (100x200 BS sieves).

2.2.2.2 Indirect / Non-digital Techniques

Indirect methods are ways of estimating shape properties through various tests that are designed to measure a value other than shape. Common examples are packing tests, flow tests and particle settling tests. They are always related to more than one shape property and cannot give more than a general idea about one specific shape property (Masad et al., 2000).

2.2.2.2.1 Packing/Filling Tests

In these tests, containers of various shapes and sizes are filled with particles and the volume of voids is measured. In determining packing density, different size fractions are separated to remove the effect of size distribution and to observe only the effect of particle shape. Packing density of each size fraction is measured by filling up a steel cylinder with the particles, subjecting the particles to prescribed tamping and filling up the cylinder with water such that no meniscus is present above the rim and weighing the amount of water inside. Then, packing density is;

$$\text{Packing density} = \frac{\text{weight of particles in cylinder}}{. \bullet \text{volume of cylinder}} \quad (2.16)$$

where . is the bulk density of the aggregate.

Kwan and Mora (2001) correlated the packing densities of aggregate samples to shape parameters to evaluate the effects of various shape parameters on packing. It was found that the shape factor and convexity ratio are the most important parameters affecting packing. Two alternative formulas revealing the combined effects of these two shape parameters on the packing density of aggregate are proposed. Packing density is a measure of how well the aggregate particles fill up the volume of the concrete.

$$\text{Packing density} = \frac{\text{solid volume of particles}}{\text{bulk volume of aggregates}} \tag{2.17}$$

Voids ratio is the ratio of the volume of voids between aggregate particles to the bulk volume occupied by the aggregates.

$$\text{Voids ratio } = 1 - \text{packing density} \tag{2.18}$$

It was found that packing density varies between 55% and 85%, depending on size distribution and shape characteristics of the aggregate.

Plum (1944) found that the number of flat particles needed to fill a volume were greater than the number of particles of desirable shape (more equi-dimensional) which in turn was greater than the number of elongated particles required. The National Crushed Stone Association developed a method (Gray and Bell, 1964) in which an index of particle shape is obtained by calculating the percentage of voids in specified size fractions (each tested separately) in a loosely compacted and in a cylindrical container, by using the following equation:

$$\text{Percent voids} = 100 \bullet \left(1 - \left(\frac{w}{v \bullet g}\right)\right) \tag{2.19}$$

where w = weight of the sand cylinder, v = volume of the cylinder in cm^3, and g = bulk specific gravity of the aggregate, determined independently on coarse particles of the same aggregate. The fractions used are ASTM sieve sizesNo.8-No.16, No.16-No.30, and No.30-No.50; the value reported is the average of the determinations on the three fractions. Values ranged from 48 to 59% for various sands (Gray, 1964).

The National Aggregate Association proposed methods (A and B) of a test for particle shape and texture of fine aggregate using uncompacted void content. A 100 cm^3

cylinder is filled with a fine aggregate of prescribed gradation by allowing the sample to flow through the orifice of a funnel into the calibrated cylinder. The cylinder with aggregate is weighed. The uncompacted void content is computed using this weight and the bulk dry specific gravity. In method A, a graded sample of specified grading is used. In method B, the void content is calculated using void content results of three individual size fractions. Both methods showed good correlations with ASTM D 3398 and were more straightforward and less time consuming (Kandhal et al., 1991). Li et al. (1993) attempted to calculate rugosity by packing volume. In this method, aggregates are poured from a cone-shaped bin into a calibrated constant-volume container, and the packing specific gravity is calculated using the weight of the calibrated volume of aggregate. The macro and micro surfaces were computed using the apparent, bulk, and packing specific gravities. The addition of the macro and micro surface voids thus obtained was done to arrive at the specific gravity. Kandhal et al. (1991) stated that since the features of surface texture are an order of magnitude smaller than the features of roundness, it is unlikely that surface texture would have a significant effect on packing density. BS 812: Part 1 (1975) introduced an angularity number as the amount by which the percentage of solid volume measured during a packing density test falls below 67 or the amount by which the percentage of voids exceeds 33. This angularity number generally varies between 0, for very rounded particles and 12, for very angular particles. Kwan and Mora (2001) suggested that the practice of estimation of angularity in terms of packing density (based on an assumption that packing density is based solely on angularity) should be abandoned.

2.2.2.2.2 Flow Tests

Several tests involving the flow of aggregates or flow of another substance through aggregates have been proposed to indirectly estimate shape properties. Tests involving the behavior of particles on an inclined plane and the measurement of the rate of flow of water through gravel are two examples (Jankar and Rao, 2004). In another technique used, Rex and Peck (1956) measured the rate at which sand flows through a 3/8-in. orifice and simultaneously evaluated the effects of shape and surface. An index is calculated as:

$$\text{Time index} = \frac{\text{rate for a given sand}}{\text{rate for the same size standard testing sand}} \tag{2.20}$$

Ishai and Tons (1977) proposed a method in which the size of the orifice depends on the size of the particles being tested. The sample was broken down into as many as six size fractions and flow test performance was reported on one-sized aggregate and corresponding one-sized glass beads. Malhotra (1964) used a mortar flow and time index test and found an inverse relationship between shape and flow time.

Methods to measure roughness indirectly by flow tests have also been proposed. Ozol (1978) proposed a method to directly determine specific surface area by measuring permeability, loss of head and rate of flow of a liquid through a column of single-sized particles using the theory of Carman (Carman, 1938).

2.2.2.2.3 Settling Velocity / Behavior Tests

Some tests involving the settling behavior of particles in a medium have been proposed to measure shape properties. A sphericity calculation based on the settling of particles was proposed as mentioned above (Wang et al., 2002). Schiel (1941) devised a formula involving specific gravity, settling velocity (function of thickness) and sieving (function of width), the results of which are expressed as values from 100 to about 70. A spherical shape gives a value close to 100, a cubical shape about 86.5, a fairly cubical shape between 83.5 and 86.5, a flat particle 80.5-83.5 and a very flat particle < 80.5.

2.2.2.2.4 Petrographic Analysis

Petrographic analysis has been performed on thin or polished sections to evaluate aggregate shape. Wright (1955) used a technique which involves tracing of the profile on a thin section. French (1991) found, using petrographic analysis, that two aspects of roundness are apparent; the degree of rounding at edges and corners and the angles defined by the surfaces making those angles and corners, and it is the latter which has the greater influence on aggregate packing, while the former is likely to affect the location of microcrack development. He proposed that calibration graphs can be drawn relating the grading of the aggregate as measured by sieving to that observed in the thin section. The measurement on the thin section or polished plate is carried out using the maximum apparent dimension of each particle or product of the minimum and maximum dimensions. The grading zone of the fine aggregate can be assessed by comparison with standard sections or by measuring the mean apparent particle size of the aggregate. The 50 percentile for the aggregate is usually about 1.77 times the measured mean size.

2.2.2.2.5 Other Indirect Tests

Several other indirect methods which can not readily be classified have been proposed. Heywood (1933) devised a method to calculate surface area by weighing the maximum amount of coating produced by immersing a particle in molten paraffin at a prescribed temperature. Tons and Goetz (1968) measured the volume of asperities by coating the particle in asphalt and then removing the excess down to the roughness peaks and used the following formula to determine rugosity (Tons and Goetz, 1968):

$$\text{Rugosity} = \frac{\mathrm{V}_{\text{asphalt remaining on particle}}\left(cm^3\right)}{\text{geometric particle area calculation from particle dimensions}} \tag{2.21}$$

Davies and Rees (1944) studied the sphericity of sand by determinations of surface area and by using an air permeability method. Some other methods employed were to measure the weight of a fine powder used to level a unit area of surface roughness, and to measure the air flow between a rock surface and an elastic membrane held against it at a given pressure (Ozol, 1978). A direct shear test was proposed to measure the internal friction angle of a fine aggregate under different normal stress conditions. In this test, a sample is consolidated in a shear mold and then placed in a direct shear device, sheared by a horizontal force while a known stress is applied (Kandhal et al., 1991).

2.2.2.3 Digital techniques

Many researchers have attempted to use digital techniques to estimate particle shape properties, particularly in the last decade. Digital imaging techniques (DIT) can be used to investigate particle shape at different scales and can distinguish among different shape properties and make it possible to quantify their distinct effects on the properties of concrete. Digital image processing (DIP) is quick, not prone to human errors and capable of performing sophisticated measurements. DIP techniques allow the determination of geometric parameters such as two-dimensional perimeter, perimeter of ellipses or rectangles with equivalent areas, shortest and longest dimensions, convex perimeters, particle count, area fraction, size distribution, shape characteristics, spatial distribution etc. The results are often derived from two-dimensional images, and occasionally from three-dimensional images. While there are certain advantages of digital methods over conventional methods, there are certain drawbacks as well. One such drawback is that sieve size can not be measured by DIP (Mora et al, 1998). This is because the dimensions measured in two-dimensions do not directly correlate with the actual dimensions of the particles. In addition, DIP results must be expressed in terms of area fractions, instead of the more customary mass fractions, which people are more used to.

Prior to introducing some DIP methods mentioned in the literature, an assumption commonly made in evaluating results of DIT must be noted. Nearly all such techniques assume that aggregates from the same source have approximately the same shape. This is a key assumption which is not always correct. It is more correct for natural aggregates or aggregates which have been crushed with the same crusher, and which are of similar size. As the source, crushing process, or particle size changes, particle shape becomes less homogeneous.

Different researchers have used different shape indices to describe the same shape attribute and even different definitions for the same shape attribute. Many researchers have worked with two-dimensional images of particles, using manual, digital or video cameras. Heigold and Lamar (1970) measured the photographic silhouettes of 10 by 14 mesh grains of calcite and 17 different limestones on a radial grid of 16 equally spaced rays (diameters) and used a computer to compare data obtained with reference data on a variety of geometrical standards. The results were expressed as the statistical correlation of each grain to the most similar shape as well as to the shape that the total sample most nearly resembled. Mueller and Hunn (1974) used computer processes for automated analysis of grain images. The image was displayed on a cathode ray tube and measurements of shape and volumetric parameters were obtained by a variety of electronic manipulations. Ehrlich and Weinberg (1970) carried out a Fourier series expansion of the radius about the center of mass of the particle, utilizing coordinates of peripheral points on the two-dimensional maximum projected area grain shape, and expressed the result as a shape equation. Czarnecka and Gillott (1977) developed a modified version of the Fourier method to express more precisely the total roughness of the particle profile as the sum of two separately measurable shape and texture factors.

Particles passing through a sieve can actually have one dimension that is larger than the size of the sieve; therefore the sieve aperture size is a measure of the lateral dimensions of the particles only. A relatively flat particle can pass through a square sieve aperture diagonally so the width of a particle passing through a certain sieve size can be longer than the sieve size. It is not possible to directly relate two-dimensional DIP results to sieve analysis. Kwan et al. (1999) proposed a correction for the sieve size – particle size relationship, to convert the breadth calculated from DIP, to an equivalent sieve size using a correction factor C as shown in the following equation:

$$\text{Equivalent square sieve size} = C * \text{breadth} \tag{2.22}$$

The value of C is dependent on the shape of the cross section of the particle and therefore has to be determined for each type and source of aggregate. It is determined by a trial and error process of matching the grading curve derived by DIP based on an assumed value of C to the corresponding curve obtained by mechanical sieving.

Mora and Kwan (2000) devised a formulation for estimating thickness of aggregate particles from two-dimensional images, assuming that aggregates from the same source have approximately the same shape characteristics, and using the measured mass of the aggregate sample:

$$\text{Mean thickness} = . * \text{breadth} \tag{2.23}$$

where . is a parameter dependent on the flakiness of the aggregate.

$$\text{Volume} = \text{mean thickness} * \text{area} = \; = . * \text{breadth} * \text{area} \tag{2.24}$$

$$\text{M (total mass of the sample)} = . * . * \sum_{1}^{n} (\text{breadth} * \text{area}) \tag{2.25}$$

where n is the total number of particles.

$$. = \frac{M}{\left(. * . * \sum_{1}^{n} (\text{breadth} * \text{area}) \right)} \tag{2.26}$$

So, this value of . is actually the mean thickness/breadth ratio of the aggregate sample.

Kuo and Freeman (2000) proposed several shape parameters using the convex hull of particles in two-dimensional images.

$$\text{Form factor} = \frac{4\pi A}{\text{Per}^2} \tag{2.27}$$

where Per is the perimeter of the convex hull. This yields 1.0 for a circle, so;

$$\text{Form factor} = \frac{\text{Per}_{\text{eq. circle}}^{\;2}}{\text{Per}^2} \tag{2.28}$$

$$\text{Aspect Ratio} = \frac{L}{W} \tag{2.29}$$

$$\text{Angularity} = \left(\frac{\text{Per}_{\text{convex}}}{\text{Per}_{\text{eq. circle}}} \right)^2 \tag{2.30}$$

$$\text{Roughness} = \left(\frac{\text{Per}}{\text{Per}_{\text{convex}}} \right)^2 \quad (2.31)$$

They propose a common image form factor as a function of the three proposed indices:

$$\frac{1}{\text{form factor}} = \frac{\left(1 + \text{Aspect Ratio}^2\right)}{\left(2 * \text{Aspect Ratio}\right)} * \text{Angularity} * \text{Roughness} \quad (2.32)$$

Many researchers have also used computer analysis of images obtained through the use of an SEM to analyze roughness. Persson (1998) looked at material passing the 63 µm sieve using SEM, the material in the 63 to 125 µm and the 125 to 250 µm ranges as thin sections using polarization microscopy with UV light. She suggested that grain size distributions from sieve analysis are based on mass percentage whereas those from image analysis are based on the percentage of particles, and that two-dimensional DIP data need to be transformed into a representation of volume or weight percentage and two-dimensional representations of the particles need to be transformed into 3-D representations. The following formula was proposed:

$$\text{Tot. \# of part. in the interval (\%), X} = \frac{L}{A_l} * S_1 + \frac{M}{A_m} * S_m + \frac{N}{A_n} * S_n \quad (2.33)$$

where L, M, N are the numbers of particles; A_l, A_m, A_n are the total numbers of particles in fraction L, M, N (< 63 µm, 63-125 µm, 125-250 µm); and S_1, S_m, S_n are the percent values passing the sieves (63µm, 125µm, 250µm). This calculation will be biased since the sieved percentages of weight are used as weights to add the number of particles percentages. This will result in an over representation of the particles. To be able to add all fractions, the relation between flat lying particles to those from cut particles has to be clarified, and another method of weighting has to be practiced.

Methods have also been proposed to measure gradation. Researchers at the Laboratoire Central des Ponts et Chaussees developed a videograder, VDG-40, an optoelectronic device designed to provide a gradation analysis of a large sample rapidly (Kuo and Freeman, 2000).

Some researchers have used alternate ways of capturing particle shape such as laser profile scans. Kim et al. (2002) proposed wavelet-based 3-D particle descriptors based on signal processing techniques and digital data obtained from automated 3-D scans of laser particles, as a way to characterize individual particles. In the system, a laser line scanner is used to obtain 3-D data of one side of a particle. The data is transformed into 8-bit grayscale digital images, where the grayscale pixel values represent the height of each datum point. This 3-D cartesian coordinate data is converted into a polar coordinate domain, which allows for a generalized 3-D particle data which interpolates missing data for the bottom portion of each particle, hidden from the scanner. Shape, angularity, and texture coefficients are obtained based on how well the signal coincides with dilated and translated versions (finer and coarser scales) of the mother wavelet. This is an example of technique that is between 2-D and 3-D. Figure 2.6 shows this particle characterization scheme using wavelet analysis.

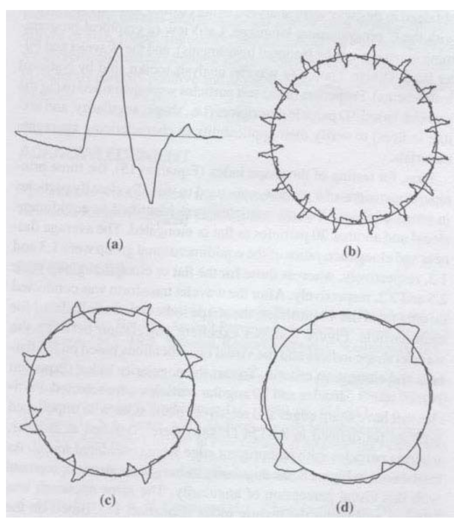

Figure 2.6 Particle characterization scheme using wavelet transform: a) Daubechies' D4 mother wavelet, b) texture measurement, c) angularity measurement, d) measurement (Kim et al., 2002)

A system developed at The University of Illinois uses three cameras to collect particle images from three perpendicular orientations. This method determines the 3-D convex shape of particles but not true shape. Such a method can estimate the weights and volumes of particles but there is a limit to the smallest particle that can be analyzed (Rao and Tutumluer, 2000). Several pattern recognition methods such as fractal dimension analysis, 2-D to 3-D reconstruction models based on stereology, model shape of choice or geometric probability and Hough transforms, have also been proposed. Wilson and Klotz (1966) used a video-based method of measuring angularity, based on the properties of the Hough transform. Hough transform is a mathematical tool commonly used to detect straight lines in video images. This method detects and measures the length of any straight edge in a two dimensional image. The angularity index is then calculated as:

$$\text{Angularity index, } S_i = 1 - \left(\frac{\overline{A}}{A_{max}} \right) \tag{2.34}$$

where A_{max} is the longest line on the edge of the particle and $\overline{A}$ is the average length of all the lengths in the A(θ) =function. If one or two lines dominate the perimeter of the object, S will approach unity. If the object is irregular or rounded, then S approaches zero since all lines are short and near the average length.

Masad et al. (2000) used erosion-dilation techniques to evaluate fine aggregate angularity and a fractal approach by measuring the fractal length of the aggregate boundary. Erosion is a morphological operation in which pixels are removed from a binary image according to the number of surrounding pixels that have different color (particle or matrix) and results in the smoothening of the object. Progressive erosion eliminates small objects and eliminates outward-pointing angularity elements of the surface. In dilation, contrary to erosion, a layer of pixels is added to the object to form a simplified version of the original object. Applying n erosion cycles followed by n dilation cycles does not restore the object to its original shape. The area of objects lost after a certain number of erosion-dilation cycles is proportional to the percentage of objects smaller than a certain size and to object angularity and is calculated by the following equation:

$$\text{Surface Parameter, SP} = \left(\frac{(A_1 - A_2)}{A_1}\right) * 100\% \quad (2.35)$$

The SP value will be higher for particles with greater angularity. Erosion dilation is further explained in Chapter 3. Fractal behavior is defined, in its simplest form, as the self-similarity exhibited by an irregular boundary when captured at different magnifications. Smooth boundaries erode/dilate at a constant rate; however, irregular or fractal boundaries have more pixels touching opposite neighbors, and therefore do not erode uniformly. This effect has been used to estimate fractal dimensions, and consequently angularity along the object boundary. Fractal length increases as the fine aggregate angularity increases.

When particles are imaged on a flat surface, there is a risk of the particles having a preferred orientation. Particles will generally rest in the most stable position, often on their flattest side, which may influence the results negatively if not taken into account. Some researchers have used set-ups which hold the particles at a particular orientation while the images are taken, to decrease the effects of orientation. Kuo and Freeman (1998) attached coarse aggregates to an L cross-section tray (with two perpendicular faces) and then imaged them from two orthogonal angles. Brzezicki and Kasperkiewicz (1999) used a form with steps which holds the aggregate particles at known angles to the camera and evaluated L, W, T from shadows observed on this special form representing a fragment of a cylindrical surface with a system of parallel indentations. The walls of the indentations were perpendicular to each other so the shadows of the grains appeared as perpendicular projections. Taylor (2005) imaged individual particles from multiple (up to 64) orientations by attaching them to a pin and estimated the surface area of the convex body using Cauchy’s theorem (Cauchy, 1850).

More sophisticated methods have also been proposed. Wang et al. (2002) used x-ray computed tomography images and estimated volume, surface area, specific surface area and sphericity. It was found that the overall specific surface of aggregates within the same sieve size range can be evaluated over few particles. Recently, Garboczi et al. (2005) used a laser ranging device (LADAR) to scan the surface of individual aggregate particles and used the data to rebuild the particles, calculate volume, surface area, and other useful three-dimensional properties. The values determined using this technique are as exact as the resolution of the LADAR scans.

Research has also been done in random particle generation using statistical techniques (Grigoriu et al., 2005). This is important in that it is not possible to characterize the shape of all the particles to be used in a mix and realistic particles need to be generated in the case of computational models which employ aggregate particles such as those in VCCTL.

2.2.3 Related Specifications and Standard

The following is a list of standards related to aggregate size and shape determination frequently used and mentioned in the literature:

ASTM C 29 (Standard Test Method for Bulk Density ("Unit Weight") and Voids in Aggregate): This standard describes the determination of bulk density and calculation of the void content in fine, coarse, or mixed aggregates.

ASTM C 125 (Standard Terminology Relating to Concrete and Concrete Aggregates): This standard defines terms such as bulk density, elongated piece of aggregate, flat piece of aggregate, fineness modulus etc.

ASTM D 4791 (Standard Test Method for Flat and Elongated Particles in Coarse Aggregates): This method requires that the operator measure each individual particle in a set of proportional calipers set up according to the specification on a 2:1, 3:1, or 5:1 basis. Prowell and Weingardt (1999) provide standard deviations for within laboratory and multi-laboratory, for the 2:1 and 3:1 cases. The standard deviation for the within lab single operator case was found to be 5.3% which means results on an identical sample of aggregates should not differ by more than 15% of their average. This difference should not be greater than 24.3%, 73.9% and 99.9%, for the 2:1 multi-laboratory, 3:1 within laboratory and 3:1 multi-laboratory cases, respectively. It is seen that the variation in this test is very high.

ASTM D 3398 (Standard Test Method for Index of Aggregate Particle Shape and Texture): This test method is used for determining a numerical index of particle shape and texture based on the weighted average void content of specified sizes. The sample is separated into nine different sizes between 19 mm and 75 μm. The bulk specific gravity for each size range is determined, and the mold is filled in three courses, each rodded ten times, and the net weight of the aggregate is determined. Then, the procedure is repeated with each layer being rodded 50 times. The index is determined using the following equations:

$$V = \left(1 - \left(\frac{W}{S * V}\right)\right) * 100 \tag{2.36}$$

$$I_a = 1.25V_{10} - 0.25V_{50} - 32.0 \tag{2.37}$$

where W is the net weight of the aggregate, S is the bulk specific gravity, V is the volume of the mold, 32 is an empirical constant representing the porosity of smooth, uniformly sized spheres at zero compactive effort. Kandhal et al. (1991) found that, on the basis of ASTM D 3398, a particle index value of 14 appears to divide the natural and manufactures sands.

ASTM D 5821 (Standard Test Method for Determining the Percentage of Fractured Particles in Coarse Aggregate): This method involves the determination of the percentage of particles having more crushed faces than a specified minimum number, by counting. Rao et al. (2002) found this test to be subjective.

ASTM C 1252 (Standard Test Methods for Uncompacted Void Content of Fine Aggregate (as Influenced by Particle Shape, Surface Texture, and Grading)): The use of this method for particle shape determination is based on the idea that void characteristics would indicate the morphological characteristics of single sized aggregates. Angular and rough textured aggregate particles generally yield higher void contents in loosely compacted samples.

ASTM C 136 (Standard Test Method for Sieve Analysis of Fine and Coarse Aggregates): This test is performed by separating the material on a nest of sieves and determining the percentage of each sieve size present. Each successive size is approximately one-half the opening of its predecessor.

ASTM C 33 (Standard Specification for Concrete Aggregates): This specification defines requirements of grading and and quality of fine and coarse aggregate in concrete. Some aspects of this standard are prescriptive due to a lack of adequate aggregate shape characterization.

BS 812 (Testing Aggregates), Part 1 (Methods for Determination of Particle Size and Shape)

Hossain et al. (2000) compared several of the standard test methods and found that voids tests based on ASTM C 1252 and the ASTM D 3398 test methods are more objective and precise than ASTM D 5821 and ASTM D 4791 voids test.

2.2.4 Measuring the Shape of Individual Particles versus Measuring Shape Properties in Bulk

In indirect methods, particle shape is determined based on measurements of bulk properties. In direct methods, particle shape is measured, described qualitatively or quantified by direct measurement of individual particles. The advantage of measuring particles individually is that different shape properties can be measured separately. However, because a large number of irregular particles must be assessed to adequately characterize an aggregate material, descriptors that can be qualified with automated machines are often preferred.

2.2.5 Effects of Different Shape Parameters on the Properties of Concrete

The influence of aggregates on the properties of concrete has been extensively discussed in the technical literature and many methods for arriving at the optimum or ideal gradings have been presented. However, none of these have been accepted as being universally applicable because of economic considerations, differences in particle shape and texture of aggregates, and the effects of entrained air and amount of cementitious material contained in the concrete. Aggregates influence the properties of fresh and hardened concrete by occupying a significant volume, imparting volume stability and increasing durability. The shape properties of aggregate particles at different scales have different effects on different properties.

2.2.5.1 Effects of Coarse-scale Properties

The overall shape of aggregate particles may have a drastic effect on the strength and workability of mixtures. French (1991) found that that if nearly all particles have aspect ratios of 3:1 or less, the shape factor has little influence on the quality of the concrete. However, the strength may be affected if more than 50% of the aggregate particles have aspect ratios in excess of 5:1, especially if these particles are oriented parallel to one another as a result of placement. Flat or elongated particles, if oriented horizontally, can trap bleed water, preventing the development of a good bond and result in reduced bulk weight and decreased compressive strength (Rao et al., 2002). Flat particles oriented vertically can cause a structural weakness in compression and also decrease strength. Equi-dimensional particles are generally preferred to flat or elongated particles for use as concrete aggregates because they present less surface area per unit volume and generally produce tighter packing when consolidated. Flat particles make for a harsh mixture with low workability at given water content, which leads to poor compaction and a high void content, resulting in low strength and durability. If the number of flat or elongated particles is not too great, then the workability problems can be overcome with the use of water-reducing admixtures. The question then becomes what quantity is considered too great. ASTM C 33 gives no limits with regard to this attribute since agencies have limits ranging between 8% and 20% maximum allowable on a 3:1 ratio (Galloway, 1994). It has also been suggested that at concentrations of 15 to 20 % or higher, flat particles can align during mixing, resulting in the lowering of the suspension viscosity, possibly to a value even lower than that of a suspension of an equal volume of spheres (Martys, 2004). The depth of carbonation is largely governed by the degree of compaction so that flat or elongated aggregate shape can influence reinforcement corrosion (French, 1991). Also, since they increase the water content for a certain consistency, they increase bleeding and can result in frost resistance problems due to excessive bleeding.

2.2.5.2 Effects of Intermediate-scale Properties

Roundness and angularity of particles may also affect certain properties of concrete. Popovics (1973) found that angularity had a greater effect on workability than overall shape. He used the average mortar layer intercept concept, which is the measured distance along a random line of the mortar layer between coarse aggregate particles, and found that there exists a minimum value of 3.8mm below which the workability of concrete is inadequate. This value seemed to be independent of particle shape. The average mortar intercept is inversely proportional to the angularity number in concrete made with the same aggregate grading and mixture proportions. French (1991) also proposed that the angularity of aggregates has a greater effect on strength and workability than the flatness index. Well-rounded particles may be expected to require less cement paste for equal workability than angular particles of equal sphericity and similar surface texture. The incentive to lower the amount of cement paste used is to lower the cost of production of concrete, to reduce the heat of hydration and drying shrinkage; both of which may cause cracking problems and are roughly proportional to the volume of cement paste in concrete. Powers (1966) suggested that the volume of concrete exceeds the volume of compacted aggregate by 3 to 10% (3% when no air entraining agent is used) thus a sufficient amount of extra volume of paste is about 3%.

Shergold (1953) found that increasing angularity directly affects the percentage of voids in aggregate which in turn affects the workability or mixture proportions in concrete. Bloem and Gaynor (1963) found that the water requirement of a mixture increases more or less linearly with the voids ratio of the aggregates used.

Rao et al. (2002) suggested that angularity improves aggregate interlock and load transfer properties of jointed concrete pavements, and that angular and rough textured particles yield higher strength concrete. It was suggested that angularity has the greatest effect of shape properties, greater than axial proportions or surface texture, on bulk void content.

2.2.5.3 Effects of Fine-scale Properties

The surface texture of particles also influences certain properties of concrete. A significant effect is on the strength of the bond developed between the aggregate and the cement paste. Kaplan (1959) found that surface texture is the most important aggregate property influencing compressive strength. It has also been suggested that flexural strength increases as roughness increases (Mather, 1966). Also, this effect increases as the strength of the concrete increases. The presence of texture on the aggregate surface results in increased strength probably due to an increase in the mechanical interlock with the matrix and an increase in the surface area and more interface with which the mortar may react (Galloway, 1994). Increased texture and increased angularity contribute to concrete strength at equivalent mixture proportions involving contributions of:

1) mechanical interlock (due to texture), 2) total surface area available for adherence of cement paste (due to particle shape and texture) (Ozol, 1978).

Kaplan (1958) proposed that texture has the largest effect on compressive strength among shape parameters which include angularity, texture, flatness and elongation. He also found that texture had no appreciable effect on workability of concrete. Tattersall (1991) also found that texture does not affect concrete flow (plastic viscosity) appreciably. Bennett and Katakkar (1965) however, found that the workability of various mixtures they tested was closely related to the specific surface of the fine aggregate.

Mather (1966) suggested that a smoother particle will require a thinner layer of paste to lubricate its movement with respect to other particles. It will therefore permit a higher packing for equal workability, hence will require a lower paste content than a rough particle of similar roundness and sphericity. As surface smoothness increases, contact area decreases and bonding area decreases (compared with a rough particle of the same volume).

Blanks (1950) suggested that salients and depressions on the particles, particularly when the sides of these roughnesses are almost perpendicular to the general surface, assist in adherence of the paste to the aggregate. Undulatory roughness is less helpful and may even be harmful to bond as the mortar changes in volume. Abrupt roughness is probably less significant than physical penetration of cement paste into the aggregate.

2.2.5.4 Effects of Grading and size

Size distribution of aggregates has perhaps the greatest effect on concrete properties (particularly workability), of all size and shape related properties. A review of codes in practice on concrete mixture proportioning indicates that the provisions regarding grading and size of aggregates are clearer than those on shape. Mather (1966) wrote:

If a grading suitable for relatively spherical particles is employed with particles that are highly non-spherical, the results may be expected to be less satisfactory than if a more appropriate grading had been employed.

For similar particles, the paste requirement increases as the particle size decreases. This is said to be because particle surface area increases but has not been shown to do so in the same proportion as surface area increases or according to the decrease in particle diameter. Ozol (1978) offered an interesting explanation to this. For mono-sized spheres, as size decreases, void content stays the same, thus the paste requirement must stay the same to fill the voids. It is suggested instead that the number of points of contact (which require separation) between a greater number of particles is the reason.

Experience has demonstrated that either very fine or very coarse sand, or coarse aggregates having a large deficiency or excess of any size fraction is usually undesirable, although aggregates with discontinuous or gap grading have sometimes been used to advantage. A well-graded material is the closest to ideal with a similar amount on each standard sieve size listed in that size specification. The scarcity of a particular sieve size could result in poor workability and even poor durability of the concrete. There exist programs which allow the combination of several aggregates with poor grading to achieve a well-graded mixture. Such programs can be used to determine the most-densely-packed system and minimum void content for the aggregates under consideration.

ASTM C 33 uses maximum size as a starting point of selecting coarse aggregate and is dependent on thickness of section, spacing of reinforcement, availability, economics and placement procedures (aggregates greater than 63 mm become more difficult to pump). The importance of maximum aggregate size (MSA) is that the smaller the aggregate size, the more mortar is needed in the mixture to surround the particle. There are, however, limits on both ends where this does not hold true. As the strength level is increased, smaller MSA must be used for the most efficient use of cement

(Schmidt, 1975). It is generally accepted that large particles have less area for bonding so higher strengths are not possible to obtain with large MSA. The effect of aggregate size on strength has also been attributed to the increase in the amount of portlandite precipitated as particle size decreases, so that much of the CH occurs on the surfaces of siliceous fine aggregate (French, 1991).

Fine aggregate grading has a much greater effect on workability of concrete then does coarse aggregate gradation. Water, the cementitious material, and the fine aggregate comprise the matrix in which the coarse aggregate is suspended and this matrix needs to coat the coarse aggregate particles and retain sufficient fluidity for placement purposes. Thus the fine aggregate can not be too coarse or harshness, bleeding, and segregation will occur. If it is too fine, the additional surface areas will require additional water and also result in segregation.

ASTM C 33 prohibits more than 45% aggregates passing any sieve and retained on the next consecutive sieve. It also limits the FM to between 2.3 and 3.1. For high-strength concretes, Schmidt (1975) found that a coarse sand with a FM of around 3.0 produced the best workability. In general, manufactured sands require more fines than natural sands for equal workability. The amount passing the No.50 sieve and the No.100 sieve have a greater influence on workability, surface texture, and bleeding of concrete (Kosmatka and Panerese, 1992).

2.3 Background on Concrete Rheology

This section is not intended to be a complete survey of the literature on concrete rheology but rather to give a background that will be helpful in understanding the motivation for performing the tests presented, and in interpreting the results obtained. A very detailed explanation of fundamental concepts, test methods, and devices which have been used to measure concrete workability and rheology can be found in (Koehler, 2004).

2.3.1 Definition of Rheology and its Relevance to Concrete Workability

Rheology simply put, is the study of deformation and flow. However, a more relevant definition could be that it is the study of the flow of materials that behave in an unusual manner. Examples of materials that flow in a normal, more familiar way are air, water, oil, and honey. Mayonnaise or peanut butter, however, flow in complex, unusual ways. Regardless of their viscosities, some being higher and some lower, normal or Newtonian fluids follow the same scientific laws. Non-Newtonian fluids do not follow these Newtonian flow laws, and behave in a wide variety of ways. Fluid rheology is applicable to fresh concrete, as fresh concrete can be considered a fluid. This said, concrete is a very complex material, due to several reasons. First, it involves a very wide range of particle size. Concrete is a suspension of fine and coarse aggregates in cement paste which is, in turn, a concentrated suspension of cement particles in water. Second, it is a time-dependent material, in that its flow properties change with time, due to hydration reactions. The rheology of concentrated suspensions is a topic which has been widely studied and can be very useful in scientifically defining concrete workability.

2.3.2 Some Properties of Fluids

Although fluids include both gases and liquids, regarding concrete rheology, it is possible to limit our discussion to liquids. When, a viscous liquid is subjected to a shear stress, it deforms continuously for the duration of the application of the stress, and the deformation is irrecoverable. In contrast, when an elastic solid is subjected to a shear stress, the strain will be finite, and related to the shear modulus, G, of the solid by the following equation:

$$\tau = G. \tag{2.38}$$

where; τ is the applied shear stress and . is the shear strain.

In viscous fluid flow, shear stress and the time rate at which shear stress is applied are related, meaning that a greater shear stress is required to shear the liquid at a greater rate. For the case of constant flow, shear stress, τ , is related to the shear rate, $\dot{\gamma}$, by the coefficient of viscosity, η, through the following equation:

$$\tau = \eta \cdot \dot{\gamma} \tag{2.39}$$

and the shear rate is equal to the velocity gradient, as shown in Figure 2.7, through the following equation:

$$\dot{\gamma} = \frac{dv}{dy} \tag{2.40}$$

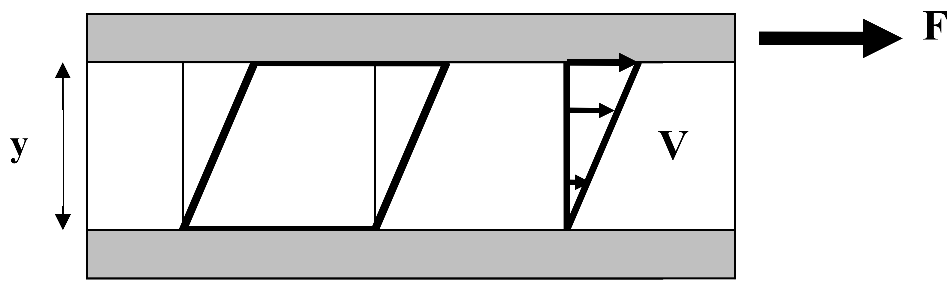

Figure 2.7 Two dimensional representation of viscous flow (Koehler, 2004)

The relationship between the shear stresses and shear rate of a fluid is often represented by a flow curve. The flow behavior of fluids can be distinguished by comparing their flow curves. Figure 2.8 shows idealized flow curves based on some of the most common models developed for fresh concrete.

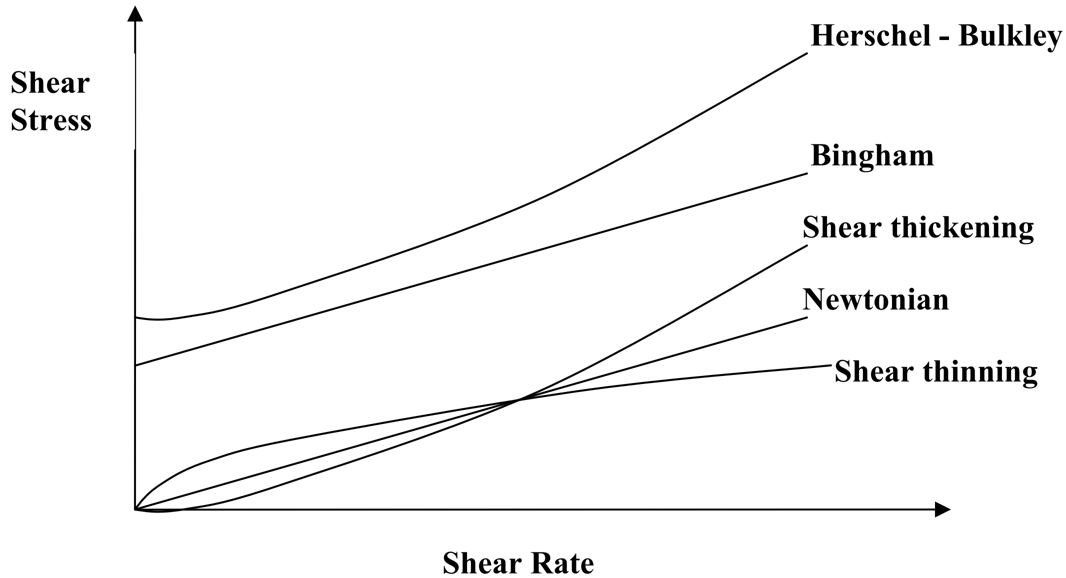

Figure 2.8 Idealized flow curves based on some common models

The most basic constitutive equation that describes fluid flow is for **Newtonian fluids**, such as water and oil at a given temperature. For such fluids, there is a linear relationship between the applied shear stress and shear rate, for the entire range of shear rates, and viscosity is a material constant. Equation (2.39), given above, describes the flow of Newtonian fluids. Unfortunately, the Newtonian model fails to satisfactorily represent the flow of concrete mixtures. This is due to the fact that ordinary concrete mixtures have a non-zero yield stress value (a viscoplastic material), which is the point at which the flow curve intersects the ordinate. Self-consolidating concretes, on the other hand, have very low yield stress, and can be represented using models which assume zero yield stress.

The **Bingham Model**, which is the most commonly used model for defining the flow of concrete mixtures, assumes a linear relationship between shear stress and shear rate and accounts for a yield stress, more correctly defining the flow behavior of concrete mixtures. The following equation describes the flow in this model:

$$\tau = \tau_o + \propto .^{\cdot} \tag{2.41}$$

where τ_o is the yield stress, $\propto$ is the plastic viscosity term and $.^{\cdot}$ is the shear rate. There is no difference between the viscosity term in the Newtonian model and the plastic viscosity term in the Bingham model other than notation. A drawback of the Bingham model is that flow curves for concrete are rarely linear.

The **Herschel-Bulkley** model, another model which is commonly used for defining concrete flow, assumes a non-zero yield stress and a non-linear relationship between the applied shear stress and the shear rate and is describes with the following equation:

$$\tau = \tau_o + a .^{\cdot b} \tag{2.42}$$

where τ_o is the yield stress, $.^{\cdot}$ is the shear rate, and a and b are material constants. This equation becomes the Bingham equation when b is set to unity. Depending on the values selected for a and b, the Herschel-Bulkley equation can define an upwards concave (shear-thickening) or downwards concave (shear-thinning) curve. Other models have been proposed and can be found in the literature.

2.3.3 Definitions of Yield Stress and Viscosity

In concentrated suspensions, solid particles interact to form a flocculated structure that resists flow at sufficiently low stresses. **Yield stress** is related to the force required to break down this flocculated structure and to initiate flow. There are differing opinions about whether or not yield stress really exists and if so, how it should be defined. Yield stress is determined from a flow curve by extrapolating back the measured data points to intercept the shear stress axis. It has been determined, based on low-shear rate viscosity measurements, that viscosity is very high at low shear rates up to a certain rate, after which the viscosity drops rapidly, which results in the transition from elastic behavior to viscous flow. Regardless of whether a yield stress actually exists, it is a parameter with practical significance. The definition of yield stress is important in measuring it, in that results can vary significantly. Values of yield stress obtained through measurements starting at a static state are often higher than the values obtained by extrapolating back data points in flow curves.

Viscosity relates shear stress to shear rate, and is a material constant for Newtonian fluids. For non-Newtonian fluids like concrete, however, it is useful to describe it in more detail.

The viscosity term in Equation (2.39), η, is the dynamic viscosity and is given in units of Pa.s. The kinematic viscosity, v, is given in units of m^2/s, is given as:

$$\nu = \frac{\eta}{\rho} \tag{2.43}$$

where ρ is density.

Apparent viscosity is equal to the shear stress divided by the shear rate. Apparent viscosity is the slope of a line drawn from the origin to a point on the curve, for non-linear cases. The differential viscosity is defined as the derivative of shear stresses with respect to shear rate:

$$\eta_{diff} = \frac{d(\tau)}{d(\dot{\gamma})} \tag{2.44}$$

Plastic viscosity, $\propto$, is the limit of the differential viscosity as shear rate approaches infinity.

$$\propto = \lim_{\dot{\gamma} \to \infty} \frac{d(\tau)}{d(\dot{\gamma})} \tag{2.45}$$

Plastic viscosity is equal to differential viscosity for Bingham materials. For materials referred to as non-ideal Bingham materials, such as ordinary concrete, for which the flow curve is non-linear at low shear rates but linear at higher shear rates, plastic viscosity is the slope of the linear portion of the curve.

Relative viscosity, η_r, is given as the ratio of the viscosity of a suspension to the viscosity of the suspending medium, and is defined as:

$$\eta_r = \frac{\eta}{\eta_s} \tag{2.46}$$

Specific viscosity, η_{sp}, is defined as:

$$\eta_{sp} = \eta_r - 1 \tag{2.47}$$

and fluidity, ϕ, is defined as:

$$\phi = \frac{1}{\eta} \tag{2.48}$$

2.3.4 Causes of and Models to Predict Viscosity of Suspensions

There are three types of forces which act on particles in suspensions: Particle interaction forces, Brownian forces, and viscous forces. Particle interaction forces are the result of attraction or repulsion between particles in the suspension and are generally relevant for the behavior of the cement paste phase of concrete. Attractive forces tend to cause flocculation, which increases viscosity. Repulsive forces, on the other hand, tend to disperse the particles, and the viscosity is related to the particle concentration, rather than the degree of dispersion. Brownian forces do not have a significant effect on concrete mixtures and will not be discussed here. Viscous forces are proportional to the local velocity difference between a given particle and the surrounding fluid. Therefore, a change in the viscosity of the suspending medium results in a change in the viscosity of the overall suspension.

Several models have been developed to relate properties of suspensions to viscosity. A few will be discussed here. The **Einstein model**, relates the viscosity of a suspension, η, to the viscosity of the suspending medium (η_s) and the solids volume concentration (φ) through the following equation:

$$\eta = \eta_s(1 + 2.5\varphi) \tag{2.49}$$

This model is based on the assumption of mono-sized spheres. Higher order terms of φ can be added to account for interaction between the particles. This model is exact for dilute suspensions (up to about 10% solids volume concentration) and modifications are required for concentrated suspensions. The **Krieger – Dougherty equation**, which is approximate and based on the Einstein model, has been derived for concentrated suspensions. It includes maximum packing fraction (ϕ_m) and intrinsic viscosity ($[\eta]$) terms, and is given as:

$$\eta = \eta_s (1 - (\phi / \phi_m))^{-[\eta]\phi_m} \tag{2.50}$$

The maximum packing fraction is defined as the concentration at which viscosity approaches infinity as there is contact between the solids in three dimensions throughout the suspensions. Intrinsic viscosity is a dimensionless number defined as the limiting value of the reduced viscosity as solids volume concentration approaches zero. It is equal to 2.5 for spheres and higher for other shapes. Figure 2.9 shows the change in viscosity with increasing solids volume content, according to the Einstein and Krieger – Dougherty models.

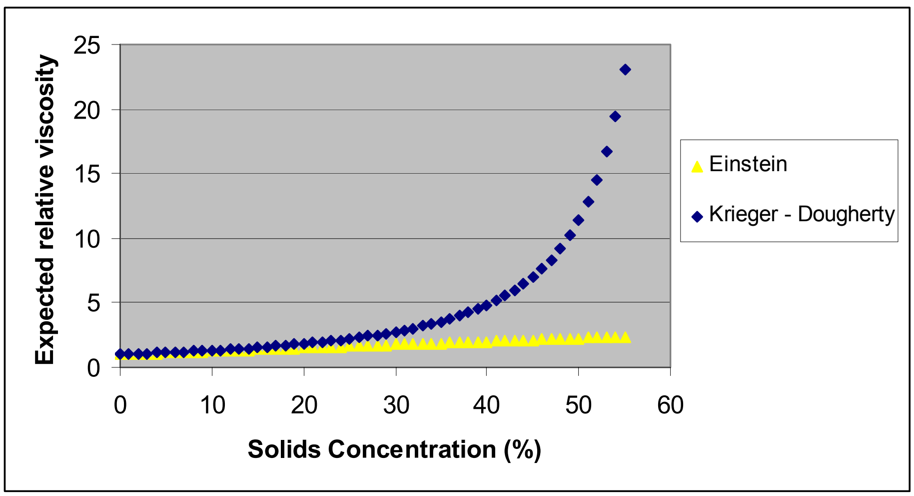

Figure 2.9 Change in viscosity with increasing solids volume content, according to the Einstein and Krieger-Dougherty models

It is clear from the figure that there is a noticeable difference in the predicted relative viscosity at solids concentrations above 10 to 15%. It has been stated that both of these models can be used for cement paste but should not be used for concrete (Ferraris, 1999).

A recently introduced computational method called “Dissipative Particle Dynamics” (DPD) appears promising for the modeling of concrete rheology. This model tracks boundaries of fluid-fluid and fluid-solid phases and can control the interparticle interactions. A current drawback of the model is that it requires significant computational power, the running of one concrete mixture case can take up to a few days running parallel on ten or more processors, simultaneously. This model, being rather new, needs to be verified against empirical results from carefully selected test cases and be calibrated if necessary.

2.3.5 Factors Affecting Fresh Concrete Rheology

Mixture proportioning, material properties, mixing time, and conditions at the job site all affect the flow properties of concrete. In addition, rheological properties can be a function of measurement technique, and results obtained using one rheometer can be significantly different than those obtained using a different rheometer. Although the effects of certain changes to mixture proportions or materials used can be examined using paste rheology, these may not always be representative of the behavior of the concrete and it is preferred to analyze the rheological behavior of concrete, including the aggregates.

It is obvious that water content has a significant effect on flow and lowers both the yield stress and the plastic viscosity of a mixture by reducing the solids volume concentration of the paste phase (cement particles). However, it must be noted that excessive water content can result in segregation resulting in a mixture with poor flow properties. For a fixed water-cement ratio, increasing cement content (relative to total aggregate volume) increases the amount of paste surrounding aggregate particles (mortar and concrete phases) and lowers both yield stress and plastic viscosity of the mixture. In addition, cement composition and fineness can influence flow, due to differences in water demand. Contrary to increasing cement content, increasing aggregate content (relative to a fixed water-cement ratio) increases viscosity, due to increased particle interactions. The effect of particle concentration on yield stress is less lucid for typical particle concentrations in concrete. Tattersall (1991) has reported that there exists an optimum sand-to-coarse ratio for which the values of yield stress and plastic viscosity are a minimum; however, this value may not be the same for both.

The particle size distribution of aggregates significantly influences workability and rheological properties. It is generally accepted that a well graded aggregate with particles of a wide range of sizes decreases viscosity. Increasing the packing density generally improves the flow; however, the optimal packing density is lower than the maximum packing density for a given aggregate. Quiroga (2003) found that uniform aggregate gradations required less water for a given slump. The morphological properties of aggregates also influence the rheology of concrete. Spherical shapes or rounded aggregates, give lower viscosity than angular ones. Rounded and smooth aggregates require less water than angular or flat and/or elongated particles to achieve the same slump. Spherical particles flow more easily around each other and result in reduced viscosity. However, it is not easy to say, for example, whether or not the viscosity of a mixture made using flat and/or elongated particles will be higher than that of a mixture made with more equi-dimensional yet angular ones. There is a need for more research on the effect of coarse and fine aggregate particle shape on rheological properties. Particle shape is important in that it affects packing, and it has been found that higher packing density produces higher slumps. Tattersall (1991) suggested that aggregate particle shape has a more significant effect on plastic viscosity than yield stress. He also found that particle surface texture does not have a significant effect on flow properties. Size distribution and particle shape can be especially important in the case of microfine aggregates (aggregate particles passing the 75μm sieve). Although microfines increase the water demand of the mixture due to increased surface area, it has been reported that they can improve flow by improving the grading of the fine aggregates.

Admixtures and supplementary cementitious materials also influence paste and concrete flow significantly, and their effect on rheology deserves greater attention. They will be covered here in brief since these materials were not used in the test program. The use of water-reducing admixtures generally results in a significant reduction of the yield stress of a mixture while the changes in plastic viscosity, increasing or decreasing, are minute. Air-entraining admixtures improve workability by rendering the concrete more cohesive; however excessive air-entrainment may cause the concrete to become sticky and hard to finish. Air entrainment reduces viscosity more than it reduces yield stress, up to about 5% (Tattersall, 1991). Above 5%, yield stress continues to decrease whereas viscosity remains the same. Viscosity-modifying admixtures increase both the yield stress and the viscosity of concrete mixtures and increase resistance to segregation and settlement. The use of fly ash generally reduces yield stress but has a variable effect on viscosity, dependent on whether the cement is replaced on a mass basis or a volume basis. This is due to the fact that fly ash particles are smaller in size than cement particles resulting in a change in surface area, the amount of which is strongly dependent on whether the replacement is made on a mass or volume basis. The effects on yield stress are also dependent on the amount of replacement. The effect of silica fume replacement of cement is dependent on amount. Tattersall (1991) found that up to a certain threshold replacement value, use of silica fume reduces plastic viscosity and does not affect yield stress considerably. Above this value, both yield stress and viscosity increase. Faroug et al. (1999) found that viscosity decreased up to a 10% replacement rate, and increased afterwards. Yield stress increased up to 20% replacement, after which it decreased. Both fly ash and silica fume have a beneficial effect, due to their rounded, spherical shapes, and a negative effect, due to the increase in the water demand of the mixture due to increased surface area, on the flow of concrete. The effect of ground granulated blast furnace slag on rheological properties is dependent on the amount of cement and the type of slag used in the mixture.

2.4 Measurement of Rheology

Rotational rheometers can be used to determine rheological parameters of concrete mixtures in fundamental units. They allow the application of a continuous shear stress to a mixture and the monitoring of changes over time and can be used to obtain a flow curve. It is possible to perform controlled-rate rheometry, in which a series of shear rates are imposed and the resulting shear stresses are calculated, or controlled-stress rheometry, in which a range of shear stresses are imposed and the resulting shear rates are measured. There are various geometries of rotational rheometers: coaxial cylinders, parallel plates, cone and plate, etc. The exact dimensions of the rheometer are used to develop analytical equations relating torque and rotation speed to the specific parameters of a given constitutive equation such as the Bingham equation or the Herschel-Bulkley equation. Derivations of such relations are available in the literature.

The rheometer used for the tests presented in the following chapters is a modification of the coaxial cylinders type. There are a few concepts worth introducing without getting into excessive detail. The first of these is that of a "dead zone". This is a region in the opening between the coaxial cylinders (opening) where there is no flow due to the shear stresses being insufficient to overcome the yield stress. In the presence of a dead zone, equations used to calculate the shear rate need to be used over the portion of the opening where flow actually occurs. The occurrence of a dead zone is based on three parameters: the speed of the rotation, the ratio of the yield stress to the plastic viscosity, and the ratio of the outer radius to the inner radius. It can be eliminated by increasing the rotation speed, reducing the ratio of the yield stress to the plastic viscosity, reducing the ratio of the outer radius to the inner radius, or a combination of these. The yield stress, plastic viscosity and the ratio of the two depend on the material being tested, the speed of the rotation is dependent on the shear rate applied, and therefore can not be modified. The ratio of the outer and inner cylinders can be controlled and a minimum rotational speed can be calculated for a given geometry and ratio of yield stress to viscosity to eliminate the formation of a dead zone. Figure 2.10 shows the influence of the dead zone on the measured torque vs. the rotation speed curve, for a fixed outer cylinder radius to inner cylinder radius ratio.

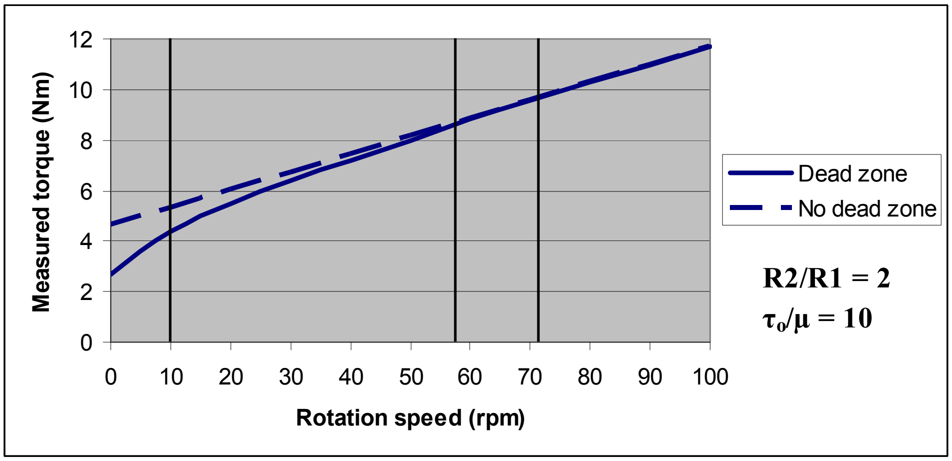

Figure 2.10 Influence of the dead zone on Measured torque vs. Rotation speed curve (Koehler, 2004)

If there is no dead zone, the dashed line in Figure 2.10 will be measured. In the presence of a dead zone, however, the solid line will be measured. This is because the amount of torque measured will decrease due to the decrease in the amount of material that flows. The magnitude of the error resulting from incorrectly ignoring the dead zone is dependent on how much lower the rotation speed for a given data point on the flow curve is than the critical rotation speed at which the dead zone is eliminated. It can be seen from Figure 2.10 that ignoring the dead zone incorrectly results in an underestimation of the yield stress and an overestimation of the plastic viscosity. Figure 2.11 shows the error resulting from ignoring the dead zone, for a range of yield stress to viscosity ratios, for a fixed outer cylinder radius to inner cylinder radius ratio.

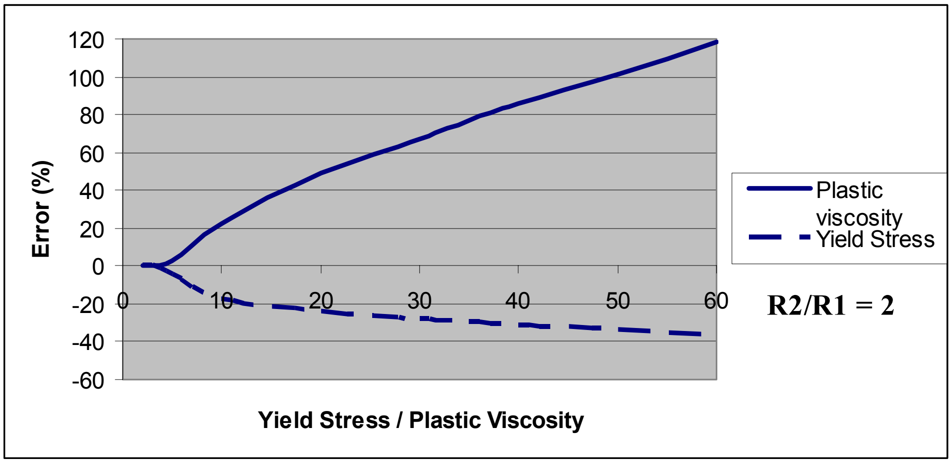

Figure 2.11 Influence of ratio of yield stress to plastic viscosity on errors due to neglecting the dead zone for rotation speed 10 rpm to 60 rpm (Koehler, 2004)

It can be seen that the stiffer a concrete (the higher the yield stress to viscosity ratio), the larger the error due to ignoring the dead zone becomes. This can be readily visualized. Several methods have been suggested to account for the presence of a dead zone and are available in the literature.

Another concept worthy of mention is that of "end effects", which occur in the case of the inner cylinder being immersed in the concrete being tested, where there is concrete above and below the inner cylinder. The shear stresses at the top and bottom ends of the inner cylinder are changed due to the presence of the material directly above or below it. Methods of approximating these effects have been suggested in the literature.

Another important concept is that of relative rheometry. It is possible to use a relative rheometer to measure values related to but not necessarily equal to the yield stress and plastic viscosity, instead of measuring fluids in an absolute rheometer and measuring rheological parameters in fundamental units. For concrete, relative rheometers measure torque at a series of fixed speeds. Figure 2.12 shows typical results from a relative rheometer. A straight line is fitted to the data points and the intercept of this line with the ordinate (torque axis), G, is related to yield stress. The slope of the line, H, is related to plastic viscosity. Methods have been suggested for relating G and H to yield stress and plastic viscosity but the existence of a dead zone creates problems, since the amount of material that flows increases with increasing rotation speed, making it difficult to distinguish between the contribution of viscosity and changing dead zone size to the increase in torque.

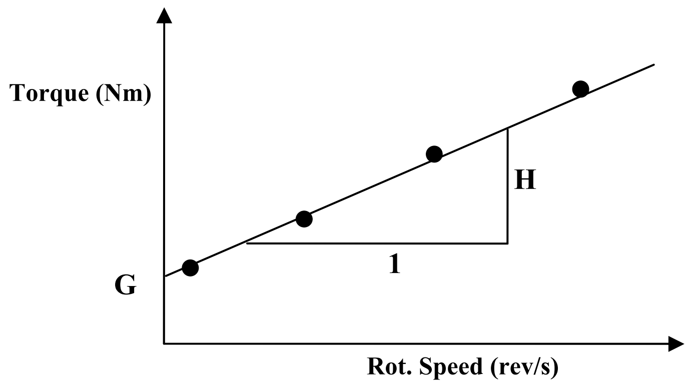

Figure 2.12 Typical results from a relative rheometer

It was previously mentioned that the rheometer used in the research presented here was a modification of the coaxial cylinders type. The difference is that the rheometer uses a vane in place of the inner cylinder. Figure 2.13 shows the vane impeller used.

Figure 2.13 Vane impeller used in the rheometer

There are various advantages of using a vane in place of the inner cylinder. An important one is that the vane cuts a cylindrical volume out of the mixture but different than the case with the inner cylinder, slippage at the cylinder surface is mitigated, because yielding occurs within the material and not at the boundary of the material (Koehler, 2004).

CHAPTER 3 CHARACTERIZATION OF AGGREGATE SHAPE USING X-RAY TOMOGRAPHIC AND MATHEMATICAL TECHNIQUES

3.1 Introduction

There are at least three reasons to mathematically characterize shape. The first is to be able to quantify the shape difference between different aggregates from different sources and classify them. The second is to be able to quantitatively relate true aggregate shape to performance properties. The third reason is so that real particles can be incorporated into many-particle computational models [Garboczi, 2002]. X-ray computed tomography and x-ray microtomography are techniques that provide complete, three-dimensional characterization of aggregate particle shape. The insertion of random particles, such as concrete aggregates, into computer models requires that each be characterized by a limited set of numbers (due to memory constraints), fewer than required by digital techniques, where the location of each pixel must be known. For this reason, spherical harmonic functions are used to analyze the data obtained from tomography. This allows the reduction of each particle to the coefficients of the spherical harmonic expansion, a limited set of numbers which fully characterize particle shape at the resolution of the original image. X-ray tomographic techniques can be used for other construction materials related applications and detail given in this chapter is intended to be sufficient for a user intending to perform such experiments. X-ray tomographic techniques, image processing techniques applied to tomography data and the spherical harmonic method used to manipulate the data, are presented in this chapter.

3.2 High-Resolution X-Ray Computed Tomography

X-ray computed tomography is a completely non-destructive technique for visualizing features in the interior of opaque solid objects, and for obtaining digital information on their 3-D geometries and properties. High-resolution x-ray CT differs from conventional medical CAT-scanning in its ability to resolve details as small as a few tens of microns in size, even when imaging objects made of high density materials (Ketcham and Carlson, 2001).

In this technique, a specimen is digitally cut using x-rays, and the interior structure is revealed, similar to slicing a loaf of bread. In x-ray CT, similar to the slices of a loaf of bread, slices of the specimen are obtained. Each slice corresponds to a certain thickness. Therefore, the slices obtained are three dimensional, with one pixel depth and are thus made up of voxels (volume elements). Figure 3.1 shows a sample slice obtained using x-ray CT.

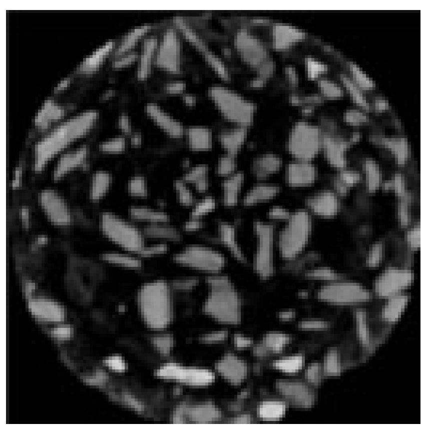

Figure 3.1 Two-dimensional image of a siliceous river gravel obtained from a CT scan

X-rays can be transmitted, scattered and absorbed as they pass through the specimen. Different parts of a specimen may scatter or absorb x-rays at different levels, resulting in a variation in the attenuation of the x-rays in going through the specimen. X-ray attenuation is dependent on the energy of the incoming x-rays and the density and atomic number of the material the rays pass through. An image is created by passing x-

rays through a single slice of a specimen, therefore a layer a
measuring the resultant decrease in intensity. An algorithm (fil
used to reconstruct the distribution of the x-ray attenuation in t
levels in the slice indicate different degrees of x-ray attenuation.
voxel thickness can be stacked computationally to obtain the inte
specimen.

The simplest scanning configuration for x-ray CT is the
to be scanned between an x-ray source and detectors which mea
the x-ray signal has been attenuated by the sample. A singl
measurements on all detectors for a given object position and sca
a *view* (Ketcham and Carlson, 2001). The scan of a slice is
multiple views, each at a different angular orientation. The scann
were third generation scanners which used a fan beam of x-ray
linear series of detectors which are both wide enough to cover
object so only the object being scanned is rotated between vie
simplified scanning configuration for a third generation scanner.

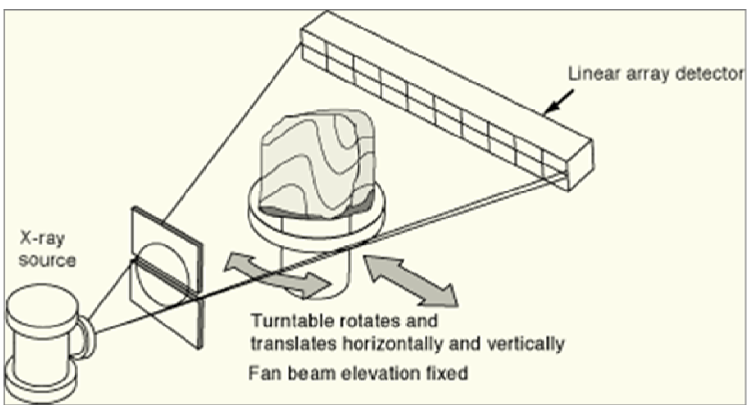

Figure 3.2 Scanning configuration for a third generation x-ray CT

in scanning an object. X-ray intensity directly affects the signal-to-noise ratio and thus higher intensity provides better image clarity. Higher intensities often require a larger focal spot. The energy spectrum describes the ability of x-rays to penetrate the object and the expected relative attenuation of the x-rays through materials of different density. While higher energy x-rays penetrate more easily through a given object than low-energy x-rays, their sensitivity to changes in density within the object is lower. This is because "photoelectric absorption" is the predominant physical process responsible for x-ray attenuation at lower energies, and it is proportional to Z^{4-5} where Z is the atomic number and Compton scattering is the process responsible for attenuation in medium energy x-rays and is proportional only to Z (Ketcham and Carlson, 2001). Thus two materials with similar density but different atomic numbers can be differentiated if the mean x-ray energy used is low enough. It is therefore important to note that the use of higher energy x-rays may not always be a good thing. Figure 3.3 shows a slice of a specimen imaged at two different energy levels.

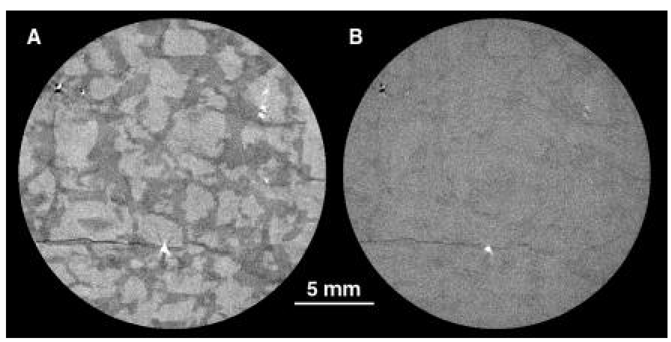

Figure 3.3 A slice of a specimen imaged at 100 keV (left) and 200 keV(right) with filtering (UT-CT)

The focal spot size determines the number of possible source-detector paths that can intersect a given point in the object. The higher the number of source-detector paths, the more the blurring of features. The x-ray tubes of the scanners used in this research were a dual spot 420 kV source with 0.8mm and 1.8mm spot sizes and maximum loads of 800W and 2000W, respectively and a 200kV ultra-high resolution tube with an adjustable focal spot with a minimum size of <10 μm at 8 W total load. Both sources had tungsten targets.

Detectors for CT scanners are made of scintillating materials. X-rays produce flashes of light in the scintillators that are counted. The size and number of detectors and their efficiency in detecting the energy spectrum generated by the source affects image quality. The size of an individual detector determines the amount of an object that is averaged into a single intensity reading, while the number of detectors determines how much data can be gathered simultaneously. In third-generation scanning, the number of detectors also defines the degree of resolution possible in a single view, and thus in an image overall. It must be remembered that higher energy x-rays more easily penetrate objects, when determining the level of expected signal after polychromatic x-rays pass through materials. The detectors used in this case were set to create 1024 virtual pixels along the width of a slice.

3.2.1 Sample Preparation

There are a few points to consider when preparing a specimen containing coarse or fine aggregate particles to be scanned with x-ray CT. The first is that the full scan field for CT is a cylinder, since the full view for a single slice is a circle. This is because the specimen is rotated around its vertical axis between each view. For this reason, the most efficient scan geometry is a cylinder. Another point to consider is that the specimen fits inside the field of view at all times during the scan. Overhangs of irregularly shaped specimens must be taken into consideration when calculating how far to place it from the x-ray source. Care must also be taken that the specimen does not move or wobble during the rotation.

Different size specimens, made of different materials were used in this research. Concrete cylinder molds, 150 mm by 300 mm (6 in. by 12 in.), were used as the molds for coarse aggregate specimens, and 75 mm by 150 mm (3 in. by 6 in.) were used as the molds for fine aggregate specimens. These specimen sizes allow for pixel sizes of about 150 ∝m and 75 ∝m, which enables the characterization of particles approximately 2 mm, and 1 mm in diameter or larger. There is a need for compromise between time efficiency and economics and resolution, when determining the sample size to be used. In general, the larger the sample is, the higher the number of particles which can be scanned at once, but the higher the size of the smallest particle that can be characterized. The selection of a material to embed the particle in depends on economy, ease of use and compatibility with the technique (such as having a density contrasting with that of concrete aggregates, and being as homogeneous as possible to keep image processing simple). Cement paste was initially tried as the matrix; however, the need to be able to recover the particles for further testing required choosing another material. Compacted cement (powder) was found to be messy and yielded mediocre images, due to the granular nature of the matrix complicating the image processing operations. Candle wax was found to be inexpensive, homogeneous and easy to work, and had a contrasting density with the aggregates. The particles can be placed individually in layers to prevent particles from touching each other or can be pre-coated with hot wax, cooled and then mixed with additional wax and molded. Specimens for fine aggregates were prepared similarly, the only difference being in size. In order to characterize particles retained on the No. 50 (0.3 mm) and No.30 (0.6 mm) sieves, specimen diameters of approximately 30 mm and 60 mm, respectively, or lower are needed.

For both coarse and fine aggregate specimens, it was determined through trial and error that aggregate volume of 40 to 45 % or less is required to prevent too many particles from touching and for the satisfactory characterization of particles.

3.2.2 Calibration

There are three basic calibrations required for third-generation scanners. These are offset and gain, which determine the detector readings with x-rays off, and with x-rays on at scanning conditions, respectively, and wedge calibration, which consists of acquiring x-rays as they pass through a calibration material over a 360º rotation. The calibration material may be air or a material with a density which is similar to that of the material of interest. A wedge calibration with non-air can provide automatic corrections for beam-hardening and ring-artifacts, which are explained in later sections.

3.2.3 Data Collection

Number of views and time per view are the two main variables in the collection of data. The number of views relates to how finely the 360° full rotation of the specimen is divided. This value can typically be between 600 and 3600. Each view represents a rotational interval equal to 360º divided by the total number of views. Time per view defines the counting time for each intensity measurement and increasing it can increase the signal to noise ratio and improve resolution.

The position of any single point in the object corresponds to a sinusoidal curve as time progresses. An image showing this is called a sinogram. Figure 3.4 shows a sample sinogram.

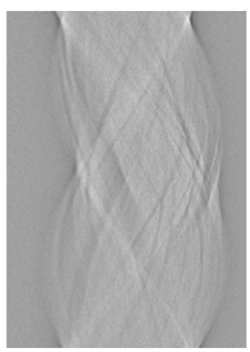

Figure 3.4 A sample sinogram (Rendahl, 1999)

The raw data are displayed such that each line contains a single set of detector readings for a view, and time progresses from top to bottom.

3.2.4 Data Reconstruction

The sinograms are converted into two-dimensional slices through a mathematical process which often involves a technique called filtered back projection. Details of this process can be found in (Kak and Slaney, 2001). The raw intensity data in the sinogram are converted to CT numbers that have a range determined by the computer system during reconstruction. Recent systems use a 16-bit scale, which allows a range from 0 to 65535. On most industrial scanners, these values correspond to the grayscale in the image files created by the systems. The CT values should map linearly to the effective attenuation coefficient of the material in each voxel. Industrial CT systems are sometimes calibrated so that the CT number corresponds roughly with density, where air has a value of 0, water of 1000, aluminum of 2700, etc. For scanning concrete aggregates such a scale may desensitize the system since the variation in densities within the specimen may not be very great. In this case, the CT value contrast within the specimen can be maximized by assigning arbitrary low and high values can be assigned to the least and most attenuating features in the scan field.

3.2.5 Resolution

The size and number of detector elements, the focal spot size and the distances between the x-ray source and the object and the object and the detectors, determine the spatial resolution of a CT image. The source to detector distance was fixed in the scanners used in this research. In such a case, the resolution of the image is maximized by minimizing the distance between the source and the object. Figure 3.5 shows two different scanning arrangements of the same specimen which will result in two different resolutions.

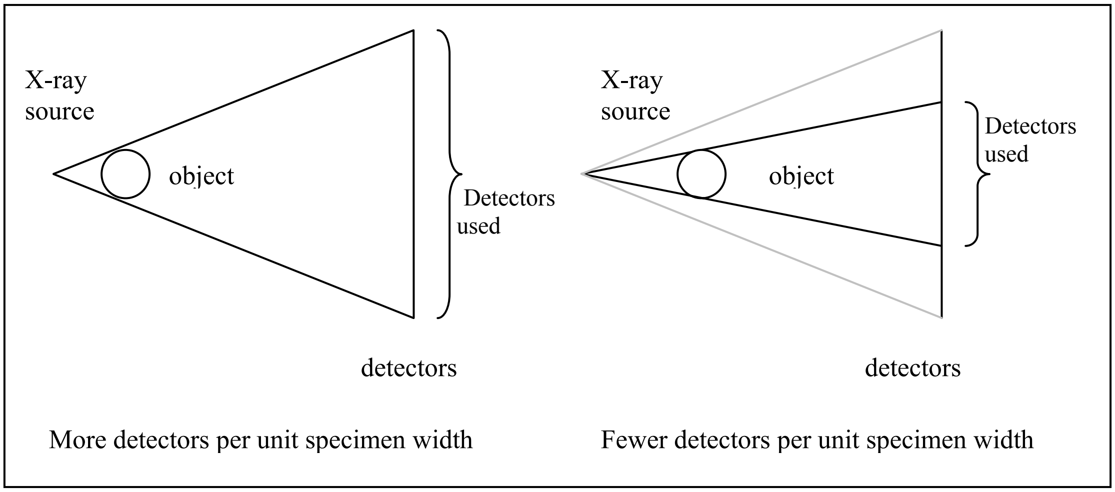

Figure 3.5 Different scan arrangements of the same specimen which will result in two different resolutions

The resolution in the vertical dimension, and therefore the thickness of the slice, is governed by the thickness of the slits in front of the detectors. There is a practical limit as to how much slice thickness can be decreased after which the need to increase the x-ray flux to maintain satisfactory counting statistics (since the area on the detector will have decreased) will tend to increase the focal spot size and cause blurring. One way around this problem is to increase the time per view. The spatial resolution required is dependent on the density resolution in the object being scanned. If the aggregates and the matrix in which they are embedded are sufficiently different in their attenuation properties, or densities, a lower resolution will suffice than when the two materials have similar density.

3.2.6 Size Limitations

There is a maximum practical limit to the size of the specimen to be scanned, because of the need to receive a sufficiently strong signal from the beam after it has passed through the object. Thicker objects will absorb more energy and result in lower image quality.

Perhaps more importantly, the size of the specimen is restricted by the resolution required/desired. High-resolution CT scanners, such as the ones used in this research can provide resolution less than 100 micrometers, enough to satisfactorily image aggregate particles retained on the No.50 sieve. The characterization of particles smaller than this size requires the use of x-ray microtomography, which is described in a following section.

3.2.7 Scanning Artifacts (Ketcham and Carlson, 2001)

Artifacts that result from scanning can make the quantitative use of the CT data difficult as they may change the CT value in certain parts of the object and obscure details of the object. Moreover, they can result in the flawed interpretation of the data. Beam hardening is the most commonly encountered artifact in CT scanning. It causes the edges of an object to appear brighter than the center of the object. Hardening refers to the increase in the mean energy of the x-ray beam as it passes through an object. This happens because the lower energy x-rays are attenuated more than their higher energy counterparts. This leaves the beam with a higher average energy than the incident beam. This also causes the attenuation coefficient of the object to decrease as the beam passes through it, making shorter paths through the object more attenuating than longer paths. This causes the parts of long ray paths corresponding to the center of the object to appear darker and the edges to appear brighter. One solution to this problem is to use a beam with a high-enough energy that the beam hardening is negligible. Another possible remedy is filtering the low-energy rays in the beam by passing it through a piece of metal such as copper. Another option is to place the object being scanned inside a cylindrical wedge material of similar attenuation properties. The wedge material would then be removed from the images during image processing. In the case of concrete aggregates, the readings in the raw scan data can be converted to a non-beam-hardened equivalent before reconstruction. A radial average of the CT values for a collection of slices can be used to perform a wedge correction in cases where the sample is pretty uniform.

Ring artifacts are full or partial circles, with centers on the rotation axis, which appear on the image. The output from an individual or a set of detectors may shift to yield abnormal values. The rings on the image are located in the positions of greatest overlap of these rays during reconstruction. They can be caused by changes in temperature or beam energy or when the beam hardness is sufficiently different than that during wedge calibration, particularly in cases where the wedge calibration was done through air. Partial rings can occur if the object being scanned is uneven, since different views will reflect different degrees of hardening. A solution is to perform the wedge calibration through a material with similar attenuation characteristics to the aggregate specimen. Software corrections are also possible; however, care must be taken to prevent the loss of parts of the actual object.

Certain other artifacts can occasionally occur, such as streaks that traverse the longest axes of the object. A starburst artifact can occur as a bright streak from the object surface into the surrounding matrix in cases where the object is much higher in density than the matrix. Another potential artifact is the blurring of the aggregate surface due to limited resolution. The CT value for a certain pixel will be the average of the attenuation properties of all the materials and areas it represents, and thus is an average of the properties of a part of the particle and a part of the surrounding matrix. This is called a partial volume effect. It is interesting to note that this effect can be constructively used to identify features of an object which are smaller than the voxel size at the selected resolution such as in the case of identification of cracks in a specimen.

3.3 X-ray Computed Microtomography Using Synchrotron Radiation

X-ray microtomographic imaging (μCT) is similar to regular CT in that virtual slices of a specimen can be obtained and processed to obtain complete, three-dimensional visualizations of features in the interior of the specimen (in this case of embedded microfine aggregate particles). It is the extension of CT to specimens between 1 mm and 1 cm in size and creates cross-sectional images with resolution approaching 1 μm. The physics of this technique, however, are different, and it is useful to understand the basics to be able to obtain clear and correct images. The geometry of illumination, x-ray energy range, and intensity requirements for μCT are well met by a synchrotron x-ray source and the μCT tests presented here were performed at the National Synchrotron Light Source (NSLS), at Brookhaven National Laboratory. It is particularly important to have a basic knowledge of μCT because experiments at synchrotrons are performed in a given, restricted amount of time, by users themselves, with limited technical support.

Details given here are those for beamline X-2B at the NSLS. This beamline is a white beamline, with a single monochromator in the hutch (where the sample is placed, and measurements are made) and the design allows an approximately 1-cm wide by 5-mm high illuminated area. An x-ray flux between ~7keV and ~40keV can be provided. Si<111> mirrors are used for routine use. A two-dimensional position sensitive detector placed directly behind the specimen simultaneously collects the projection data for many rays throughout the specimen. Figure 3.6 shows the schematic of the detector.

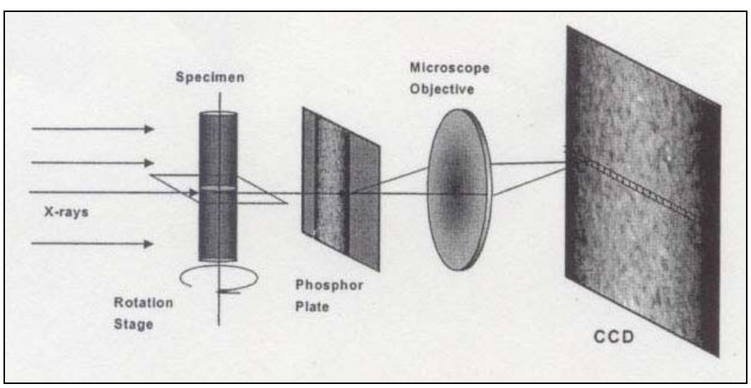

Figure 3.6 Schematic of the μCT detector (Dunsmuir, 2005)

Motorized specimen micropositioners control specimen height, horizontal translation transverse to the x-ray beam and rotation. A single crystal scintillator is used to convert the pattern of x-ray intensity transmitted by the specimen to a visible light image. The crystal is attached to a focusing stage and is moved to refocus the image after a lens change. A microscope objective magnifies the image onto the surface of a charge coupled device (CCD). Objective selection sets the image magnification. 2.5x, 5x, 10x, and 20x lenses are available at this beamline, higher magnification lenses being used to capture finer detail, however the use of the higher magnification lenses can be problematic and requires experience. A thermoelectrically cooled CCD collects image data. It is a back-thinned 1024x1024 full frame device with 24 micron pixels, ~340K electron full-well capacity, 14-bit digitization, 800 kHz readout, and 16e/sec dark current at -35°C. The CCD can be thought of as a stack of linear detectors, each associated with a single slice through the specimen.

Attenuation images are collected from many angles by rotating the specimen through small, evenly spaced, angular increments between 0 and 180 degrees using a rotation stage. The number of images needed is approximately $\frac{n\pi}{2}$, where n is the width of the specimen image in CCD pixels.

3.3.1 Sample Preparation

The importance of sample preparation in μCT can not be overemphasized. Due to the very fine scale at which the imaging is being done, the method is not as forgiving as CT to poor sample preparation. First, it is presumed that the μCT specimen will be dimensionally stable, so that it will maintain its shape during the scan, and is able to withstand the high dose of x-rays deposited. It is also important that there be heterogeneity within the sample, which will give rise to a detectable absorption contrast. In the case of aggregates, this requires that the matrix in which the microfines are embedded have sufficiently different x-ray absorption or simply varying density.

Specimen size selection is driven by several criteria including absorption, contrast and resolution. The specimen should absorb about 90% of the incident radiation along the most radio-opaque path to obtain the best signal-to-noise ratio in the reconstructed image. The absorption of the x-rays in the 7 to 40 keV energy range is described by:

$$I / I_o = e^{-\mu(\lambda)\rho x} \qquad (3.1)$$

where I is the intensity of the absorbed x-ray beam, Io is the intensity of the incident x-ray beam, ρ is the specimen density, x is the specimen thickness, and

$$\mu(\lambda) = KZ^m \lambda^n \qquad (3.2)$$

is the mass attenuation coefficient of the specimen where Z is the atomic number, m is approximately 4, λ is the x-ray wavelength and n may vary between 2.5 and 3.0. To absorb 90% of the incident radiation, the quantity μ(λ)ρx, commonly referred to as τ, should be approximately 2. To obtain this, the sample thickness or the x-ray energy can be varied. Image noise increases are noticeable in images with $\tau < 0.5$. A τ value greater than 2.5 causes reconstruction artifacts.

As mentioned previously, magnification is selected by the choice of microscope objective. Ideally, the entire specimen should remain within the field of view of the CCD, as it is rotated during the scan. As magnification increases, the field of view decreases and the specimen dimension must be adjusted accordingly. There are advantages such as being able to obtain a quantitative map of linear attenuation when the entire object stays within the field of view during the experiment ('global scanning'), whereas the image will have a relative grayscale in arbitrary units when a part of the specimen extends beyond the field of view during rotation ('local scanning'). However, this is not important in the case of scanning microfines for shape determination. The specimen size should not be greater than three times the field of view. The selection of specimen size, x-ray energy and resolution can also be driven by the differences in x-ray absorption among the different components of the sample. If the contrast among the components of the sample (between the matrix and the aggregates) is low, a lower x-ray energy and a smaller specimen will probably be needed. The concentration of the microfine particles in the specimen will clearly be a factor influencing energy selection.

It is possible to prepare a microfine aggregate μCT specimen by simply filling a thin glass or other tube with the particles. However, this can make image processing more difficult due to a great number of particles touching, therefore reducing the quality of the images and reducing the fine scale detail of the particles characterized (as will be explained in the following sections). It is also desirable to avoid using an outer layer of material through which the x-rays will have to pass. Alternatively, the particles can be mixed with epoxy and cast in a small mold. The microfines scanned for this research were mixed with marine grade epoxy and cast in plastic coffee stirrers with an inner diameter of approximately 2.5 mm. Any kind of epoxy that can support its own weight after hardening and with a density contrasting with that of the aggregate can be used. It is important, however, that the epoxy be viscous enough to suspend the particles during hardening, otherwise the particles can settle and agglomerate. Due to the size of the opening of the mold, the epoxy-aggregate mixture was sucked into the mold using a nasal syringe instead of pouring it in. Once the mixture set, the plastic peeled off the samples easily. Trials were made using glass tubes with smaller inner diameters, but demolding was difficult as the set epoxy tended to stick to the inner glass surfaces. A cylindrical core section of the specimen with a diameter smaller than that of the specimen was actually scanned in most cases, and therefore the slenderness of the sample was important mainly for minimizing the attenuation of the beam caused by the parts of the scan outside of the scan volume. In relatively few cases, the specimens were cut to an irregular cross-sectioned shape of diameter smaller than a millimeter. Different amounts (by weight percent) of microfines were mixed with epoxy and trial scans revealed two important points. The first is that it is useful to further sieve and separate the microfines to obtain clearer images with less background. When a large size range of particles is present, the smaller particles which cannot be adequately resolved (those smaller than about five to ten times the voxel size) appear as blurry particles which complicate image processing. In the scans presented, the microfines were sieved into two groups; 0-38 µm and > 38 µm (No.400 sieve). The second is that the amount of microfines in the mixture should not exceed 15% by weight. Although this value may appear to be low, higher contents caused problems with image processing and a sufficient number of particles of a certain type can be characterized with one scan at this concentration. The height of the specimen was 20 to 60 mm, however, this value can be much lower as the part of the specimen scanned was often less than 2 mm. Figure 3.7 shows three different microfine aggregate µCT specimens. The colors of the specimens are different due to the aggregate color showing through the semi-translucent epoxy matrix.

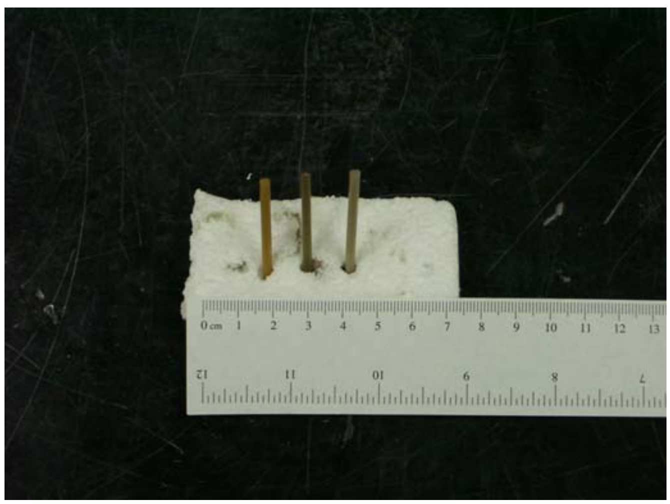

Figure 3.7 Three different microfine aggregate µCT specimens (The top scale bar shows centimeters)

It was observed that the mixing of the epoxy and the aggregate can form air bubbles which can be trapped in the specimen once the mixture has set. Such voids do not complicate the data acquisition or processing significantly (because the density of air contrasts with that of the aggregate or the matrix, and voids will appear very dark in the image); however they can reduce the efficiency of the scan. Since, the actual volume being scanned is rather small (several cubic millimeters), an air void can result in the wasting of valuable scan volume. It was found that slow mixing results in fewer bubbles, and the samples can be placed in a vacuum for 2 to 3 minutes to eliminate them, if desired. Figure 3.8 shows a close up of a μCT specimen, in which both particles (small dark spots) and air voids (larger, light in color) are apparent.

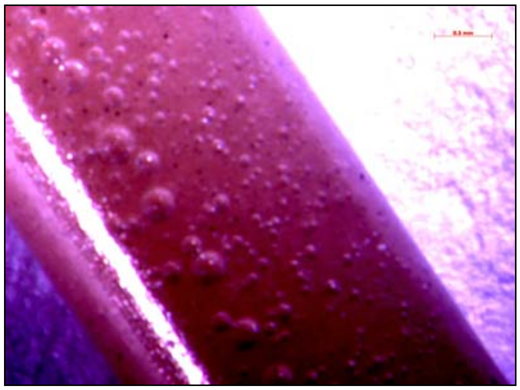

Figure 3.8 Close up of a μCT specimen (The scale bar in the top right corner shows 0.5 mm)

3.3.2 Data Collection

Initial radiography is needed to determine the specimen x-ray attenuation if the sample is of unknown composition. This is done by first determining the exposure time for the incident x-ray beam at the initial estimated energy and then collecting a Tau map of the specimen. Tau map collects the radiographic images with and without the sample in the beam and calculates the log of I/I_o. Prior to a scan, the specimen should be aligned manually on a small post on the eucentric goniometer to minimize wobble about the rotation axis. Specimens are usually adhered to the post using tacky wax, as this material does not creep and compromise specimen stability. Also, the rotation stage axis must be aligned so that it is exactly parallel to the CCD columns and perpendicular to the incident beam. An evaluation of the degree of misalignment is made through several functions in the acquisition program and corrections are made through the CT stage motors.

A scan begins by translating the specimen out of the x-ray beam and summing several I_o beam images into a calibration buffer. The specimen is moved back into the beam and images are acquired at small angular increments between 0 and 180 degrees. Since the synchrotron beam decays with time, the calibration procedure may be repeated periodically during the scan. Separate exposure times can be provided for the calibration and images. The maximum allowable exposure time for images of specimens that extend beyond the field of view of the CCD can be considerably longer than that for the unattenuated beam (during calibration) since all points in the image are attenuated by the sample. It is important to collect as many counts in a single calibration and image frame as the CCD dynamic range will allow. These counting statistics have direct impact on the signal-to-noise ratio of the reconstructed slices.

Scan times can vary considerably depending on the flux available from the synchrotron at particular x-ray energy, the image magnification, the number of view angles needed, and the signal-to-noise required in the reconstructed volume. A low magnification 256 voxel cubes, of data at 20 keV can be acquired in a few minutes, whereas a 1024 voxel cube of data may need 1 to 7 hours. The data acquisition time for the specimens tested in this study varied between 1 to 3 hours.

3.3.3 Data Reconstruction and Analysis

The projection data are stored as a series of 2-D images of x-ray opacity. The projections from a single row of pixels in the CCD must be collected together to form the sonogram (similar to in CT) data set necessary to reconstruct the corresponding 2-D slice. The final product of the reconstruction process is a single file containing a sequence of contiguous slices of the specimen (This 3-D, multiple slice file must be separated into multiple single slice files during image processing).

3.4 Processing of Images obtained from CT and μCT

Two-dimensional slices of aggregate particles are obtained from x-ray CT and μCT scans, as mentioned previously. These images need to be processed first in two-dimensions, and then in three-dimensions before they can be analyzed using spherical harmonic functions.

3.4.1 Image Processing in Two-Dimensions

A sample two-dimensional image obtained from a CT scan was given, in Figure 3.1. In the image, different shades of gray in the pixels represent different attenuation values of the material in that pixel (more accurately, the material represented by that pixel). There are a maximum of 256 (0 to 255) different shades of gray in such an image. It is seen that the background is made up of darker pixels, and the aggregate particle cross-sections are made up of lighter pixels. A transition from lighter to darker pixels can also be seen at particle boundaries. Ideally, at infinitely high resolution (infinitesimal pixel size) and excellent image quality, there should not be a transition region as the particle and the matrix differ sufficiently in density. However, due to resolution limitations, artifacts from the scan, and possibly practical effects of the behavior of the selected matrix material on aggregate surfaces (similar to the wall effect resulting in a transition zone at cement paste – aggregate interfaces), such a region, several pixels in width, occurs.

The first step in the processing of the images is separating the particles from the matrix. This is done by thresholding the image and binarizing it. The gray-scale image has a histogram of the values of gray values between 0 and 255. It is possible to use the histogram to select a cut off value for the grey scale values, below which all the pixels will be turned white, and above which all pixels will be turned black, thus binarizing the image. The process of deciding what this value should be is not trivial, as can be seen in the following figure. Figure 3.9 shows a close-up of the slice in Fig. 3.1 thresholded at different values.

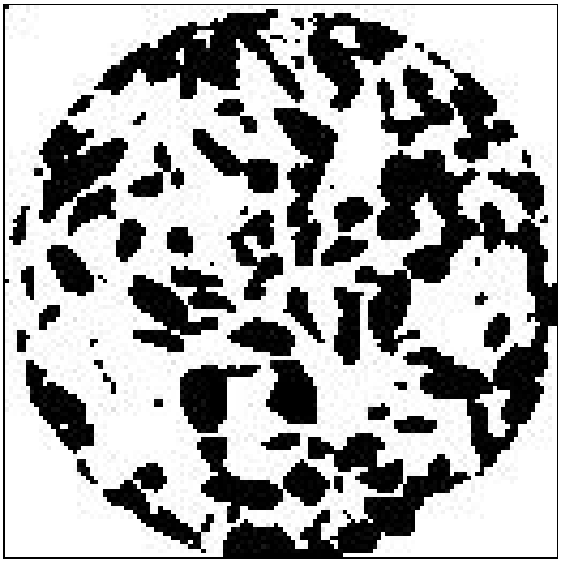

Image thresholded at gray value = 40

Image thresholded at gray value = 65

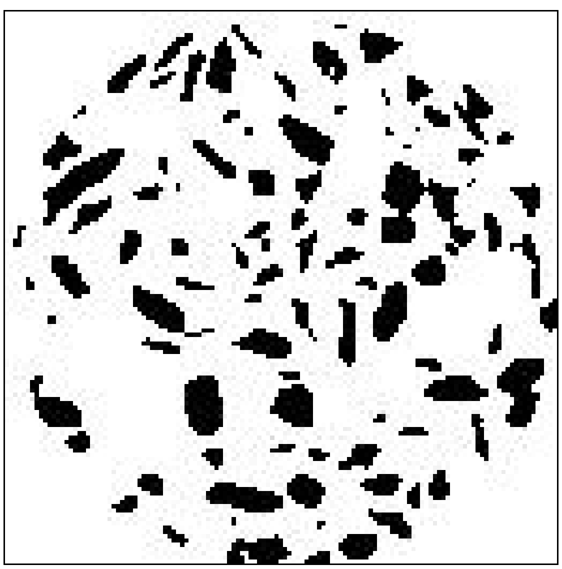

Image thresholded at gray value = 90

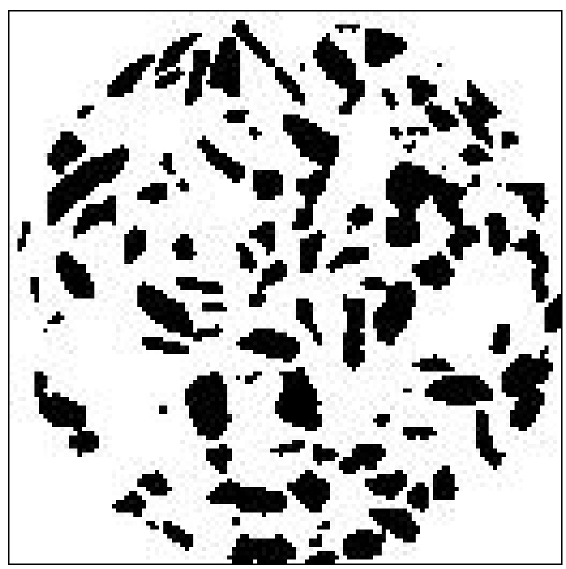

Image thresholded at gray value = 65

Figure 3.9 Images (black and white) thresholded using different grayscale values

Lower and higher threshold values are compared to a gray value (65) which is suitable value for this image. This can be checked by comparing the image thresholded at this value to the grayscale image. It is useful to compare the growth/disappearance of smaller particles in the thresholded image as the value is changed. Another useful method is to look for changes in the boundaries of larger particles. It can be seen that any calculations made using these images will yield different values. The difference from the actual values can be large if this step is done carelessly, resulting in a larger or smaller (or rougher and smoother) particle than in reality, changing values such as volume, surface area. This process is done for tens or hundreds of particles (in one slice) simultaneously which can further reduce accuracy, as the cutoff selected will be for an average of the particles, and may not be the optimal cutoff for each individual particle. It is obvious that the transition region for a smaller particle cross section will be different in size than that for a larger particle cross section. In addition, in the case of tomography scanning where there will be hundreds of 2-D images (slices) that make up the scan volume, the cutoff value determined using a single slice will generally be used to threshold all slices, for convenience, which can further introduce error.

Once all the slices have been thresholded, they are contiguously stacked (in the order they were scanned) to form a three-dimensional image or volume. It is no longer necessary to be able to see the particles within the matrix so the volume formed is a three-dimensional array of 1s (matrix) and 0s (particle). At this point, some particles can be touching each other (resulting in one large, irregular particle), and they will need to be separated before they can be analyzed with spherical harmonics. There are several methods which are used to separate touching particles which employ different algorithms. The one used in this study is an “erosion-dilation algorithm”. Although this process is performed in 3-D, it is easier to explain in two-dimensions and Figure 3.10 can be used to clarify the explanation.

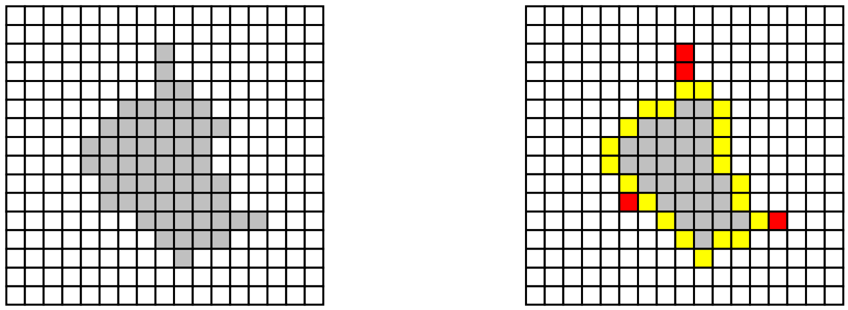

Figure 3.10 Explanation of erosion-dilation in two dimensions

Each pixel in the image corresponding to a particle (gray pixels) is asked what its neighbors are, particle or matrix. Then, depending on the rule employed, the particle under question will be turned white (matrix) or remains gray (particle). In the erosion rule in Figure 3.10, pixels for which all four neighboring pixels (side neighbors) are not gray will turn white, while those for which all four neighboring pixels are gray will remain gray. Then, in the dilation rule, the pixels for which all four neighbors are white, will remain white. Otherwise, they will turn gray. In Figure 3.10, pixels which eroded and dilated back (turned white and turned gray again) are shown yellow. The particle pixels which eroded but did not dilate (turned white and remained white) are shown red. Similar to the thresholding, particle separation through erosion-dilation is also done on all particles simultaneously. Often, one cycle of erosion-dilation does not suffice to separate all particles, and multiple cycles are needed. It is important to note that each cycle, while separating touching particles by eliminating throats between them, also irreversibly erodes fine scale surface texture and small protrusions. This causes particles to appear smoother than they actually are. Figure 3.11 shows the effect of multiple erosion-dilation cycles on a slice.

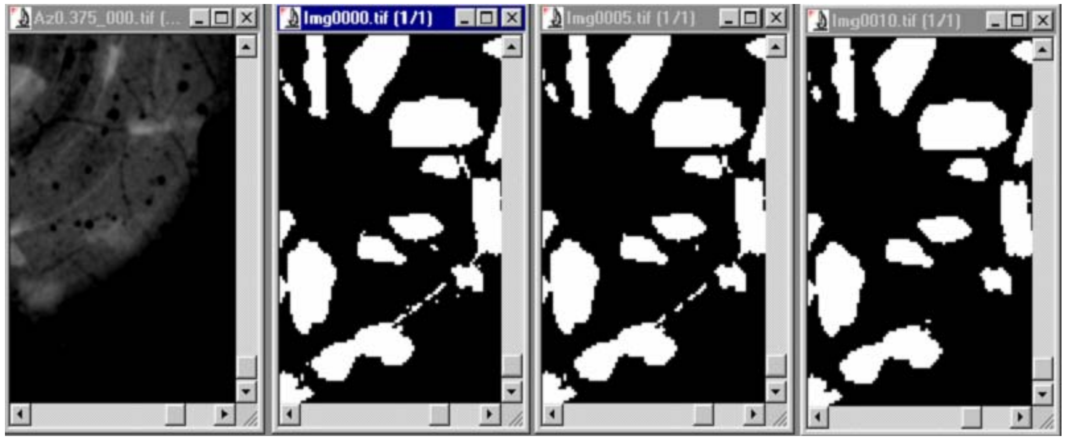

1 cycle of E/D **2 cycles of E/D** **3 cycles of E/D**

Figure 3.11 The effect of progressive erosion/dilation cycles on an image

It can be seen that impurities in the lower right corner disappear completely after three cycles of erosion-dilation, which may lead to the belief that a high number of erosion-dilation cycles should be employed. However, observation of the larger particles shows that some of the surface detail is lost and the particles are smoother which can alter the angularity and texture determined for this particle. There exist other methods such as the "watershed separation method" (Russ, 2002) which may be used in place of or in conjunction with erosion-dilation cycles.

Once the particles are separated, they can be computationally extracted from the 3-D bulk volume to be analyzed individually using spherical harmonics. The process of extraction can be done using any one of various algorithms; a "burning algorithm" in 3-D was used in this study. Figure 3.12 is used to describe this algorithm in 2-D.

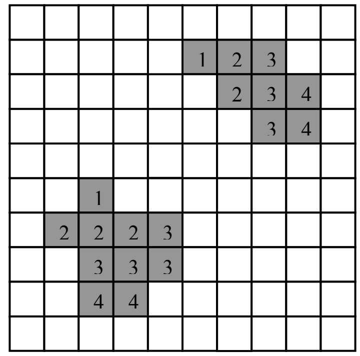

Figure 3.12 Description of the "burning algorithm" in two dimensions

In the figure above, gray pixels correspond to the particle and the white pixels correspond to the matrix. The image is scanned until a particle pixel is found (pixel 1). Then, the nearest neighbors of that pixel and any particle pixel found is labeled (pixel 2). The process is repeated and layers of pixels found in successive iterations are labeled sequentially (3, 4, and so on). The iterations continue until no more particle pixels can be found. The position of each voxel found in the 3-D image is stored with respect to a single voxel in the particle. The particles are ready to be analyzed using spherical harmonic functions.

3.5 Spherical Harmonic Analysis and its Application to Characterizing Aggregate Particles in three-dimensions

Spherical harmonic functions are the three-dimensional equivalents of the Fourier series. They can be used to completely describe the shape of a particle, by starting with a digital particle. In this case, the digital particles are aggregates extracted from a three-dimensional stack of two-dimensional slices obtained through x-ray computed tomography and microtomography, as described in earlier sections.

The process and formulas for analyzing particles in three-dimensions is given below. The process requires that the surface of the digital particle is obtained and the positions of surface voxels, relative to an arbitrary point, are stored. Often, the center of mass of the particle is used as this reference point. Line segments are drawn to surface points from the center of mass at various angles (θ_i,φ_j) where these angles are spherical polar coordinates. The lengths of these line segments, $R_{ij}(\theta_i,\varphi_j)$ are calculated from the position of the stored surface voxels, at angles corresponding to points of a double Gaussian quadrature scheme, one for each angle, where R_{ij} is the distance from the center of mass to the surface point corresponding to the direction defined by (θ_i,φ_j). Gaussian quadrature is a method for doing integrals numerically and choosing the surface points at angles corresponding to the points of a Gaussian quadrature makes the evaluation of integrals using these points straightforward. Figure 3.13 explains the spherical polar coordinate system.

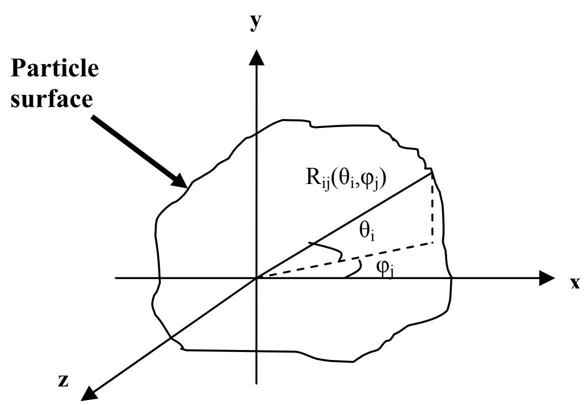

Figure 3.13 The spherical polar coordinate system used for the analysis

There is a restriction to particles that can be handled by this method. Any line segment drawn from the center of mass to a point on the surface of the particle must be contained completely within the particle. Particles with overhangs or voids do not satisfy this criterion. Figure 3.14 shows a two-dimensional representative drawing of a particle which violates the assumptions used in this method and the image which will result from the application of the technique.

Figure 3.14 A two dimensional particle with overhangs and voids and the virtual particle that will be built using it

As can be seen, a void will be interpreted as the boundary of the particle for the corresponding angles and a hole or valley will form at the radial angle corresponding to the void. Fortunately, most concrete aggregates do not have overhangs due to natural weathering or crushing. They also do not have voids larger than the minimum size which is resolved in CT and image processing can fill any voids prior to mathematical analysis.

The following is the main equation used in spherical harmonic analysis:

$$\mathrm{r}(.\ ,.\ ) = \sum_{n=0}^{8} \sum_{m=-n}^{n} a_{nm} Y_n^m(.\ ,.\ ) \tag{3.3}$$

where $\mathrm{r}(.\ ,.\ )$ is any smooth function defined on the unit sphere (0<θ<π, 0<φ<2π), and is given as $(._i, ._j, \mathrm{R}_{\mathrm{ij}})$, in this study. Y_n^m is the "spherical harmonic function" and is given by:

$$Y_n^m(.\ ,.\ ) = \sqrt{\left(\frac{(2n+1)(n-m)!}{4\pi(n+m)!}\right)} P_n^m(\cos(.\ ))e^{im\phi} \qquad .4)$$

and the functions $P_n^m(x)$ are called associated Legendre functions and are a set of orthogonal polynomials. Values of associated Legendre functions can be found in the literature (Weisstein, 2005). The computed surface points are then used to calculate the coefficients, a_{nm} which depend on both n and m, according to the following formula:

$$a_n^m = \int_0^{2\pi} \int_0^{\pi} d\phi d.\ \sin(.\ ) r(.\ ,\phi) Y_n^{m*} \tag{3.5}$$

where the asterisk denotes the complex conjugate. Choosing, a 120-point Gaussian quadrature results in the summing of this integral over 14,400 points. This can be thought of as the higher the number of points used in the Gaussian quadrature, the higher the detail obtained; however, there are limits resulting from the detail of the original digital particle. A set of coefficients can be used to completely describe the three-dimensional shape of the particle and can be used to rebuild the particle and can be thought of as a more efficient way of holding the location of each surface pixel.

The following exercise is useful in explaining the importance of being able to store particle shape information as spherical harmonic coefficients. A cube with a 20-mm side length, scanned at a resolution to yield a voxel size of 100 microns, will have greater than 236,000 surface voxels for which relative position information needs to be stored to define the particle using digital methods. The number of voxels needed for more irregular shapes can be even higher. In contrast, this particle or a more irregular one can be defined by storing 400 to 900 spherical harmonic series coefficients. In addition, it is possible to convert back to an approximate digital particle from these coefficients. The method also allows the determination of the volume, surface area, and other very useful characteristics of the particle.

The volume of a particle is given by:

$$V = \int_0^{2\pi} \int_0^{\pi} \int_0^{r(\theta,\phi)} r^2 \sin(\theta) dr d\theta d\phi \tag{3.6}$$

where the integral is over all angles and for values of r between the origin at the center of mass and the surface, r(θ,φ). The r integral can be analytically performed and the equation above becomes (in terms of r(θ,φ)):

$$V = \frac{1}{3}\int_0^{2\pi} \int_0^{\pi} r^3(\theta,\phi) \sin(\theta) d\theta d\phi \tag{3.7}$$

The calculation of surface area and some of the other characteristics such as local mean curvature or mean curvature averaged over the surface, Gaussian curvature (local and averaged over the surface), and the moment of inertia tensor are rather complicated and lengthy and can be found in (Garboczi, 2002), together with an error analysis of the method for ellipsoids. Analysis by Garboczi (2002) revealed that the accuracy of the volume and surface area of particles calculated are dependent on the digital image shape and therefore the resolution at which a particle is scanned. About 400 to 900 spherical harmonic coefficients or more (n = 20 to 30) gave good results for the actual aggregate particles presented. It is important to note that although volume can be approximated by summing voxels alone, calculation of the surface area by summing voxel surfaces will yield a result which is too high, and the value calculated using spherical harmonics is much more accurate.

CHAPTER 4 EXPERIMENTS – DETERMINATION OF AGGREGATE SHAPE USING COMPUTED TOMOGRAPHY AND COMPUTED MICROTOMOGRAPHY

4.1 Introduction

There were several reasons for scanning real coarse and fine aggregate particles using high-resolution computed x-ray tomography (CT) and microfines using x-ray microtomography (μCT) and analyzing them with the spherical harmonic method. The first was to apply these already existing methods to concrete aggregate shape determination, verify the accuracy of the algorithms used, and check for special conditions regarding this application to improve the method. The second purpose was to compare various sample preparation methods and define a method which consistently gives good results for concrete aggregates. A third was to develop an aggregate properties database which includes particles of several different typical shapes, such as round and smooth, angular and rough, elongated, flat etc. Finally, a fourth goal was to investigate the usefulness of various simple parameters defined in three-dimensions (some being the 3-D equivalents of commonly used two-dimensional parameters), and possibly define new parameters which may be useful in distinguishing particles with different shape characteristics and can perhaps be linked to their performance in concrete. The following sections give the specifics of the aggregates scanned and scanning conditions.

4.2 Experiments

The fact that CT and μCT scanners (and therefore scans) are currently expensive or not readily accessible made it impossible to scan as many aggregates as desired. Therefore, aggregates of certain types and sizes were chosen to be scanned, which could serve to fulfill the above mentioned purposes and to provide a variety of real aggregate shapes and size distributions which could be representative of similar aggregates for which extensive empirical data exist.

4.2.1 The First Group of Aggregate Scanned (Coarse and Fine)

Four different aggregate types were selected to start building a database of aggregate shape properties. These aggregates were a natural, uncrushed siliceous river gravel from Indiana, a partially crushed siliceous river gravel from Arizona, a limestone from Oklahoma, and a granite from Oklahoma. The river gravel from Arizona was received in three fractions, 1 in., 1/2-in. and 3/8-in. The fine aggregate of this type and the 3/8 in. fraction were crushed while the ½ in. and 1 in. fractions were not crushed. These aggregates had previously been used in a mixture proportioning study and had been characterized using several laboratory methods (Quiroga, 2003) and thus it was decided they would provide good starting data. In addition, these aggregate sources were intended to cover a wide range of aggregates commonly used in the U.S. in terms of particle shape and texture. The specific gravity and absorption capacity (ASTM C127), dry rodded unit weight (ASTM C29) and packing density results for these four aggregates are given in Tables A.3 to A.8. A list of the mineral compositions of the coarse and fine aggregates of the four types determined through petrographic analysis is given in Table 4.1.

Table 4.1 Mineral composition of the coarse and fine aggregates of the four types determined through petrographic analysis (Patty, 2003)

Sample	Description	Source	Rock/Mineral Identification
IN-coarse	Natural river gravel	Indiana	35% limestone, 19% shale-siltstone, 46% siliceous (quartz, chert, etc.)
IN-fine	Natural river sand	Indiana	10% limestone, 90% siliceous (quartz, chert)
AZ- coarse	Natural river gravel	Arizona	Siliceous rock types (granite, rhyolite, quartzite)

Sample	Description	Source	Rock/Mineral Identification
AZ- fine	Siliceous sand	Arizona	Siliceous rock types (granite, rhyolite, quartzite)
LS- coarse	Crushed limestone	Oklahoma	Limestone (calcite with micro fossils)
LS- fine	Crushed limestone fines	Oklahoma	Limestone (calcite with a trace of chert)
GR- coarse	Crushed granite	Oklahoma	Granite gneiss (quartz-mica)
GR- fine	Crushed granite fines	Oklahoma	Granite gneiss (quartz-mica)

A qualitative description of these aggregates, which can be used to better evaluate the data yielded by CT, is provided below:

Siliceous river gravel – Indiana: This aggregate is comprised of a variety of particles which are mostly strong and dense. Based on a sample of coarse aggregates and a sample of fine aggregates (No.8), roughly 40% are clearly rounded and smooth, 30% are clearly angular and rough, and 30% are in between. Approximately 15% of the particles are flat, and there are very few elongated particles.

Partially crushed siliceous river gravel – Arizona: Material retained on the 1/2-in. sieve is rounded and rather smooth, as it is uncrushed, and roughly 30% are clearly rounded and smooth; 40% are clearly angular and rough; and 30% are in between. The material passing the ½-in sieve is mostly angular and rough. The 3/8-in fraction contains many flat and elongated particles, and the fine aggregate fraction is composed of a mixture of flat, elongated, and rough particles.

Limestone – Oklahoma: The coarse particles are crushed and therefore mostly angular but generally not flat or elongated. The surface is smoother than that of the granite (but not as smooth as the surface of the uncrushed river gravel) and rather soft and easy to scratch. The fine fraction contains more flat and/or elongated particles.

Granite – Oklahoma: These particles are generally angular, with a rough surface. The edges of the particles are not very sharp, as this aggregate is friable. The coarse fraction has about 20% flat particles and very few elongated particles.

The particle size distribution for the coarse and fine fractions, determined by sieve analysis (ASTM C136), of these four aggregates is given in Appendix A. Figure 4.1 shows samples of the four different aggregates.

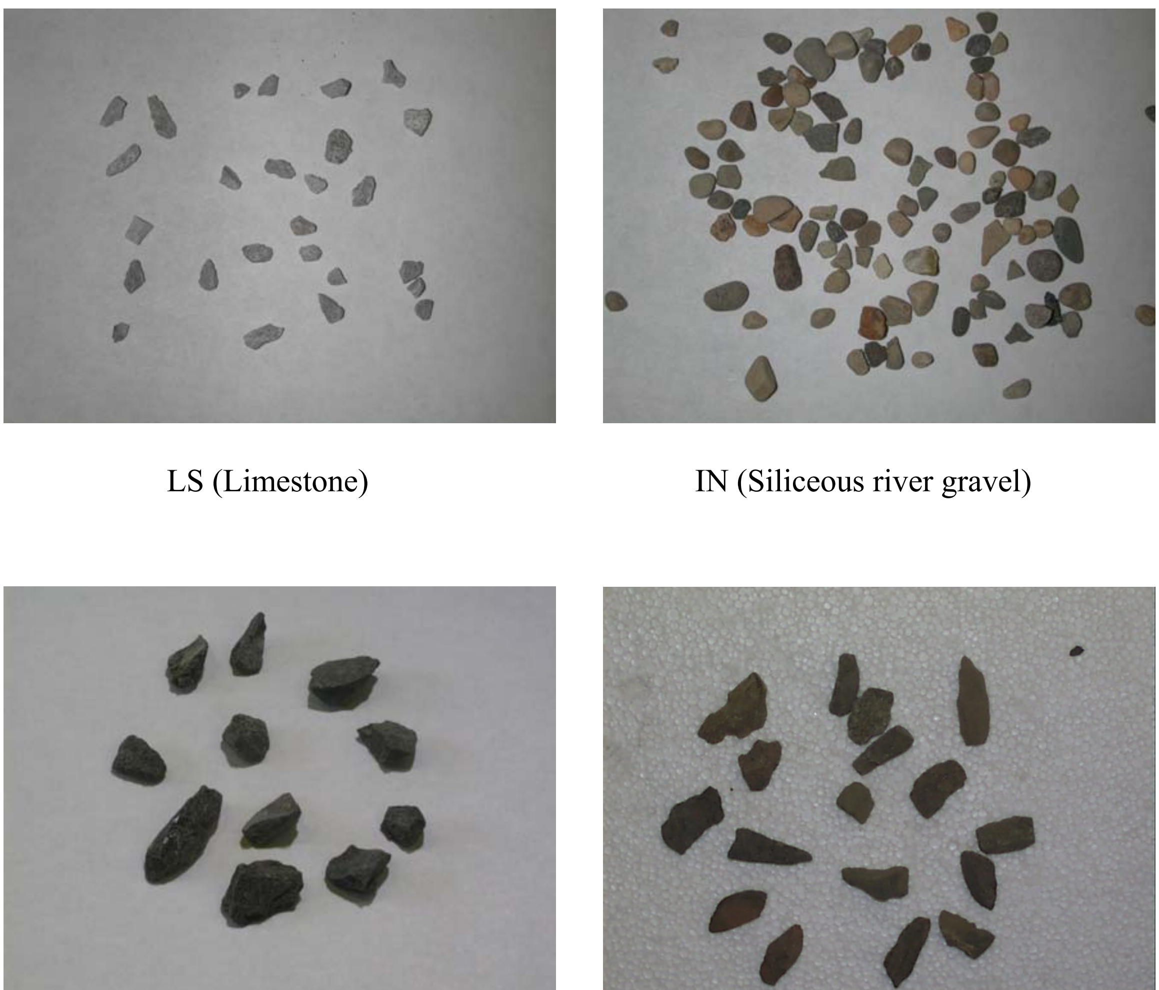

LS (Limestone) IN (Siliceous river gravel)

GR (Granite) AZ (Siliceous river gravel)

Figure 4.1 The four types of coarse aggregates scanned

4.2.2 The Second Group of Aggregates Scanned (Coarse and Microfine)

A set of twelve coarse particles chosen at random from a fully crushed granite aggregate at a commercial quarry and microfines of the same type and source were scanned using CT and μCT with the purpose of comparing the properties of the different sized particles of the same type, from the same source. The granite came from a relatively homogeneous source so the particles were expected to be more uniform than most commercial products. Six particles were selected from the 12.7 to 19 mm size range (0.5 to 0.75 in., labeled WI-0.75) and six particles were selected from the 6 to 12.7 mm size range (0.25 to 0.50 in., labeled WI-0.5). The microfine granite particles had equivalent spherical diameters (diameter of a sphere having volume identical to the volume of the particle) of 80 ∝m or less.

The principal mineral phases in this granite (by mass percent) as determined by x-ray diffraction (XRD) are given in Table 7.1. The density of each particle measured by water displacement is given in Table 7.2. A digital image for each of the twelve coarse particles is given in Figures 4.2 and 4.3.

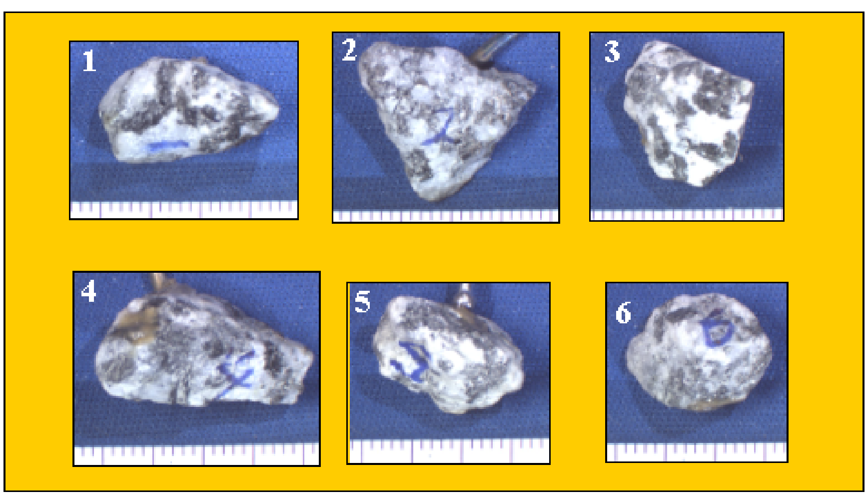

Figure 4.2 The six "WI 0.5" rocks studied from the sieve size range 6.3 mm to 12.7 mm. The lighter material is feldspar; the darker is hornblende (The smallest division in the scale bars is 1 mm).

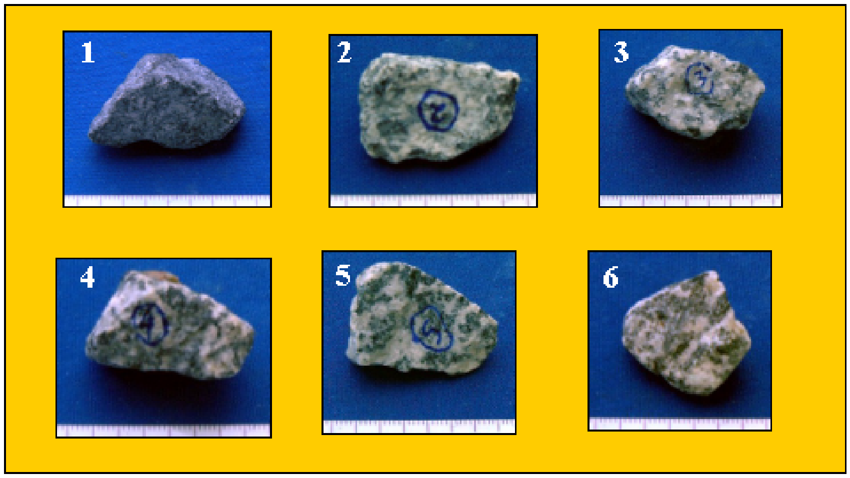

Figure 4.3 The six "WI 0.75" rocks studied from the sieve size range 12.7 mm to 19 mm. The lighter material is feldspar; the darker is hornblende (The smallest division in the scale bars is 1 mm).

4.2.3 The Microfine Aggregates Scanned

Six different types of microfine aggregates, randomly selected from a bin of microfines, were scanned using µCT. Table 4.2 lists these six aggregate types, mineralogical information, and their sources.

Table 4.2 The microfine aggregates scanned

Aggregate Label	Size Range	Information	Source
DL01a	0 – 38 µm	Dolomitic Limestone	Ontario
DL01b	38 – 75 µm	Dolomitic Limestone	Ontario
GR01a	0 – 38 µm	Granite	Georgia
GR01b	38 – 75 µm	Granite	Georgia
HG01a	0 – 38 µm	Hornblende Gabbro	North Carolina
HG01b	38 – 75 µm	Hornblende Gabbro	North Carolina
MA01a	0 – 38 µm	Marble	Maryland
MA01b	38 – 75 µm	Marble	Maryland
PF01a	0 – 38 µm	Limestone Pond Fines	Ontario
PF01b	38 – 75 µm	Limestone Pond Fines	Ontario

NS01a	0 – 38 µm	Natural Stone	Ontario
NS01b	38 – 75 µm	Natural Stone	Ontario
LS01a	0 – 38 µm	Limestone	Michigan
LS01b	38 – 75 µm	Limestone	Michigan

The NS01 microfines consisted of natural sand washings and LS01 consisted of manufactured limestone sand washings, both of which were collected in settling ponds. The remainder of the aggregates came as raw materials directly from the quarry and the microfines were sieved out of the fine aggregate fraction (ASTM C 136).

The particle size distribution for each of the microfines was determined by wet laser diffraction particle size analysis (the particles were suspended in water). This method has been shown to be the most widely used and probably the most accurate particle size analysis method (cement) by a round robin study performed by the National Institute of Standards and Technology (Ferraris et al., 2002). Table 4.3 gives results of wet laser particle size distribution analysis where d_x is the percentage of the particles having a maximum projected dimension smaller than x microns, and SSA is the specific surface area of the particles, which is a function of the size and the shape of the material.

Table 4.3 Particle size distribution statistics for the microfine aggregates scanned (Stewart, 2005)

Aggregate	**d_{10}**	**d_{50}**	**d_{90}**	**SSA (m^2/g)**
DL01	2.5	24.1	64.1	0.948
GR01	4.6	36.7	96.5	0.703
HG01	5.1	37.8	87.3	0.632
MA01	4.0	35.5	82.7	0.286
PF01	8.0	39.7	80.5	0.456
NS01	18.4	50.1	92.1	0.366
LS01	2.7	18.8	53.6	0.930

The graphical (complete) size distributions for the aggregates are given in Figure A.1 in Appendix A. The principal mineral phases in the microfines were determined qualitatively by XRD and are given in Table 4.4.

Table 4.4 Mineral phases in the microfines as determined by XRD

Aggregate	**Minerals found**
DL01	*Dolomite* – $CaMg(CO_3)_2$
GR01	Quartz – SiO_2 Albite – $NaAlSi_3O_8$
HG01	Cobalt Phosphate – $Co_2P_2O_7$ *Calcium Aluminum Silicate* – $Ca_{0.88}Xs_{0.12}Al_{1.77}Si_{2.23}O_8$ Gallium Plutonium – Ga, Pu *Ferropargasite*
MA01	*Dolomite* - $CaMg(CO_3)_2$
PF01	*Dolomite* - $CaMg(CO_3)_2$
NS01	Calcite – $CaCO_3$ Quartz - SiO_2 Manganese Bromide – $MnBr_2$ Germanium Lithium Palladium – $GeLi_2Pd$
LS01	*Calcite* - $CaCO_3$

It is unlikely that all of the compounds found are actually in the samples and the ones more likely to exist are shown italicized. The microfines of each type were further sieved using the No.400 sieve and two separate specimens were scanned for each type, to obtain better quality images, one containing 0 to 38 µm particles and one containing 38 to 75 µm particles.

CHAPTER 5 EXPERIMENTS – THE EFFECT OF AGGREGATE PARTICLE SHAPE AND SURFACE TEXTURE ON RHEOLOGICAL PROPERTIES

5.1 Introduction

Concrete aggregates can have varying shapes and degrees of surface roughness. While it is easily comprehensible that the shape of inclusions present at such high amounts (generally around 45% for coarse aggregates and 30% for fine aggregates) will influence the rheological properties (yield stress, viscosity) of the mixture, the effect of varying degrees of surface texture is not lucid. Some researchers report that particle surface texture does not have a significant effect on rheological properties (Tattersall, 1991). Other researchers have reported the opposite (Geiker et al., 2002). One problem with determining the effect of texture on flow properties is that it is difficult to empirically separate the effect of the two different scale shape properties, overall shape and surface texture on concrete flow. This is because most concrete aggregates have not only an irregular shape but also some texture. While natural aggregates tend to have more equi-dimensional and rounded shapes and manufactured aggregates tend to have more elongated and/or flat, and angular shapes, both types of aggregates may have smooth or rough surfaces.

Artificial aggregate particles of regular geometric shapes with similar texture were prepared in the laboratory in an effort to observe more quantitatively the effects of particle shape on rheological properties. Artificial coarse particles of identical shape and size but different texture were also prepared, in an effort to separate the effect of surface texture on flow properties from that of overall shape, and to provide empirical results which could be used to verify and calibrate rheological models such as the DPD model mentioned in Chapter 2. The method of preparing these artificial aggregates, other materials used and the details of the rheology tests performed are given in this chapter.

5.2 Experiments to Investigate the Effects of Overall Particle Shape on Flow (Shape Tests)

Although much research has been done recently on characterizing aggregate shape, most of this has been on the two-dimensional or partial three-dimensional characterization of aggregate shape. For this reason, it has not been possible to directly and quantitatively observe the effect of particle shape on the properties of a mix. Three-dimensional data, as yielded by X-ray CT, allow the quantitative observation of this effect and the quantitative comparison of empirical results to data from computer models. It is important that first there exist empirical data that can be compared to model data, for verification and calibration purposes. For this reason, regular shaped aggregates, like spheres, cubes and rectangular prisms were used in concrete mixtures to replicate coarse aggregate particles.

5.2.1 Materials

Two different ASTM C 150 Type I portland cements were used in all the shape tests. One was from Capitol Aggregates in San Antonio, TX (Cement 1), and the other was from Texas Industries in Hunter, TX (Cement 2). The chemical composition and physical properties of these two cements, as provided by the manufacturer, are given in Tables 5.1 and 5.2.

Table 5.1 Chemical Composition for the Type I Cements used in the Shape Tests

Chemical Analysis	Composition (%)	
	Cement 1	Cement 2
Silicon Dioxide (SiO_2), %	20.09	20.2
Aluminum Oxide (Al_2O_3), %	4.87	4.6
Iron Oxide (Fe_2O_3), %	1.87	3.1
Calcium Oxide (CaO), %	63.43	64.9
Magnesium Oxide (MgO), %	1.24	1.4
Sulfur Trioxide (SO_3), %	4.34	2.8
Sodium Oxide (Na_2O), %		0.13
Potassium Oxide (K_2O), %		0.44
Insoluble Residue	0.10	0.19
Total Alkalies (as Na_2O_{eq}), %	0.54	0.42
Limestone		3.1
$CaCO_3$ in Limestone		93
Potential Compounds		
C_3S, %	57.79	61
C_2S, %	14.02	12
C_3A, %	9.73	7
C_4AF, %	5.69	9
Ignition Loss		

Table 5.2 Physical Properties for the Type I Cements used in the Shape Tests

Physical Analysis	Cement 1	Cement 2
Fineness		
Wagner, m^2/kg	274	
Blaine, m^2/kg	552	379
Setting Time		
Initial, min (Gilmore)	105	
Final, min (Gilmore)	148	
Initial, min (Vicat)	63	155
Final, min (Vicat)	101	
Compressive Strength		
1 day, MPa	26.8	13.9
3 day, MPa	37.5	26.7
7 day, MPa	42.9	33.8
28 day, MPa	48.8	45.1
Air Content, %	7.40	5
Moisture Content, %		
False Set, % Free		
Loss on Ignition, %	2.47	2.7
Amount Retained on #325 Sieve, %	0.9	
Autoclave Soundness	0.00	0.02

Siliceous river gravel from Texas Industries in Austin, TX was used in the shape tests. The bulk specific gravity, absorption capacity and fineness modulus of this sand, as determined by ASTM C 128 and ASTM C 117 are given in Table 5.3.

Table 5.3 Physical properties for the fine aggregates used in the Shape Tests

Property	
Bulk Specific Gravity (SSD)	2.60
Absorption Capacity (%)	0.56
Fineness Modulus	2.58

The particle size distribution of the fine aggregate, as determined by ASTM C 136, is given in graphical format, in Figure 5.1.

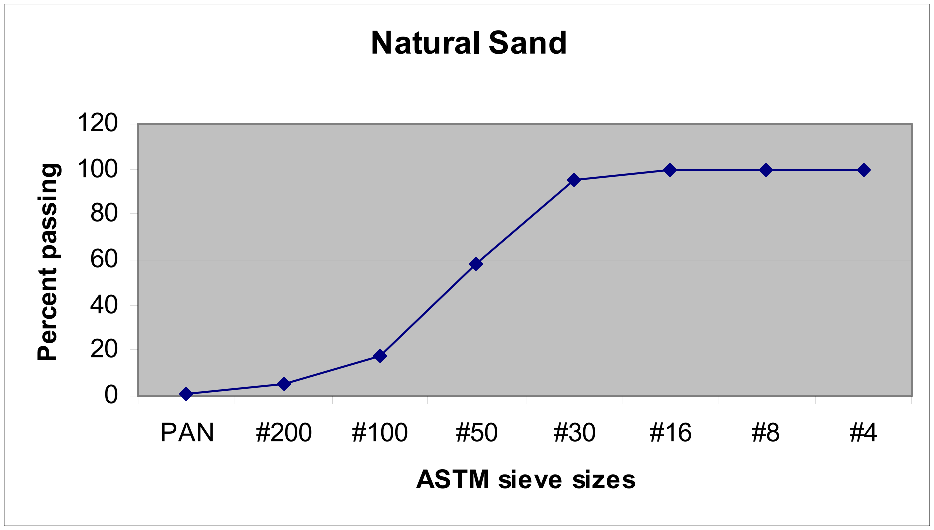

Figure 5.1 PSD of the sand used in the shape tests

Chemical admixtures were not used in any of the shape tests, and the coarse aggregates used were the artificially prepared particles (regular shapes).

5.2.2 Motivation for Choosing the Regular Shapes Used in the Study

The shape of aggregate particles are commonly defined using terms such as rounded, which describes the similarity of a particle to a sphere; angular, which describes the dissimilarity of the particle to a sphere and its faceted nature; elongated, which describes the relatively high ratio of the maximum dimension of the particle to the intermediate dimension; and flatness, the relatively high ratio of the intermediate dimension of the particle to the shortest dimension. Spheres were chosen to represent rounded particles, essentially being perfectly rounded particles. Cubes were chosen to represent angular particles, being the simplest angular shape with both an elongation and flatness of unity. Two different rectangular prisms were chosen to represent elongated, and flat particles; a 1:1:4 (height: width: length) prism, and a 1:4:4 (height: width: length) prism, respectively.

5.2.3 Preparation of Artificial Aggregates for Shape Tests

Before the artificial aggregates could be made, it was necessary to determine the volume of the particles, which would be equal for all four shapes. A few factors influenced the selection of the size of the particles. First, the size and therefore the volume of the particles were limited by the size selected for the spheres as this shape would need a readily available mold, and the other shapes could be cast in the laboratory. Second, the particles needed to be sufficiently large so as to minimize preparation time. Third, the particles had to be sufficiently small, to be able to be used in the concrete rheometer selected for this study and realistically represent actual coarse aggregate particles. Once these factors were satisfied, the fourth factor was the availability of a spherical mold that was inexpensive enough to be purchased in large quantities and discarded after one use. It was finally decided that standard table tennis balls, with a diameter of 40 mm would be used. A 5 to 10-mm-diameter hole was cut out of the plastic surface of the balls. The balls were then filled with a very fluid mortar mixture containing silica fume and a high-range water reducer. The reason for choosing to fill the balls with mortar was to give them a density and particularly buoyancy similar to that of real aggregate particles in a mortar medium. The fluid mortar made it easier to fill the balls completely so as to not create an asymmetrical weight distribution. The surface of the balls was smoothed at the fill opening, to maintain the original curvature of the surface as closely as possible. The balls were not demolded and were used with the plastic mold cover on the particle, mainly for durability purposes. Another reason was to avoid the immediate surface effects of potential air pockets inside the mold. The presence of large air pockets could negatively affect the symmetry of the balls and their behavior in translation and rotation. This was checked visually by rolling them on a flat surface and by demolding a few particles to observe the mortar surface. The balls were symmetrical and did not have noticeable cavities on the surface. Figure 5.2 shows an artificial spherical aggregate, inside the mold and demolded (Note: The surface of the demolded sphere is discolored yet smooth).

Figure 5.2 An artificial spherical aggregate in (left) and out of the mold (right)

The size of the cubes was then back calculated from the volume of the spheres to be approximately 32.2 mm per side. The mold was made out of wood in the laboratory using a table saw. It was coated with two layers of polyethylene prior to the preparation of the first set of particles and greased before every set of particles cast. A mortar mixture similar to the one used in the spherical aggregates was used. The fluid nature of the mixture allowed the top surfaces of the cubes to be reasonably smooth. Figure 5.3 shows the mold used to prepare the cube-shaped artificial aggregates and a cube, ready to be used.

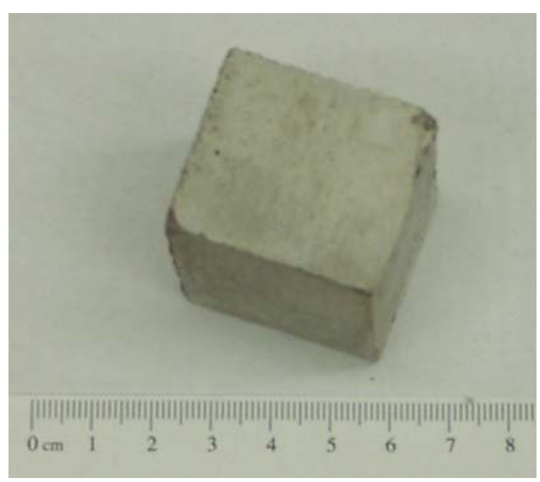

Figure 5.3 The mold used to produce the artificial cube aggregates and a cube ready to be used

The elongated and flat particles were prepared in a way similar to the cubes, with the exception that several particles were cast as a single long rectangular prism initially and then the individual particles were sawn from the longer ones. The elongated particles were approximately 20.5 mm thick, 20.5 mm wide, and 82 mm long and the flat particles were approximately 12.75 mm thick, 51 mm wide, and 51 mm long. Figure 5.4 shows an artificial elongated particle and an artificial flat particle with a sphere and a cube.

Figure 5.4 The four artificial coarse aggregate shapes

5.2.4 Special considerations for the regular shapes

The assumption while selecting and producing the four regular shapes was that the particles would have similar volumes, similar densities and similar surface texture characteristics. Due to the crudeness of the manufacturing method, the shape and volume of the particles other than the spheres could not be controlled perfectly. More particles than needed were made of the cubes, flat and elongated particles, the shape of the particles was checked visually, and particles noticeably smaller or larger than desired, those with very rough sides, or chipped edges and corners were discarded. The densities of the regular shapes were checked as well. It was discovered that there was a density difference between the spheres and the other three shapes. This difference was probably due to the lower fine aggregate content of the mixture used to make the spheres. The spheres, cubes, flat particles, and elongated particles had densities of approximately 1.85g/cm^3, 2.12 g/cm^3, 2.25 g/cm^3, 2.24 g/cm^3, respectively, measured over thirty particles. It was seen that the densities of the particles were lower than those of real aggregate particles which may have somewhat affected the flow behavior of the particles; however, in spite of this, the particles were suspended in the mortar rather than sinking or floating, as was intended. It is difficult to understand what, if any, the effect of these density differences had on the behavior of the particles. The surfaces of the cubes and the rectangular prisms were not as smooth as those of the spheres, since the smooth plastic was not removed from around the spheres and since the wooden molds roughened slightly with reuse. This difference was minimized with time however, as the surface of the spheres roughened through wear and the surface of the other shapes became smoother after a few trial runs in concrete mixtures. It is important to note that the edges of the rectangular shapes (particularly the cubes) became more rounded with time, which likely had an effect on their flow behavior. The cubes were used in trial mixtures to allow for this smoothening prior to being used in the tests presented. Figure 5.5 shows a cube which had been smoothed and had soft corners due to mixing, and a sphere for which the surface has become rougher.

Figure 5.5 The smoothened and roughened surfaces of a sphere and a cube after trial mixtures

An indirect effect of surface roughness difference could be in the water absorption of the shapes, particularly between the spheres with the impermeable coating and the other shapes with mortar surfaces. Simple, approximate absorption tests revealed that the water absorption of the spheres, cubes, flat, and elongated particles was 0.65%, 0.31%, 0.57%, and 0.44%, respectively. The higher absorption of the spheres was probably due to water entering through the filling opening (the plastic-mortar boundary) and being trapped.

5.2.5 Details of the Rheometer Used in the Experiments

The International Center of Aggregates Research (ICAR) rheometer, developed at the University of Texas at Austin, through ICAR project 105 (Koehler and Fowler, 2004) was used to measure the yield value, viscosity value, yield stress, and plastic viscosity of the mixtures made. The ICAR rheometer is a portable device for measuring concrete with workability measuring from a slump of 50 mm to self compacting concrete. Figure 5.6 shows the ICAR rheometer positioned over its container and a schematic showing its dimensions.

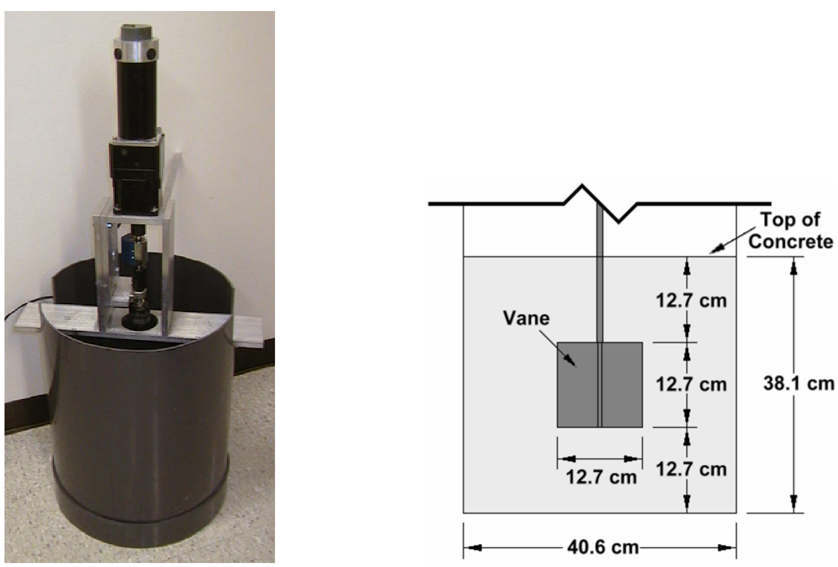

Figure 5.6 ICAR rheometer positioned over its container and the dimensions of the rheometer

The ICAR rheometer is a controlled-rate rheometer which utilizes a four-bladed vane that is immersed in the concrete and rotated at a range of fixed speeds. It is mounted in a frame and positioned over a container. Power is supplied through a standard alternating current source or an 18 V or 24 V battery. The operation of the device is automated and started through a graphical user interface on a portable computer connected to the device.

The rheometer can be used to measure a flow curve. In a flow curve test, the vane is rotated at a range of fixed speeds while the torque acting on the vane is recorded. The speeds can be arranged in decreasing or ascending order and the upper and lower bounds and the rate of change of the speed can be selected by the user. The torque vs. rotation data from a flow curve test is analyzed to determine rheological properties. A straight line is fit to the torque vs. rotation data and the slope of the line is considered to be the viscosity value (Nm.s) of the mixture, and the value of the intercept with the torque axis is taken to be the yield value (Nm) for the mixture, as explained in section 2.4. Yield stress and viscosity were determined using the Effective Annulus Method (Koehler, 2004). A five-inch impeller was used in all tests. The rheometer can also be used to test mortars, and pastes, by using a smaller vane and container.

5.2.6.1 Specific Test Settings for the Rheometer Software

All rheometer tests were of an absolute flow curve type, meaning both relative (uncorrected) parameters and absolute (corrected) parameters were calculated. Each test used a breakdown period (an initial period for the elimination of the effects of thixotropy, in which the vane turns to partially de-flocculate cement particles and realign aggregate particles, creating a repeatable, representative test state) of 15 seconds at a speed of 1.0 rev/s. Seven torque measurements were taken at equal intervals in descending order between a maximum speed of 1.0 rev/s and a minimum speed of 0.05 rev/s. Each measurement was averaged over a five-second time period.

5.2.7 Mixture Proportions for the Shape Tests

The mixture ingredients and proportions were determined with the goal of evaluating the effect of various mixture components, particularly coarse particles, on rheological properties. The following test cases were chosen:

1. Comparison of mortars with identical amounts of fine aggregates and cement but different water contents.
2. Testing of two mixtures, one made with a fixed volume (percent) of spheres, and one with a fixed volume of cubes, to check for repeatability of the results obtained from the rheometer.
3. Comparison of a fixed volume of spheres and cubes at two different water-to-cement ratios; to compare cubical shapes to spherical shapes, and the effect of suspending medium properties (changing water-to-cement ratio) on this relationship.
4. Testing of mixtures with a constant volume of coarse regular-shaped agregates (spheres, cubes, elongated prisms, and flat prisms); at a volume concentration of 35%.
5. Testing of mixtures with varying combinations of spheres and cubes.

Table 5.4 summarizes the mixture proportions used for case 1.

Table 5.4 Mixture Proportions for the Mortars with Increasing Water Content

Water (lbs)	Cement (lbs)	Fine Aggregate Type, Amount (lbs)	Coarse Aggregate Type, Amount (lbs)
27	99	Siliceous, 150	0
29	99	Siliceous, 150	0
32	99	Siliceous, 150	0
35	99	Siliceous, 150	0
38	99	Siliceous, 150	0
41	99	Siliceous, 150	0

Table 5.5 summarizes the mixture proportions used for cases 2 and 3.

Table 5.5 Mixture Proportions for Tests to Check Repeatability for Different Shape Cases and Compare Spherical and Cubical Aggregates at fixed amounts

Water (lbs)	Cement (lbs)	Fine Aggregate Type, Amount (lbs)	Coarse Aggregate Amount (by volume of container), Type
27	66	Siliceous, 100	35%, spheres
30	66	Siliceous, 100	35%, spheres
27	66	Siliceous, 100	35%, cubes
30	66	Siliceous, 100	35%, cubes

Tables 5.6-5.7 summarize the mixture proportions used for case 4 and 5.

Table 5.6 Mixture Proportions for Concretes with an Increasing Amount of Different Shaped Coarse Aggregates

Water (lbs)	Cement (lbs)	Fine Aggregate Type, Amount (lbs)	Coarse Aggregate Amount (by volume of container), Type
35	99	Siliceous, 150	0, 15, 25, 35, 45%, spheres
35	99	Siliceous, 150	0, 15, 25, 35, 45%, cubes
35	99	Siliceous, 150	0, 15, 25, 35, 45%, elongated prisms
35	99	Siliceous, 150	0, 15, 25, 35, 45%, flat prisms

Table 5.7 Mixture Proportions for Concretes Made Using a Combination of Spheres and Cubes

Water (lbs)	Cement (lbs)	Fine Aggregate Type, Amount (lbs)	Coarse Aggregate Amount (by volume of container), Type
38	99	Siliceous, 150	35%, spheres
38	99	Siliceous, 150	23 % spheres, 12 % cubes
38	99	Siliceous, 150	12 % spheres, 23 % cubes
38	99	Siliceous, 150	35%, cubes

In addition to these tests, ASTM C 143 slump tests were performed to investigate the effect of varying the amount of one component of the mixture while keeping the content of all other components constant. Three groups of tests were performed:

1. The effect of fine aggregate content on slump: The sand content of a mortar mixture was increased as the water and cement contents are kept constant.

2. The effect of coarse aggregate content and shape on slump: The coarse sphere or cube content of a mixture was increased as the sand, water and cement contents were kept constant.
3. The effect of water content (water-to-cement ratio) on slump: The water content of a mixture containing 35% coarse spheres or cubes was increased as the sand and cement contents were kept constant.

Tables 5.8-5.10 summarize the mixture proportions used for cases 6-8.

Table 5.8 Mixture Proportions for the Slump Test Mortars with Increasing Sand Content

Water (lbs)	**Cement (lbs)**	**Fine Aggregate Type, Amount (lbs)**	**Coarse Aggregate Type, Amount (lbs)**
23.5	60	Siliceous, 12-220	0

Table 5.9 Mixture Proportions for the Slump Test Mortars with Increasing Artificial Coarse Particle Content

Water (lbs)	**Cement (lbs)**	**Fine Aggregate Type, Amount (lbs)**	**Coarse Aggregate Type, Amount (%)**
12	36	Siliceous, 80	Spheres, 0,15,25,35,40
12	36	Siliceous, 80	Cubes, 0,15,25,35,40

Table 5.10 Mixture Proportions for the Slump Test Mortars with Increasing Water Content

Water (lbs)	**Cement (lbs)**	**Fine Aggregate Type, Amount (lbs)**	**Coarse Aggregate Type, Amount (%)**
8-12	30	Siliceous, 80	Spheres, 34
8-14	30	Siliceous, 80	Cubes, 34

5.2.8 Mixing Procedure for the Shape Tests

The concrete mixtures were prepared in general accordance with ASTM C 192. Batching, mixing, and testing were done at room temperature. All materials were stored in sealed containers at room temperature for at least 24 hours prior to the start of mixing. The fine aggregate was batched in moist condition, the moisture content was determined and the batch quantities were adjusted accordingly. The concrete was mixed in a rotating drum mixer. The starting batch size for all the rheometer shape tests was slightly greater than 0.05 m^3, the volume of the container used. In some of the mixtures, a mortar mixture was prepared and coarse particles were gradually added. In some, the starting mixture already had a fixed percentage of coarse particles. The fine aggregates were placed in the mixer, followed by the cement and a portion of the mixing water, and the mixer was started to blend the two components. The remaining mixing water was then added, and the mortar was mixed for 3 minutes, allowed to rest 3 minutes, and mixed for another 2 minutes. The mortar was immediately discharged into the rheometer container and tested. This test provided the result against which the results of tests using artificial coarse particles would be normalized. In the initial shape tests, the coarse particles were added directly to the container, at the prescribed volume increments. This was done by removing part of the mortar from the container with a shovel, adding the coarse particles and adding back enough mortar to fill the volume of the container. The mixture was then mixed inside the container using a shovel. The process was repeated for all the different coarse particle volumes being tested. After a few trials, it was decided that this process might not provide adequate dispersion of the relatively large artificial particles. Instead, it was decided that the mixture in the container would be put back into the mixer, the coarse particles added, and the mixture poured into the container and tested. The mixing time between each coarse particle addition was about two minutes. The increase in the total volume of the mixture (by the volume of the added coarse particles) was taken into account when determining the amount to be added to achieve the desired percent volume of coarse particles. This process increased the amount of time until the last test which could increase the viscosity of the paste due to hydration reactions. The time between the first and the last test was on the order of twenty minutes, and any stiffening in the paste due to hydration was ignored. The mixture was tested several times at each coarse concentration. The first two measurements were made following the filling of the container, then the mixture was remixed with a shovel to redistribute the coarse particles and the remaining measurements were made.

5.3 Experiments to Investigate the Effects of Particle Surface Texture on Flow (Texture Tests)

It is possible, using one technique, or a combination of several imaging techniques, to obtain the near exact three-dimensional shape of real aggregate particles. This makes it possible for models to use real irregularly shaped particles in predicting rheological and other properties of a mixture. However, the determination of fine-scale texture on the surface of particles is quite cumbersome. It is therefore important to know to what degree fine surface features affect flow. In addition, it is important to have empirical data to validate and calibrate computer models, as mentioned previously. For this purpose, glass toy marbles and small glass beads were used to serve as smooth, perfect spheres and some marbles and beads were modified to serve as rough/textured spheres, to test the effect of surface roughness of coarse particles (independently from the effect of overall shape) on viscosity and yield stress.

5.3.1 Materials

The same cements and fine aggregate used in the shape tests were used in the texture tests. Glass marbles and glass beads were used as the coarse aggregate and the fine aggregate in the concrete tests and mortar tests, respectively.

5.3.1.1 Motivation for Using Glass Spheres in the Study

Particles having a very smooth surface and particles having a relatively rough surface were needed to represent two extremes of surface roughness. The main restrictions were that the overall shape (size, volume) of the particles needed to be comparable to that of coarse aggregate particles, the density of the particles needed to be comparable to that of the paste or mortar medium to prevent settling or floating, and the particles needed to be readily available in large quantities, or be possible to produce easily and economically. It was decided that glass spheres would be suitable since they would inherently have a very smooth surface, near perfect spherical shape and consistent size. It would then be possible to coat the marbles to create rough particles while maintaining the spherical shape. Sixteen-mm glass marbles and 1-mm glass beads were selected for the concrete and mortar tests, respectively.

5.3.1.2 Preparation of Rough/Textured Particles

The most important criteria for selecting the method and materials for coating the marbles were cost and speed (since several thousand particles would need to be coated), uniformity of the thickness of the coating and the degree of roughness provided, minimizing the increase in particle volume due to the coating, and strength of the bond between the glass surface and the coating.

After trials with different sized materials, fine granite aggregate passing the No.50 sieve and retained on the No.100 sieve, was chosen as the most economical option for coating the marbles. Trials with different types of glues showed that the coating could be peeled off by hand or with a metal blade and it was decided a rather low-viscosity epoxy would work better, to develop a strong bond while keeping the volume change low. Trials showed that various types of polyurethane worked well but were cost prohibitive. A two-part, marine epoxy was strong enough but its viscosity resulted in thick coatings when the particles were immersed in a pool of epoxy, taken out and the coating layer was applied. Trials showed that a very low marine epoxy content (~10 ml per 100 particles) sufficed to coat the surface of a high number of marbles. A little epoxy in the bottom of a container could be used to coat the marbles in the container by stirring them around so that the surfaces would occasionally touch the bottom surface and each other repeatedly. A visual inspection of the surfaces of the marbles was used to determine that the particle surfaces were coated with the epoxy, a shiny surface indicating a coated surface. The particles were moved between containers to allow them to separate and for any excess epoxy to run off. Once the marbles surfaces were coated, they were thrown into a large container full of the coating sand. An effort was made to separate the marbles as they fell into the sand and the container was shaken to separate any touching particles and get a layer of sand around each particle. It is important to note that any individual handling of the particles before the epoxy set led to peeling of the layer of sand from the surface. It was important to use a large pool of sand to keep the marbles from touching while the epoxy set to prevent two or three particles from sticking to each other. Figures 5.7 and 5.8 show uncoated and coated marbles and a close up of the partially peeled coating of roughness on a particle, under a stereo microscope.

Figure 5.7 Uncoated and coated (smooth and rough) marble

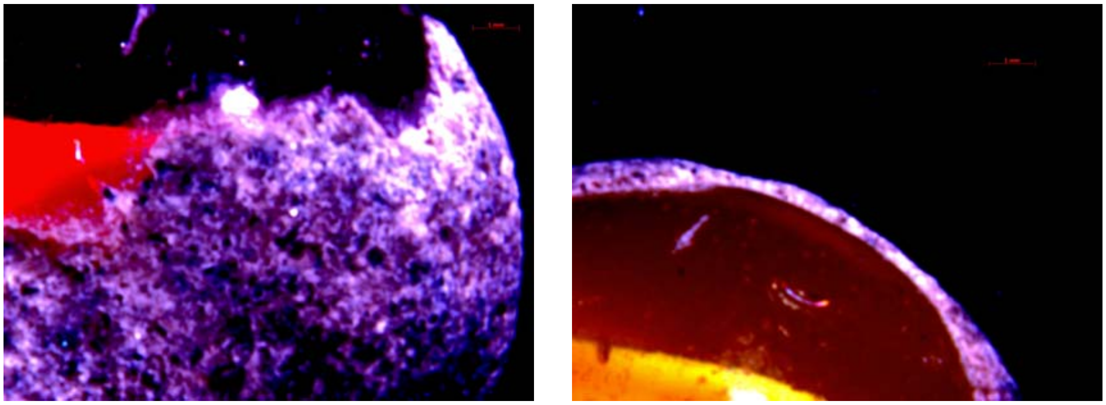

Figure 5.8 The coating of fine aggregate on a partially coated glass marble (Scale bar [top right] designates 1 mm)

The average diameter of the smooth, uncoated marbles was 16 mm. The thickness of the rough layer of fine aggregate and epoxy, though variable, was approximately 0.3 mm (~1/50 of the diameter) thus a representative diameter for the coated particles was 16.6 mm, indicating a volume increase of about 12% due to the coating. The specific gravity was determined to be ~2.42 for both the glass marbles and for the rough marbles.

The coating of the glass beads was more difficult due to their small size. To provide the particles with texture without altering their coarse scale shape, a very fine layer of coating (approximately 20 µm, for a coating ~1/50) needed to be applied. This would not have been possible using microfine aggregates due to the difficulty of separating different size microfine particles. In addition, it would not be possible to control the number of coating particles which would stick to the binder on the particle surface and therefore the material would have to be very fine. Silica fume, having an average particle size of about 0.1 µm, was chosen as the coating material. One potential problem with silica fume is that particles can agglomerate and these agglomerates can be several tens of micrometers to several hundred of micrometers in size (Juenger and Ostertag, 2004). In order to partially alleviate this problem, the silica fume was sieved using a #400 sieve to assure that the largest possible agglomerate was about 38 µm.

Another concern was the thickness of the coating material, due to its inherent viscosity. Several attempts with liquid epoxies showed that a very low viscosity epoxy was needed and most such epoxies were found to be messy and have a narrow window of workability before they set. A moisture resistant appliance epoxy in spray form was used as the binder. The coated beads were poured into a container full of silica fume, similar to the marbles and the fine aggregate, and the container was shaken to assure a full coating on all particles. Once the epoxy set, the particles were dry sieved out of the silica fume and wet sieved to remove any silica fume not in contact with the surface of the glass beads. The beads were ground during wet sieving to break apart any large agglomerates. Since all these operations were uncontrolled, the thickness and uniformity of the coating was checked under different lighting conditions and under a microscope.

5.3.4 Specifics of the Rheometer and Test Settings for the Rheometer Software

The same rheometer used for the shape tests was used for the marble texture tests. The only difference was that the container dimensions were 400 mm (height) by 270 mm (outer diameter), 140 mm (inner diameter: outer diameter minus width of vane). All rheometer tests were of an absolute flow curve type and used a breakdown period of 15 seconds at a speed of 1.0 rev/s. Seven torque measurements were taken at equal intervals in descending order between a maximum speed of 1.0 rev/s and a minimum speed of 0.05 rev/s. Each measurement was averaged over a five-second time period.

A paste/mortar rheometer of the parallel plate type with 60-mm-diameter plates was used in glass beads tests. The gap between the plates was set at 10 mm, with a space of 8 mm between the top wheel and the confinement ring. The shear rate was varied from 10 rev/s to 1 rev/s. A close up of the rheometer, the top plate, the bottom plate and confinement ring and a schematic showing the dimensions are given in Figure 5.9.

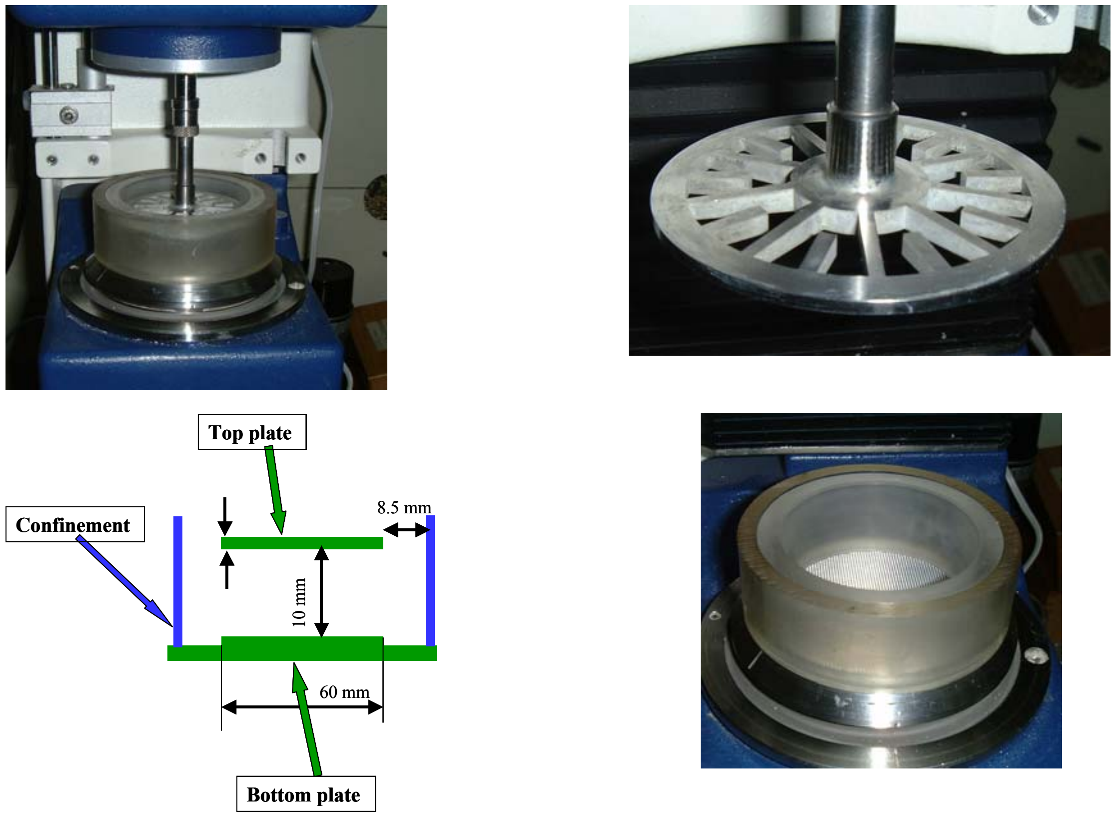

Figure 5.9 The parallel plate mortar rheometer (clockwise from top left: overall view, top plate, bottom plate and confinement ring, schematic showing dimensions)

5.3.5 Mixture proportions for Texture Tests

The mixture proportions were chosen to represent concrete mixtures having paste components with different degrees of fluidity, to determine the effect of coarse particle texture on rheological properties. The following cases were chosen:

1. Testing of mortar mixtures with an increasing volume (percent) of smooth and rough marbles, at two different water contents to evaluate the effect of particle surface texture on flow properties and the influence of changing suspending medium properties on this effect.

2. Testing of mortar mixtures made using fixed amounts of smooth glass beads and coated/rough glass beads.

Tables 5.11-5.12 summarize the mixture proportions used for cases 1 and 2.

Table 5.12 Proportions for Mixtures with Increasing Amounts of Smooth and Rough Marbles

Water (lbs)	Cement (lbs)	Fine Aggregate Type, Amount (lbs)	Coarse Aggregate Type, Amount (lbs)
19	50	Siliceous, 75	0, 10, 20, 30, 40%, smooth marbles
19	50	Siliceous, 75	0, 10, 20, 30, 40%, rough marbles
21	50	Siliceous, 75	0, 10, 20, 30, 40%, smooth marbles
21	50	Siliceous, 75	0, 10, 20, 30, 40%, rough marbles

Table 5.13 Proportions for the Mortars Made Using the Glass Beads

Water (gr)	Cement (gr)	Fine Aggregate Amount (by volume), Type
80	200	0
80	200	40%, uncoated / smooth glass beads
80	200	40%, coated / rough glass beads

5.3.6 Mixing Procedure for the Texture Tests

The marble mixtures were prepared and tested in the same way as the shape mixtures. Only the second remixing method was used in that the mixture was reloaded into the drum mixer between each coarse particle addition. The starting batch size for all the marble tests was approximately 0.02 m^3, slightly greater than the container size. The excess concrete in the drum mixer was discarded between the starting mortar mixture and the first mixture after the addition of marbles. The mixture was tested several times at each coarse concentration, similar to the procedure followed for the shape tests.

A temperature controlled mixer was used to prepare the mortars for the glass beads tests. The cement was gradually added to water over a 30 second period, while mixing at 4050 rpm. Then the mixer speed was increased to 10040 rpm and the paste was mixed for 30 seconds. The mixer was stopped and the paste left to rest for 2.5 minutes, during which the sides of the mixer were scraped down. Then, the mixture was mixed for another 30 seconds. The glass beads were then added at the desired content and the mixture was mixed in a blender. The water bath used to cool the paste during mixing was maintained at 15°C. Immediately after mixing, approximately 25 ml of the mortar was transferred to the rheometer, the plates adjusted to the correct gap size and measurement was started.

CHAPTER 6 RESULTS OF X-RAY TOMOGRAPHY AND MICROTOMOGRAPHY TESTS AND PRACTICAL APPLICATIONS

6.1 Introduction

Fine and coarse particles of various aggregate types from different sources were scanned using x-ray computed tomography and microfine particles were scanned using x-ray microtomography. Virtual particles were built using spherical harmonic (SH) functions, and several physical properties were calculated for each particle. The results have been analyzed in different ways for different size aggregate particles, and possible practical uses of CT and ∝CT results are presented.

6.2 Results of CT Scans

The scans and the mathematical analysis yielded complete shape information for the particles, as exact as allowed by the resolution of the imaging and the image analysis. Shape information is contained in a set of spherical harmonic coefficients. A sample set of coefficients for a single particle of the coarse granite scanned is shown in Table 6.1 (Only the coefficients up to n=5 have been shown to conserve space).

Table 6.1 Spherical harmonic coefficients up to n=5 for a coarse granite particle scanned

n	m	real	imaginary
0	0	22.9108039519	0.0000000000
1	1	-0.2016049973	-0.0333386190
1	0	0.6821231681	0.0000000000
1	-1	0.2016049973	-0.0333386190
2	2	-1.0313287020	-1.0804772783
2	1	2.0373026721	0.8248485438
2	0	-2.0696234570	0.0000000000
2	-1	-2.0373026721	0.8248485438
2	-2	-1.0313287020	1.0804772783
3	3	0.7640549327	-1.0253308159
3	2	0.4208081662	-0.6329251135
3	1	-1.1257224635	0.1895220335
3	0	1.4372324846	0.0000000000

3	-1	1.1257224635	0.1895220335
3	-2	0.4208081662	0.6329251135
3	-3	-0.7640549327	-1.0253308159
4	4	-0.1262188304	0.3950664394
4	3	0.0813536436	-0.6279486665
4	2	0.3230752294	0.1750956715
4	1	-0.6313965179	0.2324241917
4	0	0.4559912801	0.0000000000
4	-1	0.6313965179	0.2324241917
4	-2	0.3230752294	-0.1750956715
4	-3	-0.0813536436	-0.6279486665
4	-4	-0.1262188304	-0.3950664394
5	5	-0.3014390860	0.0173631542
5	4	0.2830661396	-0.2414075280
5	3	0.1552804259	0.0204312148
5	2	-0.6907973538	0.0405396611
5	1	0.4547879281	0.3121394022
5	0	0.0410942698	0.0000000000
5	-1	-0.4547879281	0.3121394022
5	-2	-0.6907973538	-0.0405396611
5	-3	-0.1552804259	0.0204312148
5	-4	0.2830661396	0.2414075280
5	-5	0.3014390860	0.0173631542

Columns 1, 2 and 3, 4 show the n and m values used in equations 3.3 to 3.5, and the real and imaginary parts of the coefficient, respectively. The spherical harmonic functions to which these coefficients apply are available in the literature. Certain patterns are immediately apparent from the table. The real part of a coefficient is equal in absolute value but has opposite signs for (n,m) and (n,-m) for odd values of m, and the same sign for even values of m. Differently, the imaginary part of a coefficient is equal in absolute value but has opposite signs for (n,m) and (n,-m) for even values of m, and the same sign for odd values of m. The real and imaginary parts of the coefficients for (n, m) and (n,-m), have equal sign and value for odd values of m and even values of m, respectively. The functions corresponding to each n value define a shape which is approximated to the particle being analyzed by the coefficient. The first, corresponding to n=0 is the radius of a topologically equivalent sphere, though not of equal volume as the particle, and gives a general idea about the size of the particle (a topologically equivalent sphere is one which could be made by deforming the particle in the hypothetical case that it were made of a pliant material). The second, corresponding to n=1, yields information about the elongation of a particle. The physical meaning of the other coefficients cannot be easily understood. A perfectly spherical particle would have a non-zero a_{00} coefficient only, with all other coefficients being equal to zero. The first few coefficients influence the overall shape of the particle more significantly than the higher order ones and probably the higher order coefficients influence texture more than the lower order ones, though this is not very clear. Figure 6.1 shows the coarse granite particle for which a part of the spherical harmonic coefficients of which are shown in Table 6.1, built in three-dimensions using the Virtual Reality Modeling Language (VRML).

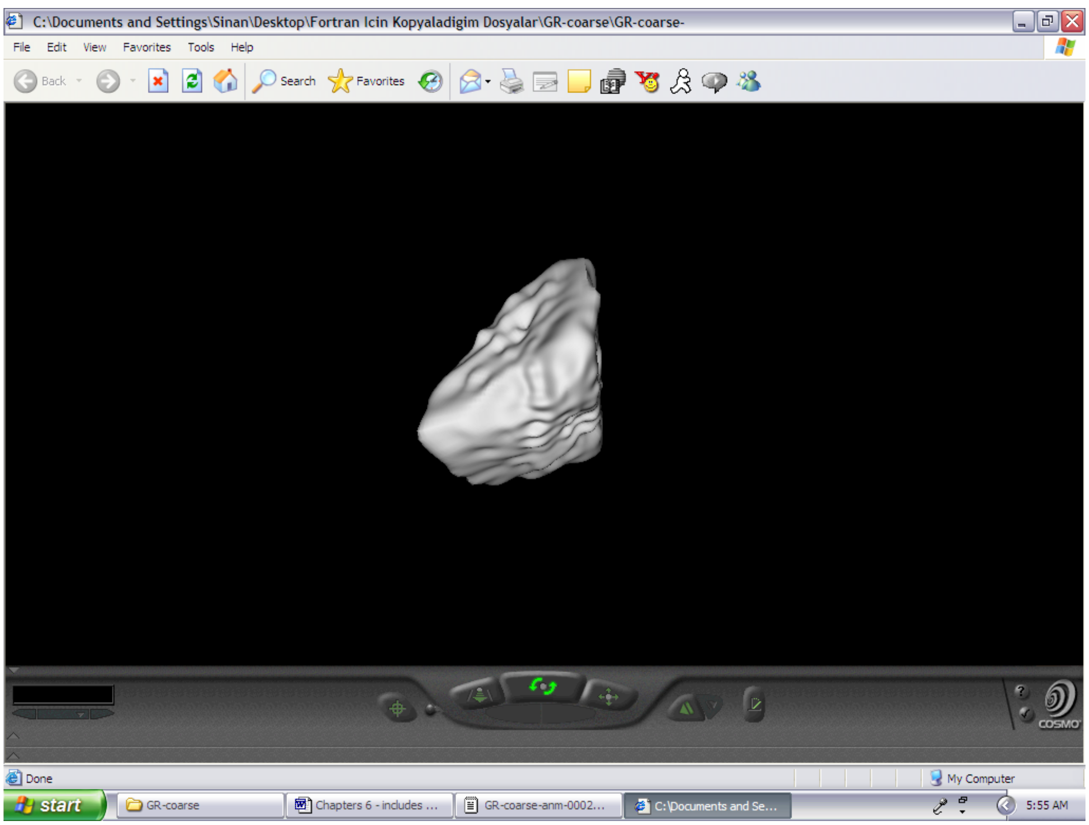

Figure 6.1 A virtual coarse granite particle built using spherical harmonic coefficients and VRML

All spherical harmonic coefficients (up to n=30) for the granite particle shown in Figure 6.1 are given in Table B.19. Having the spherical harmonic coefficients for a particle allows the calculation of values such as volume, surface area, ratio of the surface area to that of an equivalent sphere, diameter of an equivalent sphere, trace of the moment of inertia tensor for the particle, the principal dimensions of the particle, elongation and flatness ratios, etc. The moment of inertia tensor, simply put, indicates how difficult it is to rotate an object. These values are given in Appendix B for particles of the fine aggregates, coarse aggregates, and microfine aggregates scanned. The results of certain interesting applications of the results are presented in the following sections.

6.2.1 Commonly Used Shape Parameters Calculated in 3-Dimensions

Parameters were introduced in Chapter 2, some applicable to two-dimensional data, and some to 3-D data, which could be useful in interpreting shape properties of aggregate particles. Two such parameters elongation and flatness, describe the overall shape of particles. Figures 6.2 and 6.3 give the individual and average elongation and flatness values for particles of the four different coarse aggregate types scanned.

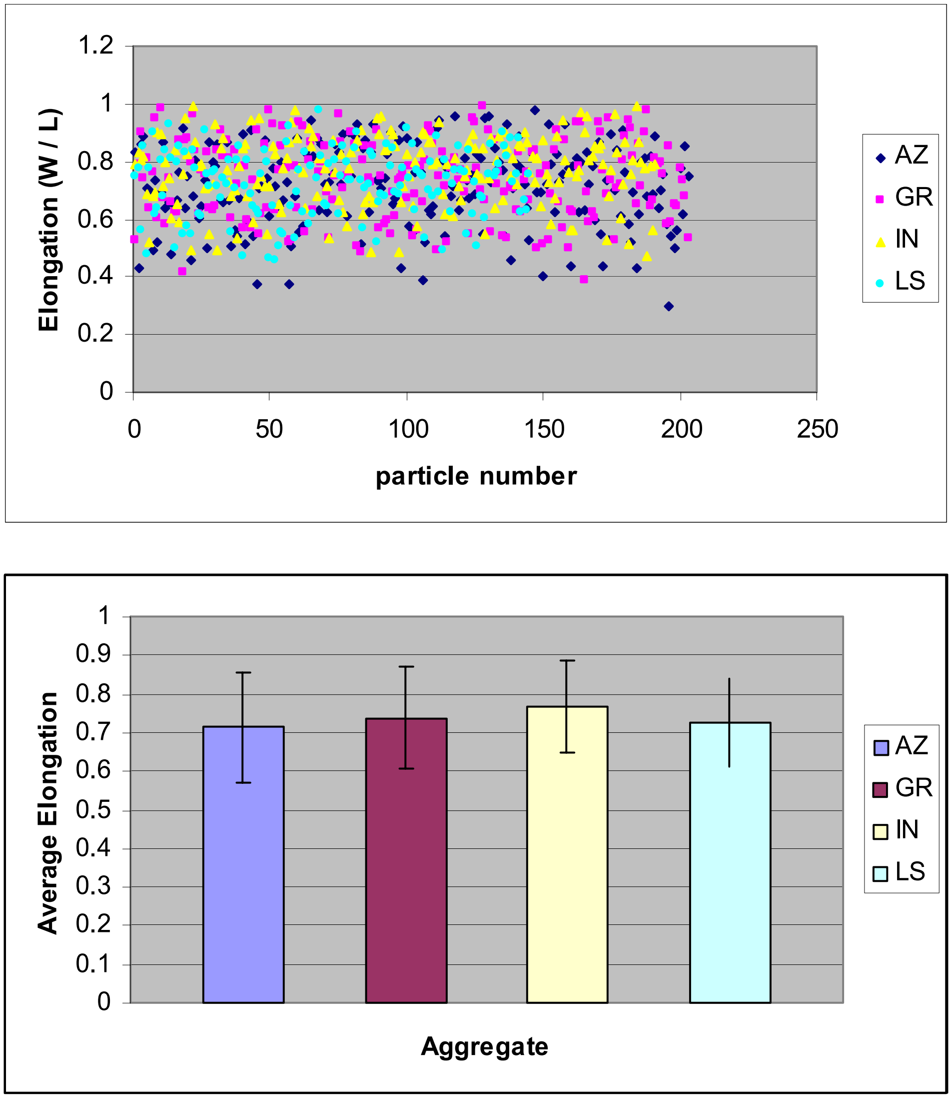

Figure 6.2 Individual and averaged elongation values for the particles of the four different coarse aggregates scanned

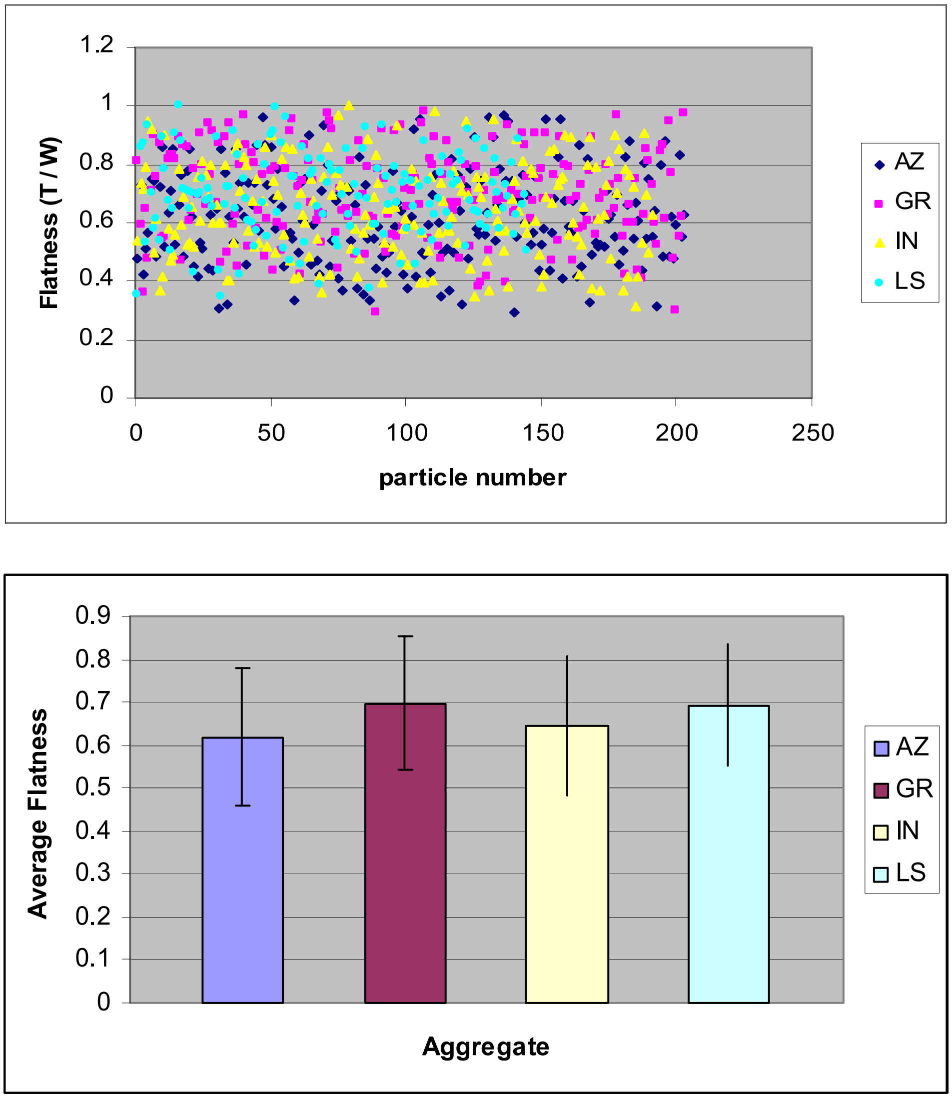

Figure 6.3 Individual and average flatness values for the particles of the four different coarse aggregates scanned

The elongation and flatness values lie mostly between 0.5 and 1.0, indicating that the particles scanned, for all four types, are generally equi-dimensional and well-shaped. The AZ partially crushed siliceous gravel appears to contain the most elongated and flattest particles. However, as the error bars (displaying one standard deviation) on the average results graphs indicate, the overall shapes of the four different coarse aggregates are similar.

The surface area-to-volume ratio of a particle, sometimes called specific surface area, is another parameter which can be useful in evaluating shape. It is dependent on size and the specific surface area (SSA) of regular shapes such as a sphere or a cube decreases at a constant rate (but different for different shapes) with increasing size. Multiplication of the SSA value by the radius of a sphere of equivalent volume (ESR), however, eliminates this size dependence. The SSA*ESR value will be 3.0 for a sphere and higher for any other shape. Figures 6.4 and 6.5 show the SSA value and the SSA multiplied by the ESR, for each individual particle of the four coarse aggregates scanned and the average values.

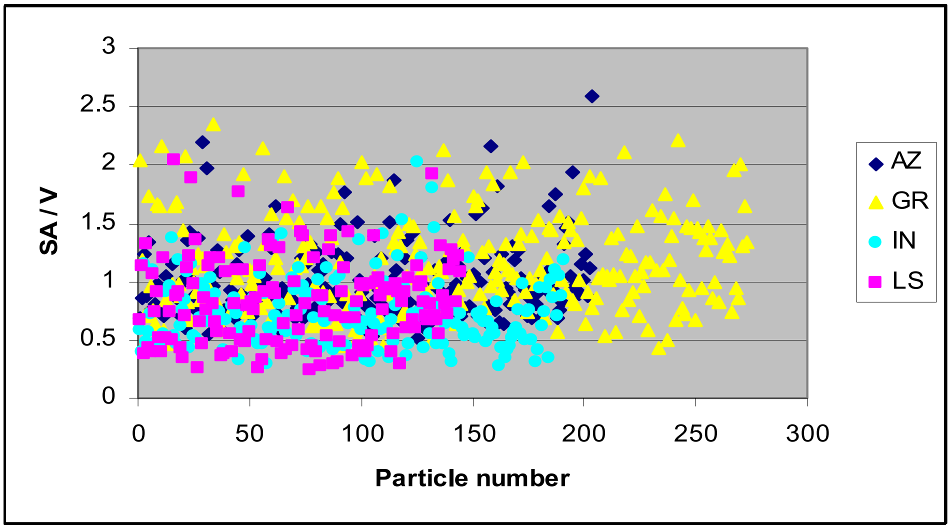

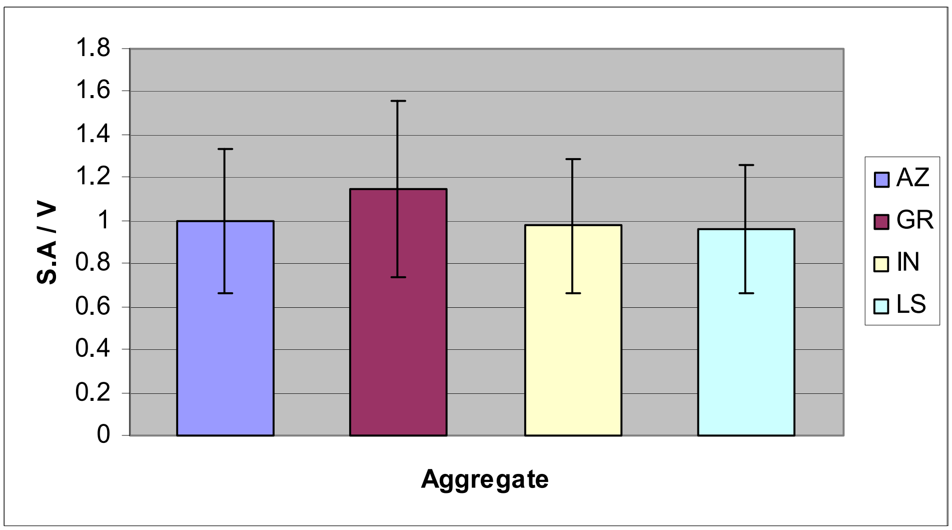

Figure 6.4 Individual and average specific surface area values for the particles of the four different coarse aggregates scanned

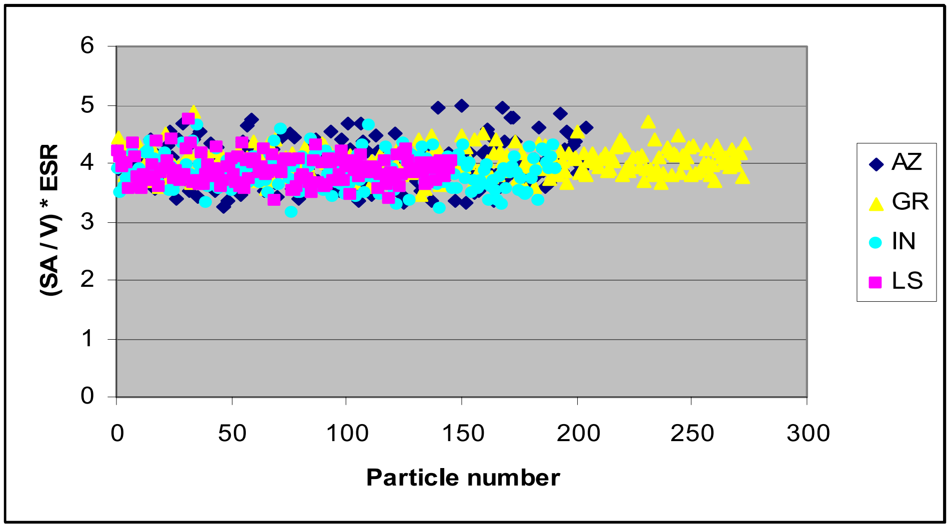

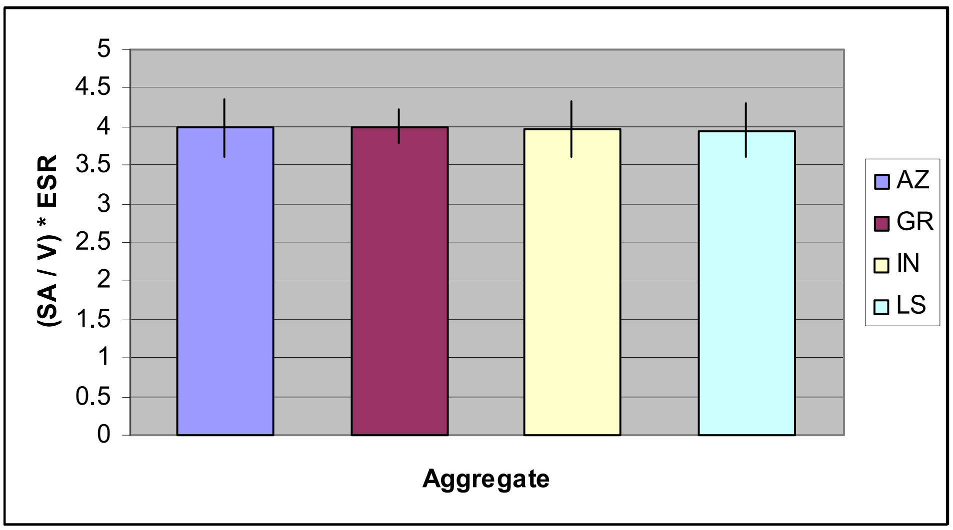

Figure 6.5 Individual and average values for specific surface area multiplied by equivalent spherical radius the particles of the four different coarse aggregates scanned

As can be seen in Figures 6.4 and 6.5, the SSA values for different particles of a single type of aggregate vary by several hundred percent. This is due to the large differences in the sizes of the particles (up to about twenty times, in volume). Once the dependence on size is eliminated, the differences are due to particle shape and are much smaller between particles of a certain type and also between the different aggregates. This is expected since the elongation and flatness values for the four aggregates revealed that the average dimensions of the four aggregates were similar.

Wadell sphericity, introduced in Chapter 2, is another useful parameter. It is the ratio of the surface area of an equivalent sphere to the actual surface area of a particle. The individual and average Wadell sphericity values for the four coarse aggregates are given in Figure 6.6.

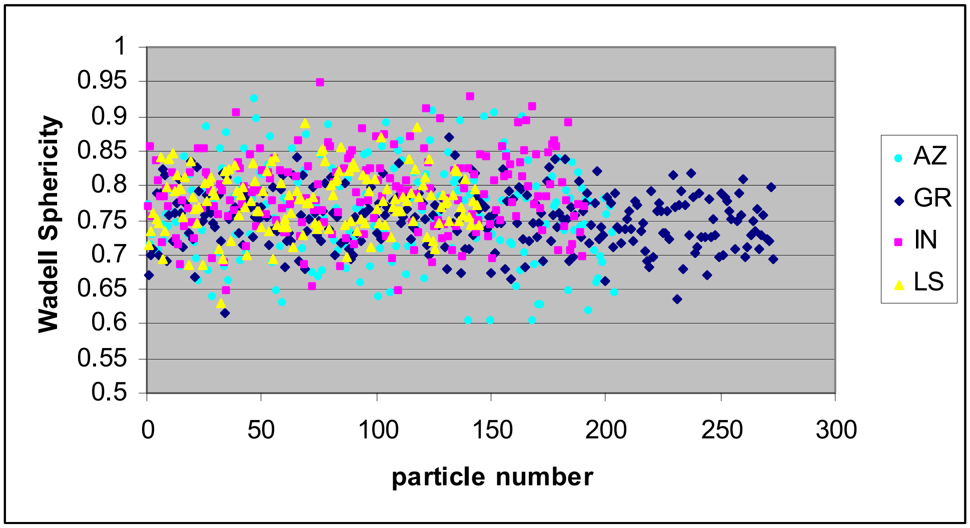

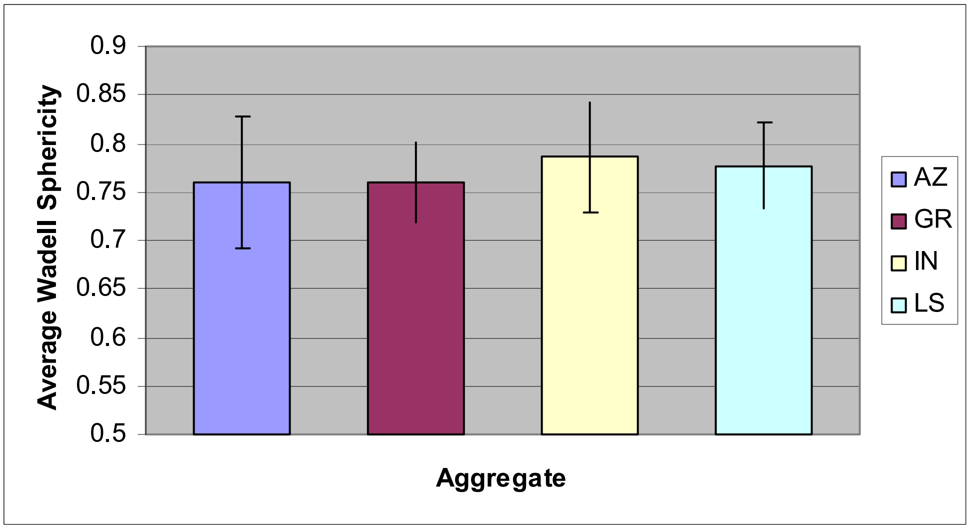

Figure 6.6 Individual and average Wadell sphericity for the particles of the four different coarse aggregates scanned

Some other well known aggregate shape parameters introduced in Chapter 2, Krumbein sphericity, Sneed and Folk sphericity, and Aschenbrenner shape factor, have been calculated for the four coarse aggregates and are given in Figure 6.7.

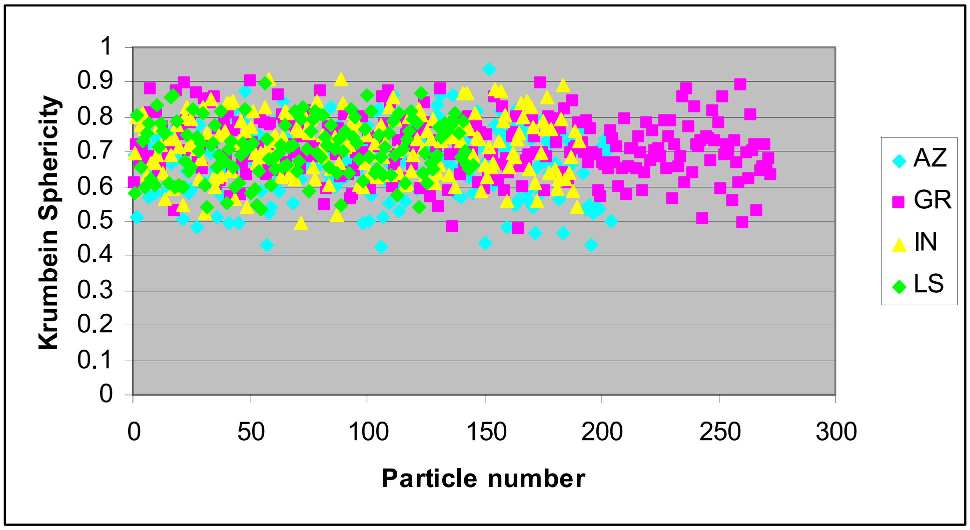

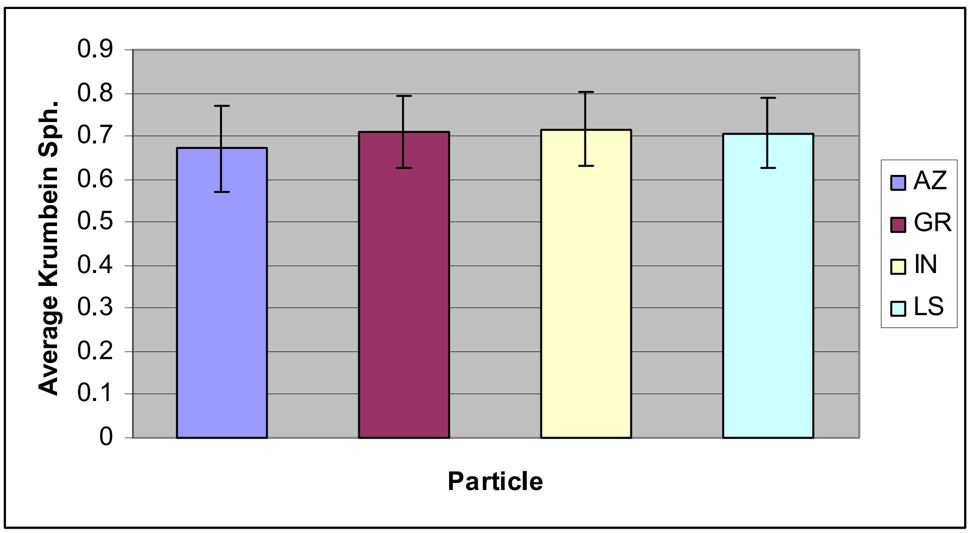

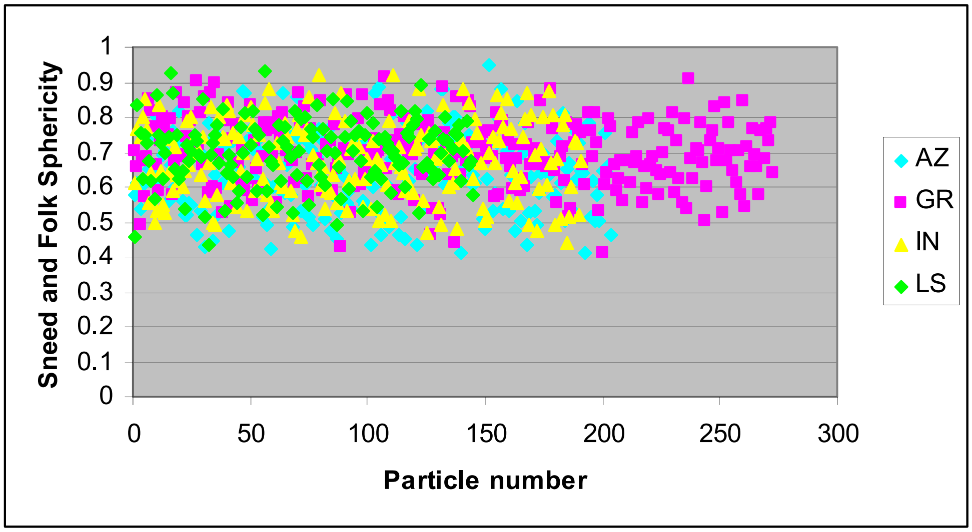

Sneed and Folk Sphericity
1
0.9
0.8
0.7
0.6
0.5
0.4
0.3
0.2
0.1
0
0
50
100
150
200
250
300
Particle number
AZ
GR
IN
LS

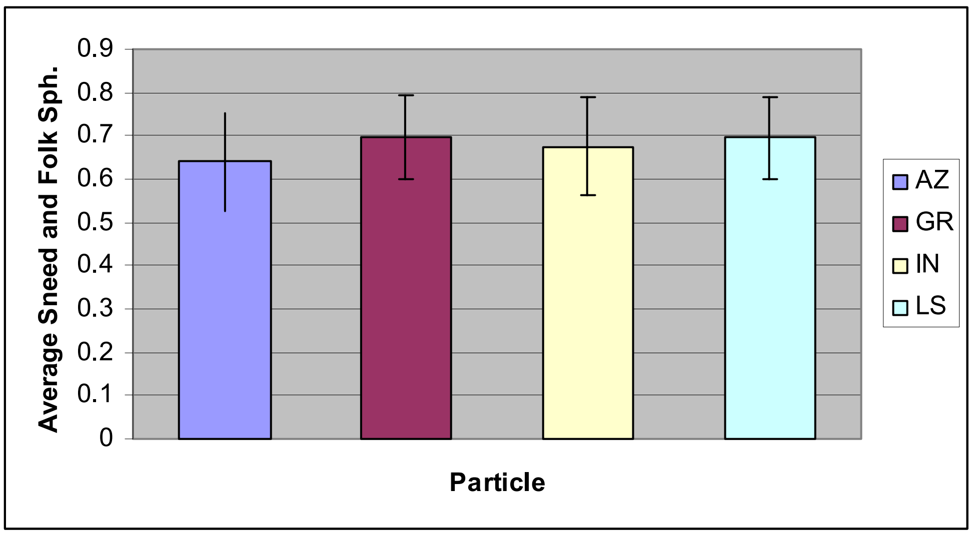

Average Sneed and Folk Sph.
0.9
0.8
0.7
0.6
0.5
0.4
0.3
0.2
0.1
0
Particle
AZ
GR
IN
LS

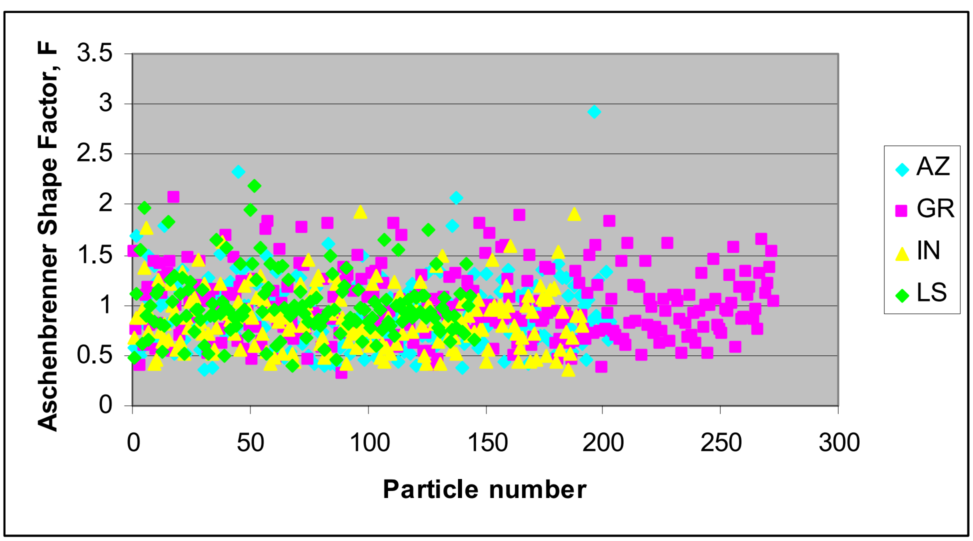

Aschenbrenner Shape Factor, F
3.5
3
2.5
2
1.5
1
0.5
0
0
50
100
150
200
250
300
Particle number
AZ
GR
IN
LS

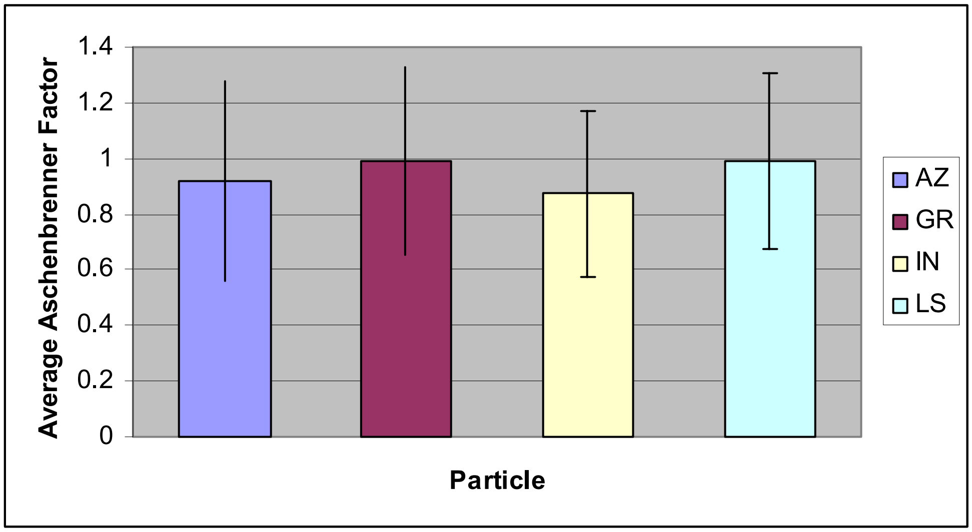

Figure 6.7 Krumbein sphericity, Sneed and Folk sphericity, and Aschenbrenner shape factor (Individual and average) for the particles of the four coarse aggregates scanned

As the combination of CT and SH functions yields the complete three-dimensional shape of the particles, any other shape parameter can easily be calculated. Analyzing Figures 6.2 to 6.7, it is clear that using a single parameter to describe the shape of an aggregate particle and then using average values for aggregates of a certain type and size may not differentiate between particles that are visually different. Therefore, it is not possible to expect a good correlation between average aggregate shape parameters and the results of mortar or concrete tests. Instead, the behavior of each particle in a system may better be treated individually, particularly when attempting to model complex phenomena. Although the average shape parameter value may be identical for two different sets of particles, their behavior as a set may be different, because of the influence of how well or poorly they interact with each other, as in the case of packing or rheology. Knowledge of the actual shape of every individual particle in a set, yielded by a combination of CT and SH analysis, is therefore more useful than a parameter for each particle or an average value. These results, for example, can be used in modeling rheology, as explained in Chapter 7, such as in the DPD model. It would never be possible to exploit the potential of this or similar models, without knowledge of true particle shape.

6.2.2 Comparison of Traditional Sieve Analysis with CT Sieve Analysis for Coarse Aggregate

It was stated in Chapter 2 that traditional sieve analysis (ASTM C136) results are influenced by the intermediate dimension (width) of particles. The sieve analysis using different particle dimensions determined by CT were compared to the results of traditional sieve analysis. Figure 6.8 shows the cumulative sieve analysis curves calculated using the length, width, and thickness dimensions of particles and ASTM C136, for the four coarse aggregates.

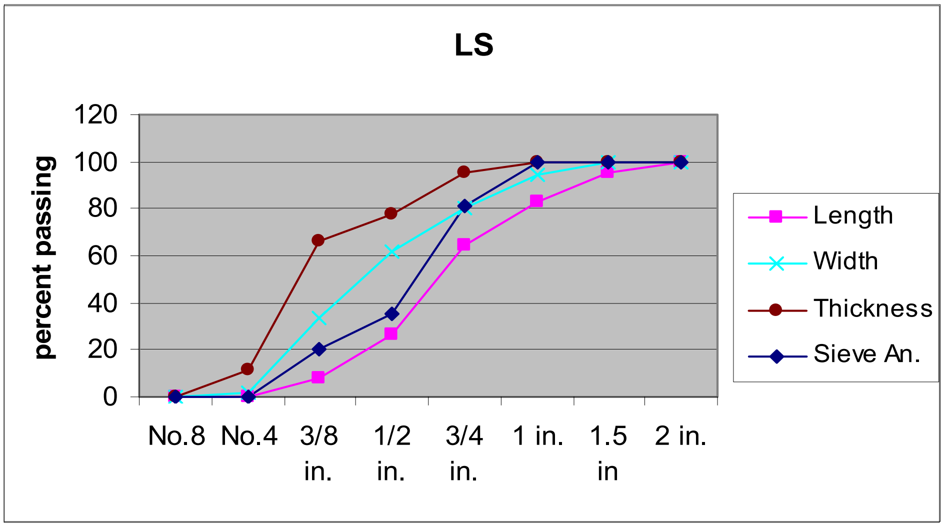
LS
percent passing
120
100
80
60
40
20
0
No.8
No.4
3/8 in.
1/2 in.
3/4 in.
1 in.
1.5 in
2 in.
Length
Width
Thickness
Sieve An.

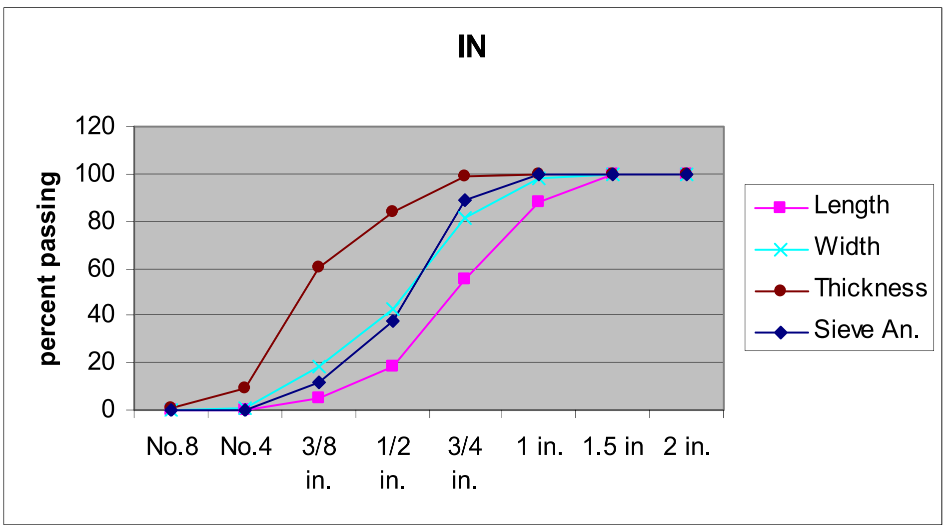
IN
percent passing
120
100
80
60
40
20
0
No.8
No.4
3/8 in.
1/2 in.
3/4 in.
1 in.
1.5 in
2 in.
Length
Width
Thickness
Sieve An.

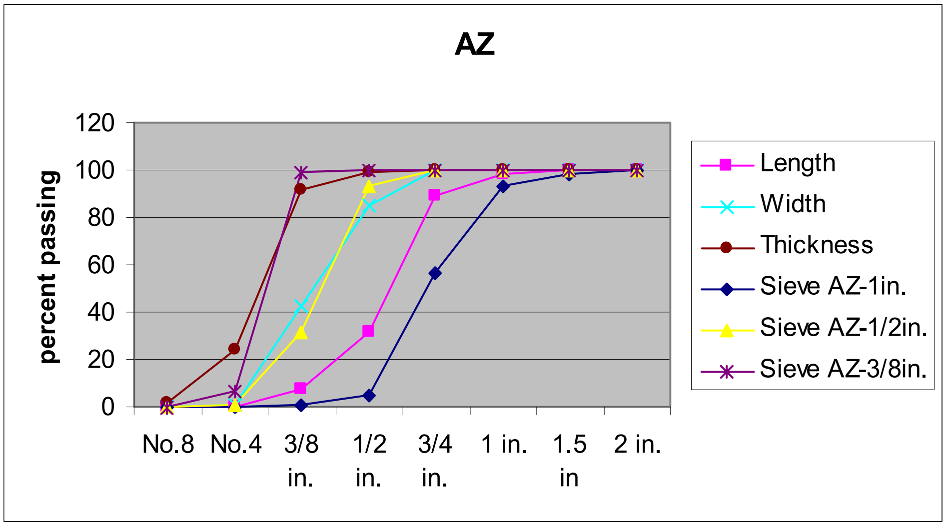

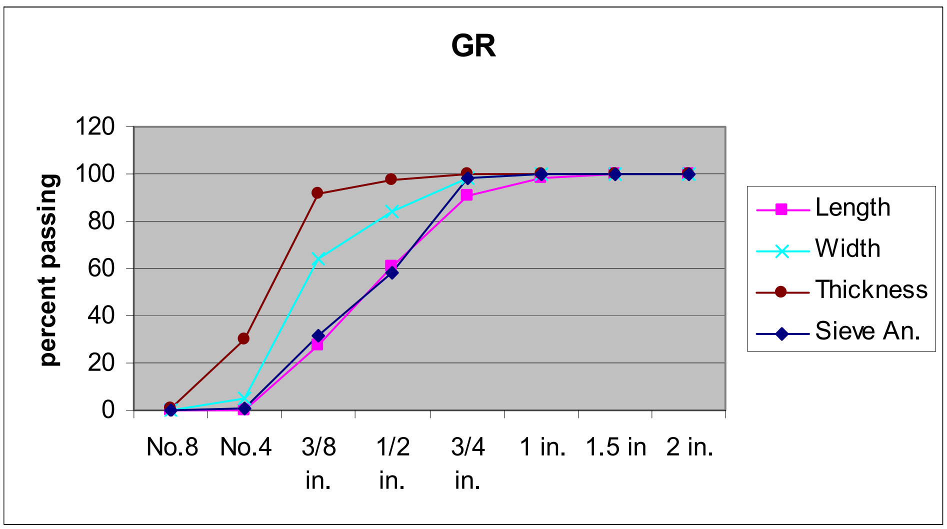

Figure 6.8 Cumulative sieve analysis curves calculated using CT and ASTM C136, for four different coarse aggregates

It can be seen that for three of the four aggregate types, the CT width distribution is the closest to the traditional sieve analysis results. For GR, the sieve distribution is between the CT width and CT length curves, closer to the length curve. Ideally the sieve analysis curve would coincide with the width curve but due to the imperfection of the process, some particles which could pass a certain sieve aperture will be retained, causing the curve to get flatter and longer towards the right of the graph, and move to between the width and the length curves. It must also be noted that the same particles were not used for both the sieve analysis and the CT scans, and while a sufficiently large amount of particles were scanned (150-250 for each type), a higher number of particles were used to determine the traditional sieve curves. There are three different sieve analysis curves for the AZ aggregate since it was in three different coarse sizes. The CT specimen contained a mixture of these three sizes, and it is seen that an equally weighted combination of the three sizes would fall between the CT width and length curves.

6.2.3 Determination of the Density of Aggregate Particles and Density Distribution within a Particle

The gray scale values of pixels (or voxels) obtained from CT is dependent on the average x-ray attenuation value of the material in the volumes represented by those voxels, as mentioned in Chapter 2. Attenuation coefficients are dependent mainly on density. Therefore, it is possible to predict the density of an aggregate particle and the density distribution within the particle, using CT. The density, although taken as one average value for a single particle of a certain type (and often one average value for many particles), can vary within a particle due to the differences in the densities of the individual minerals which make up the particle.

Taylor et al. (2005) used the set of 12 coarse granite particles introduced in Chapter 4 to compare density measurements to results obtained from CT. X-ray diffraction (XRD) was performed on powders from granite particles similar to the 12 rocks scanned with CT. The mineral phase composition is given in Table 6.2.

Table 6.2 Principal mineral phases found in the granite (Taylor et al., 2005)

Mineral phase	**Mass fraction (%)**
Quartz	7 ± 2
Hornblende	27 ± 2
Plagioclase	26 ± 2
Chlorite	25 ± 2

The density ranges commonly found for these minerals (in pure form), as reported in The Handbook of Chemistry and Physics (2004), are listed in Table 6.3.

Table 6.3 Densities of compounds commonly found in rocks (Taylor et al., 2005)

Mineral or mixture	**Density**
Granite	2.64 – 2.76
Hornblende	3.0 – 3.4
Feldspar	2.55 – 2.75
Quartz (average)	2.65
Aluminum oxide	3.44
Silica α quartz	2.648
⇓ Quartz	2.53
Tridymite	2.265
Cristobalite	2.334
vitreous	2.196

From the data in Tables 6.2 and 6.3, it can be seen that the density of the granite will lie in the range 2.6 to 3.0. It may also be noted that the values are for "pure" minerals, which are rarely found in quarries.

The densities measured experimentally were compared with the densities measured from CT. The experimental measurements were made by weighing each rock in air and measuring its volume. The measured mass was divided by the CT volume to obtain the CT density. The results of these two different methods, and the percent difference between the values calculated, are shown for each rock, in Table 6.4.

Table 6.4 Average density of the 12 granite particles measured by water displacement and by CT

Rock	Measured Density	Density using CT Volume	% diff
0.5-1	2.73	2.68	-1.8
0.5-2	2.80	2.74	-2.4
0.5-3	2.58	2.57	-0.6
0.5-4	2.79	2.74	-1.6
0.5-5	2.49	2.45	-1.3
0.5-6	2.74	2.71	-1.0
Average density = 2.69 ± 0.13 (one standard deviation)			
0.75-1	2.97	2.93	-1.3
0.75-2	2.59	2.65	2.6
0.75-3	2.80	2.80	0.3
0.75-4	2.81	2.81	-0.2
0.75-5	2.71	2.75	1.3
0.75-6	2.71	2.76	1.8
Average density = 2.76 ± 0.13 (one standard deviation)			

The differences between the values found using the two different methods is only due to the difference in volume, since the mass used was identical. The average density for the each group is within one standard deviation of that of the other, which is expected as they were taken from the same population, even though the sample size is not very large. The individual densities of the rocks vary from 2.49 to 2.97, which is quite a large range, and this is probably the effect of the multi-phase nature of the particles.

To relate the gray level of the voxels making up the particle in the 3-D image from CT, the measured values of the density of each rock was plotted against the average gray value for all the voxels making up that rock. The results for the two groups of six granite aggregates are shown in Figure 6.9.

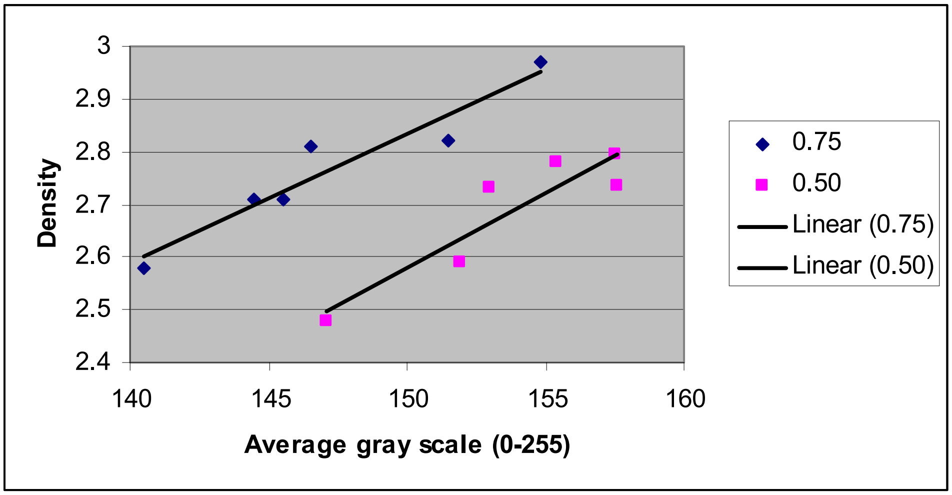

Figure 6.9 Average density of each rock plotted vs. the average gray scale of each rock

It can be seen that the average density for each rock varies linearly with average gray scale. The linear offset between the lines is due to the fact that the two groups were scanned separately with slightly different parameters. It is also possible to scan an object of known density to better determine the density value a particular gray value corresponds to in an image. The following equations give the fitted lines, where AGS is the average gray scale, and AD is the average density:

$$0.5: \quad AD = -1.74 + 0.029\,AGS \tag{6.1}$$

$$0.75: \quad AD = -0.79 + 0.024\,AGS \tag{6.2}$$

The coefficient of determination (R^2) was determined to be 0.91 and 0.97 for the 0.5 rocks and the 0.75 rocks, respectively.

Figures 6.10 and 6.11 show the distribution of density within each particle in the form of a histogram showing the fraction of the particle volume corresponding to a certain density, calculated from the equations of the lines fitted to the points in Figure 6.9.

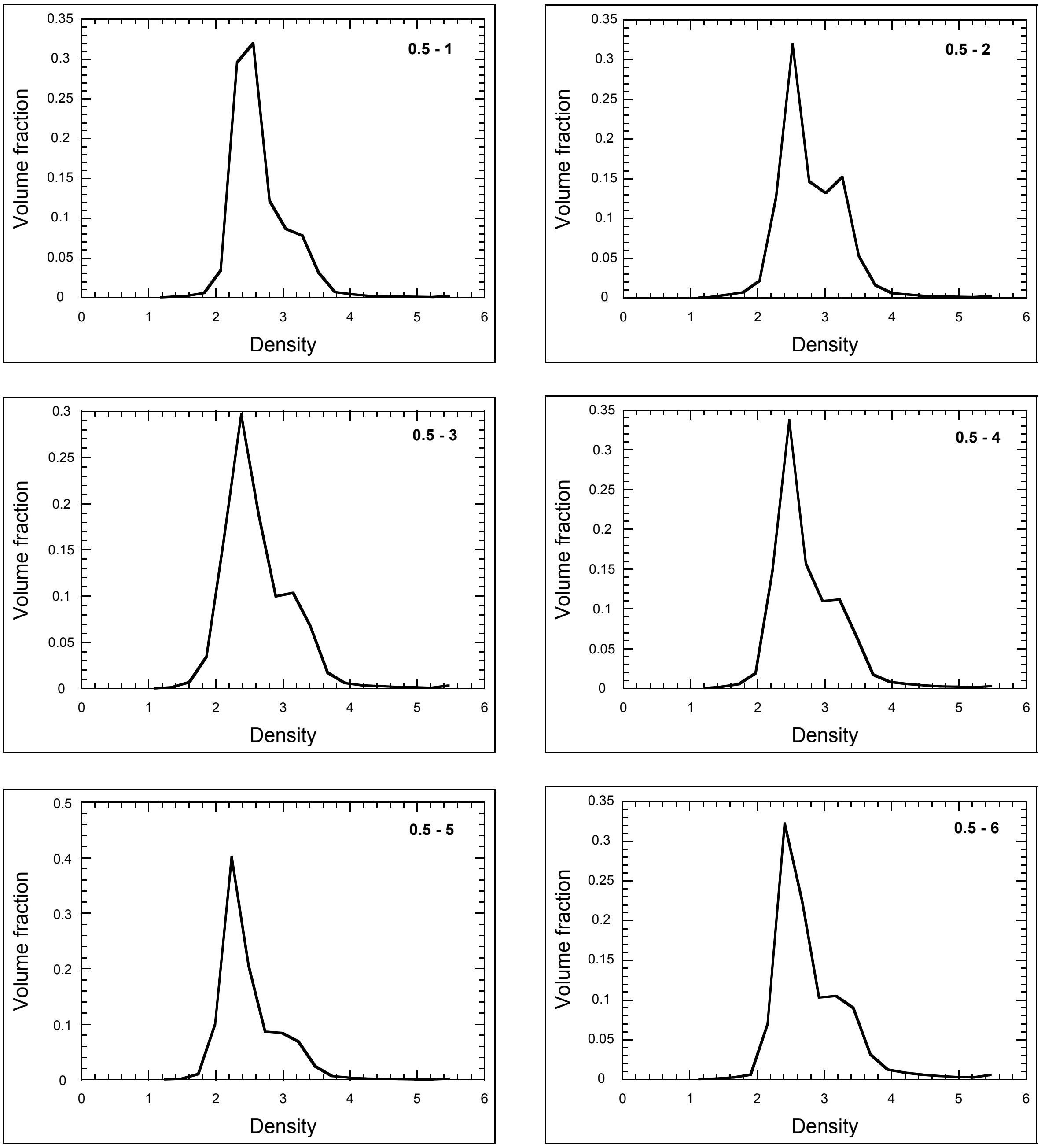

Figure 6.10 Histograms of density for the six 0.5 rocks

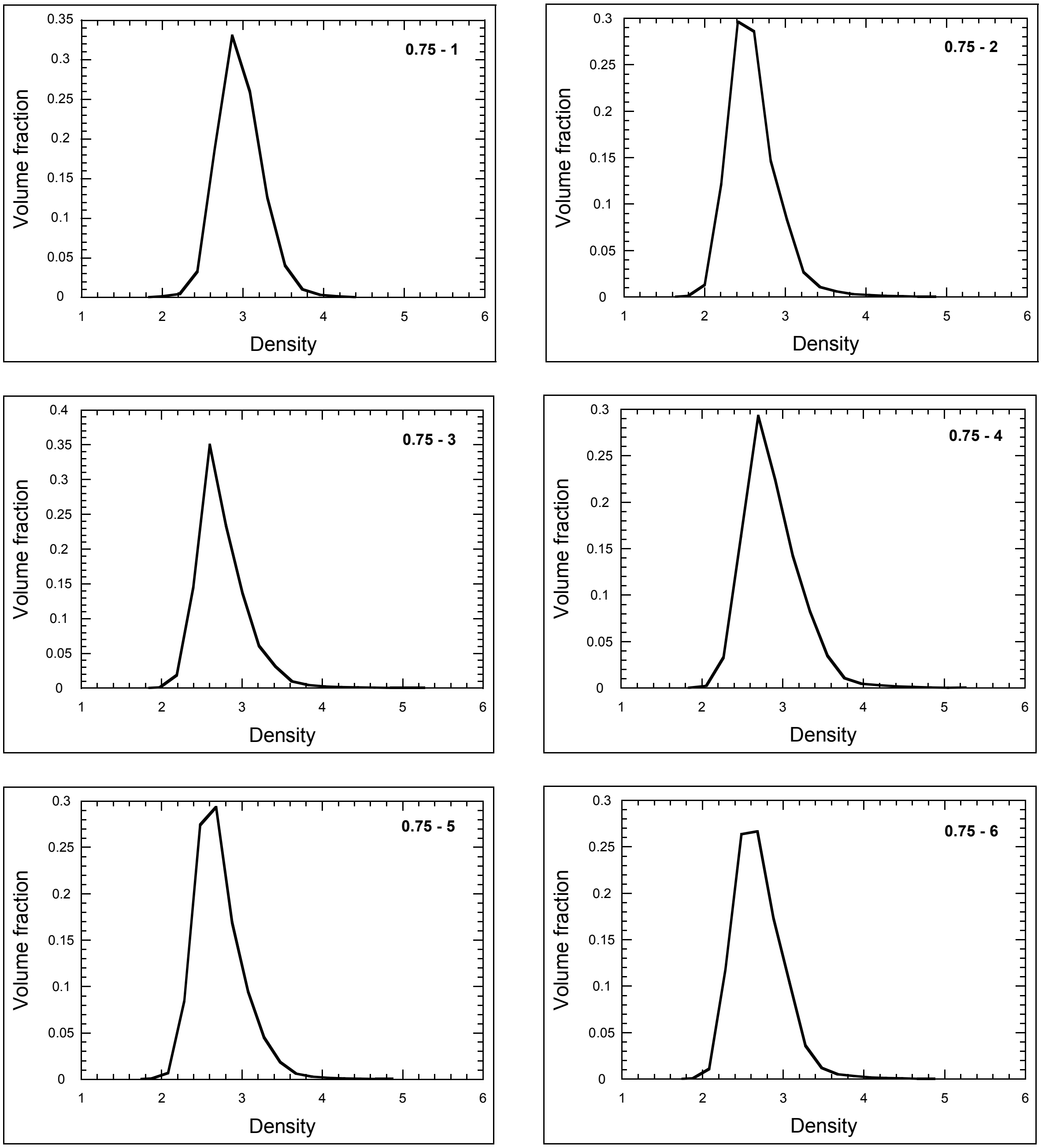

Figure 6.11 Histograms of density for the six 0.75 rocks

It is seen that the particles in one group (0.5) have at least two distinct phases which is somewhat consistent with the results from Tables 6.2 and 6.4, while those of the other group appear to have one distinct phase. It may actually be that there are multiple phases in these rocks as well, but the densities of these phases are similar enough to get interpreted as a single phase in the histogram.

6.3 Results of ∝CT Scans

The ∝CT scans yielded the same particle shape information as the CT scans; the only difference was in the size of the particles tested. This allowed for some applications of the results different than those for coarse particle results. The most practical aspect of these results is that they allow direct determination of properties which can not easily be determined physically.

6.3.1 Comparison of Particle Shape Information Obtained using 2-D cross-sectional Images and 3-D Scans of Particles

Prior to the use of microtomography, attempts were made to characterize microfines in two dimensions, as described in Chapter 2. Stewart (2005) characterized the shape of the samemicrofine aggregates scanned with ∝CT, using a Scanning Electron Microscope (SEM). There are certain advantages of two-dimensional characterization (especially in the case of microfine particles) but the morphological information yielded about a particle is limited. Due to the lack of a depth dimension, several assumptions need to be made in interpreting the results. The particles scanned using the two techniques were not the exact same particles but samples taken from the same barrel, obtained from the same source at the same time. The assumption in comparing the results from the two techniques is that the two samples analyzed are identical. The method of casting, grinding, and polishing the SEM samples is given in (Stewart, 2005). The polishing process created a very flat and smooth surface which was necessary to prevent focus problems due to varying depth of particles and background. An advantage of this method of preparing samples is that the particles are embedded in the epoxy at arbitrary orientations and self-alignment of particles in their most stable position is avoided. A disadvantage is that the particle is not necessarily sliced at its widest part (the area seen from above is not the largest possible for that orientation of the particle) but at arbitrary part. The widest cross-section of a particle from an orientation is somewhat representative of the size of the particle whereas a random section may not yield much more information than the surface roughness or angularity of the particle, provided these properties are rather uniform for the whole of the particle. The specimens were imaged at 500x magnification. Figure 6.12 shows the SEM image of a specimen of a microfine specimen.

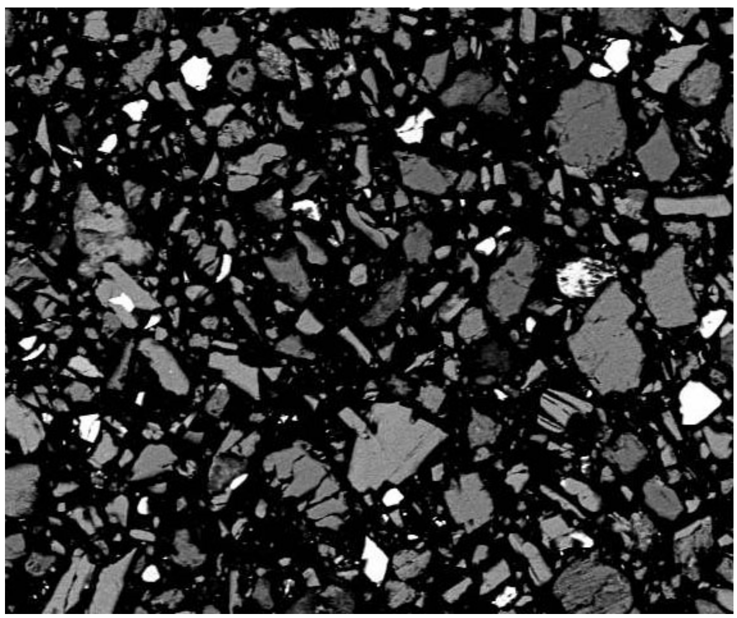

Figure 6.12 Grayscale SEM image of microfine aggregates at 500x magnification

It can be seen that the particles appear a lighter shade of gray and the epoxy background appears a darker shade. Close observation of particle boundaries reveals that there is another shade of gray along the perimeter of some particles, in irregular shapes and inside some particles, in the form of lines. While the reason for these is unclear, they are most probably defects due to sample preparation. It is possible that the lines within particles and the points which appear to be voids are due to the scratching of the surface of the particles, and the irregular surface of some particles is due to the breaking off of edge pieces or smaller adjacent particles in contact with the boundary being interpreted as part of the larger particle. These defects in the grayscale image carry over to the thresholded image used to analyze the shape of the particles. The thresholded image for Figure 6.12 is shown in Figure 6.13.

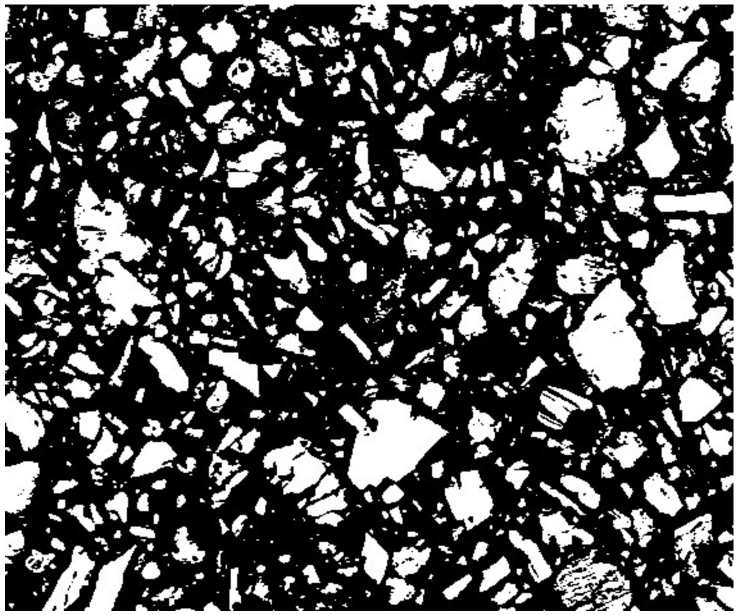

Figure 6.13 Thresholded (binarized) microfine SEM image

It is evident that the intermediate gray color boundary features of some particles in the image disappear due to the thresholding, and the resulting cross-section is unrealistic. One feature in particular of particles in the thresholded image is overhanging portions. In order for a section of a particle to have an overhang in two-dimensions, it would need to have a breaking wave-like valley or cave-like 3-D surface feature with an opening (closer to the outer part of the particle) narrower than the base (closer to the inner part of the particle). Such surface features are unlikely to survive the crushing, grinding, and weathering that the particles endure. In general, great concavities do not exist in concrete aggregates and should not exist in two-dimensional slices either. A U-shaped particle for example will more than likely need to be omitted. Stewart calculated parameters such as area, perimeter, Feret diameter, major axis length (maximum length within a particle), minor axis length (maximum length within the particle, perpendicular to the major axis), elongation etc. for each particle larger than a chosen minimum size. It is possible to compare some of these with the 3-D data and an equivalent parameter can be calculated for some in 3-D. Table 6.5 compares the aspect ratios for the particles calculated from the SEM images and the ∝CT data.

Table 6.5 Comparison of shape parameters calculated in 2-D and 3-D for microfine aggregates of the same type and source

Sample		**Aspect Ratio**		
		SEM	**∝CT (elongation)**	**∝CT (flatness)**
HG01	Mean	2.43	1.55	1.62
	Range	1.00-7.30	1.00-4.68	1.00-3.74
LS01	Mean	1.79	1.34	1.37
	Range	1.00-5.49	1.00-2.60	1.00-2.86
MA01	Mean	2.02	1.43	1.56
	Range	1.10-5.91	1.00-4.57	1.00-3.46
NS01	Mean	1.86	1.34	1.49
	Range	1.00-6.09	1.00-3.30	1.00-3.64
PF01	Mean	2.04	1.32	1.49
	Range	1.07-6.49	1.00-3.41	1.00-3.46
TR01	Mean	1.95	1.16	1.09
	Range	1.05-9.24	1.00-2.09	1.00-1.88

It is seen in Table 6.5 that the mean aspect ratio (maximum chord length within the two-dimensional particle divided by the longest dimension perpendicular to the maximum chord) calculated based on the two-dimensional SEM images is higher than both the elongation (L/W) and the flatness (W/T) value calculated from the 3-D data, for every aggregate type. In addition, the range of the two-dimensional aspect ratios is quite wide, the maximum being greater than 5.0 for all microfine types, which if the two-dimensional aspect ratio was representative of the actual overall shape of the particles would require that some particles in each type of microfine be very elongated very flat, or both. The minimum values are similar only because 1.00 is the theoretical minimum for these parameters (The elongation and flatness values have been rounded to three significant digits). There may be several reasons, as explained in the beginning of this section, for this discrepancy. It is likely that two or more particles appearing as one in the thresholded SEM images due to problems with imaging or image processing is the main reason. The sectioning of the particles at arbitrary orientations (during sawing and polishing) may be another reason. It can be concluded from these results that two-dimensional images may yield misleading results about aspect ratio (and probably other parameters as well for the same reasons) and must be verified by supplemental tests.

6.3.2 Relationship between the Shape Properties of Coarse and Microfine Aggregate Particles of the Same Type

Microfine particles of the same material as the coarse aggregate particles (12 rocks) introduced in section 4.2.2, collected from the same crushing process, were scanned with μCT at a resolution of 3.97 μm per voxel side. A total of 332 particles was obtained from the scan and the processing, with equivalent spherical diameters between 48 μm and 78μm. These microfine particles, therefore, represent the larger part of the material passing the #200 sieve. The length, L, width, W, and thickness, T, were computed for each particle from the virtual particles built using SH. The direct measurement of these values was not done, due to its difficulty.

Table 6.6 compares these microfines to the 12 coarse aggregate particles in a two-dimensional histogram using the calculated L, W, and T dimensions. The L, W, and T parameters were scaled by the T parameter to give L (equal to L/T) and W (equal to W/T) values, for both the coarse and microfine particles. Note that the Li-Wj bin has $i \leq L < i+1$ and $j \leq W < j+1$. The ranges of values for L and W have been divided into five bins. A value computed for the coarse particles and a value computed for the microfine particles is shown in each bin. The percentage of rocks falling into each bin has been listed.

Table 6.6 L - W histogram for microfines and coarse particles. There are two values in each bin, the values for the coarse particles are shaded in gray

W5									0	0
W4							0	0	0	0
W3					0	0	0	0	0	0
W2			8.3	5.4	8.3	3.3	0	0.9	0	0
W1	50	52	33	36	0	2.4	0	0.6	0	0
	L1		L2		L3		L4		L5	

All entries above the diagonal are blank, since the relation L ≥ W must hold. Even though 12 rocks are not sufficient to provide definitive statistics, it is notable how closely the two different sizes of the material match each other, especially for the two bins, L1-W1 and L2-W1, which have the largest percentage of particles. This suggests that the shape of the microfines is similar to the shape of the larger rocks formed in the same crushing process. It is possible that different types of rock crushers will give a different form to Table 6.6. Also, particles from different sources can have markedly different distributions. Based on these results, the shapes of the coarse particles and microfine particles, from the same crushing process, are nearly identical, at least in a statistical sense. Aggregates with heterogeneous mineral composition may show different trends of course, due to differences in crushing.

6.3.3 Some Three-Parameter Shape Models

The principal moments of volume (PMV) and the absolute first moments (AFM), which can be used to define sets of orthogonal dimensions alternative to the L-W-T axes commonly used, were also computed for each of the granite microfine particles, mentioned in the previous section. PMV are the elements on the diagonal of a moment of volume tensor and are three numbers that totally define the reaction of a rigid body to an applied torque since the directions associated with these moments are orthogonal. The relative values of the three PMV are indicative of particle shape. AFM are also three numbers which are characteristic of the particle. PMV and AFM are described in more detail in (Taylor et al., 2005). The PMV and AFM were used to determine three-dimensional bodies such as rectangular boxes and ellipsoids equivalent to the shape of the particle. The following six three-parameter equivalent shape models were defined, using the three choices of dimensions (L-W-T, PMV, and AFM):

1. A box with dimensions equal to L, W, and T
2. An ellipsoid with semi-axes equal to ½L, ½W, and ½T
3. A box of dimensions defined from the PMV
4. An ellipsoid, the semi-axes of which are defined from the PMV
5. A box the dimensions of which are defined from the AFM
6. An ellipsoid, the semi-axes of which are defined from the AFM.

Figures 6.14-6.17 show the results of using three-parameter equivalent shape models for the microfine aggregates, showing how well the different types of models predict the volume and surface areas of the particles. Figures 6.13 and 6.14 are for the box shape model and Figures 6.15 and 6.16 are for the tri-axial ellipsoid shape model.

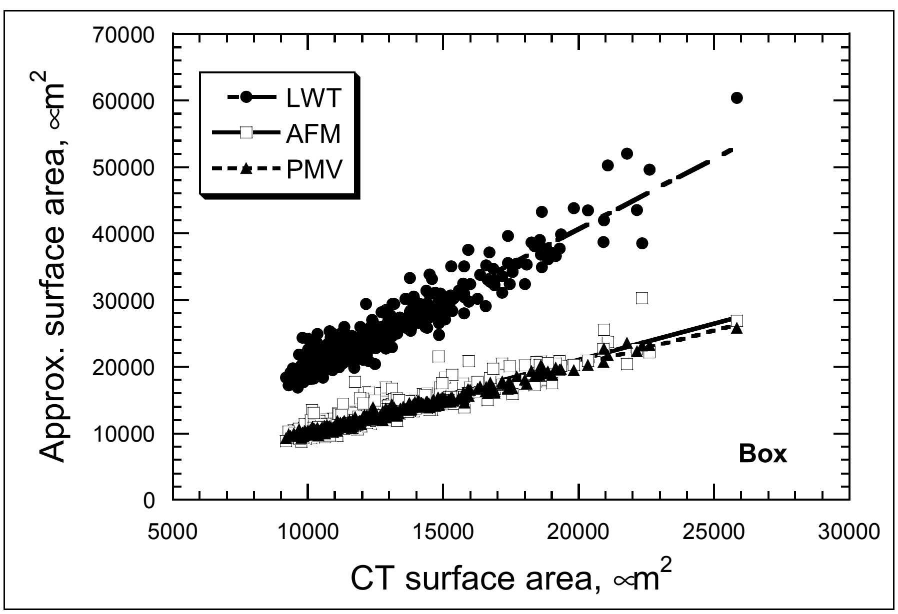

Figure 6.14 Box surface area estimates for the microfines (Taylor et al., 2005)

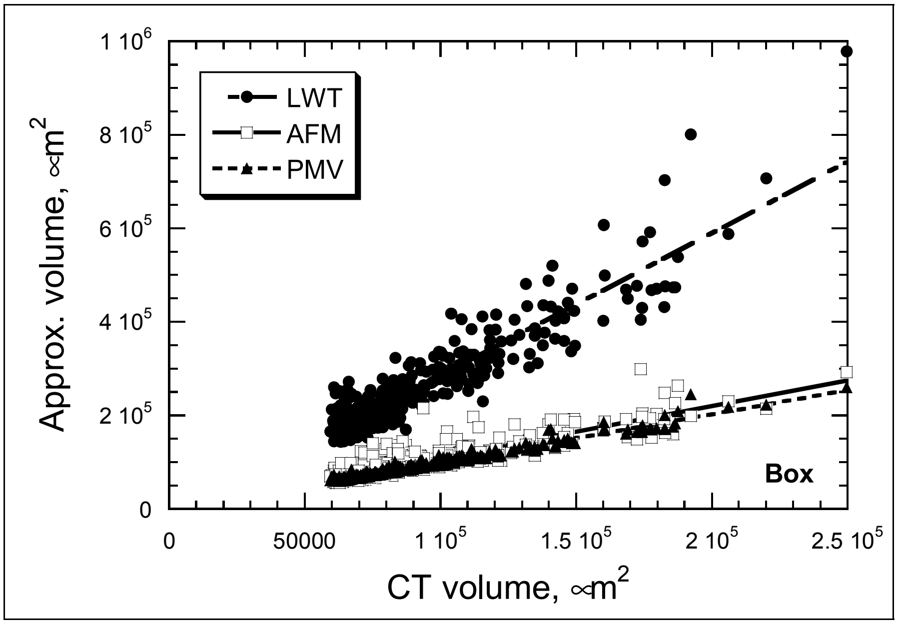

Figure 6.15 Box volume estimates for the microfines (Taylor et al., 2005)

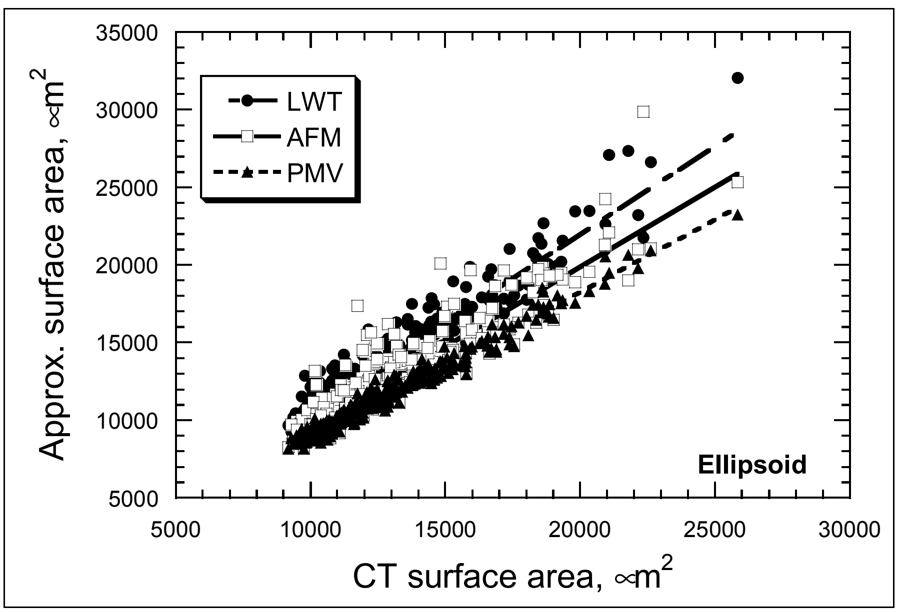

Figure 6.16 Ellipsoid surface area estimates for the microfines (Taylor et al., 2005)

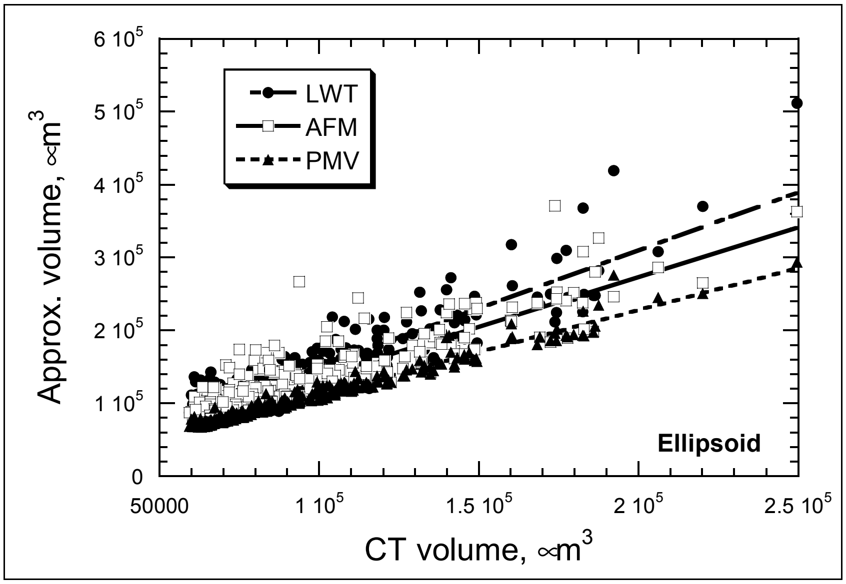

Figure 6.17 Ellipsoid volume estimates for the microfines (Taylor et al., 2005)

The usefulness of these three parameter equivalent shape models can be evaluated by whether the volume and surface area of the equivalent shape could be a good predictor of the actual values of these geometric properties of the 12 irregular test particles, which can be determined by looking at the linear parameters of the lines fitted to the data. Table 6.7 shows all the linear parameters of the various straight lines in Figures 6.14 to 6.17.

Table 6.7 Linear fit parameters for the microfine aggregates for various choices of estimating volume and surface area from various choices of dimensions (Taylor et al., 2005)

Rock type	Length parameters	Slope	Intercept	|%| of maximum value	R^2
Microfine (332)	LWT-Box-SA	2.1	-1250	5.0	0.948
	AFM-Box-SA	1.09	-700	2.8	0.927
	PMV-Box-SA	1.02	-200	0.9	0.99
	LWT-Box-V	3.04	-17000	6.8	0.922
	AFM-Box-V	1.10	300	0.1	0.884
	PMV-Box-V	1.02	-1800	0.7	0.984
	LWT-Ell-SA	1.13	-740	3.0	0.956
	AFM-Ell-SA	1.03	-700	2.8	0.920
	PMV-Ell-SA	0.93	-270	1.1	0.986
	LWT-Ell-V	1.59	-9000	3.6	0.922
	AFM-Ell-V	1.36	400	0.2	0.884
	PMV-Ell-V	1.15	-2000	0.8	0.984

An exact relation would require the intercept to be zero and the slope to be 1 so the y-intercept value expressed as a percentage of the maximum abscissa value is a check on how well the models estimate volume and surface area (0% is required for a perfect fit). All models have small values of the y-intercept compared to the maximum value of volume or surface area, so the linear relation is quite realistic. The PMV box model for surface area and the PMV box model (shaded rows) for volume have slopes of 1.02 and very small y-intercepts compared to the maximum abscissa values.

Although the PMV model for equivalent shape gave comparable results for surface area and volume of the particles, these particular models need to be studied more, and for different particles, to see if they still closely predict the volume and surface area of particles.

6.3.4 Comparison of Particle Size Distributions Obtained by Laser Diffraction and by μCT

The principal dimensions and equivalent spherical diameter (ESD) of a particle can be obtained from μCT scans, as previously mentioned. It is possible then to determine the size distribution (PSD) of the particles in the sample. Laser diffraction (LD) can also yield a PSD curve for a microfine sample. It serves as an interesting exercise to compare the PSD curves obtained for microfines of the same type and source, taken from the same batch, using the two different techniques. The assumption in comparing the results from the two techniques is that the two samples analyzed are identical. Before this can be done, however, it is important to examine how the methods determine the size of an individual particle.

Wet LD uses about 5 grams of microfines suspended in water circulating (as an ensemble or cloud) through a broadened beam of laser light which scatters the incident light onto a Fourier lens, which focuses the scattered light onto a detector array and a particle size distribution is inferred from the collected diffracted light data. Very simplistically, the PSD is determined by interpreting the shadows of a cloud of particles.

The Mie theory (van de Hulst, 1981) is used in evaluating the results, and there are many assumptions involved with this technique (Cooper, 1998). Two of these assumptions are particularly important. The first is that particles are assumed to be spherical. LD is sensitive to the volume of the particle. For this reason, particle diameters are calculated from the measured volume of the particle, but assume a sphere of equivalent volume. The second is that the suspension is dilute and particle concentration is assumed to be so low that scattered radiation is directly measured by the detector (i.e. single scattering) and not rescattered by other particles before reaching the detector (i.e. multiple scattering). The second assumption can be satisfied more easily by controlling the amount of microfine material used. The first one, however, is out of the control of the user, and it is clear that the results of this technique may be misleading especially in the case of high percentages of flat and/or elongated particles being present in the sample (This is analogous to sieve analysis yielding misleading results for elongated particles).

μCT, as mentioned previously, yields the true shape of a particle and therefore it is possible to draw PSD curves using one of various parameters of the particles. One possibility is to use the longest dimension (length) of the particles (or similarly, the shortest dimension [thickness]). This will yield the largest possible PSD curve (similarly, the smallest possible curve) for the particle set and will probably overestimate the PSD (similarly, underestimate the PSD). Another possibility is to use the intermediate dimension [width] of the particles. It has previously been suggested that the width distribution of particles obtained through image analysis is more closely correlated with the PSD obtained using sieve analysis (Fernlund, 1998). Realizing that the length distribution will overestimate the PSD and the thickness distribution will underestimate it, width distribution appears to be a reasonable way to determine PSD. One can also consider the case of observing multiple two-dimensional projections of a three-dimensional particle, in which case the maximum dimension of the average projection will be closer to the true width of the particle. Yet another possibility is to use the ESD of the particles to draw the μCT PSD curve. This will result in better results for rather equi-dimensional particles but may be misleading in the case of flat or elongated particles. Using the ESD will cause an error similar to the first assumption made in using LD and therefore may be a good choice.

LD detected particles approximately 0.5μm (it is unclear whether this was the lower limit for the instrument for the settings used or for the material in the sample) and larger. The smallest particle ESD from μCT however, was around 20 μm. For this reason, and since the microfine samples had been scanned separately as those passing, and those retained on the #400 sieve, the PSD results from the 38 to 75 μm specimens is compared to the LD PSD. In addition, the results from LD (percentages of particles of a certain size) are adjusted to include only the particles larger than 20 μm. Figure 6.18 shows the PSD curves obtained for four different microfines, using LD and using the ESD, width, and length values from μCT.

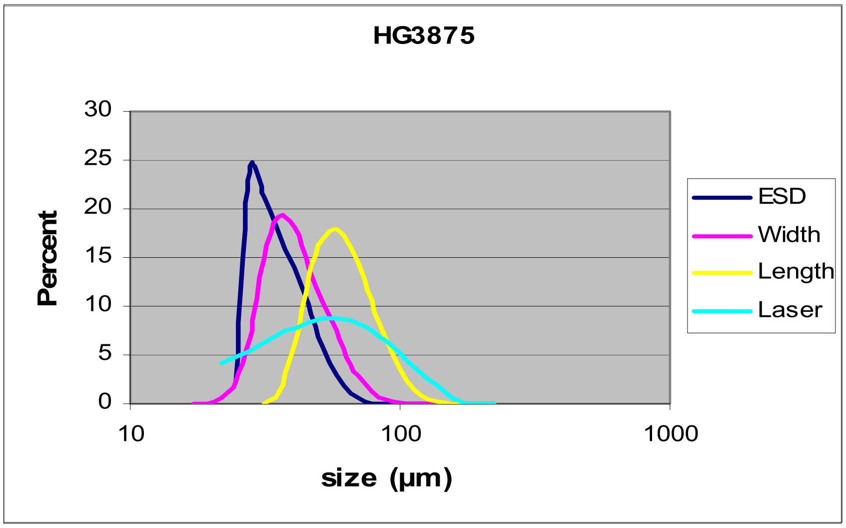
HG3875
Percent
30
25
20
15
10
5
0
10
100
1000
size (µm)
ESD
Width
Length
Laser

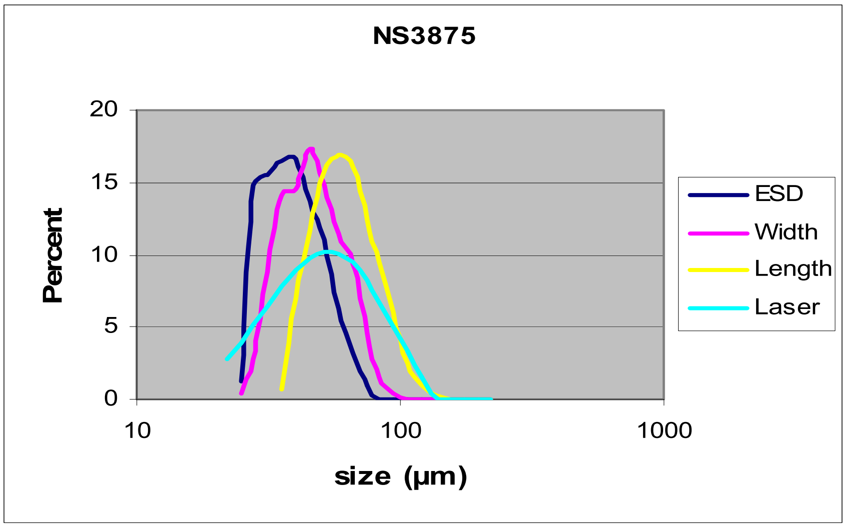
NS3875
Percent
20
15
10
5
0
10
100
1000
size (µm)
ESD
Width
Length
Laser

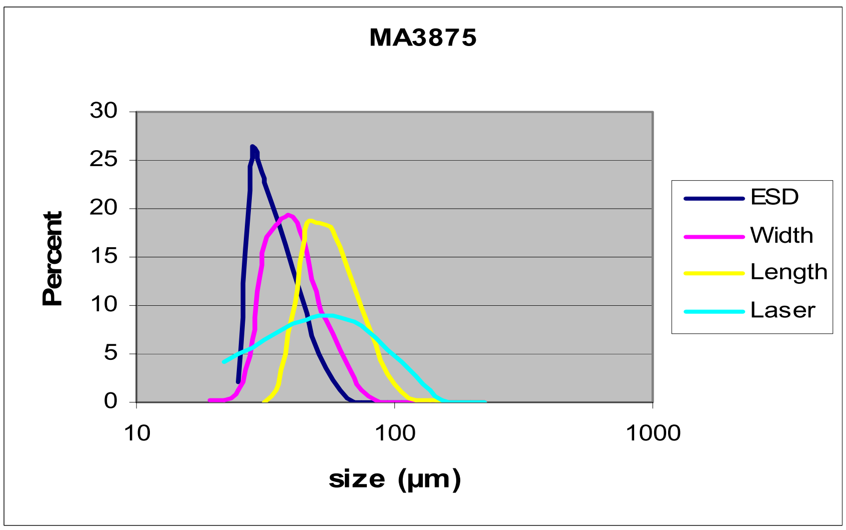
MA3875
Percent
30
25
20
15
10
5
0
10
100
1000
size (µm)
ESD
Width
Length
Laser

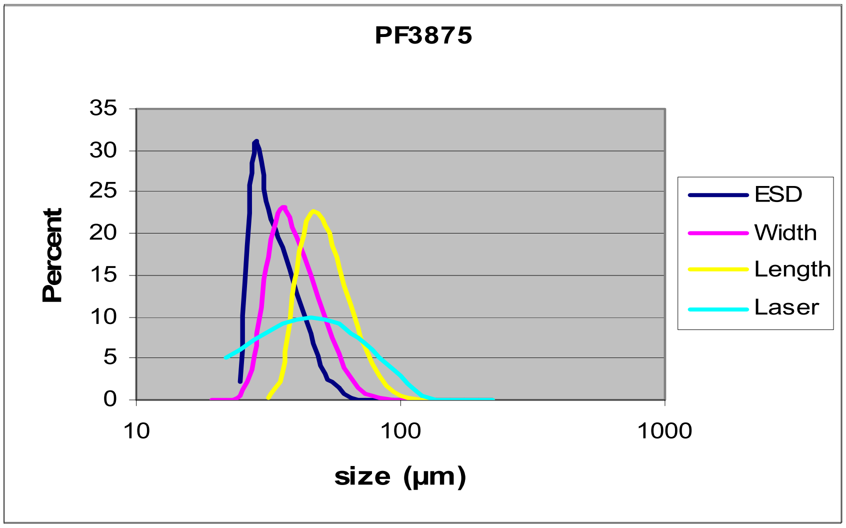

Figure 6.18 PSD curves obtained for four different microfines using wet laser diffraction and using the ESD, width, and length values from µCT

The left hand sides of the curves are intentionally left incomplete since only particles larger than a certain size (approximately 23 µm) were analyzed using µCT and connecting the curves to zero percent would suggest that there are not any particles smaller than this size in the specimen while there probably are quite a few. The laser diffraction results are also given for only particles larger than about 20 µm and have been adjusted to include only such particles, as mentioned earlier. It is seen that, naturally, the width curves for all samples are to the left of (smaller than) the length curves. The ESD values for the particles scanned are the smallest of all the parameters used. The particle sizes determined by LD are more distributed over the size range investigated. An important observation is that LD yields a considerable amount (roughly 10 to 20%) of particles larger than 75 µm. This is possibly due to the fact that the top size of the microfines was determined by sieving, and because sieving can misleadingly let pass elongated particles. However, it is unlikely that large particles will be present in such high amounts. In addition, since LD is sensitive to particle volume and calculates its size based on an equivalent sphere, such large particles would need to have even larger lengths (2 to 3 times) than the apparent size, which is very unlikely. The reason such large particles are measured may be that the particles are agglomerating and several particles are measured as one. The PSD curves from μCT, however, are exact (for the particles measured). Several thousand particles were scanned and analyzed for each microfine type, comparable in amount to the particles measured by LD. This ensures that sample size is not a factor which may lead to error in comparing the methods. One factor which can not be controlled is that the actual samples (particles) tested are different for the two techniques. It is assumed, as mentioned previously, that the two samples of a certain microfine type are identical, which is essential in any case since this assumption is made when using large quantities of aggregates of a certain source in different concrete mixtures based on characterization of a small sample of the aggregate. A trend towards a flatter PSD curve and larger median size is apparent for all microfines, from ESD to width to length to LD. This also suggests that the LD PSD is an overestimate. Another possible explanation for the existence of large particles in the LD PSD is that the ultrasonic waves used in breaking up particle agglomerations in this technique can create air bubbles which may be interpreted as particles and appear on the PSD curve.

Figure 6.19 shows the comparison of the PSD of the four microfines, calculated using the ESD, width, and length values from μCT, and using LD.

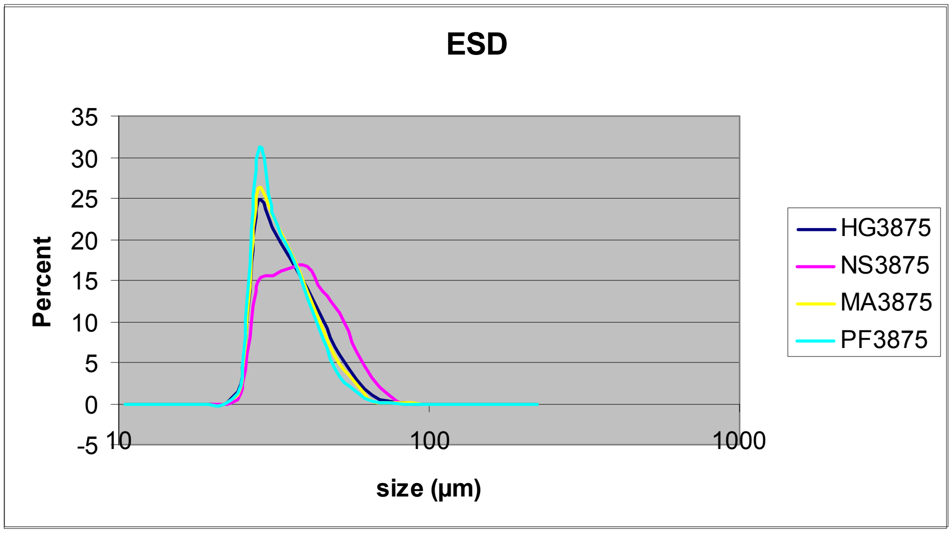
ESD
Percent
35
30
25
20
15
10
5
0
-5
10
100
1000
size (µm)
HG3875
NS3875
MA3875
PF3875

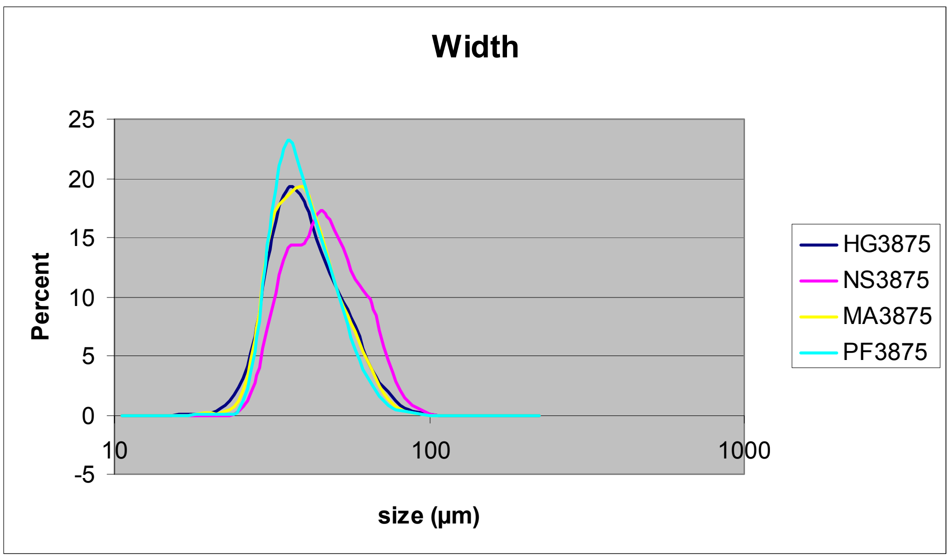
Width
Percent
25
20
15
10
5
0
-5
10
100
1000
size (µm)
HG3875
NS3875
MA3875
PF3875

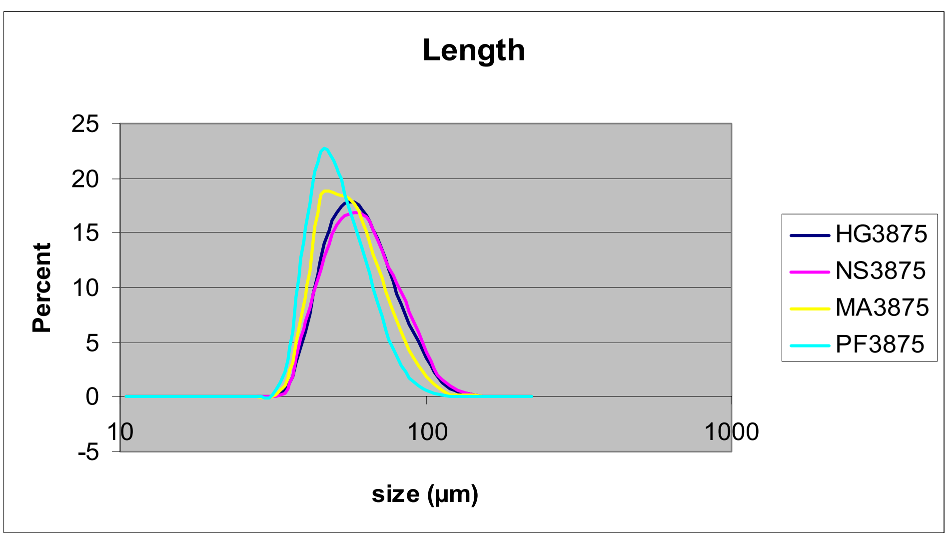
Length
Percent
25
20
15
10
5
0
-5
10
100
1000
size (µm)
HG3875
NS3875
MA3875
PF3875

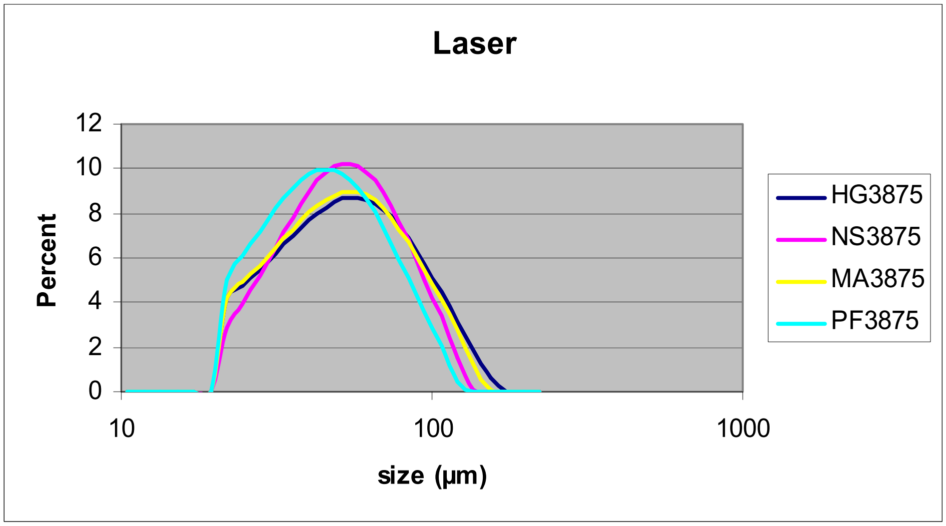

Figure 6.19 Comparison of the PSD curves for the four microfines calculated using the ESD, width, and length values from µCT, and using LD

Comparing the four microfines, the µCT results show that NS3875, the natural sand, is larger in median size and is more uniformly distributed than the remaining three aggregates, of which PF3875, the limestone, is the smallest, but are generally similarly distributed. The peaks of the ESD curves occur at around 28 µm for HG3875, MA3875, and PF3875, which are supposed to include particles retained on the #400 (38 µm) sieve. These peaks might appear to be too low for the particle size range but it is possible for such particles to have one or more dimensions that are larger than 38 µm. Figure 6.20 proves this for one of the microfines.

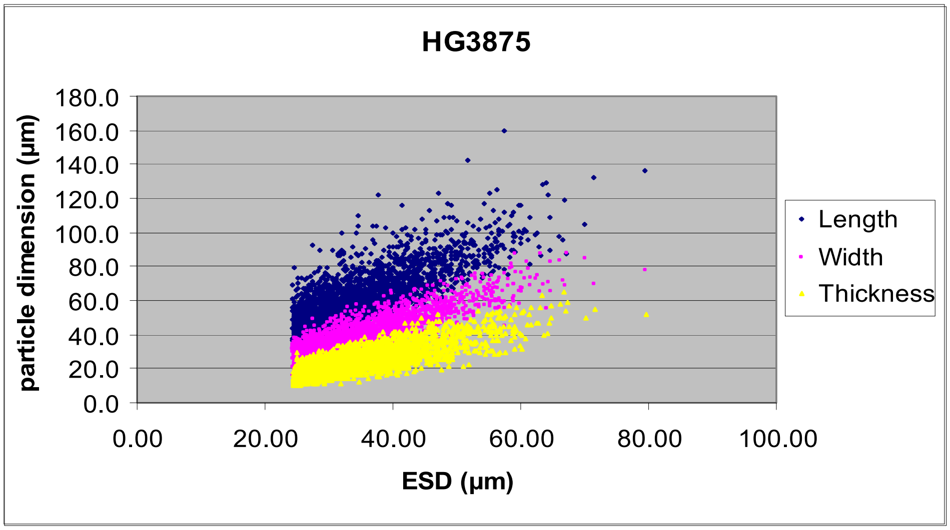

Figure 6.20 The principal dimensions of particles of HG3875 with their corresponding ESD values

For particles with an ESD of about 28 µm, the length values range between about 40 µm and 90 µm, and the width values range between about 30 µm and 60 µm. It is clear that these particles could be expected to be in this range.

It is difficult to say that a single one of the parameters can provide an accurate PSD. The choice of the correct parameter may depend on the application for which the PSD curve is to be used.

The curves in Figures 6.18 and 6.19 were plotted by binning the individual particles into several intervals, ranging in width from 2 µm to 20 µm, and representing the percentage of the particles in the intervals as a single point on the curve, for both the µCT and LD results.

CHAPTER 7 THE EFFECT OF AGGREGATE PARTICLE SHAPE AND SURFACE TEXTURE ON RHEOLOGICAL PROPERTIES – EXPERIMENTAL RESULTS AND DISCUSSION

7.1 Introduction

Various different mortar and concrete mixtures, described in Chapter 5, were tested to investigate the effect of overall aggregate shape and surface texture on the rheological properties of concrete mixtures. The results of these tests and an analysis of the results are presented in this chapter.

7.2 Results of the Shape Test Cases

Two different sets of results were calculated for each test: relative rheological values (yield value and viscosity value), and absolute values (yield stress and Bingham plastic viscosity). The absolute values are the relative values corrected to take into account the presence of a dead zone in the rheometer. The "effective annulus method" was used to make this correction. The details of this method are available in the literature. The trends of changes in relative values and absolute values are almost always similar, though the degree or rate of change due to changes in mixture proportions may differ.

7.2.1 Comparison of Mortars with Different Water Contents and Identical Fine Aggregate and Cement Content

The ability of the rheometer to measure plastic viscosity and yield stress accurately for mortars, and the effect of water content on flow were tested by running a series of tests using mortar mixtures having a range of water contents. The water contents of the mortars are approximately 100 times their respective water-cement ratio values, due to the amount of cement used. Figures 7.1 and 7.2 show the yield value (in Nm) and the yield stress (in Pa) for the different mortars.

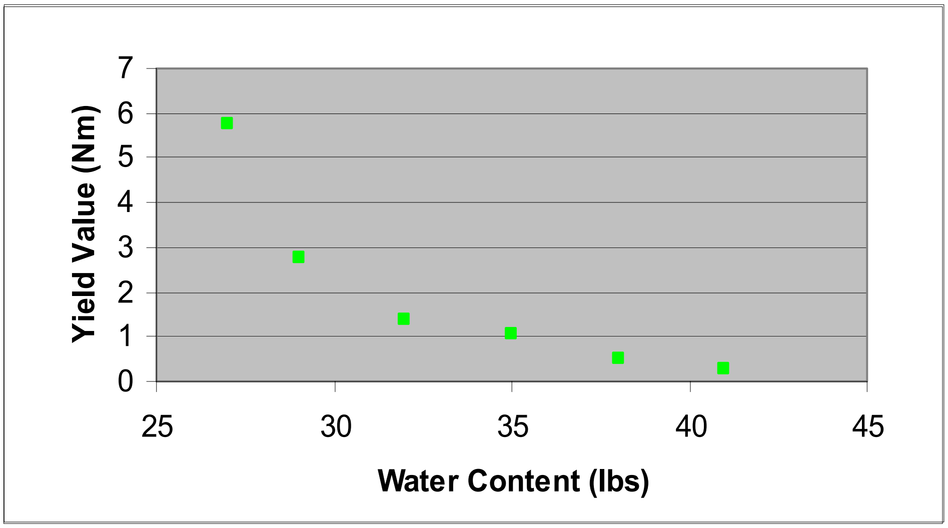

Figure 7.1 Yield values for the mortars with increasing water content

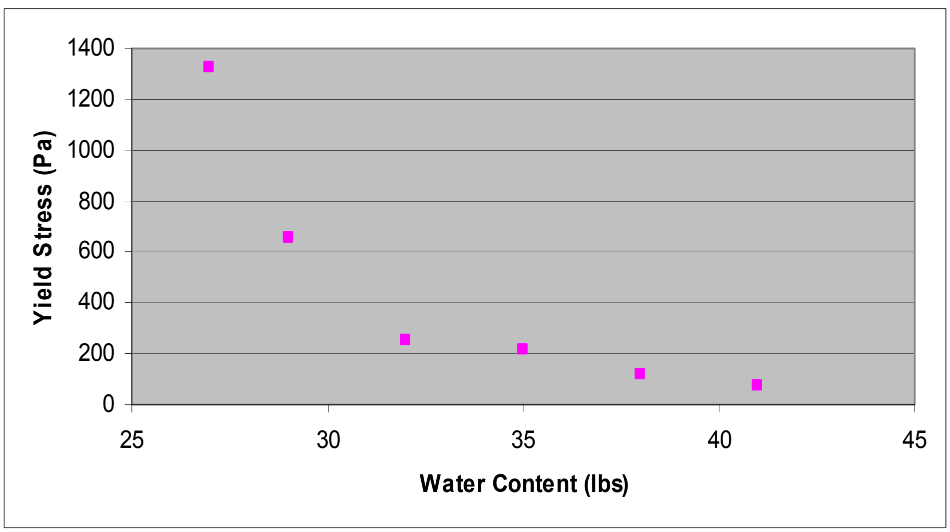

Figure 7.2 Yield stress for the mortars with increasing water content

It can be seen that the yield stress value, which is the amount of stress required initiating the flow of the mixture, increases as the water content of the mortar decreases. The rate of this increase is slow at first, but quite rapid after the water-cement ratio drops to below about 0.30. Yield stress values can be related to the results of the conventional ASTM C143 slump test. The behavior of a mixture in the slump test is dependent on its yield stress (Koehler, 2004).

Figures 7.3 and 7.4 show the viscosity values (in Nm.s) and the plastic viscosities (in Pa.s) for the different mortar mixtures.

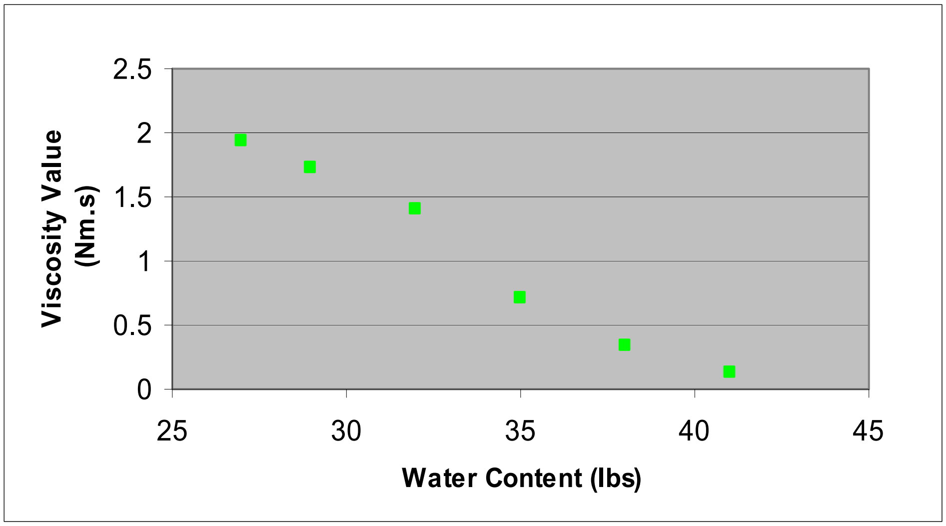

Figure 7.3 Viscosity values for the mortars with increasing water content

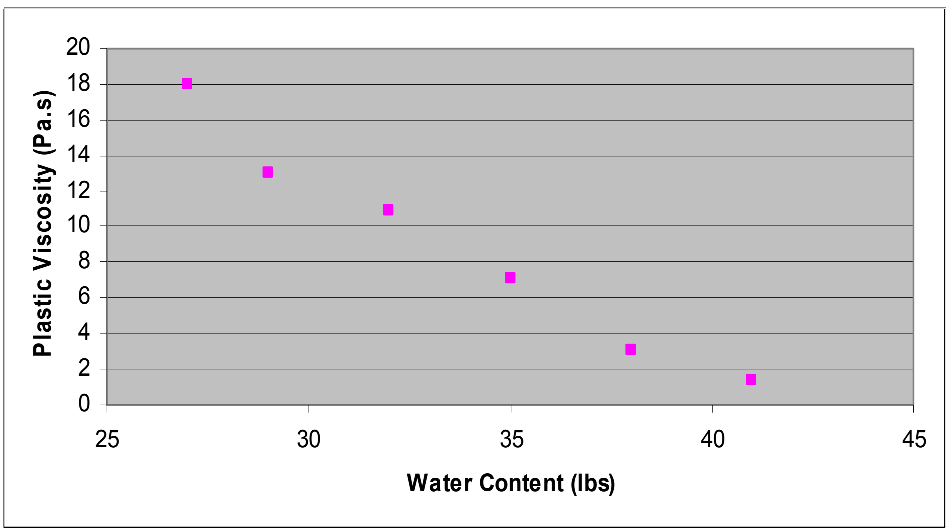

Figure 7.4 Plastic Viscosity for the mortars with increasing water content

The plastic viscosity of a mixture is the resistance of the mixture to flow under a shearing stress, once the flow has started. Therefore, it is an indication of the amount of torque required to keep the mixture flowing at a certain rate. It is seen from the figure that plastic viscosity of the mortars increases slowly at first and then the rate of the increase increases, similar to the trend of the corresponding yield stress values, but the rate of increase begins to decline between water-cement ratios of 0.32 and 0.29. This trend is probably due to experimental variation, as logically the viscosity increase should not slow down below a certain water content but rather it should increase. It is interesting to note that for three of these six mortars with lower water contents, while the stress required to start the flow was considerably higher than for the mortars with higher water contents, the torque required to keep the mortars flowing was not correspondingly higher.

7.2.2 Tests Made Using a Fixed Volume of Spheres and Cubes

Somewhat realistic concrete mixtures were made by adding artificial / laboratory-made mono-sized coarse particles to a base mortar. The goal was to determine the repeatability of results obtained for spheres and for cubes, and finally to compare the two shapes. Several measurements were made for each test case, and the results presented are averages of these tests. The determination of seven data points on a torque vs. rotation speed graph is meant by one "measurement" from which one value each for yield value, viscosity value, yield stress and plastic viscosity, can be calculated. A state of the mixture which requires measurements is termed a "test case" (e.g. increasing the sphere aggregate content from 15% to 25% by volume in a mortar medium results a new test case). The results presented for repeatability are those of a few individual measurements. Although the case of mono-sized coarse particles is neither ideal in terms of rheological properties nor realistic in terms of concrete mixtures, it was selected for reasons of control over particle shape and simplicity.

Figure 7.5 shows the yield values, yield stresses, viscosity values, and plastic viscosities calculated from individual measurements performed on the sphere mixtures with 27 lbs of water (the two data points corresponding to the same measurement number are two separate mixtures, one using spheres and one using cubes).

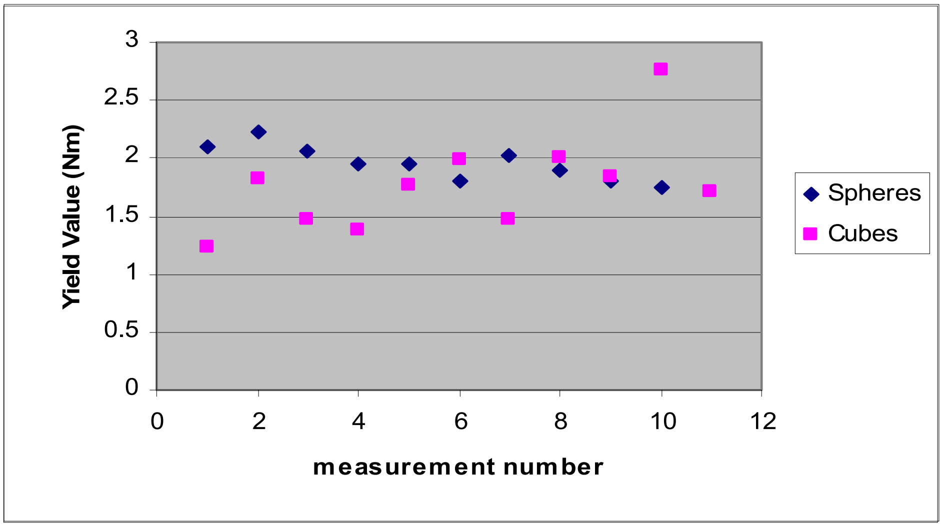

Yield Value (Nm)
measurement number
Spheres
Cubes

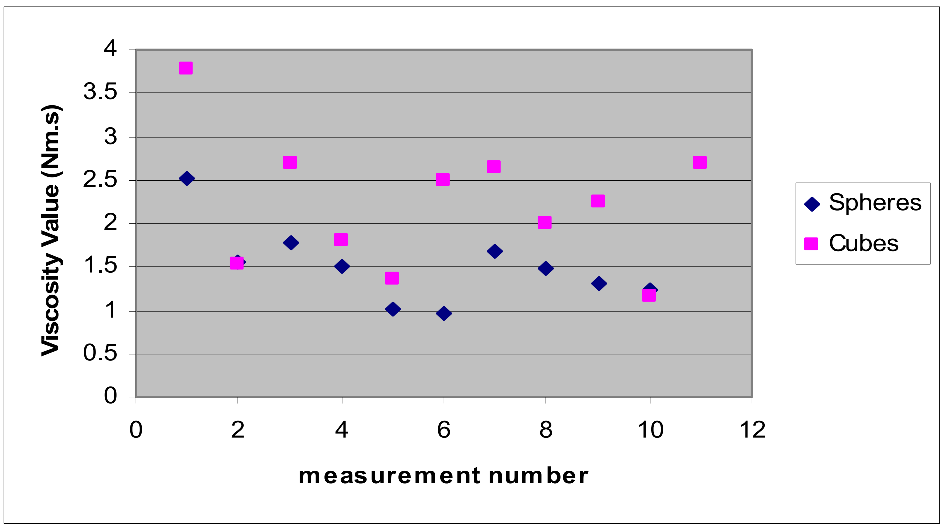

Viscosity Value (Nm.s)
measurement number
Spheres
Cubes

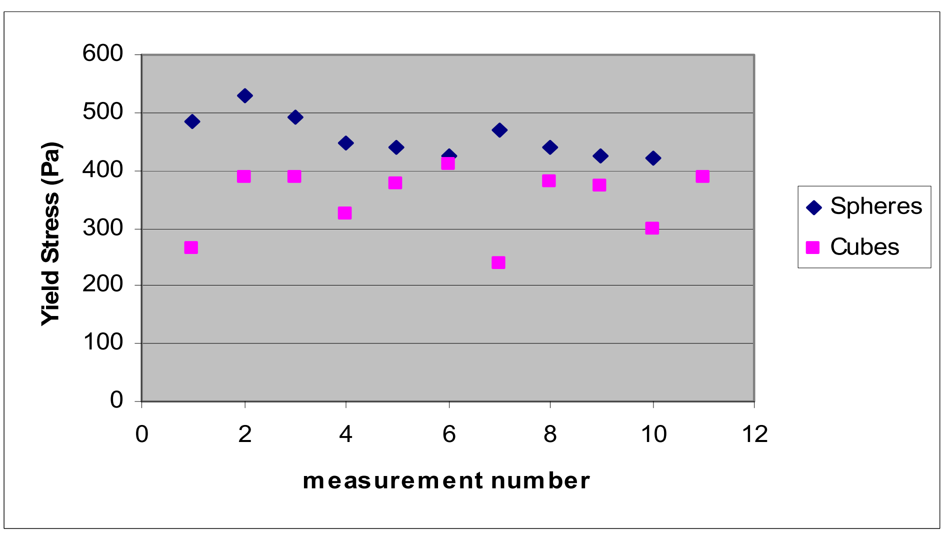

Yield Stress (Pa)
measurement number
Spheres
Cubes

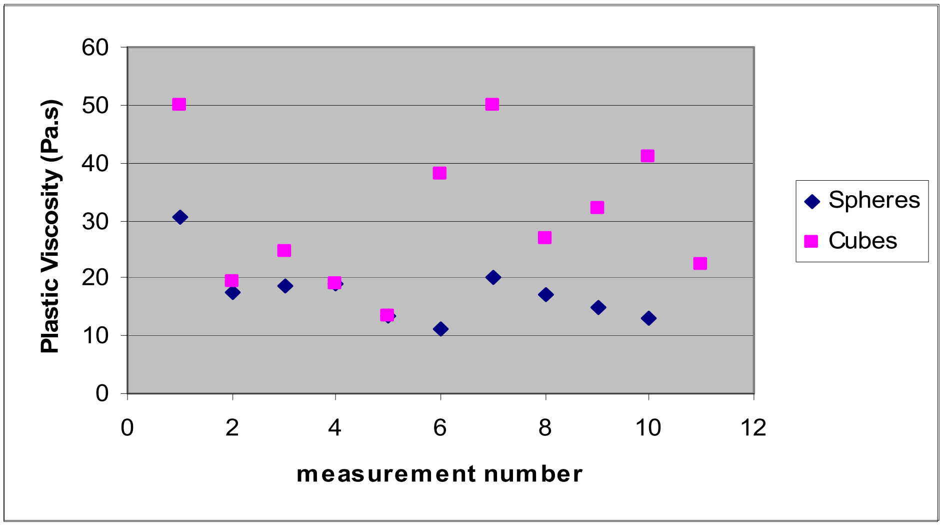

Figure 7.5 Yield value, yield stress, viscosity value and plastic viscosity measured to test the repeatability of the results for a concrete mixture.

Several important concepts are revealed by examining the graphs in Figure 7.5. First, it is seen from the sphere data that the viscosity value or plastic viscosity measured for a mixture generally decreased with each measurement. This is probably due to the artificial coarse particles (and perhaps the fine particles as well) moving out from the center of the rheometer, away from the path of the vane. As a result, the coarse aggregate concentration of the part of the mixture being tested essentially decreased, and viscosity decreased. A second observation is that there was a jump in the viscosity following a few measurements, after which the viscosity continued to drop. This is due to remixing of the mixture using a shovel, while still inside the container. Remixing may disperse the coarse particles, bringing the mixture back to its original condition, thus a viscosity close to the original viscosity was measured. The effects of remixing were dependent on how well it occurred and the jump in viscosity was not always noticeable. A third observation is that the trend of the viscosity curves for the cube mixture is unlike that for the sphere mixture. This is an artificial effect caused by the shapes selected. Again it is seen that the viscosity decreases with each measurement until remixing, after which there is a jump and continuing decrease. However, there is a lot more variation in the values. It is important, based on these three observations, that a method of obtaining and interpreting results is developed. It is obvious that making a single measurement for each test case is not a good idea because a single measurement can not capture the variation in the results (which will exist for real concrete mixtures with a combination of irregular shapes, although not as much as with mono-sized cubes), and may be higher or lower than an actual representative value. If multiple measurements are made for a test case, it must be decided which value to use, or how to average the results. This cannot be performed solely using statistics as it is known that certain conditions are changing from one measurement to another and each calculated value is not equally weighted. In addition, for the case of mixtures made using mono-sized regular shapes, there will often be outliers, due to the interlocking of coarse particles in three dimensions, resulting in very high values if the vane gets temporarily jammed but is freed before the maximum torque allowed by the rheometer is exceeded. In this research a minimum of three measurements were made for each test case, and often more. The first two measurements were generally made as is, then remixing was performed, and two or more measurements made. In cases where the values after remixing were similar to the first measurement, this value was assumed to be representative. In cases where the variation was high, an average of the measurements (without including the outliers) was used.

Prior to performing the tests, it was expected that the spheres would produce a better flowing mixture than the cubes and that the yield stress values for the spheres concrete and the cubes concrete would be nearly the same, with the value for the spheres being slightly lower. This is because yield stress is more dependent on the characteristics of the mortar (and since the mortar portions of the two concretes were approximately the same) and because the selected coarse particle content (35% by volume) is reasonably high (particularly since the particles are mono-sized), although not as high as in a typical concrete mixture.

Figure 7.6 shows a comparison of the yield values and yield stress for the concretes made using spheres and cubes at two different water contents (The water-cement ratios of the mixtures with 27 lbs and 30 lbs of water were about 0.41 and 0.45, respectively).

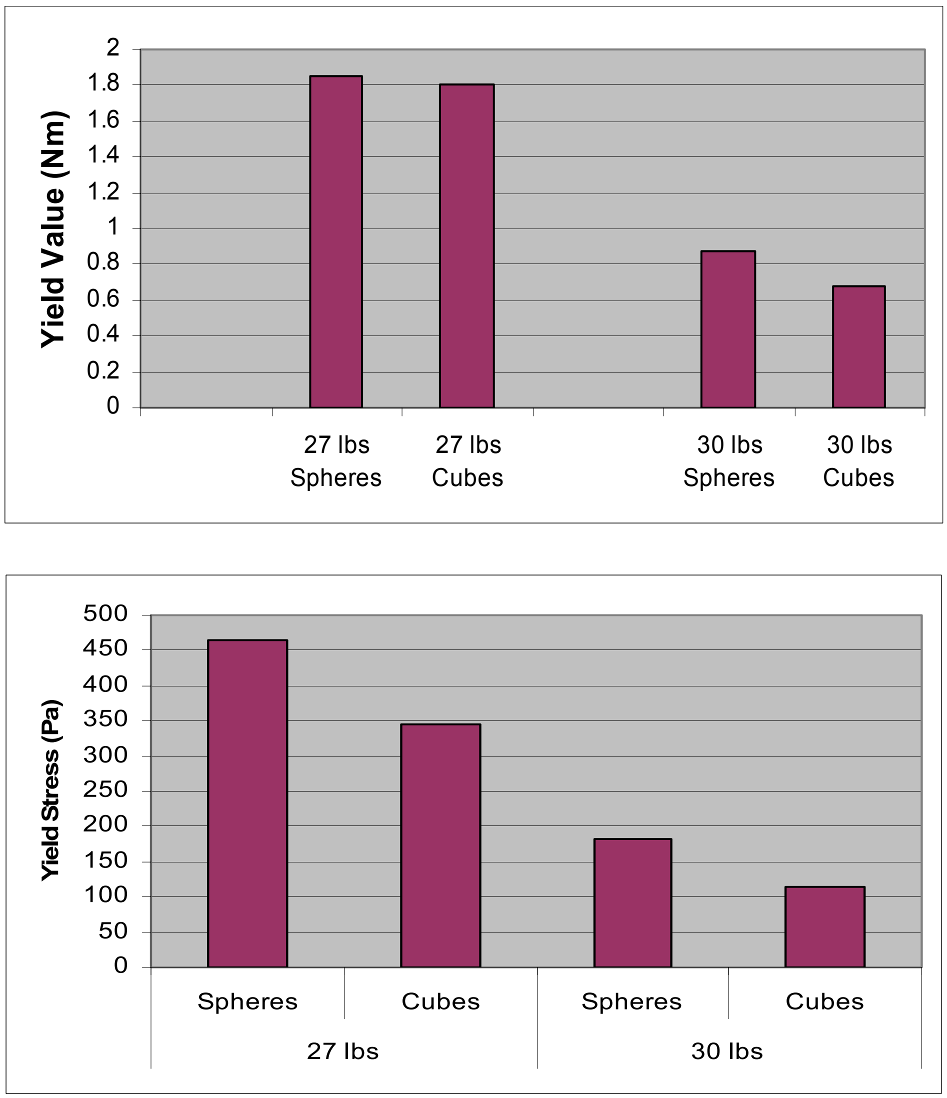

Figure 7.6 Yield values and yield stresses concrete made using spheres and cubes at two different water contents

The results show that, contrary to what was expected, the yield value for the mixture made using the spheres is slightly higher than for of the mixture made using the cubes in one case, and approximately equal in the other. The yield stress calculated for the spheres mixture is higher in both cases. Furthermore, it appears that the yield stress ratio of the cubes to the spheres is higher for the higher water content mixture. The yield value results can perhaps be explained by suggesting that the mixture behaves as a whole in the lower water content case and the coarse particles and the mortar matrix have somewhat separated effects on the yield resistance of the mixture. This could elucidate the case in which the yield values are similar. However, it is not possible to similarly explain the yield stress results, and the results may be erroneous due to a lack of a sufficient number of measurements to obtain an average value representative of the real yield stress of the mixture. Another possible cause is that the water content of the cube mixtures was higher than that of the sphere mixtures, in both cases, and the mortar mediums were not identical.

Figure 7.7 shows the viscosity values and plastic viscosities for the concrete mixtures made using the spheres and the cubes at two different water contents.

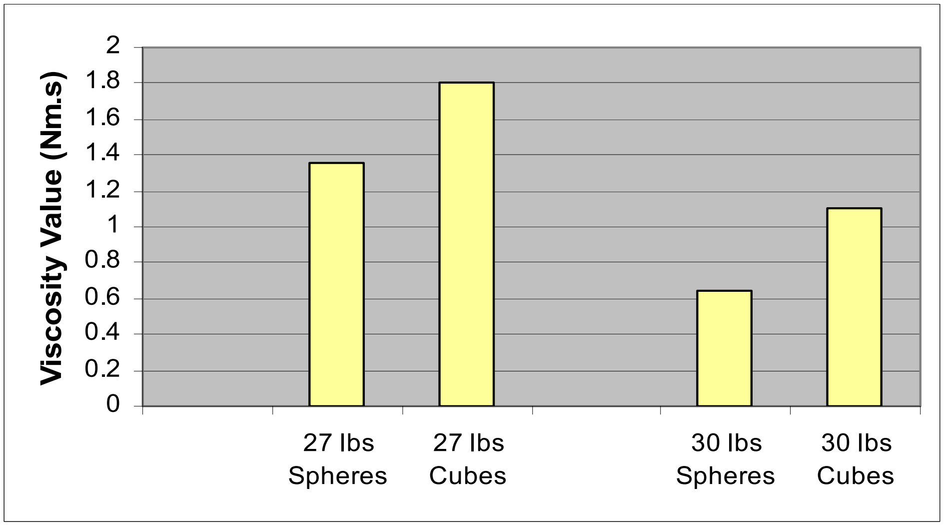

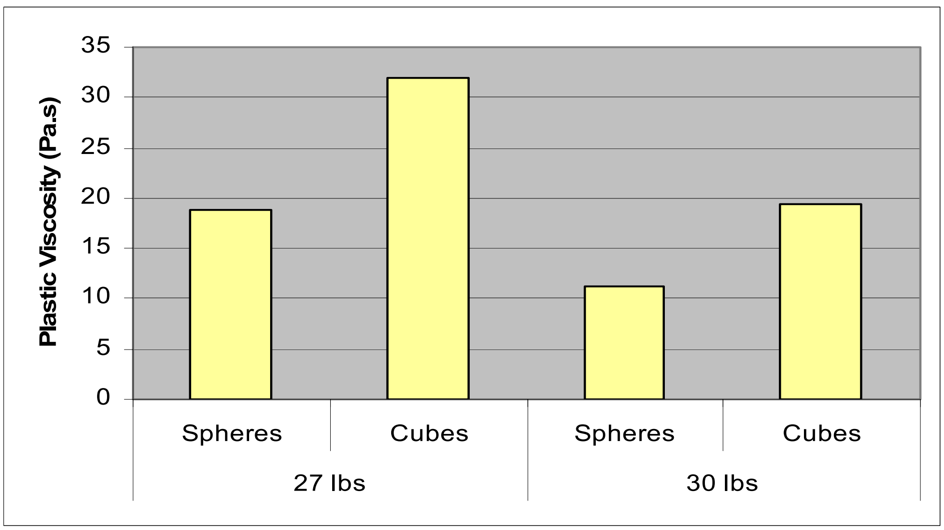

Figure 7.7 Viscosity values and plastic viscosity for concrete made using spheres and cubes at two different water contents

The viscosity of the mixtures made using the spheres is lower than that of the mixture made using the cubes at both water contents, as expected. In addition, it is seen that the viscosity for both cases decreases as the water content of the mixture is increased. The ratio of the viscosity of the cubes to that of the spheres is higher for the higher water content case, possibly as the influence of the coarse particles on flow is greater in this case.

7.2.3 Comparison of Artificial Spheres with Artificial Cubes at Increasing Coarse Particle Contents

Having tested the effect of mono-sized spheres and cubes on rheological properties, it was decided that the effect of increasing coarse particle content needed be investigated. Prior to the tests, it was expected that the concrete made using the spheres would have a lower viscosity than the concrete made using the cubes. Furthermore, a smaller difference between the viscosities was anticipated at lower coarse particle contents, and a higher difference at higher artificial particle contents, due to increased particle interaction. The coarse particle contents ranged from 0% (mortar case) to 45% (realistic coarse content in actual concrete).

Figure 7.8 shows the yield value and the yield stress for the concrete made using spheres at increasing coarse particle contents.

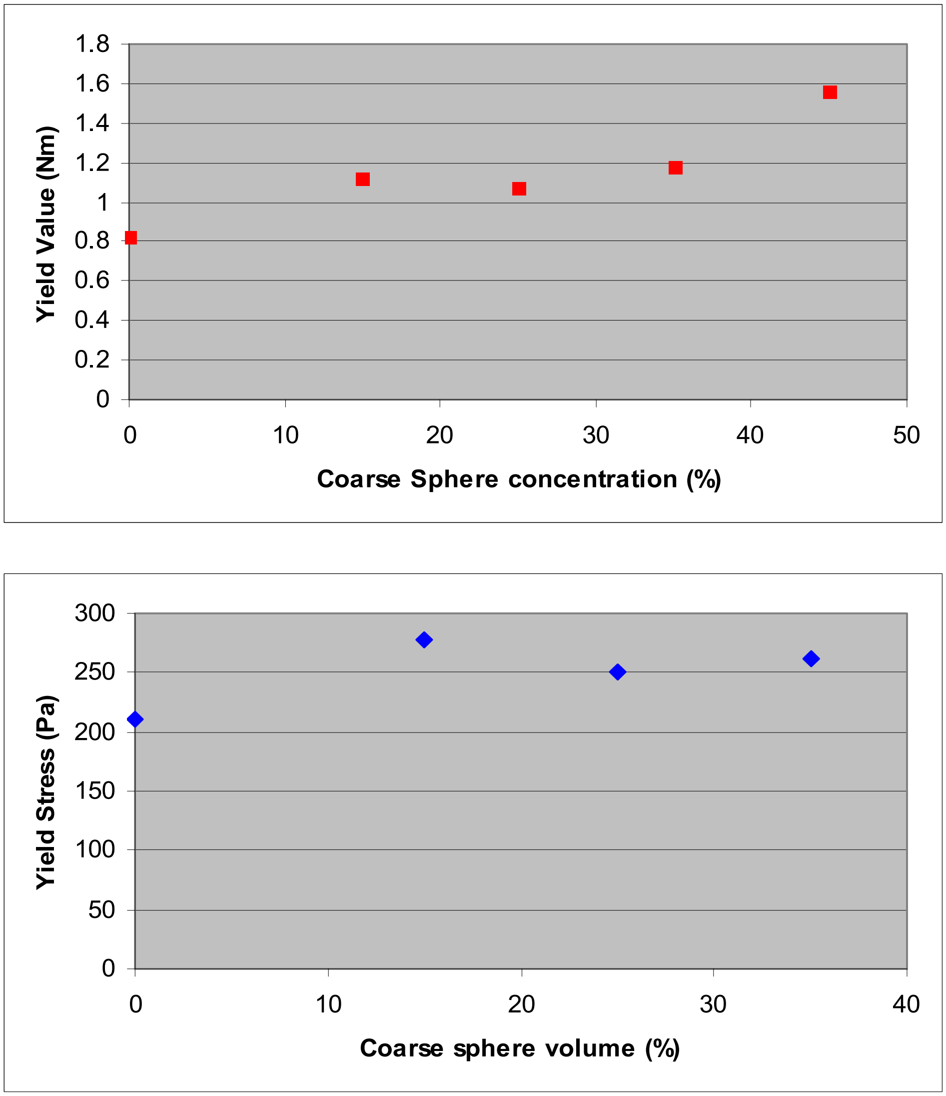

Figure 7.8 Yield values and yield stress for the concrete made using and increasing volume of of spheres

It can be seen that the yield stress values slightly increase (somewhat linearly) with increasing sphere content, as expected. This increase is small, however, perhaps because yield stress is less dependent on coarse aggregate properties than on mortar or cement paste properties, particularly at lower coarse particle contents (thus the linear curve).

Figure 7.9 shows the yield value and yield stresses for the concrete made using cubes at increasing coarse particle contents (Note: Results could not be obtained for the mixture containing 45% of mono-sized cubes as the torque required exceeded the maximum allowed by the rheometer).

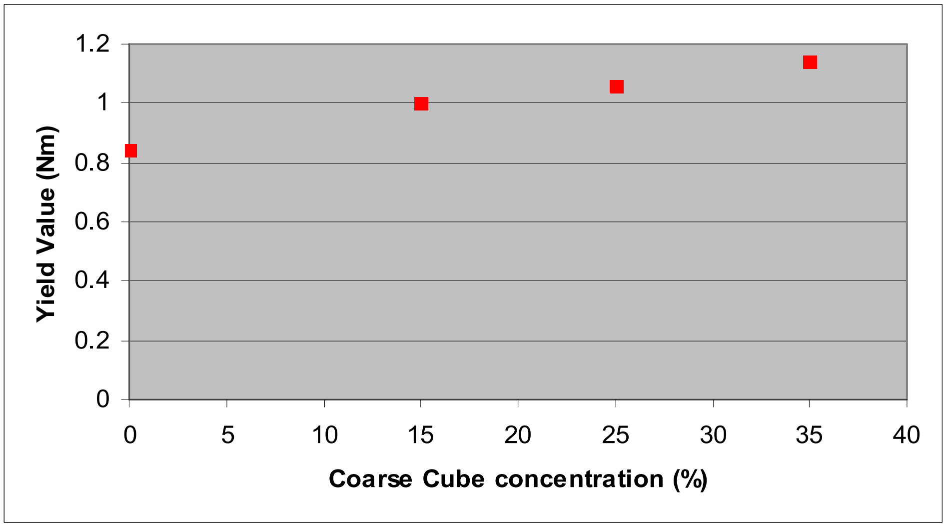

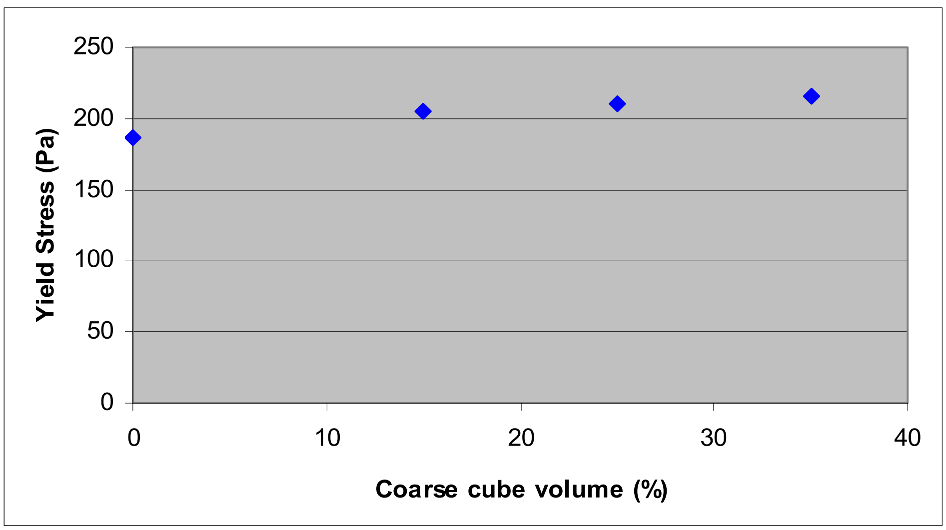

Figure 7.9 Yield values and yield stress for the concrete made using an increasing volume of cubes

Similar to the case of the spheres, the yield stress value increases as the coarse particle content increases, again somewhat linearly. Figure 7.10 shows the normalized yield values and yield stresses calculated for the concretes made using spheres and cubes. The normalization is done by dividing the values calculated for each test case by the value calculated for the mortar (0% artificial coarse particles) case (all curves start at 1.0).

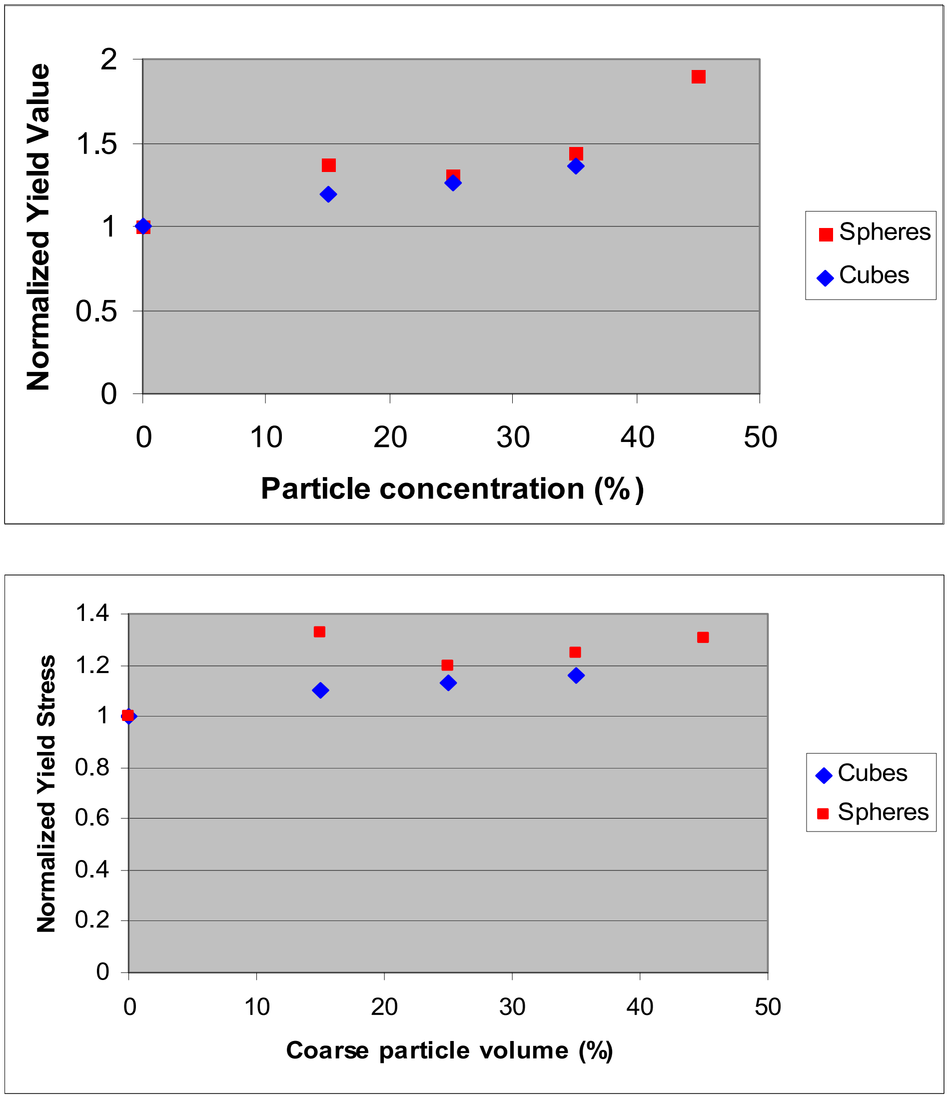

Figure 7.10 Normalized yield values and yield stresses for the concretes made using spheres and cubes, at increasing coarse contents

A comparison of the yield stress values for the spheres and cubes at identical particle contents reveals that the values are close, further suggesting that the yield stress of a concrete mixture may be more dependent on its paste or mortar characteristics than its coarse aggregate characteristics, such as shape, at least in the mono-sized coarse aggregates case.

Figure 7.11 shows the viscosity values and the plastic viscosity calculated for the concrete made using an increasing volume of spheres.

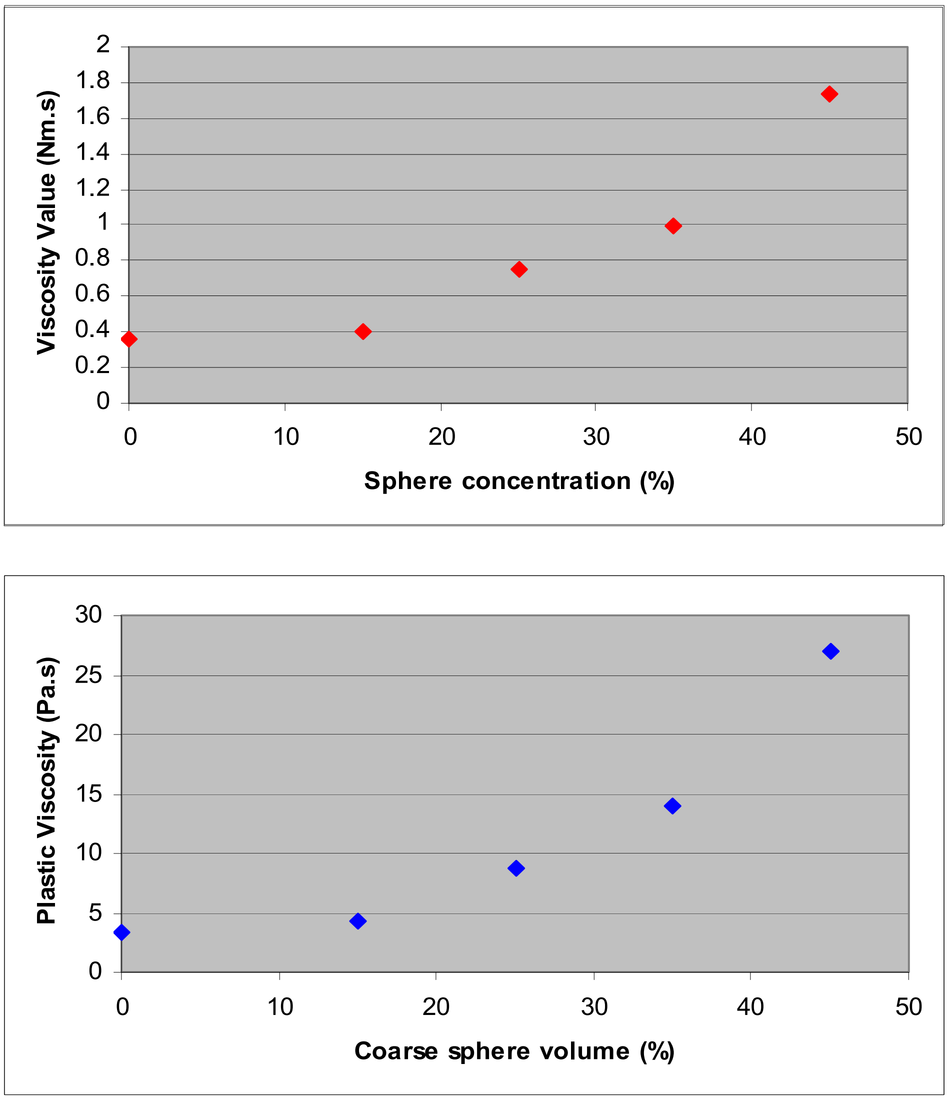

Figure 7.11 Viscosity values and plastic viscosity for the concrete made using spheres at increasing coarse particle contents

It is seen that the plastic viscosity increases significantly with increasing artificial coarse particle content. The rate of the increase increases considerably beyond 15%

particle content by volume. This is most likely due to an increased number of particle interactions. Below 15%, the mixture is still relatively dilute and there are probably not very many particles touching other particles as they move about in the mixture. Also, the particles probabilistically are far enough from each other that the trajectory of one does not appreciably affect the flow of another. Beyond 15%, the mixture begins to get concentrated enough that particles start contacting each other and interparticle forces (through contact and no contact) affect the total viscosity of the mixture. It can also be seen that the relative increase in viscosity value due to increasing particle concentration is less than the increase in plastic viscosity. This is expected because the portion of the mixture which actually flows in the rheometer gets smaller with increasing particle concentration (the dead zone gets larger), and the torque measured by the rheometer is actually required to make less concrete flow than assumed, so is lower than what would be needed for the whole (assumed) amount. When this correction is made, the relative viscosity result at a given particle concentration increases. Figure 7.12 shows the viscosity values and plastic viscosity calculated for the concrete made using an increasing volume of cubes.

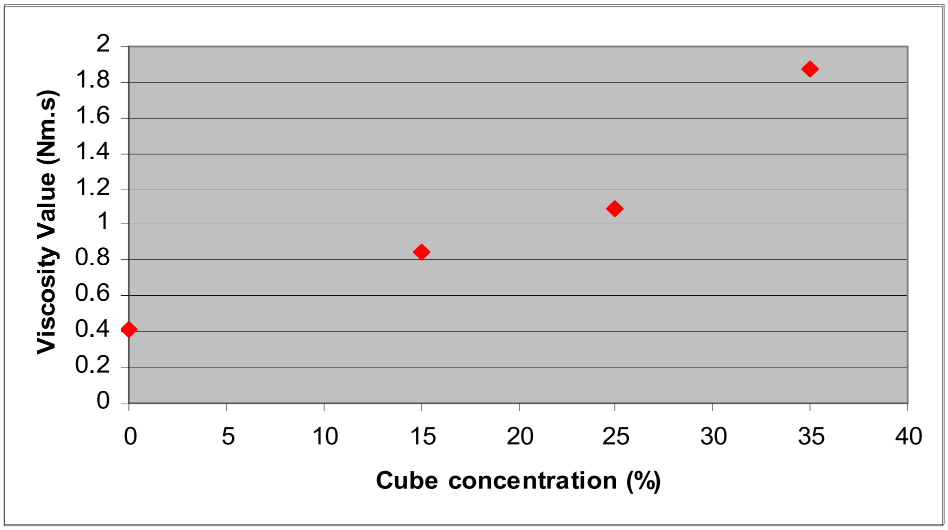

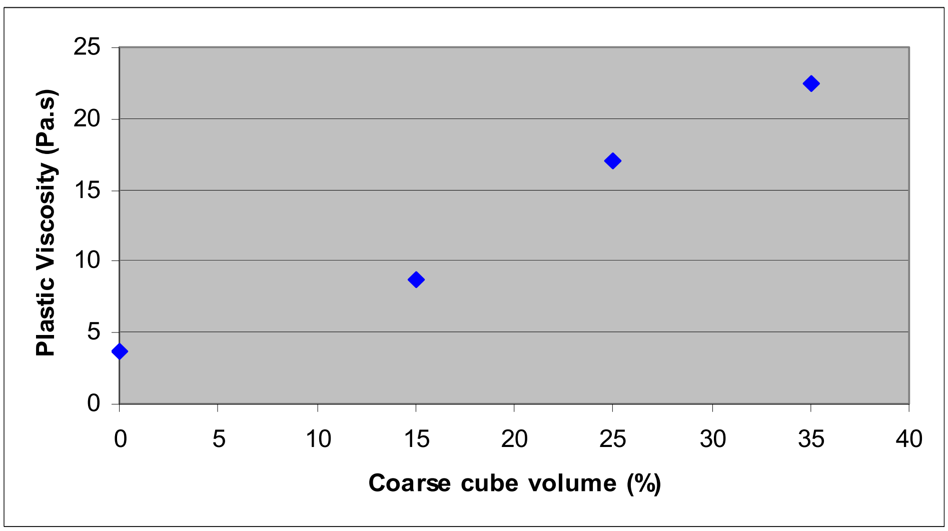

Figure 7.12 Viscosity values and plastic viscosity for the concrete made using cubes at increasing coarse particle contents

Similar to the case of the concretes made using the spheres, the plastic viscosity increases significantly with increasing artificial coarse particle content. It must be noted that the increase in the rate of the increase (slope of the curve) is apparent even at particle contents lower than 15% by volume. This is a manifestation of the shape of the cube. The flow of cubes is worse (requires a higher torque at a given shear rate) than that of spheres, even in relatively dilute solutions where particle contacts are not common. Once again, the relative increase in viscosity value is less than that of plastic viscosity, at any given concentration, due to the correction to account for the dead zone. Figure 7.13 shows the normalized viscosity values and plastic viscosities calculated for the concretes made using increasing volumes of spheres and the cubes.

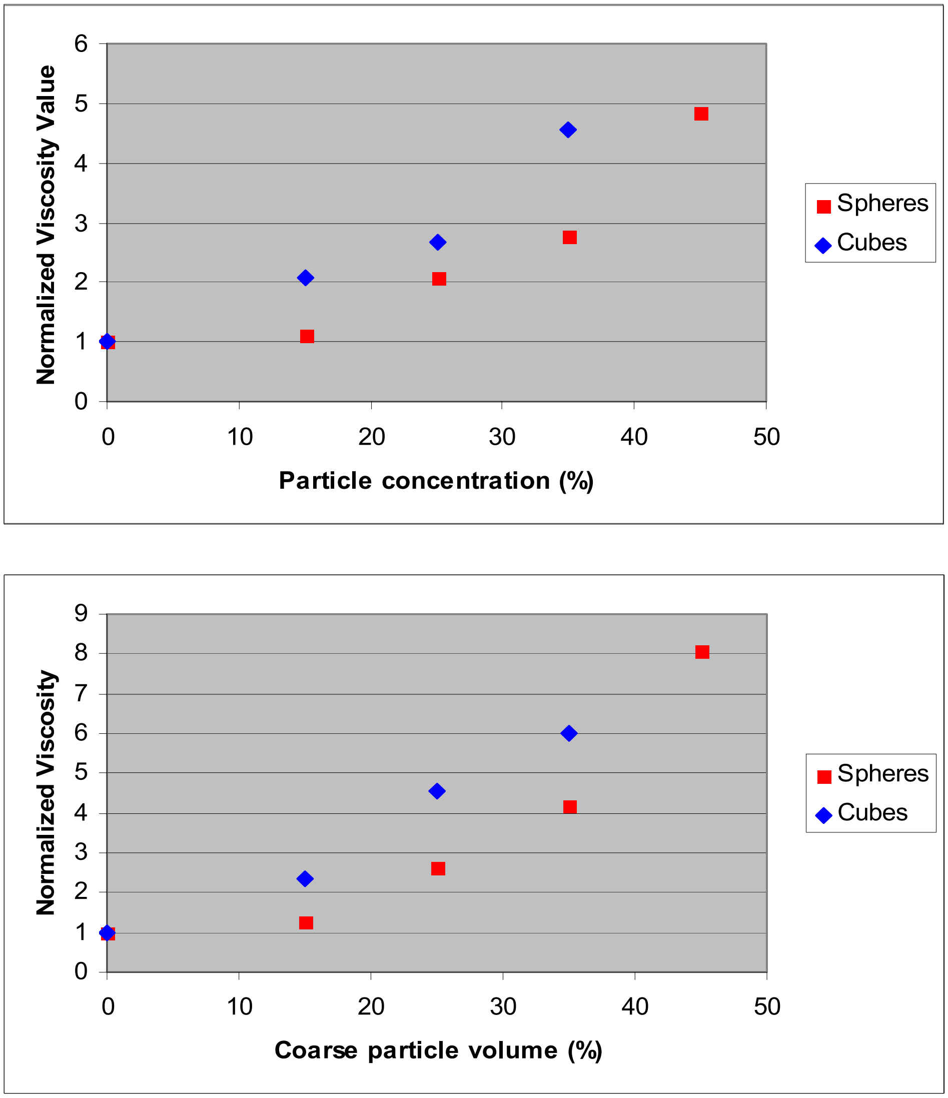

Figure 7.13 Normalized viscosity values and plastic viscosities for the concretes made using spheres and cubes, at increasing particle contents

A comparison of the curves for the concretes made using the two different shapes very clearly shows that coarse aggregate particle shape has a significant effect on the plastic viscosity of a concrete mixture, at least for the mono-sized, equal volume case.

Not only is the cube mixture noticeably more viscous than the sphere mixture at all coarse particle contents, but also the difference in viscosities increases with increasing particle content. This is consistent with the idea that particle interactions (with or without contact) increase with increasing particle concentration and that cubes affect the flow of nearby cubes much more than spheres affect the flow of adjacent spheres.

A comparison of the normalized empirical viscosity values, the predictions of the Krieger - Dougherty model, and the Einstein model for a system of mono-sized spheres is given in Figure 7.14.

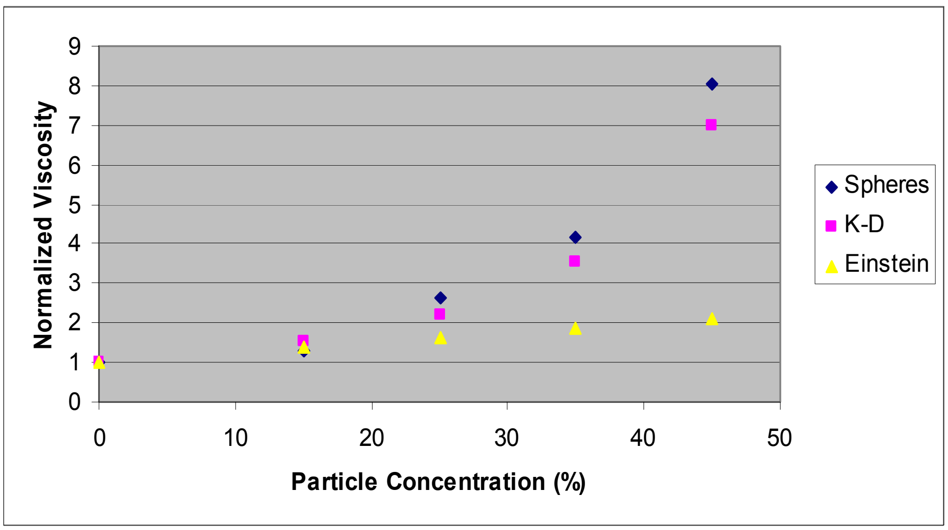

Figure 7.14 Change in viscosity for a system of mono-sized spheres with increasing concentration, as predicted empirically and theoretically by the Einstein model and the Krieger-Dougherty model

It is seen that the Einstein model works satisfactorily up to approximately 15% particle concentration. The Krieger – Dougherty model, used with the intrinsic viscosity value of 2.5 (for spheres) and maximum packing fraction of 0.64 (for random packing of spheres – although this is not the maximum for spheres, it satisfies the requirement for the Krieger – Dougherty equation that the maximum packing is when there is three dimensional contact between the particles and the viscosity is infinity) appears to correlate well with the measured data up to about 20% coarse spheres concentration, above which it calculates values lower than those measured.

It is not possible to similarly compare the measured and predicted viscosity for the case of single-sized cubes as the intrinsic viscosity value is empirical and cannot directly be measured. Empirical results can be used to back-calculate an estimate of the intrinsic viscosity for the system, though this requires knowledge of the maximum packing fraction for a mixture of mono-sized cubes, which is not constant but dependent on the packing conditions. The intrinsic viscosity for cubes will be greater than that for spheres, resulting in higher relative viscosity values. The relative viscosity value at any given particle concentration will increase as the maximum packing fraction assumed is decreased and vice versa.

The dissipative particle dynamics (DPD) model, mentioned in Chapter 2, allows the use of irregular shapes, such as cubes, prisms, or real aggregate particles. The sphere and cube mixtures of coarse particle concentration between 0% and 45% were simulated in the DPD model and viscosity predictions were made. It is important to note that, unlike the Einstein and Krieger-Dougherty models, the DPD model does not predict a fixed viscosity value for a test case and therefore the model has to be run several times for each test case, similar to making several measurements for each test case with the rheometer, and an average value has to be calculated. The predictions of the model and the empirical results are compared, for the sphere mixtures and cube mixtures, in Figures 7.15 and 7.16

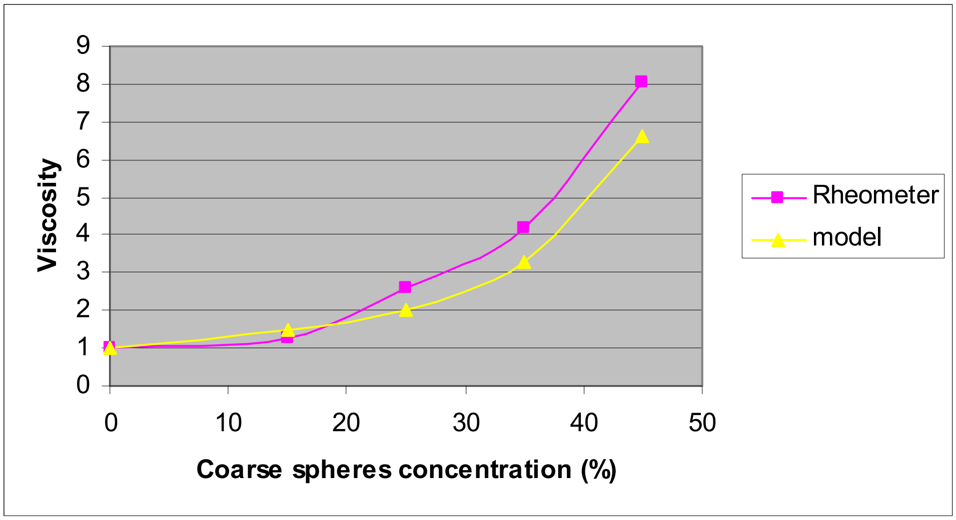

Figure 7.15 Comparison of the change in viscosity of a mixture with increasing coarse sphere concentration determined empirically and predicted by the DPD model

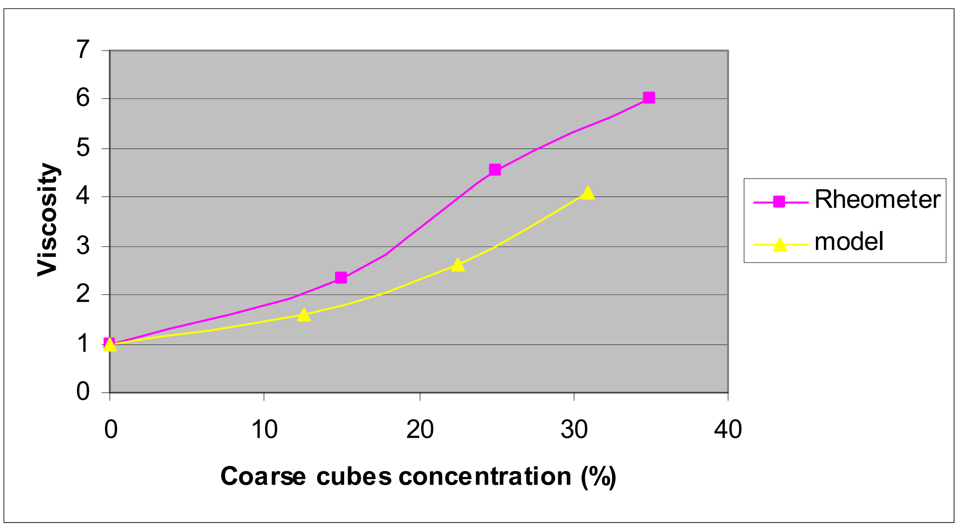

Figure 7.16 Comparison of the change in viscosity of a mixture with increasing coarse cube concentration determined empirically and predicted by the DPD model

Given the variation of the empirical results, the model is successful in predicting the increase in viscosity with coarse particle addition, for both shapes. One reason why the model predictions are lower is that the model will shear the mixture (particles in a constant viscosity medium) better or more ideally than the rheometer, that is the behavior of the particles in the simulation will be more uniform than inside the rheometer where segregation, clogging, jamming, preferential orientation of particles (due to reshoveling) etc. can occur. Another possible reason is the stiffening of the mortar medium due to ongoing hydration. Any stiffening is ignored in this research, however increases on the order of 1.25 times have been observed for the plastic viscosity of mortar mixtures, after about 25 minutes. A better way to normalize the viscosity at each concentration is then to use the viscosity of the mortar at the time the measurements are being made. This, however, would require making a second mixture (with the same properties as the medium) to be tested for the effects of aging, or sieving a part of the suspending material (mortar) out of the mixture and testing it with another rheometer. Nevertheless, the predicted values are close to the empirical values, and this is a very important step for developing confidence in the model and its ability to handle real concrete aggregates which are irregularly shaped. Although mono-sized spheres and cubes are a simplified case for rheological experiments, they in fact present a non-ideal and difficult flow situation, and it is significant that this flow can be predicted closely. This model can eventually serve as a very important tool for predicting concrete rheology in the VCCTL and experimental verification of different aspects of the model are essential.

7.2.4 Tests to Investigate the Dependence of Yield Stress (as measured by the Slump Test) on Fine and Coarse Aggregate Content and Particle Shape

The results of the rheometer tests, presented in the previous sections, suggested a weaker dependence of yield stress of a concrete mixture on the amount of coarse particles used and their shape, at least for the mono-sized case, than the plastic viscosity of a mixture. It was seen that coarse particle content seemed to increase yield stress approximately linearly and that there was not a significant difference between the yield stress values calculated for the two mixtures having similar mortars but using the spheres and the cubes as the coarse particles, respectively.

As stated previously, research has shown that the ASTM C143 slump test relates to the yield stress of a concrete mixture (Koehler, 2004). It was decided that a series of mixtures could be tested for slump values in an attempt to observe the influence of fine aggregate content, coarse aggregate content and coarse aggregate particle shape on the yield stress of a mixture. Some tests were also run on mixtures with varying water-cement ratios. Prior to the testing, it was expected that altering the water-cement ratio of a mixture would alter the slump value measured considerably and that altering the fine aggregate content in mixtures for which the water-cement ratio did not change significantly or changing the coarse particle shape in mixtures of which the water-cement ratio and coarse particle content were comparable would not affect the slump value significantly. It must be noted however, that research suggests (Koehler, 2004) that the slump test is suitable for particles of size 25.4 mm (1in.) or smaller, and the diameter of the spheres and cubes were approximately 32 mm and 40 mm, respectively.

7.2.4.1 The Effect of Fine Aggregate Content

Figures 7.17 and 7.18 show the change in the measured slump values, the cement and water contents, water-to-cement ratio, and sand-to-cement ratio for a mortar mixture, as sand is added to the mixture between each consecutive measurement, while the amounts of other constituents (cement, water) are held constant.

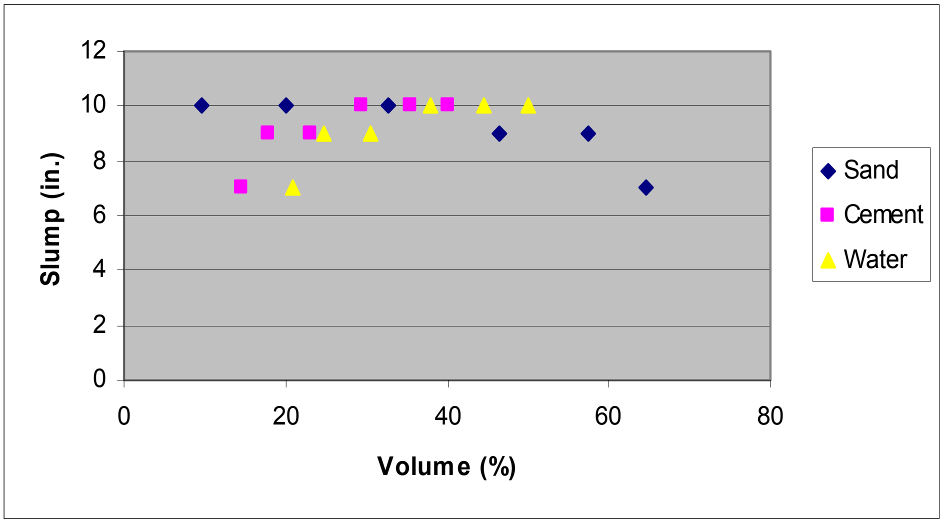

Figure 7.17 Change in the slump value and sand, cement, water contents for a mortar mixture, as the sand content is increased

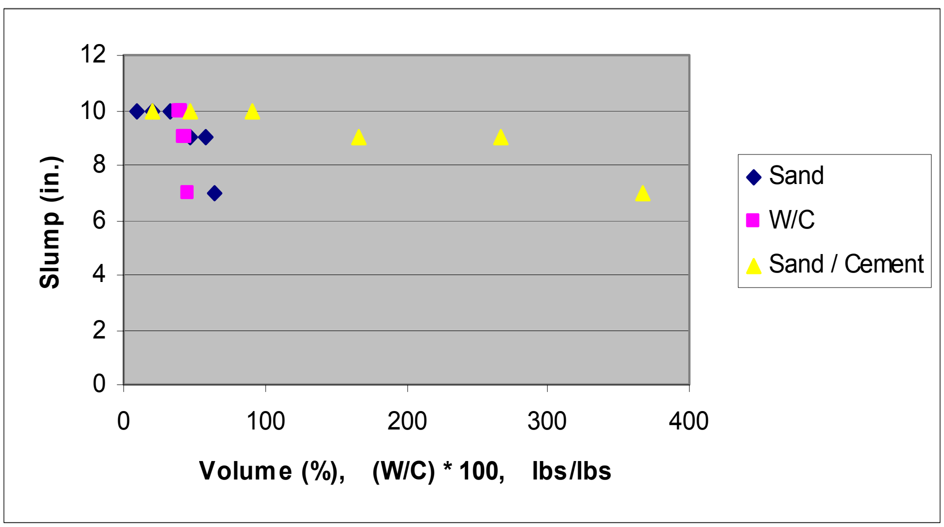

Figure 7.18 Change in the slump value, water-to-cement ratio, and sand-to-cement ratio for a mortar mixture, as the sand content is increased

It can be seen that the slump of the mortar decreases slowly and only after there is about 40% sand by volume. The percentages of cement and water (by volume) decrease, as their contents are being kept constant and the amount of sand is increased. The total volume at any slump value equals 100% (water + sand + cement). Figure 7.17 shows that the W/C for the mortar increases slightly because of the moisture contribution from the added sand. This change is from about 0.40 to 0.45. The sand-to-cement ratio increases significantly, about five fold, before any change in slump is observed. These results suggest that the effect of changing the fine aggregate content of a mortar mixture on slump is minor and less pronounced than that of water-to-cement ratio (as results that follow also show). Figure 7.19 compares the relationship between the water-to-cement ratio and the slump value with the relationship between the sand-to-cement ratio and the slump value for increasing sand content.

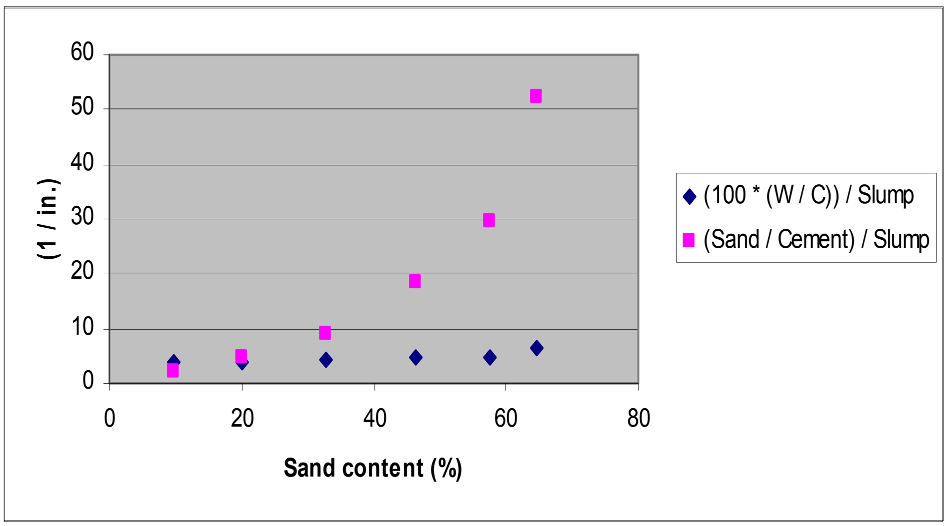

Figure 7.19 Comparison of the relationship between water-to-cement ratio and the slump value with the relationship between the sand-to-cement ratio and the slump value, for increasing sand content

7.2.4.2 The Effect of Coarse Aggregate Content and Shape

Figures 7.20 and 7.21 show the change in the slump values for mortar mixtures and sand, water, and cement contents as coarse aggregate particles are added to the mixture between each consecutive measurement, while the amounts of other constituents (cement, water, sand) are held constant.

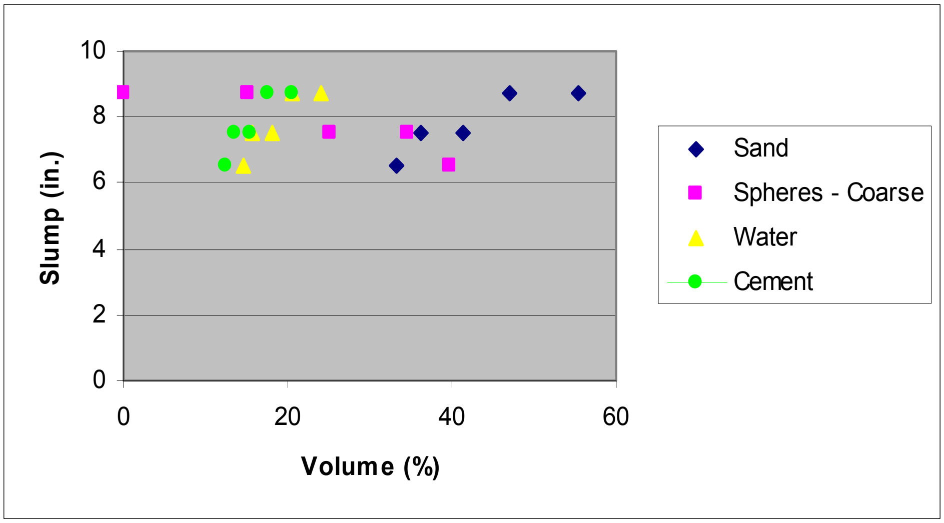

Figure 7.20 Change in the slump value and sand, cement, water, coarse spheres contents, as the sphere content is increased

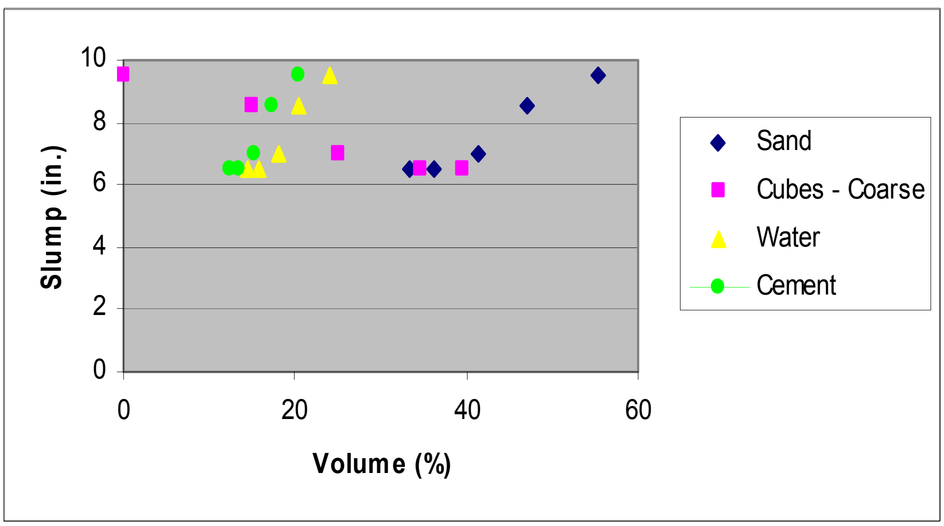

Figure 7.21 Change in the slump value and sand, cement, water, coarse cubes contents, as the cube content is increased

The volume contents of the artificial coarse particles, the spheres and the cubes, increase from 0% (the mortar case) to 40%. The slumps of both mixtures decrease slightly, approximately linearly, between 15% and 40% coarse content by volume, similar to the yield stress measurements made using the rheometer, presented in the previous sections. The sand in the mixture decreases naturally as the sand mass is kept constant. The water-to-cement ratio for the mixtures remains constant, as can be seen in Figures 7.22-7.23, as the moisture content of the coarse particles is assumed to be and is approximately zero.

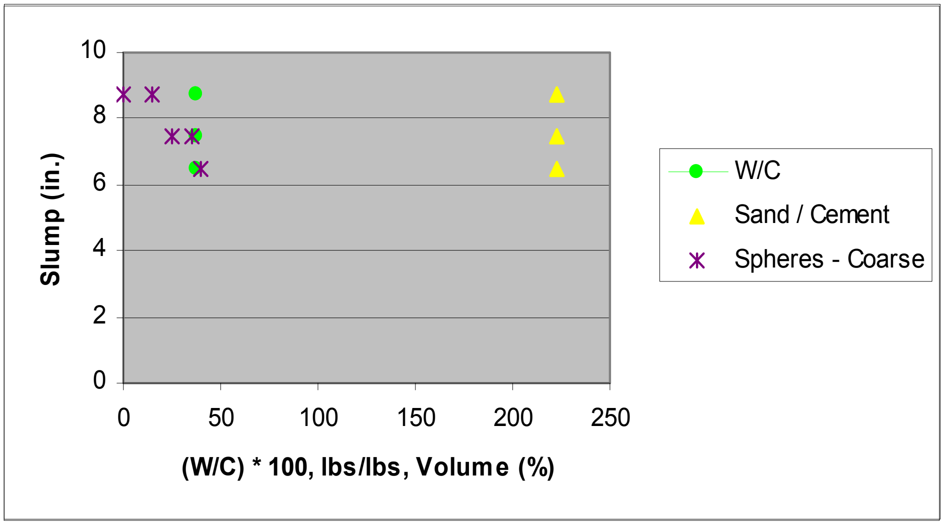

Figure 7.22 Change in the slump value, water-to-cement ratio, and sand-to-cement ratio, as the coarse sphere content is increased

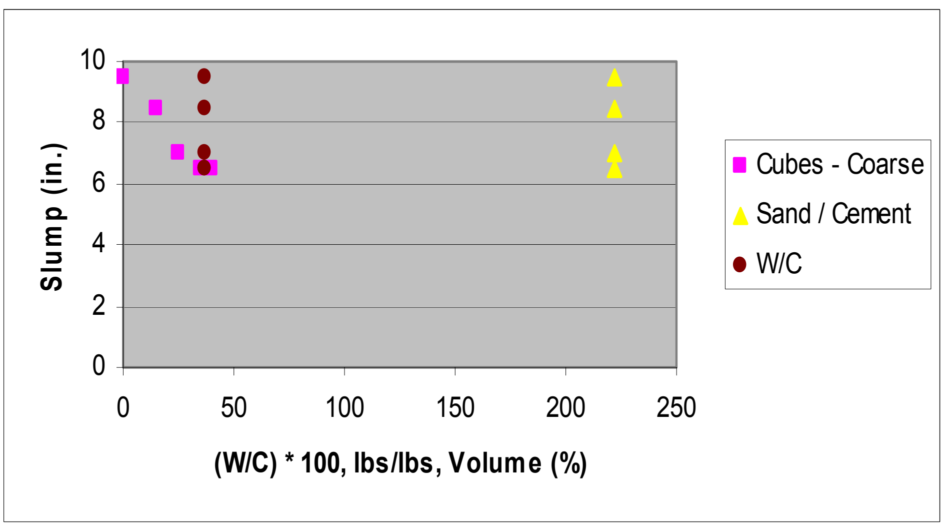

Figure 7.23 Change in the slump value, water-to-cement ratio, and sand-to-cement ratio, as the coarse cube content is increased

The sand-to-cement (S/C) ratio is also constant which makes it possible to attribute the decrease in slump to the increasing coarse particle content. This is also evident from Figures 7.24 and 7.25, which compare the relationship between the water-to-cement ratio and the slump value with the relationship between the sand-to-cement ratio and the slump value, for increasing sphere and cube contents, respectively, since the change in (W/C)/slump and (S/C)/Slump values is small.

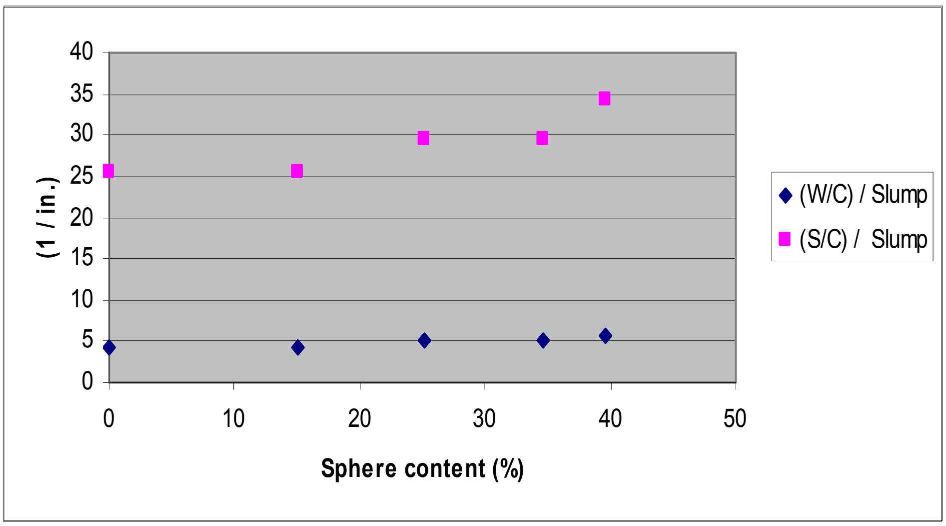

Figure 7.24 Comparison of the relationship between water-to-cement ratio and the slump value with the relationship between the sand-to-cement ratio and the slump value, for increasing coarse sphere content

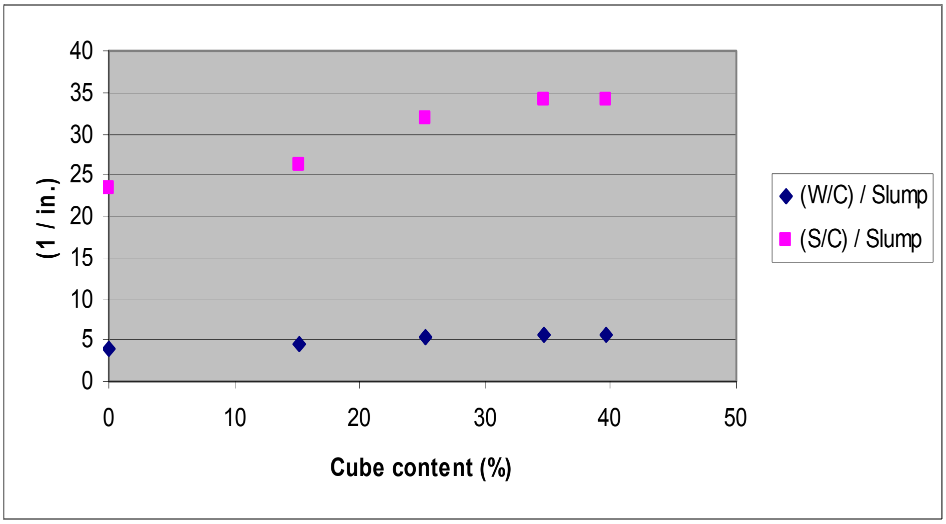

Figure 7.25 Comparison of the relationship between water-to-cement ratio and the slump value with the relationship between the sand-to-cement ratio and the slump value, for increasing the coarse cube content

It is seen, as predicted, that the change in slump (therefore yield stress) is less rapid with significant changes in coarse particle content, than with even a small change in the water-to-cement ratio. It can also be concluded, at least for the mono-sized particles case, that coarse aggregate shape does not have a considerable effect on the slump of a mixture, since the total change in slump and trend is similar for the spheres and the cubes.

7.2.4.3 The Effect of Water-Cement Ratio

The effect of water-to-cement ratio on yield stress was examined by keeping the fine and coarse aggregate contents constant. Both the artificial spheres and the cubes were used as the coarse aggregate, at a fixed volume of 35%, in two separate mixtures. Figures 7.26 and 7.27 show the change in the measured slump values, and sand, water, cement contents, as water is added to the mixture between each consecutive measurement, while the amounts of other constituents (cement, sand, and coarse particles) are held constant.

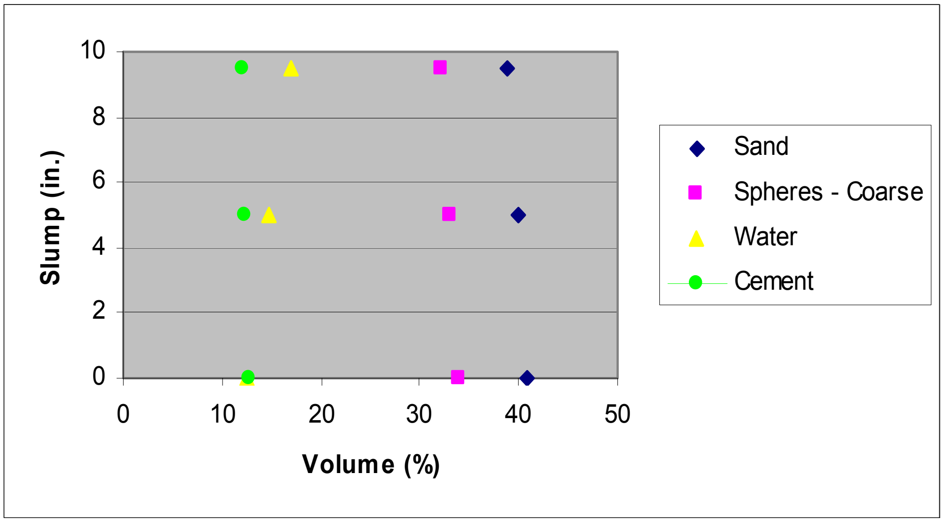

Figure 7.26 Change in the slump value and sand, cement, coarse sphere contents, as the water content is increased

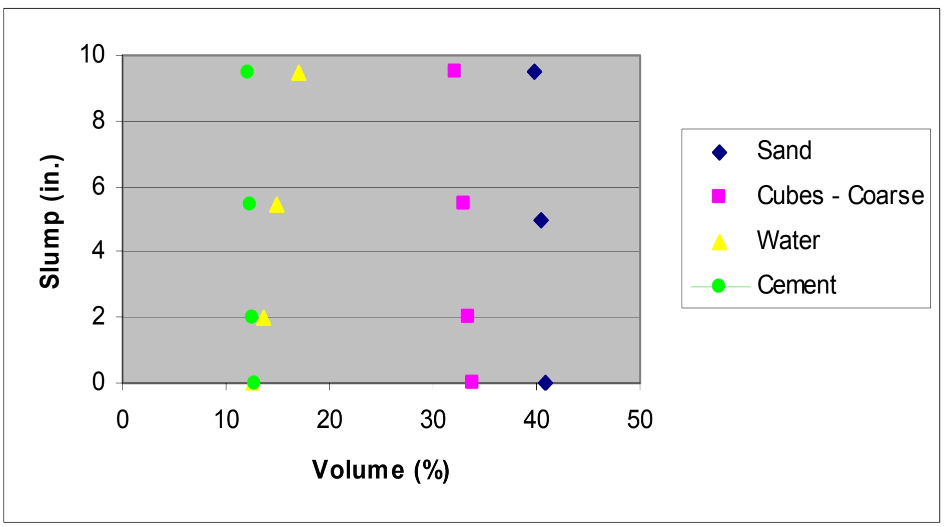

Figure 7.27 Change in the slump value and sand, cement, coarse cube contents, as the water content is increased

It is seen that the water content of the mixture increases from about 12.5% to 17%, while the change in cement and fine and coarse aggregate contents is very little. The change in slump for such a minor change in water content (and therefore in W/C), especially when compared to the small changes in slump caused by large changes in fine or coarse aggregate content, is noteworthy. Once again, it is seen that the shape of the coarse particles does not seem to have a noticeable effect on slump value (yield stress). Figures 7.28 and 7.29 further support this finding.

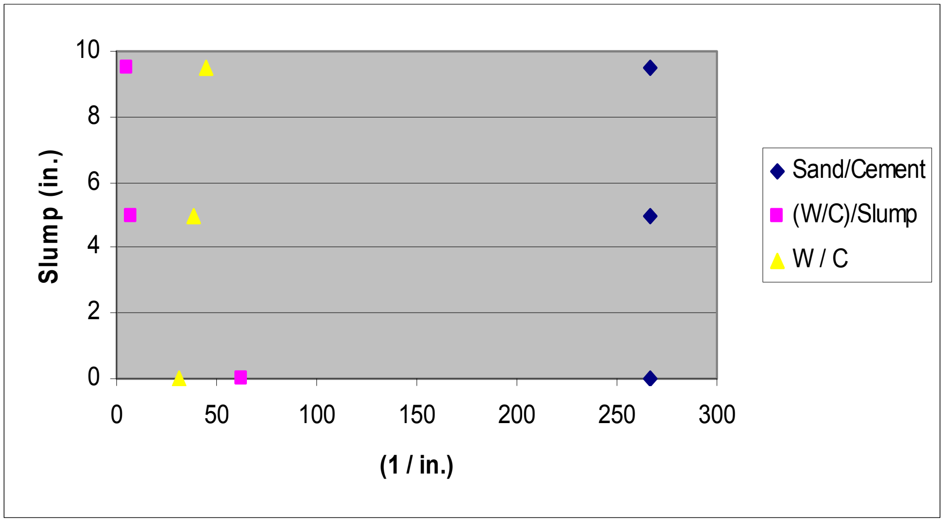

Figure 7.28 Comparison of the relationship between water-to-cement ratio and the slump value with the relationship between the sand-to-cement ratio and the slump value, for increasing water content, for a mixture using coarse spheres

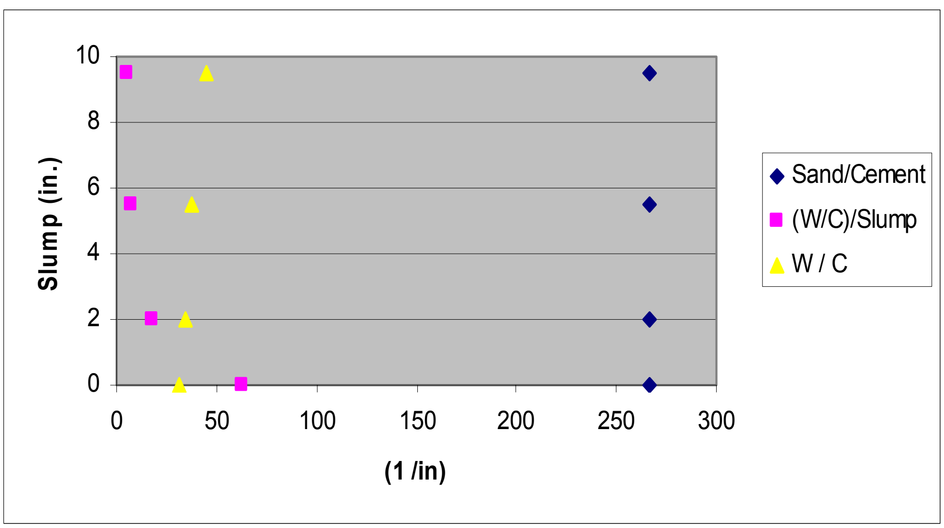

Figure 7.29 Comparison of the relationship between water-to-cement ratio and the slump value with the relationship between the sand-to-cement ratio and the slump value, for increasing water content, for a mixture using coarse cubes

7.2.5 Mixtures Made Using Two Different Combinations of Spheres and Cubes

With previous tests having provided some approximate yield stress and viscosity values for mixtures made using mono-sized spheres and cubes, it was decided that mixtures of these two shapes would be interesting to study. Two different combinations - two-thirds spheres and one-third cubes, and one-third spheres and two-thirds cubes - were tested. Prior to the tests, it was expected naturally that both of the viscosity results would be between those for the case of all cubes and case of all spheres, with the viscosity of the mixture with more cubes being higher. The position within the range (between the two limiting cases) of the values could not be predicted and would be an interesting finding. Figure 7.30 shows the normalized plastic viscosity values (against the all spheres case viscosity) measured for the mixtures made using all spheres; two-thirds spheres and one third cubes; one-third spheres and two third cubes; and all cubes.

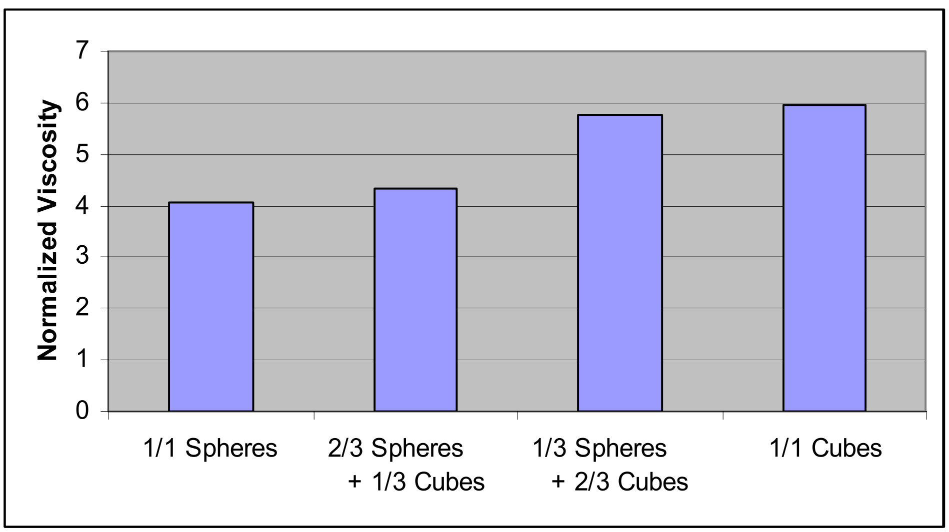

Figure 7.30 Normalized plastic viscosity for the spheres, cubes, and two combinations, at constant coarse particle concentration

The results are as expected in that the viscosity of the mixture in both combination cases lie between the two extremes of all spheres, and all cubes, with the two-thirds cube case having a higher value. It is not possible to place the values at one-third and two-thirds of the viscosity range between the all spheres result and the all cubes result, because the variation in the measured viscosity results is quite high and the range is quite narrow (approximately 1 to 2, or 100% to 200%, at 35 % coarse particle concentration).

7.2.6 Comparison of Mixtures Made Using the Four Regular-Shaped Artificial Coarse Particles

In an attempt to broaden the investigation of the influence of coarse particle shapes on flow properties, particles in the shape of flat and elongated rectangular prisms were used in addition to the spheres and cubes mentioned previously. It was difficult to predict how these shapes would affect plastic viscosity. On the one hand, they could increase viscosity since they are not equi-dimensional as are spheres and cubes, and since their surface area-to-volume ratios are higher than those of spheres or cubes. Figure 7.31 shows this ratio for the four different shapes.

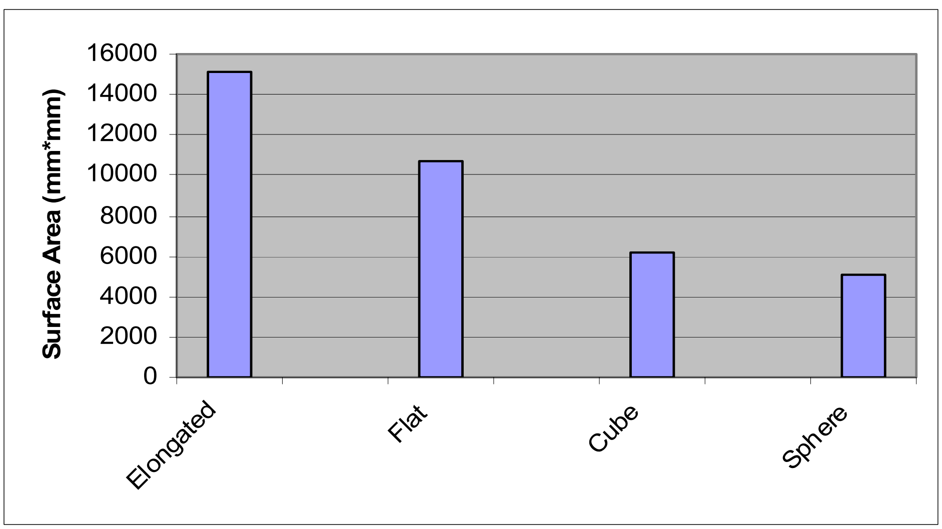

Figure 7.31 Surface area-to-volume ratio for the four regular shapes

The maximum chord within the shapes is also largest for the two rectangular prisms, which could have an effect on the results in the mono-sized particles case. Figure 7.32 shows the maximum diameter/chord lengths for the four different shapes.

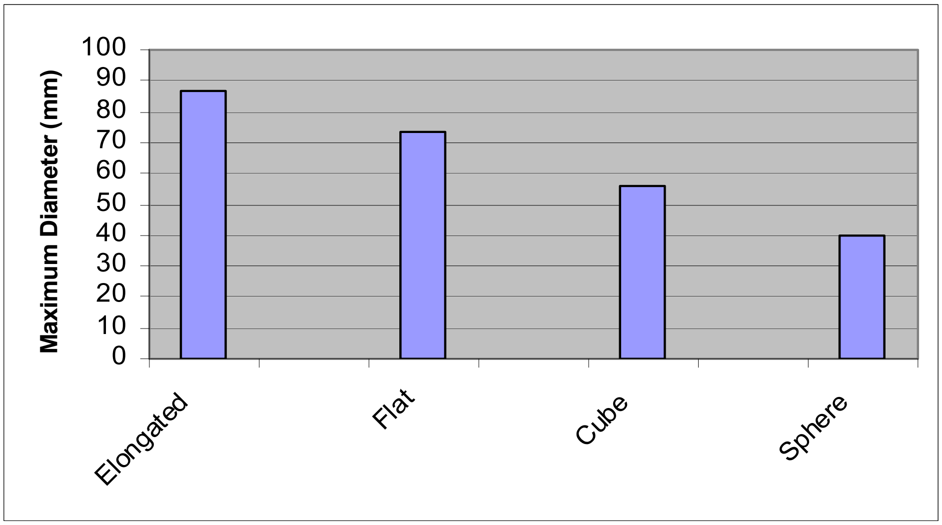

Figure 7.32 Maximum diameter/chord length for the four regular shapes

As mentioned in previous chapters, flow behavior is very complex and cannot be predicted by looking at a single parameter such as the ones given here. However, for the mono-sized case, these parameters may be useful to some extent.

On the other hand, another researcher has found (Martys, 2004), through the use of computational models, that flat particles at volume concentrations above 15-20% can result in a lowering of the suspension (concrete) viscosity due to their tendency to align (an slide past each other more easily), to lower than even the viscosity of an equivalent system (equal volume and concentration of particles) of spheres.

The results of tests on three mixtures with a constant amount of the four regular shaped aggregates are given in Figure 7.33.

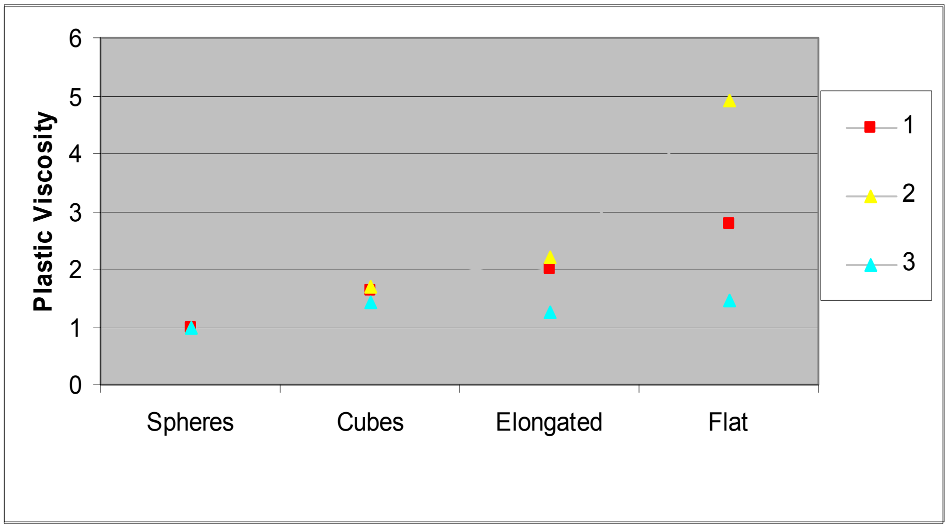

Figure 7.33 Plastic viscosity of three sets of mixtures with a fixed amount of the four regular shapes

It is seen, unfortunately, that the variation in the measured viscosities are affecting the trends, and it is not possible to conclude anything based on these results. The expected increase in viscosity for the rectangular prisms is seen in some but not all the cases. A lowering of viscosity due to flat particles is not seen. There can be several reasons for this, even assuming that the results are meaningful. First, the flat particles modeled by Martys are oblate ellipsoids and have smooth sides and no edges. The artificial flat particles used are not smooth around the edges which will clearly alter the flow of particles past each other. Second, the size of the flat particles is probably too large for the size of the vane used to take advantage of the potential alignment of the particles. Given the direction of flow in a concentric cylinders rheometer, the particles would have to be aligned with their flat sides nearly perpendicular to the vertical axis (center of the cylinders). In this position, the flat prisms would be about 50 mm long in an outward radial direction. Given that the vane used has only a 127-mm radius, and that only a part of the mixture flows due to the presence of a dead zone, such an alignment may not be taken advantage of experimentally. Third, the breakdown period may not provide sufficient shear to align the particles which will obviously be randomly oriented upon filling of the container. Similarly, the remixing of the mixture while still inside the container will probably tend to orient flat particles vertically, which will further reduce the possibility of observing this phenomenon.

7.3 Results of the Texture Test Cases

Relative and absolute rheological values, calculated using the same procedure as in the shape test cases, and an analysis of the results are presented.

7.3.1 Comparison of Smooth Marbles with Rough Marbles at Increasing Coarse Particle Contents

Prior to these tests, it was expected that the mixtures made using the smooth marbles would have a lower viscosity than the mixtures made using the rough marbles. However, it was expected that the effect of uniform surface texture would be less than that of overall shape. A smaller difference between the viscosities was anticipated at lower coarse particle concentrations, since the large spacing between the particles would reduce their effect on each other. However, since the effect of surface roughness of a single particle on the forces, developed at its marble-mortar interface, and therefore on its flow behavior, were not well known, this was not very clear. A higher difference in the viscosity of the smooth and rough marbles mixtures was expected at higher particle concentrations. Nevertheless, some researchers have found experimentally that fine-scale surface texture can actually improve flow, decreasing viscosity by influencing the spacing between the surfaces of adjacent particles, and preventing them from coming into contact (Davis et al., 2003). For this reason, the predictions of the outcome of these tests were mostly based on intuition.

The coarse particle contents ranged from 0% (mortar case) to 40% by volume. Figure 7.34 shows the normalized viscosity values and plastic viscosities for the mixture made using smooth and rough marbles with increasing coarse particle contents.

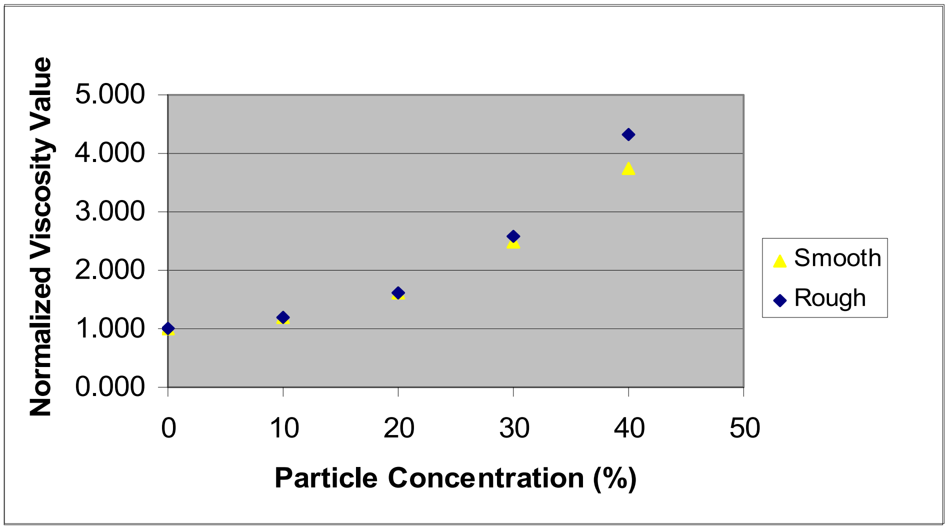

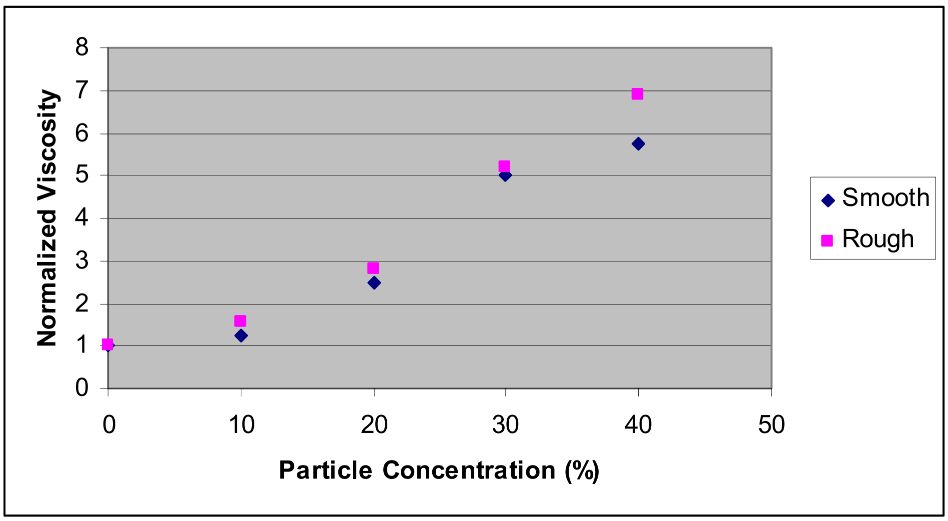

Figure 7.34 The change in viscosity value and plastic viscosity for mixtures made with increasing smooth and rough marble concentrations

It is seen that, as expected, the viscosity of a mortar mixture increases with increasing marble volume, for both the smooth and rough marbles cases, at both water contents. The trend in the increase is similar to the results for larger coarse spheres presented in section 7.2.3. The increase in relative viscosity of the mixture is slow or even negligible until about 15 % marbles have been added and more rapid, increasingly increasing, beyond about 20 % marbles.

It appears that the normalized effect of surface texture on viscosity does not change much with changing viscosity of the paste or mortar medium, for the two cases tested. While these two mixtures had noticeably different flow, it may be interesting to test mixtures with very high water content to see if the change in the normalized viscosity values with increasing coarse particle contents will be the same. It seems logical that above a certain water content (below a certain mortar paste viscosity), segregation would occur, influencing the effect of aggregate particles on concrete viscosity.

It is also seen that the mixtures made using rough marbles have slightly higher viscosity values than the mixtures made using smooth marbles, since the particle concentration reaches values more representative of concrete. This difference, however, is small and values are within experimental error, making it hard to conclude that the use of rough, textured mono-sized marbles in a mortar mixture increases viscosity more than or less than the use of smooth surface marbles. In addition, the coating on the rough marbles is not perfectly uniform, so the small difference in viscosity could also be partially due to the deviation from a perfect spherical shape. What is possible to conclude is that coarse particle surface texture does not significantly affect the viscosity of a mortar mixture, at least for the mono-sized spheres of the size used in these tests and that the overall shape of coarse particles has a greater influence on rheological properties of a mortar mixture than their fine-scale texture.

Comparing the effect of marbles on viscosity, and that of the spheres for which results were shown in section 7.2.3, it is seen that there is a small discrepancy between the viscosity values at higher coarse particle concentrations. This may be due to the differences in the size of the spheres relative to the diameter of the rheometer container, which is about 0.1 for the larger coarse spheres (table tennis balls) in section 7.2.3, and 0.06 to 0.07 for the smaller coarser spheres (smooth and rough marbles).

Figure 7.35 shows the normalized yield values and yield stresses for the mixtures made using smooth and rough marbles at increasing coarse particle contents.

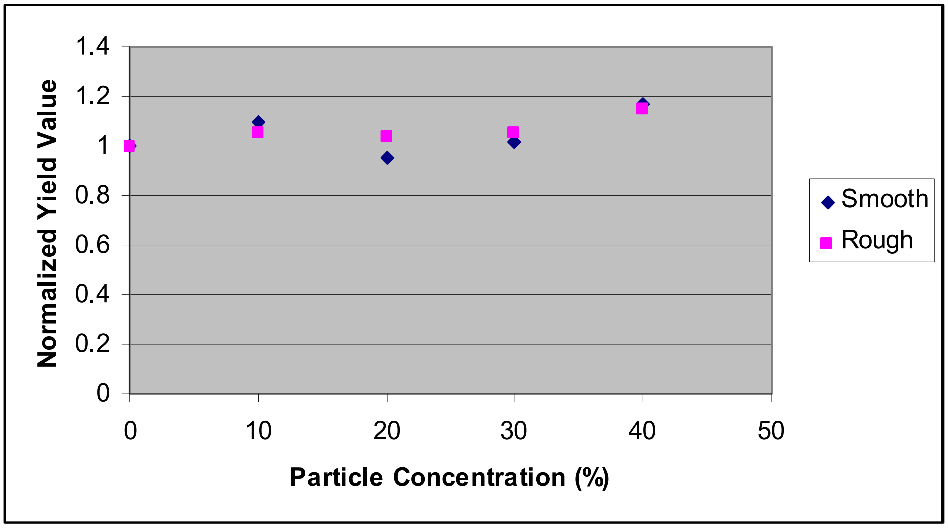

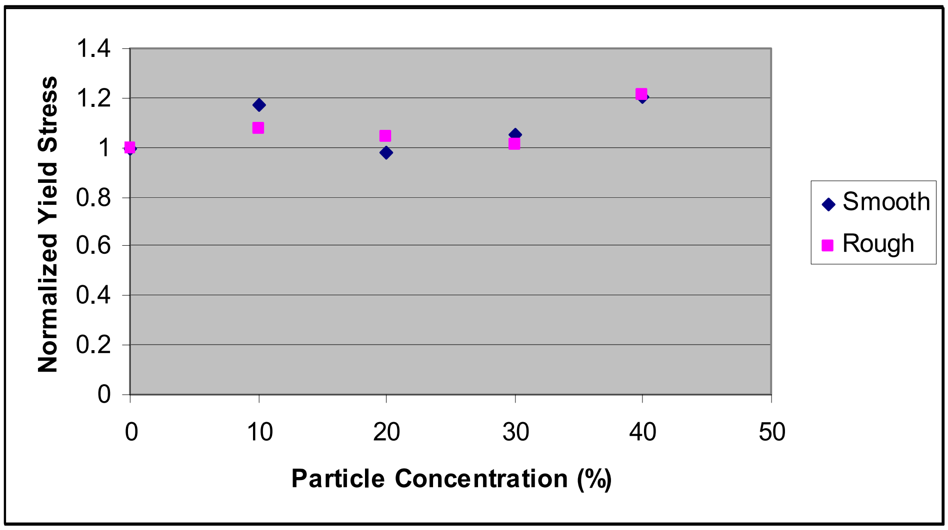

Figure 7.35 Yield value and yield stress for the mixtures made using smooth and rough marbles at increasing concentrations

Figure 7.35 indicates that the relative yield stress values for the mixtures are not affected by the increase of the concentration of smooth marbles nor that of the rough marbles, for the water content cases tested, until a coarse particle concentration above 30% is reached. This result is somewhat consistent with the results in previous sections, in that the major factor influencing the yield stress of a mortar mixture is water-cement ratio. It would be expected that the yield stress values would increase slightly, based on the previous results, with increasing marble content; however, this is not observed. The increase in yield stress is not sufficient to conclude that increasing marble content increased yield stress. There is too much variation in the individually measured values for the mortar mixtures at specific marble concentrations. It also appears that surface roughness does not have a noticeable effect on yield stress of the mixture. This is expected since overall particle shape did not have an influence on the yield stress of the mixtures in the previous sections, at least for the degree of roughness and the mono-sized particles tested.

7.3.2 Comparison of Coated and Uncoated, Rough Glass Beads in Mortar Rheology

To further investigate the influence of particle surface texture on flow properties, glass beads coated with silica fume were used, as described in Chapter 6. Figure 7.36 shows the change in the torque required to shear a cement paste, and two mortar mixtures made by adding uncoated glass beads or coated glass beads, at 40% concentration by volume, at changing rates.

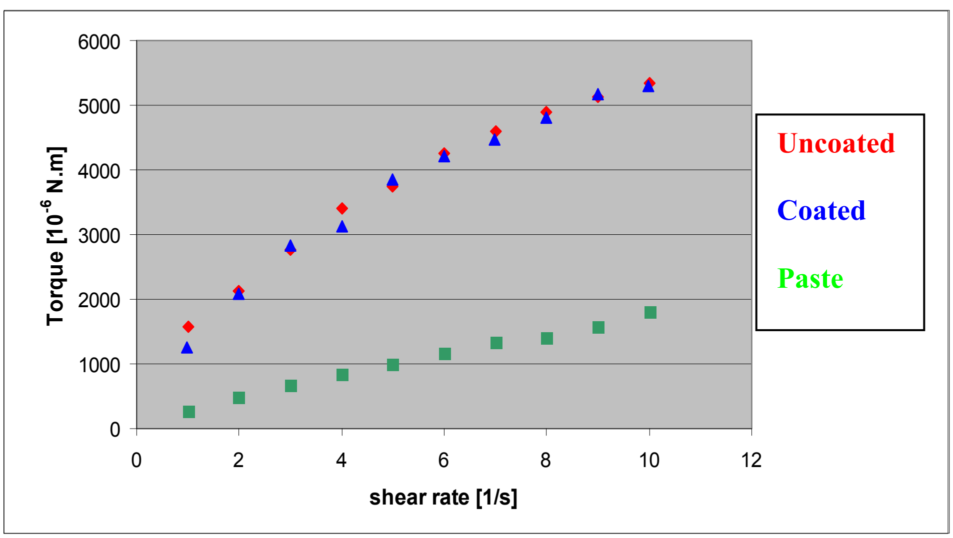

Figure 7.36 Torque required to shear mortar mixtures made using smooth glass beads, spherical beads with texture, and the paste medium.

It is can be seen that flow behaviors of the mortars made using the smooth beads and the coated beads are nearly identical. The torque required for both cases is higher than that required to shear the paste medium (with no beads) and the difference increases at higher shear rates, since the viscosity (essentially the slope of these curves) of the mortars is higher than that of the paste. Table 7.1 gives the viscosity, yield value and some mixture conditions for the mortar mixtures and the paste mixture.

Table 7.1 Results of the mortar rheology tests performed on uncoated and coated glass beads

Inclusion Type	**Concentration (%)**	**S/C**	**W/C**	**Viscosity (Pa.s)**	**Yield Stress (Pa)**
Uncoated beads	40	1.15	0.40	4.75	12.36
Coated beads	40	1.15	0.40	4.93	11.05

The torque measured for the coated beads is slightly lower than that for smooth (uncoated) beads for most of the shear rates but not for all data points and the difference is less than two percent for most, which could be due to equipment error or minor differences in water content. Similarly, it is difficult to conclude that the difference in the viscosities and yield values of the mixtures is due to the difference in texture and not just variation.

This page replaces an intentionally blank page in the original.

CHAPTER 8 AGGREGATES IN THE VCCTL AND BENEFITS OF THE VCCTL TO THE INDUSTRY

8.1 Introduction

It was mentioned in the previous chapters that the three-dimensional characterization of aggregate particles allows the inclusion of real aggregate particles in computational models which in turn improves the accuracy of the predictions made by these models. It was also mentioned that prior to the research presented here, the VCCTL models assumed regular shapes like spheres and ellipsoids for aggregates. The methods developed have allowed the inclusion of real aggregate particles into the VCCTL. The use of aggregates in the VCCTL and the benefits of VCCTL to the industry are presented in this chapter.

8.2 Aggregates in the VCCTL

The VCCTL has been designed to contain several modules, each of which is used to predict a different property or simulate a different aspect of concrete, such as rheology, hydration, transport, mechanical properties etc. Some of these properties and processes are rather independent of aggregate characteristics where as some are directly influenced by aggregate properties like shape and texture. For this reason, the VCCTL contains a database of aggregates (It is also worth noting that the methods applied to microfines in this research can be used to determine the shape of cement particles as well, and there exists a cement shape database in the VCCTL). The modular design enables the users to input aggregates into the database and/or select existing aggregates from the database and import them into models available in the other modules.

8.2.1 The Aggregate Database in the VCCTL

A screenshot of the main menu of the VCCTL version 4.0 user interface (UI) is given in Figure 8.1.

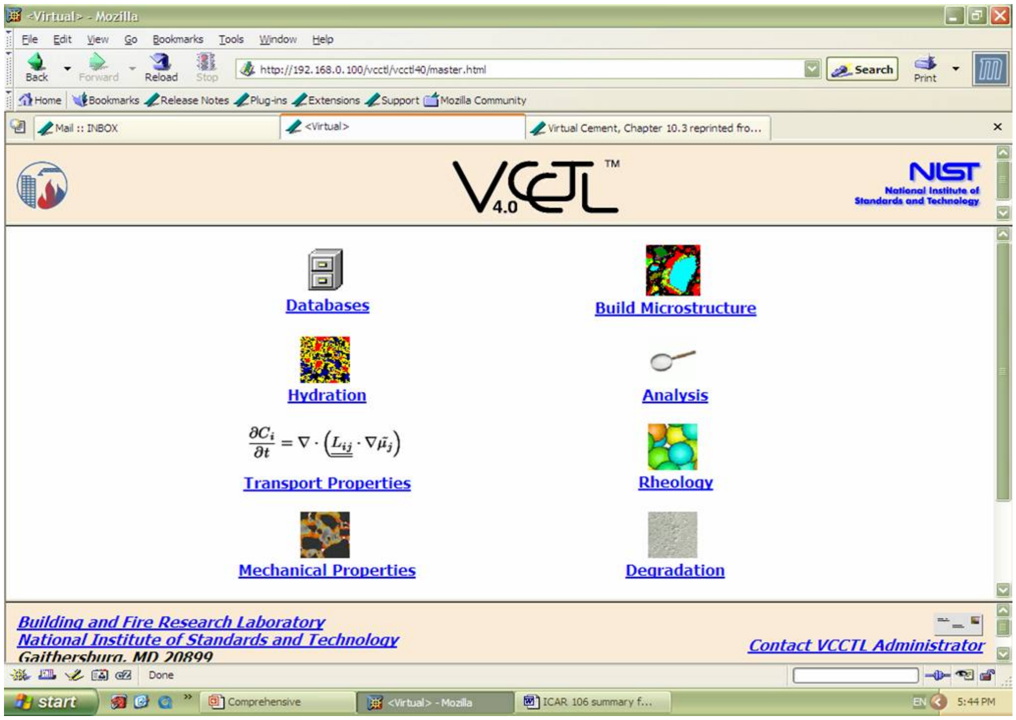

Figure 8.1 Main page of VCCTL 4.0

The modules mentioned above are seen in the figure. The databases module contains both the aggregate and the cement databases, and is used to select from existing sets of aggregates and cements of different types, sources, sizes etc. Once the user enters the aggregate database, a list of the aggregates available for viewing is displayed, as shown in Figure 8.2.

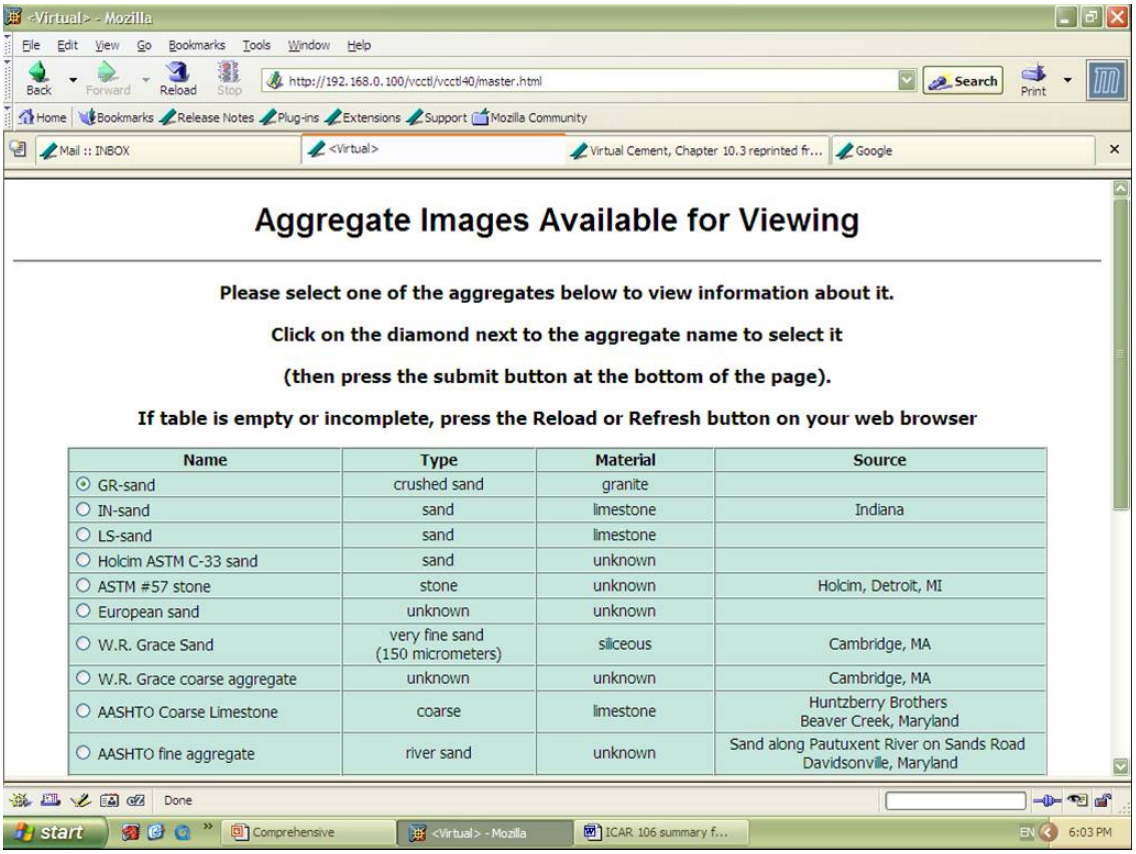

Figure 8.2 A sample list of different types of particles in the aggregates database

The name of the aggregate used by the company or institution it was received from, the type of aggregate, the size of the material, and its source are given. The user can choose one of the aggregates by clicking the radio button next to it on the list and access a list of the individual particles scanned of that aggregate, grouped into different size ranges. Figure 8.3 shows a sample list of various size bins of the "LS-sand" type in Figure 8.2, which is the limestone fine aggregate scanned in this study, introduced in Chapter 4.

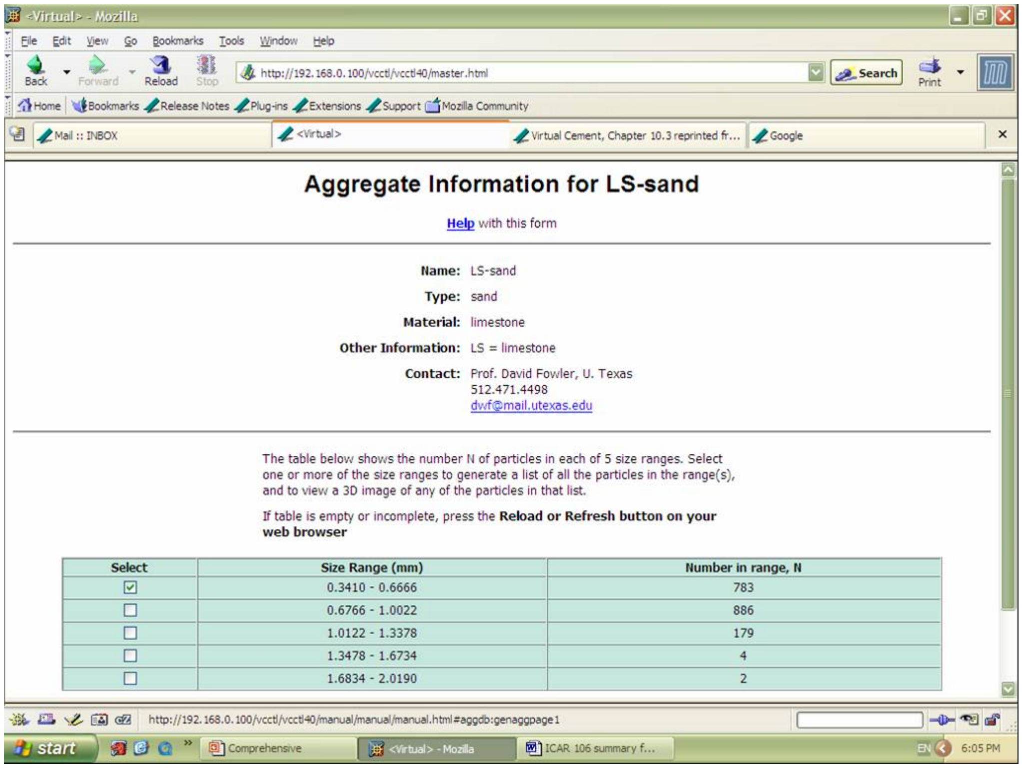

Figure 8.3 A sample list of different sizes of particles of a specific type available for viewing

As can be seen, different size ranges of particles are available. The size ranges and the number of particles that fall into that size range are shown. This information can be used to get an idea about the statistics of the scan and the approximate size distribution of the particles in the specimen scanned. The user can select a single size range or multiple size ranges from this list. The “1.3478 mm – 1.6734 mm” size range in Figure 8.3 is selected here and a list the four particles is given in Figure 8.4.

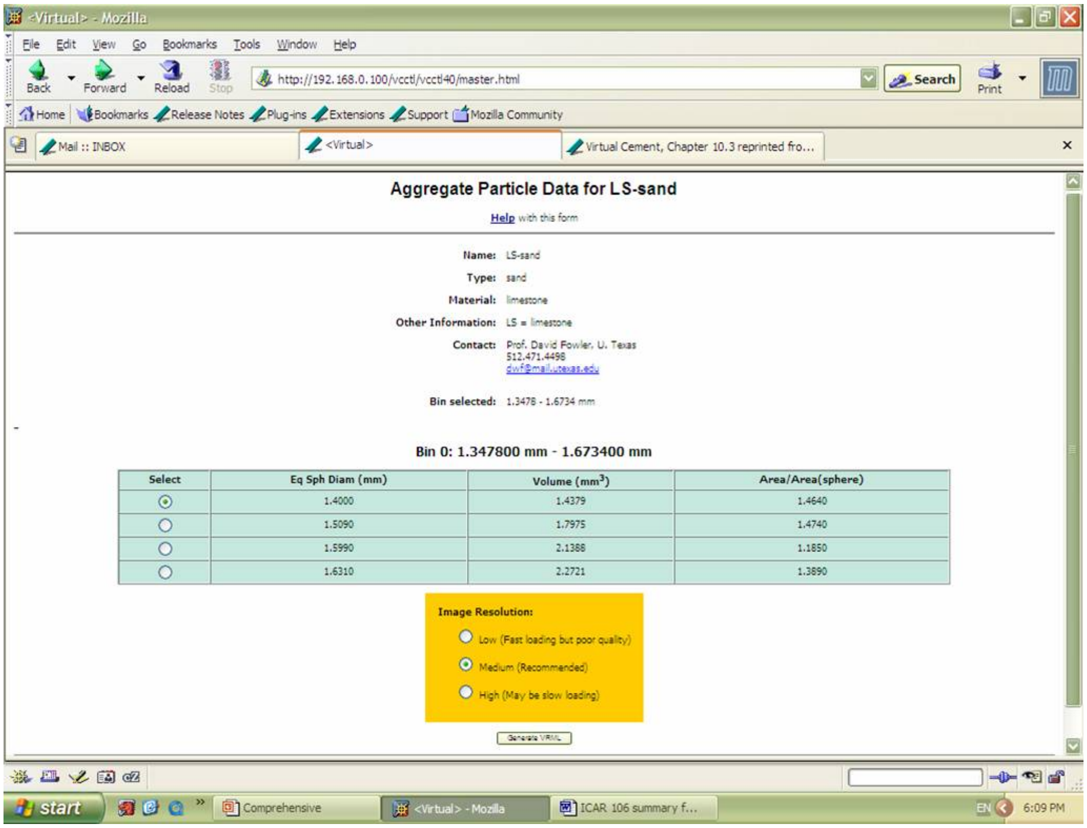

Figure 8.4 A sample list of individual particles in a certain size range available for viewing

Each row of data in Figure 8.4 represents an individual limestone sand particle scanned and stored as a collection of spherical harmonic coefficients. Some basic information such as the equivalent spherical diameter, volume, and ratio of the surface area of the particle to that of an equivalent sphere is given. The user can select a single particle to view and choose a resolution at which the particle will be built. The Virtual Reality Modeling Language (VRML) is used to build the virtual particles from the spherical harmonic coefficients. The cartesian coordinates for many surface points are determined from the coefficients and the particle is formed by a collection of plane surfaces connecting the points. One of the four sample aggregates in the list in Figure 8.4 is shown in Figure 8.5.

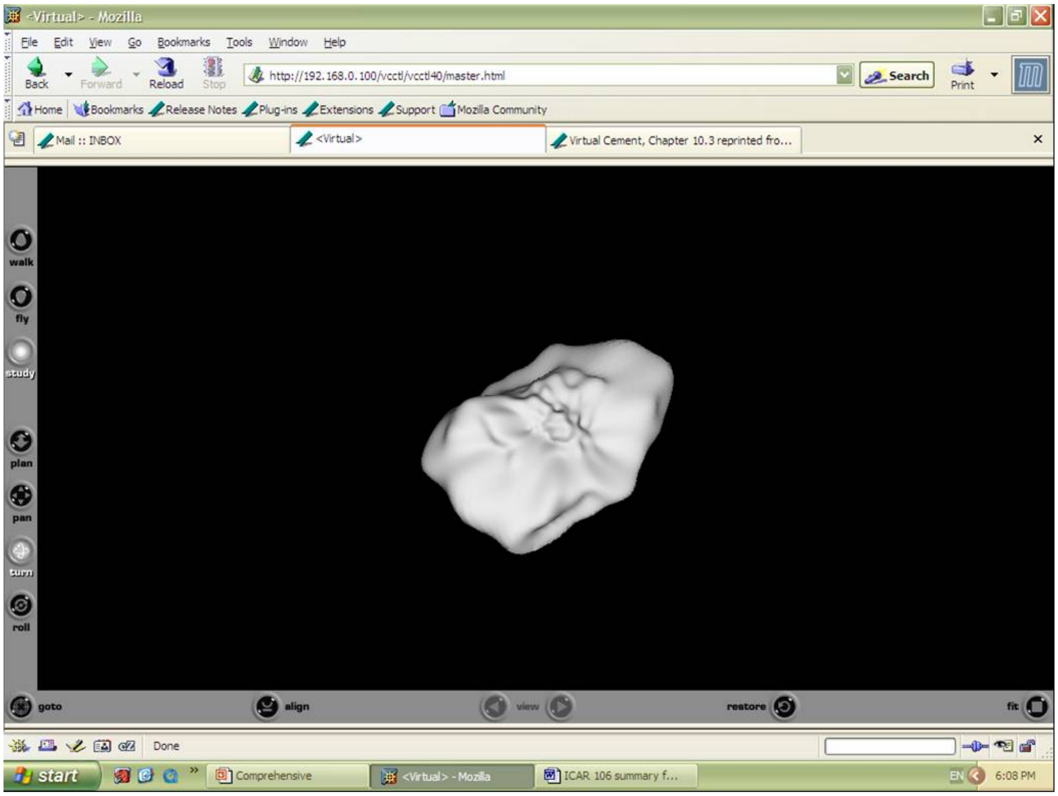

Figure 8.5 An individual limestone sand particle in the VCCTL database viewed with a VRML browser

The particles built with VRML contain three-dimensional information and the particle can be rotated and viewed from all angles and distances, under different lighting conditions etc. Particles of all sizes appear identical in size so similar relative detail can be observed for coarse, fine and microfine particles. It is important to be able to view particles to check for errors in the scanning or spherical harmonic analysis. In addition, it is useful to be able to visually compare particles of different types.

8.2.2 Adapting the Aggregates Database in the VCCTL for Specific User Applications

The aggregates database can be used in different ways. The most straightforward of these is to select particles to view, following the procedure given in the previous section. Another way in which the database is designed to be used is to select a set of particles from the database as inputs to a model. This option is not currently active but will be in the future versions of the software. This will enable the user to select a set of aggregates which closely resemble the aggregates being used in the real mixtures. Having a variety of shapes and sizes will increase the possibility of finding such a set in the database. In the case that a set with identical or similar statistics is not available in the database, the user can add the data for the particles to the database for use in the models. The spherical harmonic coefficients for each particle, obtained as mentioned in Chapter 3, are required for this. The programs to build the virtual particles and to input the particles into models have been built into the most recent version of VCCTL so scanning a representative set of particles of the aggregate of interest and determining the spherical harmonic coefficients suffice. The current procedure of adding aggregates to the database is to scan aggregates and contact the VCCTL administrator for inputting the data into the new version of the software for non-members. Members can modify the copy of the software they have to make such changes on their own. The flow chart in Figure 8.6 summarizes the procedure to use aggregates in the VCCTL.

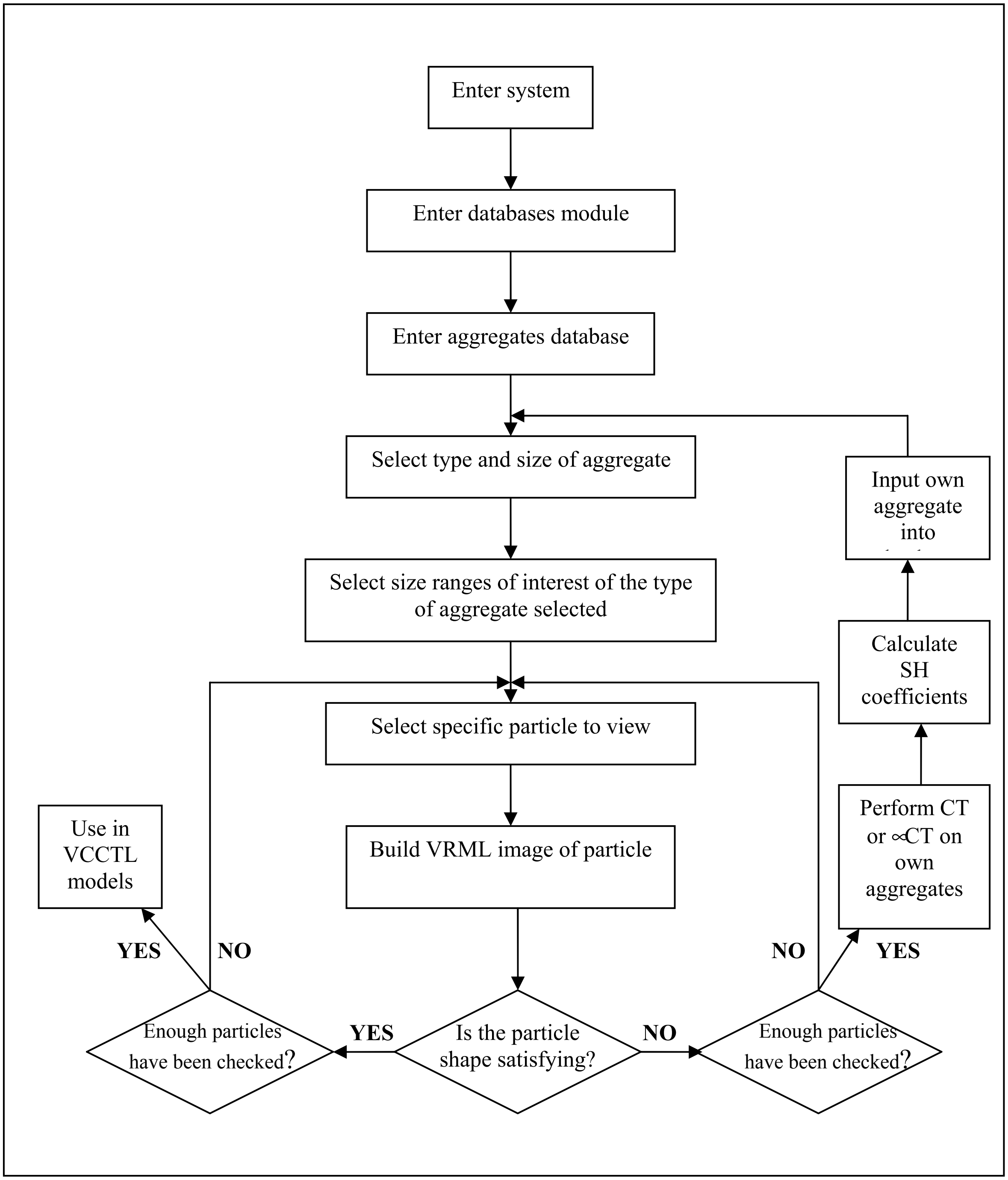

Figure 8.6 Procedure for using the aggregate database in the VCCTL

8.3 Benefits of VCCTL to the Aggregates Industry

The potential benefit to the aggregates industry from the inclusion of an aggregate database into the VCCTL and the modification of models to use real aggregate can potentially be significant. The proportioning of concrete mixtures and the evaluation of the properties of fresh and hardened concrete have been achieved mostly empirically until the present day. Conventional laboratory testing methods required to determine the suitability of an aggregate shape and size distribution for an application are costly and time-consuming. Virtual testing can reduce material and labor costs and the wait period before the behavior of a certain aggregate can be evaluated. The development of the VCCTL models will eventually allow virtual mixture proportioning, which will allow the testing of a certain set of mixture proportions, evaluation of the behavior of the mixture, and adjustment of the proportions. In the case of rheology for example, the user will be able to select an aggregate set which resembles the grading of the aggregate being used in the laboratory or the field, run the model to determine the effect of the aggregate set on the viscosity and yield stress of the mixture, and then modify the amounts of different sizes of aggregates or combine two or more aggregate sets to improve the flow properties or to increase the percentage of aggregates used while maintaining the desired flow properties. It is possible that aggregates which do not perform well alone can perform well when used in combination with each other.

Another possible use of the VCCTL is to compare aggregates of the same type but different shape, processed using different types of crushers or the same crusher with different settings. This may allow the determination of ideal crushing conditions for an aggregate source the aggregate producer uses which can optimize the performance of the aggregate.

Perhaps one of the greatest benefits of the VCCTL to the aggregate industry will be in the increased use of microfine aggregates. The increased use of manufactured aggregates has led to an increased production of microfine particles (as a by-product of the crushing), the use of which in concrete are limited and often end up as pond screenings. Although testing has shown that higher amounts of microfines than those currently allowed in specifications can be used satisfactorily, different types of microfines behave differently when used in identical amounts. While it is possible that the reason for this is occasionally mineralogy, it is likely more often physical, thus due to the shape properties and size distribution of the microfines. When virtual mixture proportioning is a reality, it will be possible to determine the maximum amount of a specific microfine aggregate (or a combination of different microfines) which can be used satisfactorily for given mixture proportions of other ingredients.

CHAPTER 9 SUMMARY, CONCLUSIONS, AND RECOMMENDATIONS

9.1 Summary

It is well known that the shape of aggregate particles can affect many properties of fresh and hardened portland cement concrete, some quite significantly (such as flow properties and elastic properties). Aggregate shape also affects various properties of asphaltic concrete. Naturally, the characterization of particle shape has been of interest to concrete researchers and others. Many methods have been proposed in the past several decades, ranging from simple, approximate, and/or subjective methods to complex methods involving the use of computers and sophisticated mathematics. Although much progress has been made, there are drawbacks to all methods, some being more significant than others. A common drawback is that most methods are not three-dimensional and while being exact in two-dimensions, can only be approximate in terms of the true particle shape. Another drawback is that most methods yield one or a few values, as desired by the industry, when it is rather obvious that aggregate particle shape is too complex to be described so simply.

X-ray tomography (CT) and microtomography (∝CT) techniques have been widely used for decades to visualize the interior features of objects and lend themselves well to the characterization of particle shape. While the equipment to perform these techniques is currently expensive, it is likely that this technology will become more economical and available, in the near future. The characterization of particle shape using these techniques is completely three-dimensional and does not have the drawbacks that other techniques have. In addition, they allow the characterization of a very wide range of particle sizes, from microfine particles of about ten-twenty micrometers in diameter to the largest coarse particles. CT and ∝CT have been applied to concrete aggregates, sample preparation guidelines developed, and scanning and processing methods and practical applications have been suggested.

Due to the complex nature of the behavior of particles in concrete, computational models are necessary to predict most concrete properties without experimentation. True, three-dimensional particle shape needs to be inputted into these models for accurate predictions, as approximated shape yields approximate results at best. The Virtual Cement and Concrete Testing Laboratory (VCCTL), which uses a suite of software modules for designing and testing cement-based materials in a virtual environment, has used spheroids as aggregates, due to a lack of a complete shape characterization method. CT and ∝CT have fulfilled this need. Another important need of such models is that particle shape and textural features can be stored using as little memory as possible, without losing vital detail. In other words, the tremendously large data yielded by CT must be compressed. The spherical harmonic method efficiently fulfills this need and makes it possible for particle shape to be efficiently used in computational models.

Another very important need of computational models is verification through experimentation, and existence of empirical data, for well-controlled cases, which can be used for this purpose. Four different regular shapes were chosen and man-made coarse aggregate particles with similar texture were tested in mortar mixtures, which were used to compare empirical results to the Dissipative Particle Dynamics rheology model. The effect of overall coarse particle shape on rheological properties was also investigated. Another set of man-made particles were used to compare the flow behavior of particles with smooth surfaces to those with rough surfaces, to determine the effect of surface texture on rheology, separately from that of overall shape. These tests also served to verify the ability of the ICAR rheometer to adequately detect changes in workability due to changing coarse particle shape and concentration.

9.2 Conclusions

Based on the literature survey, the application of x-ray tomographic methods to concrete aggregates and the development of guidelines for sample preparation and data processing, and experimental testing, the following conclusions can be reached:

9.2.1 Aggregate Shape Characterization

Test methods to characterize the shape of aggregate properties must be three-dimensional, to account for the true shape of the particle, and must be applicable to microfine particles, the use of which will keep increasing due to the increase in the use of manufactured aggregates.

It is not reasonable to expect to be able to describe particle shape using one value or a few values, such as a shape index or a texture index, and while such values might show certain trends and be useful, they can not be used to accurately predict properties. Similarly, the approach of trying to correlate shape indices to complex phenomena such as the flow of concrete should be abandoned.

X-ray CT and ∝CT are promising methods for characterizing the complete shape of aggregate particles. The three-dimensional shape analysis of microfines has never before been possible, and this is an important step in developing a better understanding of how this size material influences the properties of concrete, which is important as there is a growing need to use them in making concrete.

The spherical harmonic method provides an efficient way of storing large amounts of shape data. In addition to allowing the calculation of useful physical properties defined in three-dimensions, such as the principal dimensions of the particle, volume and surface area, and useful parameters such as the trace of the moment of inertia tensor, it can be used to build a virtual particle to visualize the shape and to check for accuracy of the results.

Comparison of CT results to traditional sieve analysis results support the idea that particle size determined by sieving relates to the width of the particle.

Shape properties calculated using two-dimensional images obtained from sections or area projections of particles, assuming that two-dimensional values can be scaled up to three-dimensions, can yield misleading results, and should be checked using supplemental techniques. A comparison of aspect ratios obtained from two-dimensional SEM images of microfine aggregates and elongation and flatness values obtained from ∝CT have shown that the values from two-dimensions can be excessively high.

Comparison of microfines and coarse particles of the same type, obtained from the same source and processed similarly have shown that there is a similarity in the elongation and flatness of larger and smaller particles formed in the same crushing process.

CT and ∝CT results can be used to predict the density of individual aggregate particles and the density distribution within each aggregate particle. This might be useful in modeling the behavior of aggregate particles in elasticity models.

The principal moments of volume and absolute first moments calculated for a particle can be used to develop three-parameter shape models, yielding the dimensions of equivalent rectangular parallelepipeds or ellipsoids, which can predict the volume and surface area of particles. The PMV model for equivalent shape appears to be especially promising.

A comparison of particle size distribution curves for microfines, obtained from wet laser diffraction and ∝CT have shown that laser diffraction tends to overestimate the size of particles, possibly due to some of the assumptions involved with this technique not being satisfied and/or agglomeration of particles during testing.

Graphical comparisons of particle size distribution are affected by the binning of particles, and the shape (and values appearing on the graph) of the PSD curve for a set of particles can change significantly between using large bin sizes and small bin sizes.

9.2.2 Effects of Aggregate Shape and Texture on the Rheological Properties of Concrete

Water content significantly affects both the plastic viscosity and the yield stress of the mixture. There is a narrow threshold range of water-to-cement ratio values, above which plastic viscosity and yield stress will be low and the change with changing water content will be slow; and below which these values will increase very rapidly, with slight changes in water content.

It is important to use absolute rheological parameters (plastic viscosity and yield stress) for mixtures containing aggregates, particularly for concrete, to account for the effect of an enlarging dead zone. The increase in viscosity will be underestimated when moving from a low concentration of particles to a higher concentration of particles, if relative parameters (yield value and viscosity value) are used.

The variation in measured values will increase when going from mortars to concrete mixtures and from well-shaped, well-graded aggregates to poorly shaped, poorly graded aggregates. The variation for repeated measurements of a mixture will also change, due to the movement of aggregates in the paste medium, and often the viscosity measured will decrease. Conversely, the viscosity will increase if the mixture is remixed. In addition, particles oriented in a particular way may falsely increase the measured viscosity or yield stress. It is therefore necessary to make several measurements for each test case of a mixture, as a single measurement will not suffice to capture this variation.

The effect of coarse aggregate particles on rheological properties is not greatly influenced by the properties of the suspending medium, meaning a set of coarse particles added to two mortar mediums, one with a high viscosity and the other with a low viscosity, will cause a similar relative change in the plastic viscosity measured, even though the absolute viscosity change will be different (e.g. a mortar with a plastic viscosity of 10 Pa.s will increase to 20 Pa.s, and a mortar with a viscosity of 20 Pa.s will increase to 40 Pa.s). This suggests that the approach of modeling the viscosity of concrete at three different levels (paste, mortar, concrete) is rational. The viscosity of the cement paste phase (therefore, the water-cement ratio and the use of admixtures) has the greatest influence on the viscosity of the concrete mixture.

The yield stress of a concrete mixture is affected only slightly by the increasing content of coarse particles. The increase is linear or slow at concentrations up to 20-30%, and then increases slightly more rapidly.

The increase in the yield stress of a concrete mixture does not strongly depend on the shape of coarse particles, provided the gradation of the coarse aggregate is identical. Mono-sized spheres and cubes at equal concentrations yielded similar yield stresses.

The viscosity of a mixture is drastically influenced by the amount of coarse particles, above a concentration of approximately 15%. The increase becomes more rapid with increasing particle content.

The overall shape of coarse particles greatly affects the viscosity of a mixture. At realistic coarse particle contents (40%-45%), the plastic viscosity measured for a mixture made with mono-sized cubes and another made with mono-sized spheres differed by about 100%.

Comparisons of empirical results for the cases of an increasing content of mono-sized spheres and mono-sized cubes with predictions of the dissipative particle dynamics model have shown that this model is promising for predicting the viscosity of mortar and concrete mixtures, with irregular shaped aggregates.

Slump tests have shown that coarse particle shape does not have a noticeable effect on slump values, water-to-cement ratio has a dramatic effect on the slump value of concrete mixtures and changing fine aggregate content does not greatly affect slump until very high volume content, higher than those typically used in concrete.

Elongated or flat particles appear to increase plastic viscosity more than equi-dimensional particles, at a given particle content, for the same gradation. However, the variation in the measured values is too high to be certain, or to compare mono-sized flat particles with mono-sized elongated particles.

The surface texture of coarse particles does not seem to affect the yield stress or plastic viscosity of mortar or concrete mixtures noticeably, independently from overall particle shape, for the case of mono-sized spheres.

The ICAR rheometer has proven to be easy to use with its lightweight structure, portability, uncomplicated user interface and adjustable containers for mixtures containing aggregates of different maximum size to avoid having to make excessive amounts of concrete. The repeatability of the rheological values measured was found to be good for concrete mixtures and excellent for mortar mixtures.

9.3 Recommendations for Future Work

Better methods of sample preparation for x-ray CT and ∝CT, and better image processing for the scan data should be developed.

The usefulness of principal moments of volume and absolute first moments should be further investigated and other useful parameters be developed.

The absolute results of CT and ∝CT data should be further compared to results from other techniques to evaluate the accuracy of these techniques.

Since tomography tests are expensive, it is not currently cost-efficient to scan very many aggregates of a certain type and size. In order to avoid having to do this, and since it is assumed that a number of particles which are statistically representative of a certain larger set of aggregates can be found, statistically sound particle generation methods should be developed to build a large virtual set of particles which can be used to model real concrete mixtures.

Several mixture proportioning models based on particle packing have been suggested, as aggregate packing greatly influences certain properties of concrete. Packing models often use regular shapes, due to the simplicity of tracking these shapes, and the due to the unavailability of a shape characterization method which can be used to model an actual packing test for which empirical results exist. Now that CT allows the determination of true particle shape, aggregate packing should be further investigated.

More tests using regular-shaped coarse particles should be conducted. Smaller coarse particles should be used to assure increased homogeneity and more realistic and better behaving basic shapes, such as oblate ellipsoids in place of flat particles and prolate ellipsoids in place of elongated prisms should be chosen, to minimize the effects of sharp edges on the interaction of particles.

The effect of coarse particle gradation on concrete viscosity should be investigated. Tests using regular-shaped particles of three, or more sizes should be designed and different combinations of particles of different sizes tested.

More tests should be performed to investigate the effect of particle surface texture on rheological properties. Higher particle concentrations should be tested for the mono-sized particles case, and different shapes and gradations should be tested. If it is determined that fine texture does not noticeably affect viscosity, then the threshold scale of shape (between angularity and texture) should be investigated experimentally and computationally.

REFERENCES

Ahn, N., "An Experimental Study on the Guidelines for Using Higher Contents of Aggregate Microfines in Portland Cement Concrete", Ph.D. Dissertation, The University of Texas at Austin, 2000.

Alexander, K.M., Wardlaw, J., Gilbert, D.J. "Aggregate-Cement Bond, Cement Paste Strength, and the Strength of Concrete." Proceedings, International Conference on the Structure of Concrete, London, Sept. 1965, pp. 59-81.

Aschenbrenner, B.C. "A New Method of Expressing Particle Sphericity", Journal of Sedimentary Petrology, Vol. 26, 1956, pp 15-31.

ASTM C 29 Standard Test Method for Bulk Density ("Unit Weight") and Voids in Aggregate, American Society for Testing and Materials, Philadelphia, PA, 1997.

ASTM C 125 Standard Terminology Relating to Concrete and Concrete Aggregates, American Society for Testing and Materials, Philadelphia, PA, 2003.

ASTM D 4791 Standard Test Method for Flat and Elongated Particles in Coarse Aggregates, American Society for Testing and Materials, Philadelphia, PA, 2005.

ASTM D 3398 Standard Test Method for Index of Aggregate Particle Shape and Texture, Philadelphia, PA, American Society for Testing and Materials, Philadelphia, PA, 2000.

ASTM D 5821 Standard Test Method for Determining the Percentage of Fractured Particles in Coarse Aggregate, American Society for Testing and Materials, Philadelphia, PA, 2001.

ASTM C 1252 Standard Test Methods for Uncompacted Void Content of Fine Aggregate (as Influenced by Particle Shape, Surface Texture, and Grading), American Society for Testing and Materials, Philadelphia, PA, 2003.

ASTM C 136 Standard Test Method for Sieve Analysis of Fine and Coarse Aggregates, American Society for Testing and Materials, Philadelphia, PA, 2005.

ASTM C 33 Standard Specification for Concrete Aggregates, American Society for Testing and Materials, Philadelphia, PA, 2003.

ASTM E 1441 Standard Guide for Computed Tomography (CT) Imaging, American Society for Testing and Materials, Philadelphia, PA, 1992.

Barret, P.J. “The Shape of Rock Particles, a Critical Review”, Sedimentology 27 (1), 1980, pp. 15-22.

Bennett, E.W. and Katakkar, S.H. “A Comparative Study of Twelve Types of Sand Used as Fine Aggregate in Concrete”, Journal, British Granite and Whinstone Federation, London, 1965.

Blanks, R.F. “Modern Concepts Applied to Concrete Aggregate”, Transactions, ASCE, Vol. 115, 1950, p. 403.

Bloem, D.L. and Gaynor, R.D. “Effect of Aggregate Properties on Strength of Concrete”, Journal of American Concrete Institute, Vol. 60, No. 10, 1963.

Brzezicki J.M. and Kasperkiewicz J. “Automatic Image Analysis in Evaluation of Aggregate Shape”, ASCE Journal of Computing in Civil Engineering 13 (2), April 1999, pp. 123-128.

BS 812 Testing Aggregates, Part 1 (Methods for Determination of Particle Size and Shape), British Standards Institution, 1990.

Bullard, J.W., Ferraris, C., Garboczi, E.J., Martys, N. and Stutzman, P. “Virtual Cement”, Chapter 10.3, *Innovations in Portland Cement Manufacturing*, pp. 1311-1331, J.I. Bhatty, F.M. Miller and S.H. Kosmatka, eds., Portland Cement Association, 2004.

Carman, P.C. “The Determination of the Specific Surface of Powders”, Journal, Society of the Chemical Industry, Vol. 57, No. 7, July 1938, pp. 225-234.

Cauchy, A. “Memoire sur la rectification des courbes et de la quadrature des surfaces courbes”, Mem. Acad. Sci. Paris 22, No. 3, 1850.

Chamberlin, W.P. “Influence of Natural Sand Fine Aggregate on Some Properties of Hardened Concrete Mortar”, HRB Record No. 124, Aggregates for Concrete, Highway Research Board, 1966.

Chatterji, S. and Jeffery, J.W. “The Nature of the Bond between Different Types of Aggregates and Portland Cement”, Indian Concrete Journal, Vol. 45, Aug. 1971, pp. 346-349.

Cheok, G.S., Stone, W.C., Garboczi, E.J. “Using LADAR to Characterize the 3-D Shape of Aggregates: Preliminary Results,” Cement and Concrete Research, 2005, in review.

Cooper, J. “Sizing Up the Composition”Materials World, Vol. 6, no. 1, January 1998, pp. 5-7.

Czarnecka, E.T. and Gillott, J.E. “A Modified Fourier Method of Shape and Surface Texture Analysis of Planar Sections of Particles”, Journal of Testing and

Evaluation, American Society for Testing and Materials, Vol. 5, No. 4, 1977, pp. 292-298.

Davies, W. and Rees, W.J. Journal, Iron and Steel Institute, Vol. 40, No. 2, 1944, pp. 19-47.

Dilek, U. and Leming M.L. "Relationship between Particle Shape and Void Content of Fine Aggregate", Cement, Concrete, and Aggregates 26 (1), Jun 2004, pp. 14-20.

Dunsmuir, J. H. "X-2B Synchrotron Microtomography", unpublished draft, 2004.

Ehrlich, R. and Weinberg, B. "An Exact Method for Characterization of Grain Shape", Journal of Sedimentary Petrology, Vol. 40, No. 1, March 1970, pp. 205-212.

Erdoğan, S.T. "The Effect of Aggregates on the Properties of Concrete and Proportioning Methods", M.S. Thesis, The University of Texas at Austin, 2003.

Erdoğan, S.T., Quiroga, P.N., Fowler, D.W., Saleh, H.A., Livingston, R.A., Garboczi, E.J., Ketcham, P.M., Hagedorn, J.G., and Satterfield, S.G. "Three-dimensional Shape Analysis of Coarse Aggregates: Methodology and Preliminary Results on Several Different Coarse Aggregates", Cement and Concrete Research, 2004, in review.

Faroug F., Szwabowski J., Wild S. "Influence of Superplasticizers on Workability of Concrete", Journal of Materials in Civil Engineering 11 (2), 1999, pp. 151-157.

Fernlund, J.M.R. "The Effect of Particle Form on Sieve Analysis: A Test by Image Analysis", Engineering Geology 50 (1), September 1998, pp. 111-124.

Ferraris, C.F. "Measurement of the Rheological Properties of High Performance Concrete : State of the Art Report", Journal of Research of the National Institute of Standards and Technology, 104 (5), 1999, pp. 461-478.

Ferraris, C.F.; Hackley, V.A., Aviles, A.I., Buchanan, C.E., Jr. "Analysis of the ASTM Round-Robin Test on Particle Size Distribution of Portland Cement: Phase 2", NISTIR 6931, December 2002.

Folk, R.L. "Petrology of Sedimentary Rocks", Hemphill Publications, Austin, Texas, 1968.

French, W.J. "Concrete Petrography – A Review", Quarterly Journal of Engineering Geology, 24 (1), 1999, pp.17-48.

Galloway, J.E., Jr. "Grading, Shape and Surface Properties", Significance of Tests and Properties of Concrete and Concrete-Making Materials, ASTM STP 169C, edited by Klieger, Paul and Lamond, Joseph F., American Society for Testing and Materials, West Conshohocken, Pennsylvania, 1994, pp. 401-410.

Garboczi, E.J. "Three-dimensional Mathematical Analysis of Particle Shape Using X-ray Tomography and Spherical Harmonics: Application to Aggregates Used in Concrete", Cement and Concrete Research 32 (10), October 2002, pp. 1621-1638.

Garboczi, E.J., Bullard, J.W., Bentz, D.P. "Virtual Testing of Cement and Concrete−USA 2004", Concrete International 26 (12), 2004, pp. 33-37

Geiker, M.R., Brandl, M., Thrane, L., Nielsen, L.F. "On the Effect of Coarse Aggregate Fraction and Shape on the Rheological Properties of Self-Compacting Concrete", Cement, Concrete, and Aggregates, Vol. 24, No. 1, June 2002, pp. 3-6.

Gray, J.E. and Bell, J.E. "Stone Sand", Engineering Bulletin No. 13. National Crushed Stone Association, 1964.

Grigoriu, M., Garboczi, E.J., Kafali, C. "Spherical Harmonic-Based Random Fields for Aggregates Used in Concrete", Powder Technology, in review.

Heigold, P.C. and Lamar, J.E. "Two-Dimensional Shape of Sand Made by Crushing Illinois Limestones of Different Textures", Industrial Minerals Notes 41, Illinois State Geological Survey, August 1970.

Heywood, H., Proceedings, Institute of Mechanical Engineers, Vol. 125, 1933, p.383.

Hossain, M.S., Parker F., Kandhal P.S. "Comparison and Evaluation of Tests for Coarse Aggregate Particle Shape, Angularity, and Surface Texture" Journal of Testing and Evaluation 28 (2), March 2000, pp. 77-87.

Hudson, B. "Fine Aggregates Need Better Testing Methods", Aggregates Manager, March 1998.

Hudson, B. "Modifications to the Fine Aggregate Angularity Test", Proceedings of the Seventh ICAR symposium, Austin, TX, 1999.

Ishai, I. and Tons, E. "Concept and Test Method for a Unified Characterization of the Geometric Irregularity of Aggregate Particles", Journal of Testing and Evaluation, 5 (1), 1977, pp. 3-15.

Jamkar S.S. and Rao C.B.K. "Index of Aggregate Particle Shape and Texture of Coarse Aggregate as a Parameter for Concrete Mix Proportioning", Cement and Concrete Research 34 (11), November 2004, pp. 2021-2027.

Jones, F.E. "The Physical Structure of Cement and Its Effect on Durability", Proceedings, 3rd International Symposium on the Chemistry of Cement, London, 1952, published 1954, p. 368.

Juenger M.C.G. and Ostertag C.P. "Alkali-Silica Reactivity of Large Silica Fume-Derived Particles", Cement and Concrete Research 34 (8), August 2004, pp. 1389-1402.

Kak, A.C. and Slaney, M. "*Principles of Computerized Tomographic Imaging",* Society of Industrial and Applied Mathematics, 2001.

Kaplan, M.F. "Flexural and Compressive Strength of Concrete as Affected by the Properties of Coarse Aggregate", Journal, American Concrete Institute, Vol. 30, No. 11, May 1959, pp. 1193-1208.

Kaplan, M.F. "The Effects of Properties of Coarse Aggregates on the Workability of Concrete", Magazine of Concrete Research, Vol. 10, No. 29, August 1958, pp. 63-74.

Ketcham, R.A. and Carlson, W.D. "Acquisition, Optimization and Interpretation of X-ray Computed Tomographic Imagery: Applications to the Geosciences", Computers and Geosciences, 27, 2001, pp. 381-400.

Kim H., Haas C.T., Rauch A.F, Browne, C. "Wavelet-Based Three-Dimensional Descriptors of Aggregate Particles" Transportation Research Record (1787), 2002, pp. 109-116.

Koehler, E.P. "Development of a Portable Rheometer for Fresh Portland Cement Concrete", M.S. Thesis, The University of Texas at Austin, 2004

Koehler, E.P. and Fowler, D.W. "ICAR 105-3F: Development of a Portable Rheometer for Fresh Portland Cement Concrete"**,** 2004, pp. 306.

Koehler, E.P., Fowler, D.W., Ferraris, C., Amziane, S. "A New Portable Rheometer for Fresh, Self-Consolidating Concrete", Proceedings of the ACI Convention, New York, NY, April 2005.

Kosmatka, S.H. and Panarese, W.C. "Design and Control of Concrete Mixtures", Portland Cement Association, 13th ed. Charlottsville, VA, p. 34.

Krumbein, W.C. "Measurement of Geological Significance of Shape and Roundness of Sedimentary Particles", Journal of Sedimentary Petrology, Vol. 11, No. 2, 1941, pp. 64-72.

Kuo, C.Y., Frost, J.D., Lai, J.S., Wang, L.B. "Three-Dimensional Image Analysis of Aggregate Particles from Orthogonal Projections", Transportation Research Record 1526, National Research Council, Washington D.C., 1996, pp. 98-103.

Kuo C.Y., Rollings R.S., Lynch L.N. "Morphological Study of Coarse Aggregates Using Image Analysis", Journal of Materials in Civil Engineering 10 (3), August 1998, pp. 135-142.

Kuo C.Y. and Freeman R.B. "Image Analysis Evaluation of Aggregates for Asphalt Concrete Mixtures", Transportation Research Record (1615), 1998, pp. 65-71.

Kuo C.Y. and Freeman R.B. "Imaging Indices for Quantification of Shape, Angularity, and Surface Texture of Aggregates", Transportation Research Record (1721), 2000 pp. 57-65.

Kwan A.K.H., Mora C.F., Chan H.C. "Particle Shape Analysis of Coarse Aggregate Using Digital Image Processing", Cement and Concrete Research 29 (9), Sep 1999, pp. 1403-1410.

Kwan A.K.H. and Mora C.F. "Effects of Various Shape Parameters on Packing of Aggregate Particles", Magazine of Concrete Research 53, No. 2, April 2001, pp. 91-100.

Lafrenz, J.L. "Aggregate Grading Control for PCC Pavements: Improving Constructibiliy of Concrete Pavements by Assuring Consistency of Mixes" Proceedings of the Fifth Annual Symposium, International Center for Aggregates Research, Austin, Texas, 1997.

Laughlin, G.R. "Limestone Fine Aggregate in Portland Cement Concrete", Highway Research Laboratory, Lexington, KY, 1960.

Li, L., Chan, P., Zollinger, D.G., Lytton, R.L. "Quantitative-Analysis of Aggregate Shape-Based on Fractals", ACI Materials Journal 90 (4), Jul - Aug 1993, pp. 357-365.

Maerz, N.H. "Technical and Computational Aspects of the Measurement of Aggregate Shape by Digital Image Analysis" Journal of Computing in Civil Engineering 18 (1), Jan 2004, pp. 10-18.

Martys, N., Personal communication, 2005.

Masad E. and Button J.W. "Unified Imaging Approach for Measuring Aggregate Angularity and Texture", Computer Aided Civil and Infrastructure Engineering 15 (4), July 2000, pp. 273-280.

Masad E., Button J.W., Papagiannakis T. "Fine-Aggregate Angularity - Automated image analysis approach" Transportation Research Record (1721), 2000, pp. 66-72.

Mather, B. "Shape, Surface Texture, and Coatings", in: Significance of Tests and Properties of Concrete and Concrete Aggregates, ASTM STP 169A, American Society of Testing Materials, Philadelphia, 1966, pp. 415-431.

Malhotra, V.M. "Correlation between Particle Shape and Surface Texture of Fine Aggregates and Their Water Requirement", Materials Research and Standards, American Society for Testing and Materials, Vol. 4, Dec. 1964, pp. 656-658.

Mora C.F., Kwan A.K.H., Chan H.C. "Particle Size Distribution Analysis of Coarse Aggregate Using Digital Image Processing", Cement and Concrete Research 28 (6), June 1998, pp. 921-932.

Mora C.F. and Kwan A.K.H. “Sphericity, Shape Factor, and Convexity Measurement of Coarse Aggregate for Concrete Using Digital Image Processing”, Cement and Concrete Research 30 (3), March 2000, pp. 351-358.

Mueller, W. and Hunn, H. “Texture Analyzer-System”, Industrial Research, Nov. 1974.

Orchard, D.F, Yandell, W.G, Lye, B.R.X. “A Quick Method for Measuring the Surface Texture of Aggregate”, Proceedings, 5th Conference of the Australian Road Research Board, Vol. 4, Part 5, 1970, pp. 325-341.

Ozol, M.A. “Shape, Surface Texture, Surface Area, and Coatings”, in Significance of Tests and Properties of Concrete and Concrete Making Materials, American Society for Testing and Materials, Philadelphia, Special Technical Publication 169 B, pp. 584-628.

Ozol, M.A. “The Portland Cement Aggregate Bond – Influence of the Surface Area of the Coarse Aggregate as a Function of Lithology”, Report No. 71-R40, Virginia Highway Research Council, June 1972.

Palasamudram, S.L. and Bahadur, S. “Particle Characterization for Angularity and the Effects of Particle Size and Angularity on Erosion in a Fluidized Bed Environment” Wear 203-204 (1) 1997, pp. 455-463.

Patat, F. and Schliebener, C. “Die Adsorption von Makromolekülen” I. Uber Eine Neue Meszmethode”, MakroMolekulare Chemie, Vol. 64-66, 1961, pp. 643-668.

Patty, T. “Mineralogical Identification / Rock Type of Five Aggregate Sources”, Report WJE No. 2003.3293, October 2003.

Pettijohn, F.J. “Sedimentary Rocks”, Harper & Brothers, New York, NY, 1949.

Persson A.L. “Image Analysis of Shape and Size of Fine Aggregates”, Engineering Geology 50 (1-2), Sep 1998, pp. 177-186.

Plum, M.N. “Concrete Manual”, Bulletin #39, Christiani and Nielsen, Copenhagen, 1944.

Popovics, S. “Aggregate Grading and the Internal Structure of Concrete”, HRB Record No. 441, Highway Research Board, Washington D.C., 1973.

Powers, T.C. “The Nature of Concrete”, Significance of Tests and Properties of Concrete and Concrete Making Materials, ASTM STP 169A, American Society for Testing and Materials, 1966.

Quiroga, P.N. “The Effect of the Aggregates Characteristics on the Performance of Portland Cement Concrete” Ph.D. Dissertation, The University of Texas at Austin, 2003

Rao, C. and Tutumluer, E. “Determination of Volume of Aggregates - New Image-Analysis Approach”, Transportation Research Record (1721), 2000, pp. 73-80.

Rao, C., Tutumluer, E., Stefanski, J.A. “Coarse Aggregate Shape and Size Properties Using a New Image Analyzer”, Journal of Testing and Evaluation 29 (5), Sep 2001, pp. 461-471.

Riley, N.A. “Projection Sphericity”, Journal of Sedimentary Petrology, Vol. 11, No.2, 1941, pp. 94-97.

Rendahl, A. “Reconstruction and Viewing of Microtomography Bone Samples”, 1999, www.phys.washington.edu/users/savage/REU99/rendahl/rendahl_paper.html

Rex, H.M. and Peck, R.A, “A Laboratory Test to Evaluate the Shape and Surface Texture of Fine Aggregate Particles”, Public Roads, Vol. 29, No. 5, December 1956, pp. 118-120.

Russ J.C., *The Image Processing Handbook*, 4th ed., CRC Press, 2002.

Schiel, F. “Die Kornform der Betonzuschlagstoffe und Ihre Prufung” (The Shape of Concrete Aggregates and Its Testing), Betonstrasse, Vol. 16, Berlin, 1941, pp. 181-186; Road Abstracts, Vol. X., No. 3, 1943.

Schmidt, W., and Hoffman, E.S. “9000 psi Concrete – Why, Why Not?” Civil Engineering, Vol. 45, No. 5, May 1975, p. 48.

Scrivener, F.H. and Hudson, W.F. “A Modification of the AASHO Road Test Serviceability Tridex Formula”, HHR, No. 46, 1963.

Shergold, F.A. “The Percentage of Voids in Compacted Gravel as a Measure of its Angularity”, Magazine of Concrete Research, No. 13, August 1953, pp.3-10.

Sneed, E.D. and Folk, R.L. “Pebbles in the Lower Colorado River, Texas – A Study in Particle Morphogenesis”, Journal of Geology, Vol. 66, No. 2, 1958, pp. 114-150.

Stewart, J.G. “Correlating Characteristics of Minus No.200 Fine Aggregate to Concrete Performance”, M.S. Thesis, The University of Texas at Austin, 2005.

Tattersall, G.H. “Workability and Quality Control of Concrete”, London, E&FN Spon, 1991.

Taylor, M.A., Personal communication, 2005.

The Handbook of Chemistry and Physics, ed. David R. Lide, CRC Press, 2004.

Tons, E. and Goetz, W.H. “Packing Volume Concepts for Aggregates”, HRB Record No. 236, NRC 1968, Washington D.C.

Tyler, I.L. "Concrete of Norris Dam", Bulletin, Engineering and Construction Department, Tennessee Valley Authority, Sept. 1937.

UT-CT, High-resolution X-ray CT Facility website, University of Texas at Austin, Department of Geological Sciences, http://www.ctlab.geo.utexas.edu/

Van de Hulst, H.C. *Light Scattering by Small Particles*, New York, Dover, 1981.

VCCTL, http://vcctl.cbt.nist.gov/

Verspui, M.A., van der Velden, P., de With, G., Slikkerveer, P.J. "Angularity Determination of Abrasive Powders", Wear 199 (1), 1996, pp. 122-126.

Wadell, H. "Volume, Shape, and Roundness of Rock Particles", Journal of Geology, Vol. 40, 1932, pp. 443-451.

Wadell, H. "Volume, Shape, and Roundness of Quartz Particles", Journal of Geology, Vol. 43, 1935, pp. 250-280.

Wang, L., Frost, D. "Quantification of the Specific Aggregate Surface Area Using X-Ray Tomography", Proceedings of the Pavement Mechnaics Symposium at the 15th ASCE Engineering Mechanics Conference, Eds. E. Tutumluer, Y. M. Najjar, and E. Masad, New York, June 2002, pp. 241.

Weisstein, E. "Legendre Polynomial." From *MathWorld*--A Wolfram Web Resource. http://mathworld.wolfram.com/LegendrePolynomial.html

Wenzel, R.N. "Surface Roughness and Contact Angle", Journal of Physical and Colloid Chemistry, Vol. 53, 1949, p. 1466.

Wilson, J.D., Klotz, L.D., Nagaraj, C. "Automated Measurement of Aggregate Indices of Shape", Particulate Science and Technology, 15 (1), Jan-Mar 1997, pp.13-35.

Wright, P.J.F. "A Method of Measuring the Surface Texture of Aggregate", Magazine of Concrete Research, Nov. 1955.

Yudhbir, R., and Abedinzadeh, R. "Quantification of Particle Shape and Angularity Using the Image Analyzer", ASTM Geotech Test J. 14 (3) 1991, pp. 296-308.

APPENDIX A CHARACTERISTICS OF AGGREGATES SCANNED USING X-RAY TOMOGRAPHIC METHODS

Table A.1 Sieve analysis of the coarse aggregates scanned (percentage retained)

Size	IN	LS	GR	AZ		
				1 in.	½ in.	3/8 in.
1 1/2 in.	0.0	0.0	0.0	3.3	0.0	0.0
1 in.	0.0	0.0	0.0	4.0	0.0	0.0
3/4 in.	10.5	17.8	1.5	37.5	0.0	0.0
1/2 in.	53.1	47.2	40.3	49.4	6.7	0.0
3/8 in.	25.7	15.0	26.3	5.3	60.7	0.5
N 4	10.7	20.0	30.2	0.4	31.7	92.1
N 8	0.0	0.0	1.8	0.0	0.9	7.5

Table A.2 Sieve analysis of the fine aggregate scanned (percentage retained)

Size	IN	LS	GR	AZ
N 4	2.2	0.1	5.0	0.1
N 8	10.3	12.8	18.5	12.9
N 16	12.3	28.1	13.6	14.5
N 30	19.6	19.9	10.8	26.3
N 50	42.6	14.2	12.1	32.9
N 100	11.8	8.0	15.2	8.7
N 200	0.9	3.1	8.8	3.3
MF	0.2	13.8	16.0	1.3

Table A.3 Characteristics for the coarse and fine aggregates scanned

Aggregate	Fraction		BSG (SSD)	BSG (OD)	Fineness Modulus	AC (%)	microfines cont.%
Arizona	**Coarse**	**1"**	2.62	2.59		1.04	
		1/2"	2.62	2.58		1.48	
		3/8"	2.64	2.60		1.52	
	Sand		2.60	2.57	2.78	1.02	1.3
Indiana	**Coarse**		2.64	2.59		2.25	
	Sand		2.61	2.58	2.69	1.30	0.2
Limestone	**Coarse**		2.62	2.58		1.79	
	Sand		2.60	2.54	3.72	2.38	13.8
Granite	**Coarse**		2.77	2.76		0.39	
	Sand		2.73	2.72	2.48	0.25	16.0

Notes: SSD = Saturated surface dry

OD = Oven dry
AC = Absorption capacity

Table A.4 Packing density for the siliceous river gravel from Indiana

Size	Packing Method			
	Loose	Rodded	Drop	Vib+Pressure
¾ in.	0.60	0.64	0.66	0.68
½ in.	0.57	0.62	0.64	0.66
3/8 in.	0.57	0.61	0.62	0.64
N 4	0.59	0.62	0.64	0.66
N 8	0.57	0.62	0.63	0.65
N 16	0.57	0.61	0.64	0.65
N 30	0.57	0.62	0.65	0.66
N 50	0.57	0.63	0.66	0.67
N 100	0.57	0.61	0.64	0.65
N 200	N/A	N/A	N/A	N/A
MF	N/A	N/A	N/A	N/A

Table A.5 Packing density for the coarse and fine limestone aggregate

Size	Packing Method			
	Loose	Rodded	Drop	Vib+Pressure
¾ in.	0.59	0.64	0.65	0.66
½ in.	0.58	0.62	0.65	0.66
3/8 in.	0.56	0.62	0.63	0.64
N 4	0.56	0.61	0.62	0.64
N 8	0.56	0.60	0.62	0.62
N 16	0.52	0.57	0.61	0.62
N 30	0.50	0.56	0.59	0.59
N 50	0.49	0.55	0.59	0.61
N 100	0.47	0.54	0.55	0.58
N 200	0.47	0.54	0.55	0.57
MF	0.39	0.43	0.48	0.56

Table A.6 Packing Density for the coarse and fine granite aggregate

Size	Packing Method			
	Loose	Rodded	Drop	Vib+Pressure
¾ in.	0.58	0.63	0.66	0.65
½ in.	0.58	0.62	0.65	0.65
3/8 in.	0.57	0.61	0.63	0.62
N 4	0.51	0.60	0.61	0.61
N 8	0.49	0.52	0.55	0.58
N 16	0.48	0.52	0.55	0.58
N 30	0.47	0.51	0.53	0.56
N 50	0.46	0.50	0.53	0.55

N 100	0.44	0.50	0.52	0.54
N 200	0.43	0.49	0.53	0.54
MF	0.36	0.42	0.49	0.54

Table A.7 Packing density for the siliceous river gravel Arizona

Size	Packing Method			
	Loose	Rodded	Drop	Vib+Pressure
1 in.	0.61	N/A	N/A	0.69
¾ in.	0.59	0.63	0.66	0.69
½ in.	0.56	0.61	0.63	0.63
3/8 in.	0.49	0.55	0.57	0.58
N 4	0.55	0.60	0.61	0.61
N 8	0.51	0.55	0.59	0.60
N 16	0.52	0.56	0.59	0.61
N 30	0.53	0.57	0.59	0.60
N 50	0.52	0.57	0.60	0.61
N 100	0.52	0.58	0.61	0.62
N 200	N/A	N/A	N/A	N/A
MF	N/A	N/A	N/A	N/A

Table A.8 Loose Packing Density for the coarse and fine aggregates scanned determined by ASTM 1252

Size	IN	LS	GR	TR	AZ
N 8	0.61	0.57	0.56	0.59	0.57
N 16	0.58	0.52	0.51	0.55	0.53
N 30	0.56	0.48	0.48	0.52	0.52
N 50	0.56	0.47	0.45	0.51	0.51
N 100	0.55	0.45	0.44	0.49	0.50
N 200	0.55	0.44	0.39	0.48	0.47
MF	N/A	0.33	0.37	0.40	N/A

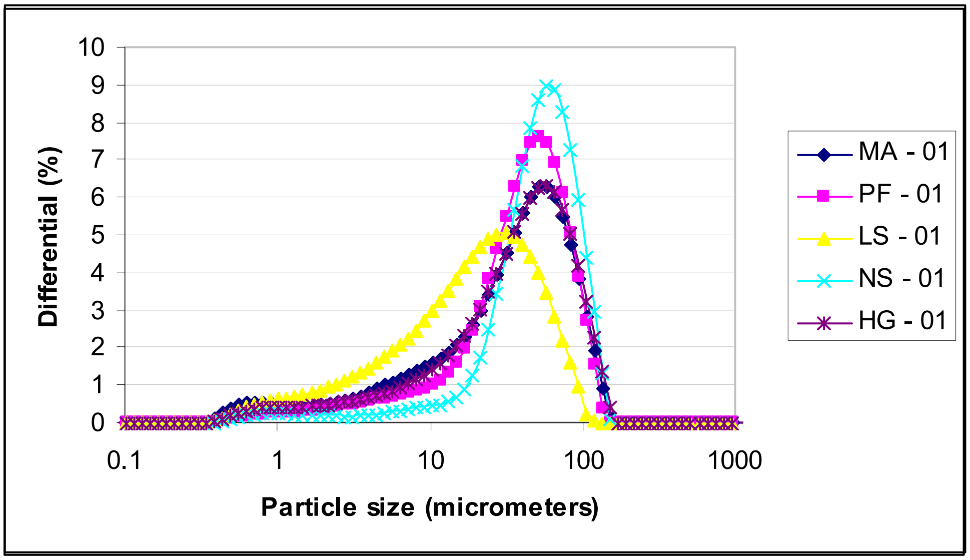

Figure A.1 Particle size distribution curves of the microfine aggregates scanned with µCT as determined by wet laser diffraction.

APPENDIX B RESULTS OF THE X-RAY COMPUTED TOMOGRAPHY AND MICROTOMOGRAPHY SCANS

Notes: Only data for 150 or 200 of the particles scanned is given for each type of aggregate to conserve space while still providing a statistically representative set.

The abbreviations in the column titles are explained below:

S.A = Surface area

Saeq = Surface area of a sphere with the same volume as the particle

ESD = Diameter of a sphere with the same volume as the particle

Tr = Trace of the moment of inertia tensor for the particle

Treq = Trace of the moment of inertia tensor for a sphere with the same volume as the particle

Max = maximum n value used for building the virtual particle

L, W, T = Length, width, thickness of the particle

Table B.1 Results of the CT scans of the granite fine aggregate

#	Vol	SA	SA/Saeq	ESD	Tr/Treq	Max	L	W	T
1	0,20495	2,39828	1,427	0,732	2,034	28	1,69439	0,69733	0,38807
2	0,04826	0,90147	1,406	0,452	1,538	16	0,73623	0,55803	0,40034
3	0,28	2,94508	1,423	0,812	1,591	22	1,35048	1,20342	0,45746
4	0,02292	0,51416	1,318	0,352	1,326	18	0,56198	0,42224	0,29988
5	0,22561	2,36549	1,32	0,755	1,368	22	1,13582	1,05127	0,65545
6	0,04004	0,74986	1,325	0,424	1,226	26	0,73102	0,51971	0,36859
7	0,02433	0,57903	1,426	0,36	1,479	20	0,61787	0,4956	0,25075
8	0,05994	1,03375	1,396	0,486	1,351	24	0,74478	0,68642	0,31747
9	0,08492	1,25704	1,345	0,545	1,737	20	1,11323	0,50725	0,38911
10	0,02218	0,49078	1,286	0,349	1,308	16	0,5337	0,41783	0,27952
11	0,03631	0,67151	1,266	0,411	1,205	18	0,57454	0,50676	0,38175
12	0,02976	0,61552	1,325	0,384	1,224	16	0,60651	0,45825	0,39941
13	0,33473	3,19795	1,372	0,861	1,347	22	1,49628	1,25262	0,67711
14	0,13197	1,66376	1,327	0,632	1,237	22	1,06819	0,72252	0,51689
15	0,237	2,64433	1,428	0,768	1,466	20	1,19053	1,1696	0,46961
16	0,11487	1,4339	1,255	0,603	1,312	12	0,98924	0,62657	0,55086
17	0,13024	1,87796	1,511	0,629	2,15	22	1,25752	0,95287	0,29806
18	0,03746	0,83633	1,545	0,415	1,601	24	0,73733	0,55136	0,32081

19	0,18882	2,07618	1,304	0,712	1,413	26	1,16164	0,92107	0,47625
20	0,02307	0,50601	1,291	0,353	1,241	18	0,52273	0,47125	0,31991
21	0,07429	1,1867	1,389	0,522	1,56	20	1,04731	0,69059	0,319
22	0,48224	3,70633	1,246	0,973	1,163	24	1,26194	1,2265	0,93469
23	0,046	0,85902	1,384	0,445	1,571	14	0,78725	0,60153	0,29251
24	0,03611	0,77443	1,466	0,41	1,716	16	0,77374	0,50639	0,30821
25	0,06205	1,01945	1,345	0,491	1,901	16	1,00808	0,48097	0,37933
26	0,20681	2,38209	1,409	0,734	1,332	16	1,17449	0,92435	0,64327
27	0,14036	1,8931	1,449	0,645	1,649	20	1,08722	0,88127	0,41715
28	0,03038	0,57336	1,218	0,387	1,195	18	0,58592	0,41005	0,37147
29	0,02244	0,50911	1,323	0,35	1,171	22	0,50607	0,42047	0,40347
30	0,05172	0,89152	1,328	0,462	1,403	16	0,8372	0,4721	0,44181
31	0,29832	2,83003	1,311	0,829	1,261	30	1,26855	0,97121	0,77663
32	0,15949	1,96191	1,379	0,673	1,555	20	1,21756	0,85893	0,37311
33	0,15161	1,88181	1,369	0,662	1,325	24	1,0657	0,9338	0,52036
34	0,02453	0,53685	1,315	0,36	1,276	16	0,56698	0,46087	0,25054
35	0,02309	0,52254	1,333	0,353	1,345	20	0,57683	0,39829	0,32051
36	0,29227	2,58693	1,215	0,823	1,183	28	1,19915	1,06498	0,63101
37	0,03086	0,71307	1,499	0,389	1,944	14	0,82785	0,48842	0,19486
38	0,05633	0,9358	1,317	0,476	1,304	20	0,85981	0,53257	0,44433
39	0,05475	1,01504	1,456	0,471	1,8	22	1,01619	0,46296	0,35462
40	0,07462	1,2078	1,409	0,522	1,735	16	0,9927	0,61676	0,32513
41	0,04576	0,82487	1,333	0,444	1,358	20	0,72344	0,56204	0,37376
42	0,05913	0,89351	1,217	0,483	1,23	18	0,66463	0,6466	0,38345
43	0,07918	1,20382	1,35	0,533	1,409	20	0,89402	0,71415	0,37505
44	0,0291	0,61971	1,354	0,382	1,375	20	0,63052	0,45111	0,28847
45	0,12925	1,7337	1,402	0,627	1,392	14	0,96391	0,84437	0,56728
46	0,02921	0,62083	1,354	0,382	1,289	22	0,71343	0,41291	0,37224
47	0,02093	0,49426	1,346	0,342	1,379	20	0,59118	0,33905	0,31346
48	0,043	0,82226	1,385	0,435	2,09	14	0,96108	0,37501	0,32853
49	0,02341	0,50698	1,281	0,355	1,19	20	0,55095	0,38715	0,32177
50	0,23041	2,70742	1,49	0,761	2,119	12	1,45816	1,19787	0,36653
51	0,43191	3,82007	1,382	0,938	1,559	24	1,74118	1,0812	0,54796
52	0,12668	1,60795	1,318	0,623	1,282	14	0,94479	0,63776	0,60031
53	0,03857	0,69202	1,254	0,419	1,124	22	0,59944	0,47181	0,43195
54	0,08367	1,2039	1,301	0,543	1,354	16	0,8743	0,63534	0,42463
55	0,05917	0,95402	1,299	0,483	1,361	16	0,79537	0,55498	0,42305
56	0,3696	2,99866	1,204	0,89	1,126	20	1,25911	0,92043	0,82111
57	0,14057	1,70449	1,304	0,645	1,586	16	1,10201	0,75802	0,39585
58	0,30466	2,86362	1,308	0,835	1,652	20	1,64866	0,76836	0,68042
59	0,46498	3,88383	1,338	0,961	1,456	28	1,75857	0,98316	0,75723
60	0,02306	0,54143	1,382	0,353	1,602	14	0,65975	0,40766	0,21856
61	0,02805	0,6233	1,396	0,377	1,581	14	0,71409	0,3999	0,32004
62	0,02432	0,54526	1,343	0,359	1,571	20	0,66156	0,41309	0,25786
63	0,02069	0,51745	1,42	0,341	1,913	18	0,69663	0,36155	0,24754
64	0,17658	2,00306	1,316	0,696	1,251	24	1,13133	0,88931	0,55229
65	0,02265	0,50534	1,305	0,351	1,154	20	0,49644	0,43464	0,36337
66	0,15857	1,88085	1,328	0,672	1,736	12	1,40887	0,61613	0,47752
67	0,03907	0,7612	1,367	0,421	1,251	20	0,66384	0,54936	0,40806
68	0,11998	1,4947	1,271	0,612	1,24	22	0,9231	0,76555	0,50953

69	0,0336	0,70778	1,405	0,4	1,699	14	0,74705	0,4896	0,26119
70	0,15536	1,79622	1,285	0,667	1,234	24	0,98695	0,8685	0,47153
71	0,08997	1,35434	1,395	0,556	1,473	22	0,98916	0,8028	0,32847
72	0,05477	0,95216	1,365	0,471	1,213	14	0,66951	0,64281	0,49703
73	0,02679	0,62553	1,445	0,371	1,589	14	0,64428	0,40668	0,36093
74	0,17201	1,99083	1,331	0,69	1,364	24	1,0958	0,92726	0,51234
75	0,0642	1,14743	1,48	0,497	1,634	14	0,86044	0,70064	0,29301
76	0,11813	1,53473	1,318	0,609	1,405	22	1,00258	0,82804	0,45496
77	0,13973	1,72007	1,321	0,644	1,35	18	0,98544	0,92916	0,42603
78	0,05044	0,86471	1,31	0,458	1,473	20	0,83052	0,45948	0,31813
79	0,0356	0,71229	1,361	0,408	1,341	22	0,68942	0,56468	0,33683
80	0,06251	0,99456	1,306	0,492	1,57	18	0,92234	0,46289	0,40971
81	0,0916	1,24609	1,268	0,559	1,33	12	0,78437	0,70306	0,44827
82	0,14769	1,73557	1,284	0,656	1,452	18	1,0388	0,78034	0,3943
83	0,04291	0,88442	1,492	0,434	2,023	22	0,91262	0,46224	0,22775
84	0,08562	1,21264	1,291	0,547	1,252	18	0,81823	0,689	0,42802
85	0,16573	2,0845	1,429	0,682	1,592	28	1,23547	0,87349	0,39955
86	0,02661	0,5403	1,254	0,37	1,185	20	0,57866	0,36848	0,33969
87	0,02286	0,53827	1,382	0,352	1,255	16	0,52233	0,48507	0,3902
88	0,20594	2,25125	1,335	0,733	1,258	20	1,12086	1,04202	0,65351
89	0,16207	2,01587	1,402	0,676	1,555	14	1,29923	0,77918	0,4771
90	0,03493	0,74712	1,446	0,406	1,82	20	0,81286	0,45006	0,24921
91	0,0212	0,47511	1,282	0,343	1,229	22	0,52409	0,37108	0,30801
92	0,07014	1,22161	1,485	0,512	2,607	20	1,29888	0,49968	0,26797
93	0,08205	1,16696	1,278	0,539	1,16	20	0,69861	0,66808	0,49801
94	0,12563	1,63861	1,351	0,621	1,421	26	1,05572	0,87975	0,38544
95	0,11098	1,44284	1,292	0,596	1,374	16	1,00762	0,70039	0,53434
96	0,04916	0,8424	1,298	0,454	1,435	22	0,77292	0,52876	0,32857
97	0,02158	0,53763	1,434	0,345	1,764	14	0,66721	0,49958	0,20847
98	0,06045	0,98747	1,326	0,487	1,361	12	0,85234	0,59404	0,38132
99	0,02391	0,60664	1,511	0,357	1,67	16	0,68555	0,51229	0,17049
100	0,02164	0,52112	1,387	0,346	1,575	22	0,59473	0,37458	0,22934
101	0,04007	0,7722	1,364	0,425	1,74	12	0,83543	0,52911	0,24766
102	0,05558	1,18193	1,678	0,473	2,043	24	1,02482	0,6365	0,19458
103	0,44936	3,92058	1,382	0,95	1,411	18	1,56653	1,18797	0,68953
104	0,04254	0,92264	1,566	0,433	2,639	18	1,14831	0,46069	0,26972
105	0,02837	0,61065	1,358	0,378	1,455	16	0,70293	0,41939	0,30852
106	0,30695	2,62263	1,192	0,837	1,205	24	1,27182	0,86799	0,70087
107	0,1908	2,12287	1,325	0,714	1,402	22	1,17171	0,90827	0,49919
108	0,22304	2,31834	1,303	0,752	1,486	24	1,35626	0,86944	0,48835
109	0,02589	0,63335	1,496	0,367	1,733	16	0,77109	0,4949	0,31785
110	0,2912	2,66029	1,252	0,822	1,267	18	1,26549	0,95517	0,6681
111	0,05847	1,03697	1,423	0,482	1,914	26	0,94374	0,50055	0,27307
112	0,0279	0,61244	1,377	0,376	1,534	14	0,68378	0,40818	0,3298
113	0,0311	0,64223	1,343	0,39	1,243	20	0,55301	0,53285	0,3361
114	0,04169	0,75582	1,3	0,43	1,683	12	0,83906	0,40215	0,33482
115	0,03031	0,6355	1,352	0,387	1,254	28	0,59888	0,38283	0,35424
116	0,02668	0,61468	1,423	0,371	1,588	18	0,68627	0,55007	0,25162
117	0,1046	1,38748	1,292	0,585	1,468	16	0,93188	0,71326	0,35187
118	0,10961	1,58097	1,427	0,594	1,736	26	1,18749	0,61463	0,32431

119	0,15126	1,77891	1,296	0,661	1,186	22	0,9033	0,87552	0,57309
120	0,44887	3,36542	1,187	0,95	1,086	22	1,18911	1,06288	1,02554
121	0,08738	1,32153	1,388	0,551	1,65	20	1,11485	0,6507	0,36754
122	0,39452	3,34993	1,288	0,91	1,386	20	1,47884	1,00419	0,68814
123	0,04181	0,84496	1,451	0,431	1,414	22	0,88013	0,45395	0,43287
124	0,13964	1,79233	1,377	0,644	1,574	18	1,19754	0,73388	0,5016
125	0,06607	1,10336	1,396	0,502	1,311	24	0,76772	0,68295	0,43792
126	0,06796	1,06662	1,324	0,506	1,383	16	0,78513	0,61151	0,44384
127	0,06922	1,13428	1,391	0,509	1,467	14	0,83047	0,64213	0,40081
128	0,27485	2,70036	1,321	0,807	1,271	14	1,24689	1,07	0,67987
129	0,14096	2,08255	1,59	0,646	1,84	20	1,18561	1,11836	0,318
130	0,02569	0,64555	1,533	0,366	1,569	22	0,68144	0,42275	0,30502
131	0,18208	2,28812	1,473	0,703	1,775	26	1,25794	0,98824	0,35753
132	0,08555	1,26116	1,343	0,547	1,289	16	0,87752	0,5829	0,53367
133	0,02696	0,60694	1,396	0,372	1,253	22	0,58863	0,46229	0,3741
134	0,11537	1,45269	1,268	0,604	1,198	14	0,88339	0,81884	0,59861
135	0,14362	1,83939	1,387	0,65	1,424	20	1,05465	0,89108	0,46564
136	0,06085	1,0606	1,418	0,488	1,995	16	1,04512	0,48939	0,30019
137	0,22792	2,65951	1,474	0,758	1,536	14	1,37995	1,05401	0,56943
138	0,03487	0,74952	1,452	0,405	1,688	16	0,8088	0,53035	0,26797
139	0,02788	0,60241	1,355	0,376	1,466	22	0,69618	0,3788	0,29131
140	0,03106	0,75241	1,575	0,39	1,846	22	0,85719	0,46488	0,25514
141	0,16787	1,99192	1,354	0,684	1,472	18	1,15371	0,67568	0,6242
142	0,58748	4,10059	1,209	1,039	1,183	22	1,60414	1,24764	0,89851
143	0,34512	3,13007	1,316	0,87	1,272	26	1,31171	1,16572	0,67571
144	0,07993	1,26791	1,413	0,534	1,811	16	1,03341	0,68071	0,31471
145	0,02199	0,51469	1,356	0,348	1,652	12	0,66938	0,33747	0,27958
146	0,02328	0,50001	1,268	0,354	1,085	22	0,49207	0,42862	0,33666
147	0,09088	1,47243	1,506	0,558	1,82	20	1,16236	0,81669	0,27107
148	0,02902	0,74452	1,63	0,381	2,001	18	0,84854	0,58932	0,20326
149	0,03704	0,758	1,41	0,414	1,806	18	0,79883	0,40773	0,28135
150	0,13561	1,63551	1,281	0,637	1,302	20	0,9665	0,74114	0,5335
151	0,07428	1,19781	1,402	0,522	1,277	28	0,81262	0,70435	0,46382
152	0,14523	1,84014	1,377	0,652	1,452	26	1,09415	0,80932	0,31295
153	0,06273	1,11542	1,461	0,493	1,717	24	1,03649	0,55264	0,32768
154	0,26268	2,66617	1,344	0,795	1,305	22	1,23317	1,04565	0,65451
155	0,02242	0,61792	1,607	0,35	2,165	24	0,82146	0,43668	0,13297
156	0,03248	0,67958	1,38	0,396	1,752	16	0,78463	0,42875	0,26256
157	0,05927	1,04372	1,42	0,484	1,355	16	0,81444	0,58185	0,44781
158	0,02317	0,51134	1,301	0,354	1,242	22	0,52639	0,38618	0,27969
159	0,18577	2,26836	1,441	0,708	1,725	16	1,29541	0,99349	0,38984
160	0,02223	0,58352	1,526	0,349	2,236	18	0,83581	0,35348	0,19926
161	0,14265	1,6743	1,268	0,648	1,223	26	0,99349	0,85794	0,50953
162	0,02225	0,47915	1,252	0,349	1,135	22	0,49037	0,38267	0,34025
163	0,0267	0,63894	1,479	0,371	1,933	20	0,78891	0,3899	0,27726
164	0,0689	1,17751	1,449	0,509	2,002	18	1,18259	0,56369	0,34787
165	0,16346	1,78239	1,233	0,678	1,228	12	0,98616	0,85903	0,53069
166	0,02724	0,55871	1,276	0,373	1,185	20	0,52984	0,4733	0,34817
167	0,08836	1,43273	1,493	0,553	2,083	12	1,12329	0,72308	0,20828
168	0,06374	1,03584	1,342	0,496	1,321	20	0,85361	0,70584	0,36544

169	0,02881	0,58759	1,293	0,38	1,37	18	0,62936	0,41424	0,28036
170	0,18453	2,16728	1,383	0,706	1,479	22	1,21867	0,84295	0,52627
171	0,02551	0,51469	1,228	0,365	1,047	22	0,45908	0,44738	0,39714
172	0,09238	1,30962	1,325	0,561	1,402	12	0,95667	0,56466	0,50125
173	0,07364	1,1953	1,407	0,52	1,291	12	0,77515	0,69482	0,48817
174	0,26539	2,71303	1,358	0,797	1,626	12	1,4897	1,09082	0,42504
175	0,42326	3,51621	1,29	0,932	1,289	20	1,52516	1,09507	0,70703
176	0,06654	1,18369	1,491	0,503	1,74	26	1,06302	0,50195	0,41948
177	0,03662	0,65793	1,234	0,412	1,205	18	0,588	0,45523	0,35153
178	0,08238	1,24212	1,357	0,54	1,41	26	0,90354	0,65926	0,3584
179	0,06416	1,16446	1,502	0,497	1,878	16	0,96236	0,56591	0,30047
180	0,02906	0,61894	1,354	0,381	1,329	16	0,60775	0,47093	0,27835
181	0,24241	2,5984	1,382	0,774	1,41	22	1,20377	1,11837	0,46803
182	0,05178	0,89038	1,325	0,462	1,341	16	0,71079	0,68554	0,35945
183	0,03895	0,6858	1,234	0,421	1,215	20	0,60636	0,56576	0,36091
184	0,21476	2,19981	1,268	0,743	1,129	22	1,00257	0,91107	0,79685
185	0,03144	0,65406	1,358	0,392	1,559	16	0,69242	0,41598	0,31633
186	0,10515	1,4397	1,336	0,586	1,357	24	1,00957	0,60497	0,53153
187	0,02306	0,62402	1,593	0,353	3,227	24	0,9502	0,29401	0,1419
188	0,02108	0,52285	1,417	0,343	1,385	16	0,54089	0,43211	0,27668
189	0,02543	0,59901	1,432	0,365	1,346	26	0,64659	0,4106	0,34151
190	0,23843	2,53772	1,365	0,769	1,398	26	1,29236	1,04536	0,64289
191	0,32679	2,88048	1,255	0,855	1,252	20	1,27824	1,01298	0,70022
192	0,07192	1,30971	1,566	0,516	2,121	20	1,14319	0,7207	0,19955
193	0,03466	0,77946	1,516	0,405	1,618	26	0,69846	0,60751	0,19234
194	0,02641	0,5899	1,376	0,369	1,226	18	0,56626	0,4582	0,42458
195	0,02748	0,62257	1,414	0,374	1,439	22	0,64245	0,44773	0,29525
196	0,26271	2,70735	1,365	0,795	1,361	18	1,2597	1,08168	0,66736
197	0,04809	0,87353	1,366	0,451	1,864	14	0,86819	0,47657	0,22989
198	0,03855	0,81216	1,472	0,419	1,645	20	0,74364	0,65896	0,19986
199	0,0404	0,8494	1,492	0,426	2,205	18	0,86892	0,4644	0,17038
200	0,03164	0,67033	1,386	0,392	1,361	20	0,62429	0,47306	0,29565

Table B.2 Results of the CT scans of the siliceous river gravel fine aggregate from Indiana

#	Vol	SA	SA/Saeq	ESD	Tr/Treq	Max	L	W	T
1	0,03536	0,81851	1,571	0,407	1,66	26	0,73885	0,56093	0,19856
2	0,29063	2,92981	1,381	0,822	1,658	30	1,54493	0,88855	0,63508
3	0,02101	0,46874	1,273	0,342	1,209	20	0,59039	0,36359	0,31644
4	0,29116	3,04166	1,432	0,822	1,48	26	1,29437	1,05273	0,57915
5	0,02903	0,66087	1,447	0,381	1,437	22	0,67349	0,55922	0,3024
6	0,70577	5,32684	1,39	1,105	1,597	18	2,06856	1,23765	0,76117
7	0,33279	2,97229	1,28	0,86	1,256	14	1,32773	1,08298	0,70081
8	0,12501	1,53709	1,271	0,62	1,176	16	0,90528	0,71776	0,56712
9	0,13578	1,64118	1,285	0,638	1,363	12	1,10159	0,75594	0,42509
10	0,02444	0,59283	1,456	0,36	1,491	20	0,69599	0,41528	0,30394
11	0,99589	5,54183	1,149	1,239	1,155	30	1,68714	1,31278	1,04551
12	1,69938	8,16749	1,186	1,481	1,353	30	2,45694	1,43252	1,2488
13	0,42389	3,46337	1,269	0,932	1,456	20	1,5871	0,98135	0,68971

14	0,82643	4,98196	1,17	1,164	1,214	30	1,59119	1,35978	0,73587
15	0,04786	0,90201	1,415	0,45	1,638	28	0,83421	0,51177	0,21918
16	1,19453	6,04026	1,109	1,316	1,074	26	1,72845	1,36523	1,33252
17	0,17062	1,81833	1,222	0,688	1,144	26	0,94042	0,81843	0,5434
18	0,24966	2,59323	1,352	0,781	1,45	30	1,30555	0,92831	0,44955
19	1,03292	6,14476	1,243	1,254	1,249	24	1,96862	1,46918	0,99003
20	1,31034	6,7808	1,171	1,358	1,239	30	2,12535	1,30101	1,16506
21	0,0655	1,02362	1,303	0,5	1,716	22	0,91784	0,42632	0,40605
22	0,02121	0,52137	1,407	0,343	1,346	22	0,54534	0,42803	0,30634
23	0,04626	0,84724	1,36	0,445	1,449	12	0,78823	0,45279	0,41106
24	0,42025	3,53279	1,302	0,929	1,323	28	1,43005	1,12062	0,73754
25	0,13997	1,6078	1,233	0,644	1,166	28	0,85548	0,8256	0,5037
26	0,21618	2,69668	1,548	0,745	1,854	20	1,40286	1,01211	0,36878
27	0,66427	4,72128	1,282	1,083	1,296	28	1,57833	1,46141	0,71825
28	1,18248	7,21389	1,334	1,312	1,45	28	2,48029	1,39032	0,88339
29	0,73978	4,82383	1,219	1,122	1,22	26	1,60369	1,37584	0,87649
30	0,15616	1,95328	1,393	0,668	1,578	24	1,1855	0,72197	0,48967
31	0,02083	0,51939	1,419	0,341	1,905	12	0,72966	0,35745	0,24498
32	0,03806	0,73639	1,346	0,417	1,494	12	0,70883	0,4526	0,30818
33	0,60057	3,83176	1,113	1,047	1,123	24	1,38752	1,15828	0,91402
34	1,00012	5,66406	1,171	1,241	1,121	30	1,63688	1,41744	1,05209
35	0,07036	1,22106	1,481	0,512	1,806	18	0,91682	0,7592	0,19776
36	0,98557	5,38781	1,125	1,235	1,124	30	1,60847	1,4768	0,92029
37	1,20354	6,42516	1,174	1,32	1,208	30	1,86613	1,51367	0,97531
38	0,04808	1,00736	1,575	0,451	2,313	20	1,08002	0,51737	0,26351
39	0,54733	4,12646	1,275	1,015	1,395	12	1,68268	1,13832	0,7
40	1,35062	6,98239	1,182	1,371	1,177	30	1,98271	1,32823	1,25557
41	0,8871	5,19787	1,164	1,192	1,16	28	1,85904	1,35794	1,03706
42	0,34442	3,06593	1,29	0,87	1,347	18	1,3202	1,25347	0,64502
43	0,03086	0,73485	1,544	0,389	1,676	24	0,68659	0,56154	0,16493
44	0,24248	2,68155	1,426	0,774	1,846	20	1,59201	0,84748	0,49497
45	0,67038	4,59155	1,24	1,086	1,218	20	1,52195	1,2877	0,75044
46	1,17746	5,98129	1,109	1,31	1,109	30	1,75529	1,39673	1,11575
47	0,28835	3,06774	1,453	0,82	1,631	28	1,66787	0,99266	0,53935
48	0,48553	4,32561	1,448	0,975	1,74	24	1,76572	1,16665	0,66602
49	0,56703	4,45292	1,344	1,027	1,234	12	1,43471	1,35335	1,04284
50	0,47079	3,57397	1,221	0,965	1,12	26	1,27394	1,18197	0,89064
51	0,46847	3,63576	1,246	0,964	1,3	26	1,53389	1,06607	0,74661
52	0,93596	5,45348	1,179	1,214	1,167	30	1,63197	1,22979	1,04413
53	0,81915	4,97552	1,175	1,161	1,084	26	1,49663	1,33098	1,15958
54	1,53365	7,2319	1,124	1,431	1,245	30	2,13184	1,3466	1,04077
55	0,02748	0,65433	1,486	0,374	1,69	12	0,65363	0,52325	0,17373
56	0,21844	2,32389	1,325	0,747	1,303	24	1,26686	0,90317	0,49046
57	0,09279	1,43515	1,448	0,562	1,547	22	0,96335	0,77663	0,29462
58	0,6511	4,06783	1,12	1,075	1,141	24	1,46265	1,03126	0,95206
59	0,23471	2,15292	1,17	0,765	1,144	12	1,01882	0,97191	0,59642
60	1,06521	6,11068	1,211	1,267	1,313	28	2,08866	1,18087	1,14269
61	0,15868	2,0732	1,463	0,672	1,76	30	1,38631	0,77631	0,41756
62	0,34127	2,77935	1,177	0,867	1,103	30	1,11715	0,91139	0,85657
63	0,15017	1,9207	1,406	0,659	1,613	28	1,21968	0,75898	0,40991

64	0,11416	1,63928	1,44	0,602	1,535	24	1,05432	0,79531	0,29994
65	0,12493	1,94839	1,612	0,62	1,875	26	1,27705	0,89375	0,33986
66	0,05499	1,10229	1,576	0,472	1,9	22	0,97034	0,62061	0,22404
67	0,04485	0,89225	1,462	0,441	1,763	16	0,86894	0,53458	0,28958
68	0,05381	0,98827	1,434	0,468	1,539	22	0,83363	0,57475	0,28218
69	0,92666	5,26698	1,146	1,21	1,162	22	1,66339	1,39322	0,91252
70	0,02716	0,61049	1,397	0,373	1,234	22	0,60012	0,48623	0,28119
71	0,22526	2,09483	1,17	0,755	1,148	28	0,99976	0,81882	0,62489
72	0,05794	1,07662	1,487	0,48	1,863	20	0,9696	0,61823	0,19854
73	0,46344	3,59127	1,24	0,96	1,429	30	1,52997	1,06659	0,62564
74	0,67716	4,85665	1,302	1,09	1,425	20	1,70225	1,50232	0,7845
75	0,23585	2,73916	1,484	0,767	1,987	14	1,53202	0,84574	0,47978
76	0,18455	2,18098	1,391	0,706	1,661	28	1,29491	0,75479	0,43704
77	0,25997	2,67534	1,358	0,792	1,645	30	1,36468	0,91415	0,38014
78	1,44952	7,70624	1,244	1,404	1,494	26	2,41952	1,52289	0,86042
79	0,06952	1,1605	1,419	0,51	1,667	26	0,89864	0,65083	0,25599
80	0,0515	1,01801	1,521	0,462	2,097	28	0,93616	0,521	0,16446
81	0,67712	4,7466	1,273	1,089	1,413	30	1,64495	1,41025	0,54195
82	1,93485	8,90019	1,185	1,546	1,392	30	2,46121	1,34158	1,24422
83	0,99419	5,57412	1,157	1,238	1,181	30	1,74887	1,26928	1,08998
84	0,03945	0,80325	1,433	0,422	1,601	18	0,77715	0,52521	0,28187
85	0,36635	3,87739	1,566	0,888	2,132	24	2,02733	1,10263	0,52217
86	0,17138	2,14376	1,437	0,689	1,544	18	1,12836	0,93872	0,36981
87	1,04149	5,9173	1,191	1,258	1,154	30	1,82857	1,55544	1,06056
88	0,27361	2,89565	1,421	0,805	1,478	28	1,29105	1,10073	0,38202
89	0,08282	1,24732	1,358	0,541	1,352	26	0,83678	0,67078	0,33963
90	0,32887	3,19805	1,388	0,856	1,677	18	1,50269	1,13573	0,36147
91	0,62838	4,49519	1,267	1,063	1,238	30	1,61221	1,17886	0,89849
92	0,16792	2,26851	1,541	0,684	1,763	20	1,21578	1,1	0,31557
93	0,29897	3,15421	1,459	0,83	1,974	28	1,77863	0,92909	0,33826
94	0,63801	4,47985	1,25	1,068	1,303	30	1,49348	1,34913	0,71333
95	0,05276	0,9711	1,428	0,465	1,626	12	0,8151	0,61239	0,31027
96	0,81243	5,15086	1,223	1,158	1,293	20	1,79435	1,53397	0,74345
97	0,02938	0,71994	1,563	0,383	2,123	20	0,83009	0,44461	0,16576
98	0,14833	2,02639	1,495	0,657	1,547	22	1,09457	1,0089	0,46515
99	0,77695	4,74465	1,161	1,141	1,173	16	1,54815	1,4027	0,78191
100	0,74247	4,978	1,255	1,123	1,278	30	1,67164	1,30136	0,815
101	1,84447	10,54383	1,45	1,522	2,285	30	3,56216	1,49104	0,6358
102	0,63314	4,88176	1,369	1,065	1,485	22	1,71148	1,43922	0,64183
103	0,24873	2,27012	1,187	0,78	1,117	16	1,03444	0,81081	0,77009
104	0,47132	3,94459	1,347	0,966	1,57	30	1,61197	1,13375	0,59378
105	0,06104	1,06932	1,426	0,489	2,232	12	1,15719	0,44815	0,36011
106	1,08432	5,9001	1,156	1,275	1,274	30	2,05399	1,29626	0,92854
107	0,21431	2,42049	1,398	0,742	1,729	26	1,40429	0,76143	0,57562
108	0,09795	1,31967	1,284	0,572	1,161	16	0,82207	0,67143	0,50534
109	0,29458	3,08749	1,442	0,826	1,647	20	1,43555	1,24592	0,36388
110	0,76432	4,98079	1,232	1,134	1,222	26	1,56901	1,40045	0,86821
111	0,09192	1,47441	1,497	0,56	2,052	24	1,15934	0,71804	0,23174
112	0,81674	5,2529	1,243	1,16	1,33	30	1,71726	1,54399	0,71946
113	0,51092	3,86849	1,252	0,992	1,302	22	1,51132	1,1504	0,7592

114	0,67444	4,75998	1,28	1,088	1,201	28	1,61067	1,39067	1,01563
115	0,77947	5,12791	1,252	1,142	1,254	20	1,65559	1,44887	0,81902
116	0,53915	4,26052	1,33	1,01	1,415	28	1,75682	1,18732	0,72275
117	0,1264	1,52581	1,253	0,623	1,165	28	0,89682	0,68846	0,60226
118	1,22875	7,83967	1,413	1,329	2,559	22	3,29121	1,04225	0,78527
119	0,9189	5,28027	1,155	1,206	1,061	28	1,59599	1,33902	1,17269
120	0,08164	1,48238	1,629	0,538	2,399	18	1,27749	0,63268	0,23218
121	0,90891	5,32796	1,174	1,202	1,189	30	1,7692	1,2692	1,07331
122	0,04535	0,84388	1,372	0,442	1,657	18	0,78134	0,47487	0,28914
123	0,03555	0,75394	1,442	0,408	1,485	16	0,69446	0,42819	0,35779
124	0,44803	3,46138	1,222	0,949	1,127	28	1,35549	1,09761	0,98578
125	0,36681	2,93952	1,186	0,888	1,104	12	1,11345	1,02402	0,84462
126	0,48154	3,95406	1,331	0,972	1,512	24	1,69284	1,16403	0,50823
127	0,02253	0,59583	1,545	0,35	1,632	22	0,67659	0,50954	0,2368
128	1,23704	6,52946	1,172	1,332	1,159	28	1,98116	1,41735	1,05872
129	0,19394	2,22706	1,374	0,718	1,825	16	1,40652	0,65428	0,5358
130	0,03118	0,76157	1,59	0,391	2,1	22	0,80765	0,47052	0,16416
131	1,00577	5,63911	1,162	1,243	1,179	14	1,71075	1,27057	1,01794
132	0,19256	1,9965	1,238	0,716	1,195	30	1,0261	0,76232	0,60534
133	0,2145	2,04058	1,178	0,743	1,092	30	0,94899	0,84673	0,67984
134	0,49209	4,02397	1,335	0,98	1,402	28	1,71324	1,14424	0,8262
135	0,50913	3,96715	1,287	0,991	1,428	16	1,6592	1,14364	0,66702
136	0,03787	0,68511	1,256	0,417	1,6	12	0,72927	0,41073	0,31896
137	0,74916	5,03489	1,262	1,127	1,351	30	1,62522	1,47568	0,67285
138	1,0658	6,01568	1,192	1,267	1,234	24	1,80008	1,43773	0,92937
139	0,16937	1,98376	1,34	0,686	1,546	18	1,23698	0,77244	0,53169
140	0,11795	1,60442	1,379	0,608	1,354	26	1,06843	0,69044	0,43073
141	0,11983	1,83197	1,559	0,612	1,885	22	1,36992	0,78612	0,40773
142	0,93562	5,85416	1,265	1,213	1,425	26	2,05666	1,17282	1,03325
143	0,76979	5,31136	1,308	1,137	1,48	28	1,90099	1,33056	0,56265
144	0,79114	4,97927	1,204	1,147	1,125	30	1,54226	1,36346	0,97494
145	0,15245	1,65856	1,202	0,663	1,102	22	0,85962	0,78006	0,65479
146	0,24704	2,62273	1,377	0,778	1,514	20	1,4172	0,90212	0,54632
147	0,16399	1,98344	1,369	0,679	1,282	24	1,08293	0,86765	0,62329
148	1,03348	6,41563	1,298	1,254	1,416	30	1,99157	1,62902	0,81359
149	0,88885	5,42383	1,213	1,193	1,217	24	1,72827	1,35205	0,96002
150	0,05487	0,84446	1,209	0,471	1,221	12	0,73692	0,47156	0,43871
151	0,06273	1,05457	1,381	0,493	1,494	30	0,75647	0,58444	0,23576
152	0,0931	1,70986	1,721	0,562	1,705	14	0,93792	0,88286	0,28572
153	0,85929	5,834	1,335	1,18	1,364	24	2,03046	1,51581	1,04762
154	0,64287	4,6971	1,304	1,071	1,412	30	1,74872	1,40204	0,55326
155	0,82433	5,06645	1,192	1,163	1,242	28	1,65264	1,36631	0,78104
156	0,92666	5,09829	1,109	1,21	1,074	30	1,46598	1,42525	1,20744
157	0,43245	3,49654	1,264	0,938	1,455	24	1,59873	1,0114	0,69274
158	0,02584	0,60025	1,42	0,367	1,464	22	0,6369	0,4671	0,19068
159	0,84498	5,66966	1,312	1,173	1,445	24	2,10661	1,13435	1,15936
160	0,07486	1,13862	1,326	0,523	1,342	18	0,80248	0,61032	0,40604
161	0,05866	1,17176	1,605	0,482	3,307	18	1,32	0,4778	0,16922
162	0,03508	0,84237	1,625	0,406	1,965	18	0,8219	0,5408	0,19377
163	0,09946	1,35174	1,302	0,575	1,184	26	0,83199	0,73117	0,52528

164	0,41285	3,38358	1,262	0,924	1,254	16	1,30503	1,17602	0,62444
165	1,28504	6,57189	1,15	1,349	1,218	30	1,98826	1,53579	1,00022
166	0,64148	4,39227	1,221	1,07	1,182	18	1,46939	1,30034	0,87322
167	0,2651	2,29944	1,152	0,797	1,116	28	1,04255	0,86787	0,67205
168	0,08424	1,2864	1,384	0,544	1,471	16	0,92387	0,83597	0,37114
169	0,08964	1,51635	1,565	0,555	3,119	22	1,45521	0,50724	0,19492
170	1,41751	7,75476	1,271	1,394	1,415	28	2,43663	1,52726	1,00962
171	1,06496	5,85941	1,162	1,267	1,109	28	1,64391	1,45432	1,10757
172	0,12264	1,92109	1,609	0,616	1,916	18	1,27842	0,79537	0,30438
173	0,38263	3,40123	1,334	0,901	1,515	26	1,6416	0,93307	0,65222
174	0,02198	0,51239	1,35	0,348	1,415	14	0,58629	0,4765	0,25926
175	1,56211	7,70182	1,183	1,44	1,322	26	2,40846	1,43871	1,1322
176	0,82335	5,91199	1,392	1,163	1,735	24	2,10534	1,60783	0,59051
177	1,14276	6,11828	1,157	1,297	1,231	30	1,88821	1,38838	0,88623
178	0,83181	5,02255	1,174	1,167	1,189	28	1,576	1,5267	0,81075
179	0,27768	3,07	1,492	0,809	1,702	20	1,5659	1,00505	0,54223
180	0,83549	5,19837	1,212	1,169	1,143	28	1,53545	1,44576	0,93179
181	0,17631	2,09061	1,375	0,696	1,746	18	1,41627	0,71815	0,48871
182	1,19813	6,78437	1,244	1,318	1,348	30	2,05138	1,59012	0,89777
183	0,1002	1,43887	1,379	0,576	1,532	26	0,9805	0,67549	0,34145
184	0,69626	4,67697	1,231	1,1	1,304	22	1,73486	1,2735	0,77383
185	0,53462	4,34131	1,363	1,007	1,48	30	1,7913	1,20599	0,7118
186	0,04792	0,9823	1,54	0,451	1,705	20	0,79308	0,7127	0,19777
187	0,1714	1,91074	1,28	0,689	1,354	18	1,10447	0,86617	0,42716
188	0,40719	3,39261	1,277	0,92	1,189	30	1,295	1,08353	0,77122
189	1,28417	6,5207	1,141	1,349	1,117	28	1,85581	1,37317	1,26835
190	0,65949	4,67226	1,275	1,08	1,389	24	1,62638	1,35147	0,56893
191	0,1574	2,27733	1,615	0,67	1,817	30	1,22515	0,97768	0,31573
192	0,17016	1,83336	1,235	0,688	1,209	30	0,9982	0,6985	0,55217
193	1,56104	7,25109	1,114	1,439	1,196	30	2,05185	1,2831	1,16983
194	0,98556	5,49635	1,148	1,235	1,116	28	1,62389	1,46462	1,03798
195	0,50848	3,45191	1,12	0,99	1,051	30	1,13822	1,16494	0,927
196	0,25159	2,77604	1,44	0,783	1,524	30	1,37873	0,9957	0,59679
197	0,6699	5,45829	1,474	1,086	1,672	26	1,90738	1,56255	0,58733
198	0,07336	1,20683	1,424	0,519	1,872	16	1,06121	0,45199	0,38139
199	1,05514	6,01683	1,2	1,263	1,183	28	2,09196	1,24648	1,16764
200	1,21355	6,61619	1,203	1,323	1,323	30	2,08329	1,49296	0,92935

Table B.3 Results of the CT scans of the limestone fine aggregate

#	Vol	SA	SA/Saeq	ESD	Tr/Treq	Max	L	W	T
1	0,20462	2,15192	1,281	0,731	1,214	16	1,06266	0,89625	0,70451
2	1,43787	9,02161	1,464	1,4	1,796	24	2,66763	1,70292	0,82472
3	0,25699	2,98685	1,528	0,789	1,798	16	1,42742	1,1835	0,36798
4	4,31229	16,42562	1,282	2,019	1,511	30	3,41255	2,09171	1,16195
5	0,98421	6,81544	1,424	1,234	1,638	18	2,33792	1,28828	0,85479
6	1,79752	10,53563	1,474	1,509	1,691	28	3,06763	1,74249	1,01888
7	0,1979	2,31266	1,408	0,723	1,515	22	1,2231	0,96225	0,43081
8	0,3343	2,90004	1,245	0,861	1,198	20	1,29765	0,9411	0,71612
9	0,63654	4,9944	1,396	1,067	1,857	22	2,20543	1,05442	0,74818

10	0,29142	2,92242	1,375	0,823	1,787	18	1,68605	0,75464	0,58887
11	0,25172	2,43589	1,263	0,783	1,462	12	1,3587	0,86548	0,63075
12	0,14056	1,67566	1,282	0,645	1,287	16	1,0156	0,67987	0,62166
13	0,22638	2,36323	1,316	0,756	1,385	24	1,33488	0,84726	0,56881
14	3,08764	13,23885	1,291	1,807	1,369	26	2,85656	2,16857	1,26247
15	0,50011	3,82874	1,257	0,985	1,315	20	1,61456	1,02045	0,86209
16	0,24224	2,81767	1,499	0,773	1,931	24	1,54338	0,85467	0,43007
17	0,9121	6,05497	1,331	1,203	1,559	16	2,26703	1,12399	0,88894
18	0,23703	2,20761	1,192	0,768	1,209	26	1,20279	0,77822	0,6394
19	0,16982	1,95237	1,316	0,687	1,253	28	1,06549	0,75273	0,56784
20	0,12236	1,6286	1,366	0,616	1,372	18	1,061	0,72097	0,50322
21	0,14432	1,83613	1,38	0,651	1,572	20	1,19757	0,83336	0,40522
22	0,24764	2,49102	1,306	0,779	1,264	18	1,27687	1,06907	0,67692
23	0,14666	1,86926	1,39	0,654	1,577	20	1,17671	0,78642	0,43419
24	0,06347	1,10673	1,438	0,495	1,465	24	0,87897	0,60061	0,3479
25	0,10281	1,54631	1,457	0,581	1,639	22	1,09867	0,68181	0,40443
26	0,47054	3,98345	1,362	0,965	1,542	30	1,65952	1,1609	0,47258
27	0,21987	2,49902	1,419	0,749	1,618	22	1,22747	0,9652	0,41875
28	0,39482	3,35758	1,29	0,91	1,425	22	1,59311	0,95078	0,73559
29	0,41384	4,01515	1,495	0,925	2,202	18	2,01826	1,05233	0,50846
30	0,72148	5,0152	1,289	1,113	1,389	24	1,77951	1,13658	0,81873
31	0,17254	2,21548	1,478	0,691	2,132	20	1,66832	0,66095	0,48639
32	0,16548	1,92855	1,323	0,681	1,382	16	1,12521	0,88746	0,50843
33	0,20001	2,08459	1,26	0,726	1,449	16	1,21113	0,74989	0,52734
34	0,27149	2,86325	1,412	0,803	1,633	24	1,5335	1,06116	0,45305
35	0,17247	2,25551	1,505	0,691	1,723	24	1,34471	0,87784	0,41237
36	2,27208	11,60859	1,389	1,631	1,904	28	3,45599	1,579	1,22127
37	0,29552	3,00248	1,399	0,826	1,787	18	1,61164	0,91832	0,48883
38	0,24776	2,43442	1,276	0,779	1,396	22	1,37396	0,78835	0,59171
39	0,2904	2,98904	1,409	0,822	1,669	22	1,58203	1,02164	0,4999
40	0,18324	1,95024	1,25	0,705	1,146	22	0,99732	0,89181	0,62574
41	0,19639	2,18884	1,34	0,721	1,561	14	1,2691	0,87899	0,50117
42	0,3423	3,26244	1,379	0,868	1,562	24	1,59667	1,03854	0,51207
43	0,16598	1,86157	1,275	0,682	1,164	26	0,93475	0,89495	0,65223
44	0,18251	1,95316	1,255	0,704	1,246	20	1,04209	0,74311	0,68318
45	0,18304	2,41829	1,551	0,704	2,177	22	1,45761	0,81198	0,31289
46	0,11185	1,43178	1,275	0,598	1,305	24	0,93343	0,67922	0,40783
47	0,37524	3,31933	1,319	0,895	1,383	20	1,39123	1,15963	0,64563
48	0,12702	1,7577	1,438	0,624	1,488	22	1,04028	0,88547	0,41886
49	0,18083	1,97803	1,279	0,702	1,238	14	1,07831	0,78505	0,62867
50	0,19278	2,16658	1,343	0,717	1,478	20	1,36955	0,8039	0,55073
51	0,40936	3,24315	1,216	0,921	1,107	26	1,26676	1,01226	0,88638
52	0,17914	2,10672	1,371	0,699	1,552	24	1,40247	0,70964	0,56302
53	0,39591	3,35673	1,287	0,911	1,458	28	1,58335	0,90376	0,68489
54	0,31006	3,33051	1,503	0,84	2,29	24	2,07092	0,87449	0,46918
55	0,12732	1,81269	1,481	0,624	1,62	24	1,0715	0,93932	0,41805
56	0,15286	1,79582	1,299	0,663	1,393	18	1,14094	0,7983	0,50166
57	0,15866	1,94668	1,373	0,672	1,291	28	1,0177	0,97431	0,50896
58	0,59697	4,66138	1,36	1,045	1,587	22	1,87235	1,14875	0,69689
59	0,14118	1,6906	1,289	0,646	1,214	26	0,9365	0,79735	0,5591
60	0,18801	2,32797	1,467	0,711	1,647	26	1,31988	0,86416	0,4511

61	0,68225	4,62579	1,234	1,092	1,393	28	1,82167	1,00134	0,76584
62	0,15728	1,8489	1,312	0,67	1,61	12	1,23252	0,70587	0,44721
63	0,18154	2,11241	1,362	0,703	1,361	22	1,15718	0,95283	0,52228
64	0,79729	5,6877	1,368	1,15	1,694	22	2,22963	1,30382	0,8113
65	0,61965	4,48339	1,276	1,058	1,278	24	1,76442	1,13956	0,88713
66	0,29324	2,90127	1,359	0,824	1,432	22	1,35899	0,99458	0,56119
67	0,22375	2,35779	1,323	0,753	1,288	30	1,30453	0,82778	0,72264
68	0,31044	2,829	1,276	0,84	1,383	24	1,42851	0,9098	0,62321
69	0,5994	4,18265	1,217	1,046	1,176	28	1,56559	1,2987	0,98188
70	0,2867	2,99033	1,422	0,818	1,553	22	1,48042	1,2513	0,47921
71	0,15834	2,1012	1,485	0,671	1,748	14	1,19245	1,04278	0,33948
72	0,09723	1,28379	1,255	0,571	1,386	20	0,93558	0,55639	0,42089
73	0,09442	1,40923	1,405	0,565	1,422	24	0,89713	0,81777	0,36958
74	0,28877	2,79735	1,324	0,82	1,301	26	1,28351	1,08628	0,59591
75	0,67784	5,10986	1,369	1,09	1,414	20	1,84207	1,20467	1,0382
76	0,23416	2,35119	1,28	0,765	1,306	22	1,17766	0,93461	0,58157
77	0,19401	2,17992	1,345	0,718	1,407	24	1,28346	0,75717	0,62126
78	0,50112	3,79273	1,243	0,985	1,222	24	1,50146	1,14586	0,77433
79	0,21953	2,45565	1,395	0,748	2,043	16	1,57991	0,80906	0,36711
80	0,25143	2,66285	1,382	0,783	1,828	22	1,62913	0,81678	0,50899
81	0,11358	1,81399	1,599	0,601	1,984	18	1,23568	0,86245	0,33827
82	0,16642	1,90712	1,303	0,682	1,294	22	1,07684	0,8343	0,53316
83	0,1562	1,87017	1,333	0,668	1,364	18	1,03551	0,86933	0,63272
84	0,15781	1,79272	1,269	0,67	1,457	14	1,09441	0,69812	0,49423
85	0,24282	2,35736	1,252	0,774	1,312	20	1,17471	0,82945	0,52925
86	0,1513	1,88748	1,375	0,661	1,48	16	1,13488	0,9724	0,40393
87	0,10019	1,35135	1,295	0,576	1,286	22	0,96037	0,6307	0,53
88	0,40709	3,33868	1,257	0,92	1,139	26	1,28277	1,14762	0,83688
89	0,46702	3,86163	1,327	0,963	1,444	20	1,62346	1,26695	0,58368
90	0,12075	1,66961	1,413	0,613	1,529	18	1,06556	0,75442	0,52403
91	0,40684	3,49357	1,316	0,919	1,39	18	1,60313	0,98893	0,69973
92	1,09244	6,3313	1,234	1,278	1,316	30	2,05287	1,29227	0,94495
93	0,4923	4,04236	1,341	0,98	1,441	24	1,76283	1,08779	0,73555
94	0,5711	4,44901	1,337	1,029	1,421	28	1,80823	1,22508	0,69535
95	0,52803	4,59338	1,454	1,003	1,602	18	1,71809	1,59017	0,66104
96	0,04234	0,75835	1,291	0,432	1,17	14	0,58392	0,5086	0,41401
97	0,10262	1,34721	1,271	0,581	1,237	20	0,88439	0,65638	0,56294
98	0,12656	1,55485	1,275	0,623	1,246	18	0,98086	0,79657	0,45315
99	0,14286	1,74667	1,322	0,649	1,308	22	0,95676	0,90361	0,44571
100	0,02092	0,46136	1,257	0,342	1,121	18	0,50428	0,40076	0,30667
101	0,21749	2,94744	1,685	0,746	2,495	20	1,73559	0,96069	0,32521
102	0,02859	0,58239	1,288	0,379	1,21	18	0,60123	0,4242	0,32975
103	0,19815	2,11564	1,287	0,723	1,16	24	1,07456	0,79356	0,75938
104	0,39002	3,39122	1,314	0,906	1,437	24	1,70153	1,05966	0,68657
105	0,11396	1,60404	1,411	0,602	1,58	14	1,08519	0,86693	0,41405
106	0,17808	1,88945	1,234	0,698	1,149	26	0,95459	0,8137	0,67939
107	0,13212	1,82682	1,456	0,632	1,604	18	1,19354	0,7886	0,41564
108	0,27103	2,60486	1,286	0,803	1,229	30	1,2957	0,93425	0,66817
109	0,31884	3,32797	1,475	0,848	1,655	22	1,60722	0,97508	0,65048
110	0,80786	5,75516	1,372	1,156	1,714	22	2,40416	1,13379	0,72501
111	0,27135	2,59376	1,28	0,803	1,279	18	1,25036	0,90026	0,78874

112	0,03329	0,78136	1,561	0,399	1,872	24	0,88182	0,45343	0,22519
113	0,45059	4,23441	1,49	0,951	1,704	26	1,74291	1,43539	0,50608
114	0,09951	1,50657	1,451	0,575	1,429	20	0,97277	0,65223	0,42012
115	0,25757	2,8375	1,449	0,789	1,85	12	1,57927	1,04587	0,47399
116	0,22164	2,34359	1,323	0,751	1,395	24	1,31053	0,87213	0,53517
117	0,06237	1,19954	1,577	0,492	1,585	24	0,83226	0,78876	0,28738
118	0,32504	2,97868	1,303	0,853	1,459	22	1,53362	0,83213	0,68013
119	0,1011	1,48173	1,412	0,578	1,527	14	0,93537	0,86262	0,38633
120	0,19514	2,24004	1,377	0,72	1,376	22	1,17384	0,9986	0,55645
121	0,30953	2,78186	1,257	0,839	1,367	16	1,31732	0,88164	0,62645
122	0,19308	2,1513	1,332	0,717	1,254	26	1,1022	0,9275	0,61904
123	0,56869	4,50046	1,356	1,028	1,551	16	1,83303	1,21877	0,73411
124	0,0316	0,70735	1,464	0,392	1,553	20	0,68527	0,40893	0,3268
125	0,4128	3,58536	1,337	0,924	1,495	24	1,64825	0,94806	0,70297
126	0,07172	1,26439	1,515	0,515	1,679	20	0,9953	0,70541	0,32516
127	0,16359	2,08599	1,442	0,679	1,458	26	1,20309	0,89599	0,48688
128	0,26467	2,49895	1,254	0,797	1,227	26	1,16752	0,93263	0,68158
129	0,27756	2,68511	1,305	0,809	1,202	24	1,10203	0,93083	0,74437
130	0,16279	1,85082	1,284	0,677	1,277	22	1,01577	0,78235	0,49742
131	0,28869	2,88796	1,367	0,82	1,468	24	1,2957	1,08158	0,46652
132	0,50731	3,7556	1,221	0,99	1,165	26	1,29051	1,2701	0,83238
133	0,87643	6,04023	1,364	1,187	1,459	26	2,07438	1,26743	1,05837
134	0,20795	2,41291	1,421	0,735	1,624	20	1,19868	1,02386	0,40963
135	0,11599	1,62359	1,412	0,605	1,526	24	1,00583	0,7857	0,36869
136	0,14052	1,72507	1,32	0,645	1,351	20	1,01956	0,80618	0,51309
137	0,06043	1,19495	1,605	0,487	2,313	20	1,13615	0,47669	0,27658
138	0,08373	1,4293	1,544	0,543	1,985	16	1,1176	0,70116	0,24731
139	0,81212	5,76011	1,368	1,158	1,659	28	2,16463	1,3002	0,68069
140	0,83423	5,48599	1,28	1,168	1,294	28	1,90328	1,23466	0,98305
141	0,32312	3,09972	1,361	0,851	1,51	28	1,45066	0,97283	0,70518
142	0,12352	1,82326	1,52	0,618	1,743	18	1,14602	0,83403	0,45217
143	0,15515	1,67932	1,203	0,667	1,124	24	0,91351	0,80154	0,5869
144	0,33062	3,01702	1,305	0,858	1,283	24	1,38419	0,89433	0,8105
145	0,36218	3,81952	1,554	0,884	2,026	18	1,81601	1,12603	0,48466
146	0,4085	3,49214	1,312	0,921	1,275	22	1,46011	0,96343	0,81348
147	0,6481	5,18421	1,431	1,074	1,848	26	2,12362	1,11319	0,67832
148	0,19918	2,21428	1,342	0,725	1,423	22	1,14939	0,96648	0,45409
149	0,02302	0,56166	1,435	0,353	1,576	18	0,69814	0,40289	0,26885
150	0,30078	2,88478	1,329	0,831	1,416	18	1,42336	0,88109	0,66216
151	0,10952	1,52436	1,377	0,594	1,683	16	1,17531	0,76752	0,30667
152	0,17014	1,81083	1,22	0,687	1,223	22	1,02461	0,72079	0,6356
153	0,51299	4,21922	1,361	0,993	1,613	20	1,97538	0,97166	0,66529
154	0,13947	1,61835	1,244	0,643	1,114	30	0,88786	0,77857	0,6579
155	0,14618	1,68812	1,258	0,654	1,19	30	0,95686	0,76881	0,48742
156	0,47042	3,74793	1,281	0,965	1,252	28	1,50307	1,2096	0,82195
157	0,06505	1,0935	1,398	0,499	1,559	18	0,95529	0,59231	0,38371
158	0,17434	2,12267	1,406	0,693	1,633	24	1,32618	0,76724	0,48588
159	0,77546	6,16426	1,51	1,14	2,38	20	2,71553	1,23723	0,61862
160	0,03827	0,72434	1,319	0,418	1,217	14	0,59884	0,51028	0,40239
161	0,20265	2,09052	1,253	0,729	1,22	20	1,09846	0,87117	0,56651
162	0,24407	2,55056	1,35	0,775	1,478	26	1,38117	0,83286	0,60962

163	0,29639	2,83613	1,319	0,827	1,513	20	1,38222	0,93475	0,63431
164	0,13121	1,64819	1,32	0,63	1,54	22	1,16428	0,59311	0,53684
165	0,49523	3,97341	1,313	0,982	1,497	22	1,79324	1,0498	0,72967
166	0,26241	2,57362	1,298	0,794	1,359	22	1,24047	1,06458	0,53553
167	0,98558	6,5753	1,373	1,235	1,634	28	2,39284	1,51106	0,73349
168	0,58061	4,45337	1,323	1,035	1,412	26	1,85665	1,15197	0,86456
169	0,34269	3,05187	1,289	0,868	1,366	30	1,58831	0,94107	0,69761
170	0,86425	5,86387	1,336	1,182	1,657	24	2,28326	1,1627	0,75196
171	0,2303	2,47538	1,362	0,76	1,459	26	1,32984	0,98765	0,45725
172	0,19727	2,28405	1,394	0,722	1,769	22	1,54603	0,76893	0,57115
173	0,14952	1,90107	1,395	0,659	1,542	16	1,09124	0,94258	0,41702
174	0,16725	1,82128	1,241	0,684	1,158	28	0,9513	0,9207	0,59805
175	0,2518	2,83903	1,472	0,783	2,21	14	1,67882	0,76064	0,50753
176	0,46422	4,23688	1,461	0,961	1,703	16	1,77966	1,25843	0,59782
177	0,10486	1,4301	1,33	0,585	1,349	20	0,92978	0,5804	0,54349
178	0,09189	1,50107	1,524	0,56	1,966	14	1,19332	0,65587	0,36683
179	0,28394	2,7173	1,301	0,815	1,396	28	1,40246	0,94426	0,53596
180	0,30924	2,82503	1,277	0,839	1,218	24	1,27138	1,02449	0,697
181	0,38929	3,52995	1,369	0,906	1,783	24	1,83784	0,88489	0,58708
182	0,51366	4,76146	1,535	0,994	2,221	22	2,16924	1,06565	0,55504
183	0,0941	1,41373	1,413	0,564	1,749	16	1,12394	0,63515	0,39936
184	0,31215	2,89338	1,3	0,842	1,409	28	1,49217	0,90964	0,62528
185	0,35542	3,16798	1,306	0,879	1,348	28	1,46287	1,0599	0,5572
186	0,20159	2,20177	1,324	0,727	1,327	20	1,16862	0,82742	0,53947
187	0,02708	0,51498	1,181	0,373	1,078	16	0,49014	0,42761	0,3334
188	0,17392	2,14132	1,421	0,693	1,764	22	1,36722	0,89147	0,36838
189	0,25607	2,73566	1,403	0,788	1,336	26	1,26816	0,86012	0,67541
190	0,23985	2,73196	1,463	0,771	2,113	18	1,73887	0,85979	0,44363
191	0,44885	3,70911	1,308	0,95	1,449	18	1,71274	1,01377	0,70431
192	0,21255	2,38304	1,384	0,74	1,481	24	1,21946	1,03296	0,41399
193	0,2208	2,33091	1,319	0,75	1,384	18	1,21486	0,82117	0,55468
194	0,32089	2,93351	1,294	0,849	1,311	26	1,28917	1,05476	0,59156
195	0,48801	3,74315	1,249	0,977	1,341	14	1,58336	1,19248	0,74092
196	0,28156	2,53675	1,221	0,813	1,106	28	1,07521	1,02292	0,71372
197	0,09747	1,47412	1,439	0,571	1,952	16	1,2417	0,60073	0,3412
198	0,38673	3,84582	1,498	0,904	1,966	22	2,12685	0,93352	0,58545
199	0,34758	3,18168	1,331	0,872	1,508	24	1,44788	1,02395	0,51976
200	0,11711	1,61689	1,397	0,607	1,669	12	1,11974	0,70964	0,50342

Table B.4 Results of the CT scans of the granite microfine aggregate from California

#	Vol	SA	SA/Saeq	ESD	Tr/Treq	Max	L	W	T
1	76299.4	10932.55	1.257	52.62	1.265	20	86.4	55.4	40.5
2	82181.9	11819.00	1.293	53.94	1.216	22	79.8	51.6	51.7
3	68903.5	10355.65	1.274	50.86	1.197	16	72.9	66.3	49.7
4	80993.6	12858.69	1.42	53.68	1.666	16	106.5	70.6	31.3
5	107493.6	13786.00	1.261	58.99	1.29	20	87.5	74.3	45.7
6	107858.2	14461.88	1.32	59.06	1.325	16	103.6	63.8	42.2
7	131937.6	15764.89	1.258	63.16	1.17	24	99.1	72.5	60.4
8	64842.0	10466.00	1.341	49.84	1.69	18	101.8	53.2	31.6

9	139825.3	18251.50	1.401	64.40	1.469	12	103.3	87.7	53.9
10	102372.9	15069.06	1.424	58.04	1.72	20	107.1	60.3	42.4
11	132704.9	15761.37	1.253	63.28	1.253	18	93.6	66.7	48.5
12	74232.3	11931.10	1.397	52.14	1.464	20	99.1	66.7	38.5
13	83585.7	11372.23	1.23	54.25	1.147	22	76.6	67.0	46.6
14	64820.1	10638.30	1.363	49.84	1.308	20	79.1	68.7	37.4
15	62304.0	9852.29	1.296	49.19	1.358	16	75.7	59.4	36.0
16	66349.4	9681.80	1.222	50.23	1.137	20	68.7	58.9	41.7
17	97794.2	13115.46	1.278	57.16	1.281	16	97.8	66.1	50.5
18	85211.7	12865.04	1.374	54.60	1.669	16	96.6	66.6	30.3
19	100957.5	12925.23	1.233	57.77	1.117	26	77.8	63.0	50.4
20	64150.2	9855.19	1.272	49.67	1.155	20	71.5	59.1	41.6
21	79725.3	11620.29	1.297	53.40	1.144	24	82.6	60.9	50.8
22	74315.3	10779.51	1.261	52.16	1.155	22	75.5	58.5	47.4
23	69373.0	10073.89	1.234	50.98	1.361	14	81.8	50.7	37.1
24	107526.0	14619.08	1.337	59.00	1.354	22	87.9	86.0	37.8
25	67336.9	10115.97	1.264	50.48	1.128	24	68.9	56.5	45.7
26	94059.9	12661.80	1.266	56.42	1.182	22	84.8	58.6	52.0
27	60851.8	10350.43	1.383	48.80	1.421	12	82.9	60.5	51.8
28	73978.8	10755.77	1.262	52.08	1.149	14	71.1	61.9	51.2
29	67101.9	10103.82	1.265	50.42	1.214	20	73.9	59.0	40.8
30	89930.1	12456.80	1.283	55.59	1.363	20	102.2	54.4	45.9
31	69442.6	10817.88	1.324	51.00	1.232	18	77.7	54.4	51.4
32	116185.2	14188.67	1.232	60.54	1.268	18	91.6	78.9	39.5
33	68848.9	11274.70	1.388	50.85	1.571	22	98.9	55.0	36.5
34	85415.6	12902.94	1.376	54.64	1.544	22	102.0	69.3	34.5
35	65763.7	9796.69	1.243	50.08	1.179	16	72.2	68.0	52.0
36	73391.1	10724.64	1.265	51.95	1.184	18	71.9	66.5	50.2
37	126804.9	14798.54	1.212	62.33	1.219	18	90.0	79.8	44.7
38	69318.3	10172.43	1.247	50.97	1.183	18	76.1	58.2	41.9
39	169104.0	17712.52	1.198	68.61	1.136	20	90.2	76.0	65.6
40	78710.5	11443.56	1.288	53.17	1.173	24	75.6	66.5	50.3
41	64150.3	9740.68	1.257	49.67	1.155	16	67.1	56.3	51.0
42	74079.8	10795.40	1.266	52.11	1.356	18	89.4	51.6	41.8
43	65982.6	10926.26	1.384	50.14	1.589	20	91.2	59.3	31.0
44	77649.0	12313.51	1.399	52.93	1.739	18	107.8	62.0	27.5
45	64411.8	10152.25	1.306	49.73	1.86	12	99.2	46.5	31.3
46	68255.9	10220.11	1.265	50.70	1.329	14	82.7	53.3	43.9
47	69709.3	10387.96	1.268	51.06	1.187	20	74.5	68.0	39.1
48	89509.4	12366.20	1.278	55.50	1.306	18	97.1	60.1	48.8
49	73486.1	12466.68	1.469	51.97	1.631	22	94.6	66.7	32.3
50	100049.7	13765.05	1.321	57.60	1.337	20	101.6	62.6	47.3
51	87887.9	12310.98	1.288	55.16	1.168	18	78.0	72.8	48.5
52	64571.7	10156.70	1.305	49.78	1.192	16	77.6	60.1	51.2
53	82928.9	11346.03	1.234	54.10	1.167	20	77.7	71.6	45.3
54	173784.8	22333.53	1.483	69.24	2.759	20	166.6	62.0	39.2
55	63253.7	10384.78	1.353	49.43	1.173	24	78.0	63.3	45.0
56	94743.0	13068.98	1.3	56.56	1.258	18	90.2	60.9	53.5
57	134750.9	16886.64	1.329	63.61	1.318	24	108.1	63.3	56.4
58	63985.3	9476.36	1.225	49.62	1.471	12	88.4	43.4	40.8
59	70525.6	10173.97	1.232	51.26	1.16	18	74.4	53.3	49.0
60	92513.6	12997.23	1.314	56.11	1.403	22	96.1	61.8	41.5
61	88610.9	13295.51	1.383	55.31	1.497	24	104.6	64.9	40.3

62	174458.4	20350.72	1.348	69.33	1.366	26	116.6	90.2	54.3
63	83272.0	12408.72	1.346	54.18	1.647	14	99.5	57.6	42.7
64	79719.6	11231.56	1.254	53.40	1.219	20	74.5	67.1	48.8
65	73713.7	10629.88	1.25	52.02	1.183	18	74.2	58.1	51.9
66	65846.8	10368.21	1.315	50.10	1.263	20	80.9	70.0	37.7
67	63084.8	9642.64	1.258	49.39	1.301	20	82.4	47.0	44.0
68	79640.9	12077.91	1.349	53.38	1.974	16	117.8	47.3	35.2
69	80033.6	12878.97	1.434	53.47	1.933	18	108.9	52.4	35.9
70	111377.7	16626.22	1.485	59.69	1.529	24	110.0	64.7	54.1
71	72727.0	11390.17	1.352	51.79	1.296	20	74.5	60.8	50.7
72	67713.0	11896.99	1.481	50.57	2.372	20	124.3	47.7	30.5
73	63274.3	9625.45	1.253	49.44	1.187	18	70.4	51.6	39.4
74	67642.4	10078.23	1.255	50.55	1.223	18	81.7	51.8	44.2
75	66124.2	10827.87	1.369	50.17	1.37	20	95.0	61.7	40.5
76	71302.9	10650.20	1.281	51.45	1.178	22	74.0	61.8	47.0
77	106196.3	14846.94	1.369	58.75	1.435	24	106.4	56.0	44.9
78	106012.3	14892.08	1.375	58.72	1.478	22	103.5	64.8	41.3
79	122449.6	13898.00	1.165	61.61	1.074	22	85.8	66.4	62.9
80	249696.0	25846.92	1.348	78.13	1.423	20	134.6	88.7	81.9
81	104836.1	13589.80	1.264	58.50	1.194	20	83.8	71.2	47.0
82	106605.5	13414.70	1.234	58.83	1.181	24	81.1	70.0	50.3
83	87316.2	12473.63	1.311	55.04	1.586	18	96.1	57.0	31.0
84	85844.3	12366.51	1.314	54.73	1.569	18	101.2	55.1	38.3
85	112319.8	14890.23	1.323	59.86	1.263	22	89.7	79.5	46.2
86	107741.4	14572.76	1.331	59.04	1.183	22	88.5	71.8	63.8
87	62884.3	9974.76	1.304	49.34	1.358	18	80.4	64.9	33.7
88	70054.9	10012.29	1.218	51.15	1.206	18	75.0	67.5	37.1
89	182598.9	21068.11	1.354	70.39	1.458	18	144.9	76.2	63.6
90	115535.5	13758.43	1.199	60.43	1.096	20	81.0	77.3	65.8
91	82129.6	11195.29	1.225	53.93	1.204	14	73.9	72.3	38.3
92	100162.8	13606.73	1.305	57.62	1.243	22	93.9	74.6	47.9
93	112160.7	15939.06	1.417	59.83	1.855	22	131.7	60.7	35.9
94	107691.0	13805.60	1.261	59.03	1.299	20	90.9	70.9	48.1
95	64900.2	10559.59	1.352	49.86	1.526	20	85.3	56.4	30.8
96	64255.0	10480.40	1.351	49.69	1.374	22	88.9	55.4	41.3
97	148177.7	17178.31	1.269	65.65	1.562	18	119.1	59.4	47.6
98	64642.7	10700.17	1.374	49.79	1.371	20	86.7	50.8	41.0
99	67046.3	10003.26	1.253	50.40	1.196	20	72.8	56.6	40.4
100	65764.7	10255.80	1.302	50.08	1.3	22	75.9	56.7	37.4
101	106884.6	13953.01	1.281	58.88	1.334	14	97.2	67.0	51.2
102	62783.8	9978.47	1.306	49.31	1.241	14	76.2	63.7	51.9
103	108323.9	15271.19	1.39	59.14	1.35	18	103.5	71.2	45.7
104	66952.5	9631.60	1.208	50.38	1.256	16	73.1	56.8	35.6
105	91188.8	12677.01	1.294	55.84	1.363	22	92.9	58.5	44.7
106	83313.3	12139.60	1.316	54.19	1.288	18	86.0	82.2	45.6
107	84774.2	14124.84	1.514	54.50	2.113	18	110.2	68.2	32.2
108	220018.9	22620.28	1.283	74.90	1.297	16	118.4	98.3	60.8
109	109926.6	14078.10	1.269	59.43	1.263	22	86.6	82.0	45.4
110	115632.8	14841.30	1.293	60.45	1.357	22	94.2	71.1	34.4
111	76942.4	11041.54	1.262	52.77	1.25	18	76.5	74.5	38.2
112	60597.2	9444.53	1.266	48.73	1.227	16	73.2	54.7	46.1
113	63814.0	10046.69	1.301	49.58	1.196	18	76.2	61.4	42.6
114	110535.7	14240.44	1.279	59.54	1.358	20	90.7	78.8	37.5

115	71431.5	11724.20	1.408	51.48	1.497	16	89.3	61.9	41.6
116	140715.4	18596.53	1.421	64.53	1.673	12	115.9	79.9	46.8
117	107753.6	14397.21	1.315	59.04	1.503	20	109.5	68.2	41.0
118	159925.3	18637.44	1.308	67.35	1.761	16	125.3	62.0	51.8
119	78710.7	12134.98	1.366	53.17	1.482	20	83.0	73.1	28.7
120	70457.0	10156.16	1.231	51.24	1.305	16	89.8	53.8	41.0
121	72283.6	10787.58	1.286	51.68	1.161	22	77.3	60.7	45.3
122	62889.7	9351.43	1.223	49.34	1.183	16	74.4	55.3	42.0
123	72618.5	10195.80	1.211	51.76	1.182	20	69.4	62.6	41.2
124	75960.0	10281.54	1.185	52.54	1.063	22	64.0	60.6	53.8
125	82869.4	12002.14	1.306	54.09	1.334	18	83.8	69.4	39.0
126	185815.8	18837.94	1.196	70.80	1.088	24	93.8	78.0	64.8
127	86084.7	12766.75	1.354	54.78	1.192	26	77.3	67.8	52.9
128	146892.6	18070.26	1.342	65.46	1.251	22	100.4	68.4	64.1
129	66047.7	10294.80	1.303	50.15	1.304	18	84.8	61.4	41.1
130	68336.0	10325.11	1.277	50.72	1.155	24	72.2	58.8	48.8
131	182878.6	18808.96	1.207	70.42	1.147	26	98.7	85.4	56.5
132	74089.1	10511.87	1.232	52.11	1.091	18	68.4	62.0	52.8
133	72965.7	11537.61	1.366	51.84	1.446	12	83.8	72.6	36.5
134	71850.9	11541.26	1.381	51.58	1.581	20	90.5	63.5	32.2
135	105195.1	14709.58	1.365	58.57	1.305	22	93.5	72.5	52.9
136	72847.2	11474.47	1.36	51.82	1.449	18	80.6	76.0	34.9
137	126142.8	15569.64	1.28	62.22	1.209	26	97.8	71.4	51.6
138	106087.4	14413.21	1.33	58.73	1.392	22	90.9	68.1	42.4
139	70753.1	10805.12	1.306	51.32	1.23	22	82.3	59.4	40.9
140	81107.2	11366.96	1.254	53.71	1.205	16	84.4	60.9	51.0
141	81451.3	12117.49	1.334	53.78	1.35	20	82.4	73.0	35.2
142	75723.2	11467.92	1.325	52.49	1.267	24	76.2	64.8	41.6
143	66991.7	10702.50	1.342	50.39	1.279	26	73.6	62.8	37.7
144	77012.6	10604.82	1.211	52.79	1.265	16	79.9	58.1	37.3
145	100030.6	14530.47	1.394	57.59	1.421	22	93.2	84.2	36.8
146	61308.3	9908.18	1.318	48.92	1.328	16	73.8	68.6	36.1
147	71413.0	10678.29	1.283	51.47	1.195	24	73.5	55.8	48.6
148	60841.4	10409.45	1.391	48.80	1.753	20	99.7	48.0	33.4
149	92378.7	12878.84	1.303	56.09	1.353	12	91.1	70.9	48.2
150	142421.6	16586.21	1.258	64.79	1.307	22	108.1	84.2	44.2
151	89166.2	13600.29	1.409	55.43	1.595	20	124.7	56.6	44.4
152	89598.9	12387.40	1.279	55.52	1.24	22	80.6	68.9	40.9
153	69313.2	10728.00	1.315	50.97	1.116	24	69.6	59.2	51.6
154	64486.5	10141.39	1.304	49.75	1.33	16	78.9	64.2	38.3
155	103887.6	12973.04	1.214	58.33	1.155	18	88.4	59.6	56.9
156	116875.1	13870.89	1.2	60.66	1.135	24	82.7	64.4	56.5
157	88534.8	12641.09	1.316	55.30	1.296	20	93.0	59.1	48.0
158	99636.1	12871.03	1.238	57.52	1.067	24	71.5	67.0	57.9
159	65192.3	11083.32	1.415	49.93	1.289	26	80.1	63.0	41.8
160	115125.1	15371.12	1.343	60.36	1.409	26	108.8	69.0	43.0
161	67228.6	10511.08	1.315	50.45	1.23	22	78.7	63.4	42.0
162	60907.4	10978.37	1.466	48.82	1.689	14	88.4	58.7	36.9
163	59917.5	9671.93	1.306	48.55	1.459	12	78.0	57.4	47.5
164	69641.7	11534.72	1.409	51.05	1.545	18	89.3	74.6	31.0
165	71311.4	10262.65	1.234	51.45	1.108	18	68.0	58.7	50.2
166	70751.5	12238.30	1.479	51.32	2.273	14	114.9	52.9	25.9
167	86000.3	13095.33	1.39	54.76	1.695	14	105.6	59.5	36.2

168	64859.1	10056.30	1.288	49.85	1.269	20	73.3	59.8	38.4
169	82868.4	12599.47	1.371	54.09	1.354	22	92.9	66.3	36.3
170	71437.6	10341.02	1.242	51.48	1.283	16	75.5	54.0	42.4
171	129092.4	16892.12	1.368	62.70	1.33	22	105.0	66.9	53.1
172	67546.4	11114.64	1.386	50.53	1.655	22	99.6	44.5	41.5
173	88307.4	12717.72	1.326	55.25	1.251	20	82.2	77.8	48.0
174	82693.5	12381.07	1.349	54.05	1.315	22	94.2	68.7	42.6
175	60365.3	10048.81	1.35	48.67	1.36	20	79.5	62.9	37.7
176	93168.9	13106.60	1.319	56.25	1.614	12	97.1	50.2	44.9
177	82946.9	13810.24	1.501	54.11	1.974	18	120.0	62.6	29.6
178	67836.0	10216.77	1.27	50.60	1.262	20	74.9	59.9	40.5
179	61161.1	10266.36	1.368	48.88	1.393	14	82.6	61.3	35.0
180	103243.9	13876.84	1.304	58.20	1.355	20	96.4	67.3	49.7
181	81007.4	11965.15	1.322	53.68	1.194	24	75.2	64.3	42.7
182	73101.2	11707.69	1.385	51.88	1.67	20	91.1	64.9	25.8
183	82447.3	12029.80	1.313	54.00	1.791	18	102.3	50.7	34.9
184	149186.1	18442.15	1.356	65.80	1.572	18	119.3	94.0	37.7
185	74823.6	10898.31	1.269	52.28	1.129	26	68.4	61.3	42.8
186	80141.2	12179.28	1.355	53.49	1.638	18	98.2	53.4	37.4
187	135800.4	16564.06	1.296	63.77	1.313	24	95.9	74.0	43.8
188	67787.4	11143.72	1.386	50.59	1.781	16	99.3	52.7	31.1
189	118199.1	14469.90	1.242	60.89	1.17	24	92.5	65.5	59.5
190	62124.9	10927.19	1.441	49.14	1.671	24	97.7	49.7	34.1
191	121787.3	15735.24	1.324	61.50	1.434	16	98.6	88.0	38.3
192	61886.7	9606.01	1.27	49.08	1.2	16	72.4	54.1	44.2
193	71311.4	10618.45	1.277	51.45	1.079	22	70.7	55.2	52.1
194	118086.4	15755.21	1.354	60.87	1.253	26	89.8	77.4	55.1
195	74211.3	10810.63	1.266	52.14	1.269	16	83.7	65.8	41.4
196	97398.0	12871.25	1.257	57.08	1.216	22	86.8	65.0	48.2
197	65999.1	10063.47	1.274	50.14	1.351	12	84.0	54.2	38.5
198	179644.2	19293.53	1.253	70.01	1.292	18	106.0	81.9	54.3
199	62134.7	9539.93	1.257	49.14	1.247	18	77.4	57.8	38.5
200	65433.2	9611.84	1.224	50.00	1.206	18	66.7	63.4	38.5

Table B.5 Results of the ∝CT scans of HG3875

#	Vol	SA	SA/(SA)eq	ESD	Tr/(Tr)eq	Max	L	W	T
1	14485.7	4413.24	1.536	30.24	1.966	12	62.2	36.6	19.4
2	8128.2	2726.13	1.394	24.95	1.389	18	41.0	33.6	19.2
3	11117.2	3111.12	1.292	27.69	1.199	24	41.4	30.7	21.1
4	27535.5	5609.42	1.272	37.47	1.296	18	57.8	45.1	36.6
5	21619.4	4983.69	1.328	34.56	1.253	28	56.6	38.4	33.0
6	10799.4	3377.19	1.429	27.42	2.006	20	59.1	28.0	19.2
7	9118.5	2677.09	1.268	25.92	1.222	22	36.5	32.3	20.2
8	15367.6	3863.53	1.292	30.85	1.26	24	52.8	35.6	25.9
9	7773.9	2641.25	1.392	24.58	1.808	14	48.7	27.5	14.7
10	43484.1	8146.23	1.362	43.63	1.737	26	85.7	43.6	26.6
11	8833.4	2722.47	1.317	25.65	1.299	20	40.8	28.9	19.8
12	71942.5	11632.68	1.391	51.60	2.084	12	106.1	48.8	30.9
13	12255.5	3742.19	1.456	28.61	1.437	22	52.9	28.7	26.3
14	31983.6	6029.45	1.237	39.38	1.154	26	56.2	48.1	34.7
15	21320.7	5231.16	1.407	34.40	1.458	24	54.4	54.4	23.2
16	24163.4	5711.66	1.413	35.87	1.597	24	71.6	40.1	26.9

17	21427.5	4818.87	1.292	34.46	1.276	24	55.6	45.4	27.5
18	17152.1	4015.68	1.249	32.00	1.211	22	45.6	39.7	23.7
19	18695.8	4711.42	1.383	32.93	1.383	16	55.3	36.2	30.5
20	10798.1	3006.70	1.273	27.42	1.236	22	42.3	27.6	26.3
21	42690.1	8274.48	1.401	43.36	1.493	22	69.8	65.6	25.1
22	72933.4	10497.74	1.244	51.84	1.163	28	72.3	63.0	44.1
23	7759.0	2628.44	1.387	24.56	1.439	18	39.5	36.0	15.0
24	108423.3	14884.45	1.354	59.16	1.468	24	97.9	87.0	44.2
25	27186.3	5968.29	1.365	37.31	1.541	20	63.4	42.0	24.2
26	22279.3	5645.48	1.474	34.91	1.77	20	75.1	39.9	22.9
27	26489.5	5698.66	1.326	36.98	1.408	20	71.2	43.2	28.5
28	14980.1	3828.22	1.303	30.58	1.415	16	52.4	36.0	24.6
29	29596.9	6948.93	1.502	38.38	2.111	16	78.3	55.5	23.5
30	18155.7	4387.31	1.313	32.61	1.37	20	55.5	36.7	20.6
31	11061.8	3474.28	1.447	27.64	1.512	20	46.5	42.2	19.1
32	11116.4	3388.03	1.407	27.69	1.662	22	54.0	31.8	19.2
33	33011.1	5999.24	1.206	39.80	1.263	18	63.4	48.9	34.1
34	49215.9	8412.07	1.295	45.47	1.368	18	75.1	50.9	35.1
35	13002.2	3633.96	1.359	29.17	1.402	22	45.9	36.0	22.8
36	16907.7	4185.03	1.314	31.84	1.536	16	54.9	34.2	19.0
37	11509.7	3586.96	1.455	28.01	1.658	14	51.8	29.1	22.7
38	8263.5	2705.35	1.369	25.08	2.001	18	50.1	21.4	15.7
39	18828.3	4084.67	1.193	33.01	1.092	24	43.3	41.3	30.3
40	9633.4	3106.62	1.419	26.40	1.721	24	54.5	25.6	18.3
41	15827.8	4589.95	1.506	31.15	1.757	18	62.3	39.9	19.3
42	25944.1	5713.13	1.348	36.73	1.447	20	63.5	45.3	22.6
43	69335.6	11376.05	1.394	50.97	1.466	26	86.5	73.4	34.1
44	89879.4	11871.51	1.223	55.58	1.187	28	77.3	67.4	46.3
45	132694.9	15627.49	1.242	63.28	1.153	28	86.5	87.2	63.6
46	43026.0	8399.84	1.415	43.48	1.558	16	77.6	54.4	29.5
47	31914.7	6082.10	1.25	39.35	1.311	22	63.4	41.7	34.0
48	35340.1	6655.78	1.278	40.72	1.3	24	67.2	50.7	33.2
49	8161.2	2994.90	1.528	24.98	1.771	16	54.4	37.0	15.0
50	27591.2	5897.14	1.335	37.49	1.328	20	61.1	48.8	34.1
51	50466.1	8590.46	1.301	45.85	1.367	28	83.7	49.0	34.5
52	37894.2	6991.42	1.281	41.67	1.471	26	70.6	39.5	29.8
53	9699.3	3181.61	1.447	26.46	1.939	16	57.4	30.3	16.6
54	37214.8	7288.10	1.352	41.42	1.681	18	82.2	43.3	30.5
55	11052.7	3217.84	1.341	27.64	1.443	18	48.3	38.8	17.6
56	9166.6	2976.94	1.405	25.97	1.326	22	39.2	29.7	25.4
57	20412.4	4302.08	1.191	33.91	1.165	20	47.4	41.6	27.1
58	17487.9	4513.05	1.385	32.20	1.198	28	51.7	38.2	30.6
59	42778.8	7756.65	1.311	43.39	1.472	26	78.2	47.2	28.9
60	21011.3	5297.04	1.439	34.24	2.088	22	77.9	30.5	26.0
61	10894.4	3617.45	1.522	27.50	1.924	14	53.5	38.5	13.3
62	26212.7	5412.84	1.268	36.86	1.438	22	62.7	36.5	30.6
63	35167.7	8101.92	1.561	40.65	2.652	16	97.5	42.5	17.7
64	19357.2	4528.33	1.299	33.31	1.23	22	51.9	37.2	33.7
65	18567.2	4313.57	1.272	32.85	1.166	26	47.3	40.5	26.0
66	7947.1	2535.59	1.317	24.76	1.177	22	38.3	29.5	23.3
67	36818.5	6962.14	1.301	41.28	1.231	26	63.9	49.2	34.6
68	14447.3	3708.06	1.293	30.22	1.272	20	45.7	34.5	23.8
69	37786.0	7081.77	1.3	41.63	1.588	18	69.9	42.2	31.2
70	12346.9	3427.87	1.327	28.68	1.343	16	42.5	37.6	19.2
71	13082.1	3582.78	1.334	29.23	1.491	14	46.6	40.0	18.3
72	18617.9	4582.75	1.349	32.88	1.514	18	53.7	48.8	18.5

73	9641.8	2978.74	1.36	26.41	1.584	16	48.9	30.3	17.1
74	34678.5	7295.15	1.419	40.46	1.623	18	76.8	55.6	26.2
75	28565.0	6429.90	1.423	37.93	1.717	20	75.0	42.1	21.6
76	9534.6	2781.65	1.279	26.31	1.237	18	40.2	28.9	23.5
77	8738.5	2640.62	1.287	25.56	1.185	24	35.7	32.2	22.2
78	37114.7	7904.66	1.469	41.39	1.667	16	73.4	60.8	21.5
79	11089.0	3334.77	1.387	27.67	1.566	18	50.9	40.5	17.4
80	19633.0	4621.68	1.313	33.47	1.497	18	61.6	37.7	24.5
81	8747.8	2750.74	1.34	25.56	1.58	16	43.8	33.4	14.2
82	70458.8	11013.53	1.335	51.24	1.515	16	86.9	54.0	42.5
83	18475.7	4304.73	1.274	32.80	1.425	20	57.7	36.6	23.7
84	17652.9	4371.45	1.333	32.31	1.997	14	66.7	27.4	21.3
85	9554.0	2702.84	1.241	26.33	1.283	16	39.8	29.4	20.8
86	20099.7	4522.73	1.265	33.73	1.309	22	51.4	43.4	20.7
87	40989.5	7889.38	1.372	42.78	1.625	18	79.9	46.7	32.9
88	18746.9	4740.97	1.389	32.96	1.562	22	61.0	30.8	29.3
89	14866.5	4201.49	1.437	30.51	1.67	20	59.4	32.7	22.8
90	21624.1	5066.23	1.35	34.57	1.424	18	57.2	43.8	26.5
91	15947.7	4382.55	1.43	31.23	1.704	16	60.4	34.5	19.4
92	44046.5	7497.93	1.243	43.82	1.145	26	65.1	52.7	37.7
93	11272.5	3801.00	1.563	27.82	2.465	12	64.4	32.0	12.7
94	10771.2	3090.23	1.31	27.40	1.29	22	43.5	28.7	20.9
95	21280.0	4767.53	1.284	34.38	1.363	24	59.2	36.2	27.7
96	60744.5	9694.58	1.297	48.77	1.358	28	78.3	58.5	34.3
97	26965.2	6437.26	1.48	37.21	1.798	20	75.6	46.7	30.1
98	14823.5	4014.44	1.376	30.48	1.81	18	64.6	31.5	22.3
99	10593.8	3460.90	1.484	27.25	2.497	14	67.5	27.6	17.0
100	10565.6	2991.29	1.285	27.22	1.326	20	38.4	38.6	17.2
101	11611.1	3070.97	1.238	28.09	1.147	22	41.3	34.9	26.1
102	64470.2	10505.26	1.351	49.75	1.421	26	92.5	53.1	37.9
103	10402.2	2978.64	1.293	27.08	1.307	20	39.8	32.9	22.9
104	10724.0	3324.36	1.414	27.36	1.566	22	48.7	30.7	20.9
105	22205.3	4627.25	1.211	34.87	1.206	22	55.4	38.6	30.1
106	11402.2	3558.18	1.452	27.93	1.709	22	54.8	31.7	18.6
107	51301.0	9205.70	1.379	46.10	1.407	18	76.3	54.3	40.1
108	16335.1	4589.78	1.474	31.48	2.342	16	75.7	33.0	18.9
109	9557.6	3262.46	1.498	26.33	2.264	22	67.1	26.1	16.6
110	21145.0	4877.95	1.319	34.31	1.478	18	56.5	51.2	18.9
111	17915.5	4368.10	1.319	32.46	1.419	20	61.6	33.5	26.7
112	42923.9	7812.78	1.318	43.44	1.317	26	72.9	46.7	38.3
113	19391.8	4578.34	1.312	33.33	1.614	22	59.2	31.9	27.2
114	14765.2	3645.82	1.253	30.44	1.154	24	42.2	37.4	26.3
115	25521.9	5551.01	1.324	36.53	1.709	20	70.9	38.1	18.9
116	9528.7	3232.53	1.487	26.30	2.257	18	63.7	25.2	20.3
117	7769.7	2451.22	1.292	24.57	1.396	16	40.7	28.1	17.5
118	17343.9	4130.15	1.275	32.12	1.293	22	53.2	35.5	26.6
119	23385.6	5144.51	1.301	35.48	1.435	18	61.8	42.7	22.2
120	38564.2	7369.47	1.335	41.92	1.632	24	89.6	38.6	31.5
121	14991.7	3848.87	1.309	30.59	1.298	26	53.3	30.6	25.7
122	12492.9	3402.97	1.307	28.79	1.268	20	46.3	34.5	20.5
123	26408.1	5637.35	1.315	36.95	1.427	22	70.4	36.9	28.6
124	9116.7	2988.07	1.416	25.92	1.479	20	48.3	30.0	17.2
125	10117.9	3198.38	1.414	26.83	1.735	24	50.0	32.1	14.4
126	38386.2	7538.54	1.37	41.85	1.474	26	80.6	53.2	30.0
127	17759.0	4406.50	1.339	32.37	1.263	28	53.5	37.6	24.2
128	19687.0	4763.90	1.351	33.50	1.353	24	60.8	38.9	31.1

129	15556.1	4255.57	1.412	30.97	2.15	20	68.9	27.2	20.0
130	43106.6	8276.82	1.392	43.50	1.825	22	75.0	43.8	31.8
131	54745.9	8616.32	1.236	47.11	1.115	20	65.6	58.1	48.4
132	9823.5	3133.48	1.413	26.57	1.857	16	55.0	27.6	17.6
133	9979.7	3429.34	1.53	26.71	2.232	16	66.0	23.6	21.5
134	46296.8	7751.40	1.243	44.55	1.214	28	70.0	48.9	36.8
135	13712.4	3660.98	1.321	29.70	1.448	24	51.4	31.4	24.5
136	12572.8	3550.06	1.358	28.85	1.358	24	43.0	37.1	22.4
137	10920.9	3375.21	1.418	27.53	1.554	14	49.1	38.3	16.8
138	32804.5	6411.70	1.294	39.72	1.367	14	60.3	51.7	26.0
139	16646.4	4236.52	1.344	31.68	1.556	14	60.2	32.6	27.7
140	13711.5	3472.24	1.253	29.70	1.343	18	46.6	37.0	20.5
141	8342.0	2685.07	1.35	25.16	1.154	24	36.3	28.8	25.5
142	11782.1	3313.63	1.323	28.23	1.768	18	54.0	29.2	17.5
143	67618.7	10522.52	1.311	50.55	1.2	28	74.1	59.1	46.1
144	10430.4	3321.74	1.439	27.11	1.5	18	48.0	32.9	17.9
145	40527.4	8302.92	1.455	42.62	1.689	26	83.1	56.2	29.4
146	14214.3	3999.31	1.409	30.05	1.507	22	55.3	34.2	20.5
147	13919.8	4010.56	1.433	29.85	1.616	14	54.2	42.6	17.6
148	44065.8	8712.32	1.444	43.82	1.831	26	87.6	50.4	25.5
149	12896.3	3304.73	1.243	29.10	1.237	18	46.0	31.1	27.3
150	8150.8	2563.82	1.309	24.97	1.398	18	42.3	24.7	19.8
151	17525.5	4240.38	1.3	32.23	1.406	22	59.1	38.4	19.1
152	17804.6	4794.20	1.454	32.40	1.628	20	55.2	44.6	18.8
153	7645.7	2763.65	1.472	24.44	1.91	12	50.4	34.5	13.7
154	11409.5	3264.46	1.332	27.93	1.452	18	47.2	36.0	17.2
155	10524.2	2991.22	1.288	27.19	1.214	22	39.2	36.3	23.1
156	8819.8	2824.99	1.368	25.63	1.493	20	47.8	32.3	20.0
157	20806.7	5007.80	1.369	34.12	1.442	26	67.7	32.9	28.4
158	8112.1	2662.02	1.363	24.93	1.252	22	36.1	31.1	20.4
159	9238.8	2615.92	1.229	26.03	1.129	22	37.7	29.6	21.4
160	12218.6	3217.43	1.254	28.58	1.42	16	45.8	32.7	21.4
161	20171.7	4908.49	1.37	33.77	1.178	28	49.9	43.2	31.0
162	7970.8	2535.19	1.314	24.78	1.238	18	39.0	29.6	19.4
163	38066.6	6962.82	1.272	41.74	1.253	24	60.2	53.4	37.5
164	13479.4	3550.19	1.296	29.53	1.364	18	46.9	37.1	21.3
165	36994.4	7070.50	1.317	41.34	1.292	26	66.4	53.3	29.4
166	19380.2	4760.63	1.364	33.33	1.428	20	55.2	37.4	28.2
167	53537.5	8610.56	1.253	46.76	1.219	26	70.7	53.0	43.9
168	12790.2	3471.09	1.312	29.02	1.318	20	49.8	38.1	21.3
169	41538.7	7490.92	1.291	42.97	1.445	22	80.3	42.5	32.6
170	8363.7	2883.39	1.447	25.18	1.9	20	57.2	25.8	17.8
171	19463.5	4552.08	1.301	33.37	1.715	18	65.3	33.3	21.9
172	12356.8	3119.15	1.207	28.68	1.274	18	43.6	30.0	20.8
173	13079.9	4095.87	1.526	29.23	2.8	14	74.5	28.0	13.3
174	9572.2	2898.70	1.33	26.34	1.652	14	49.6	27.4	18.9
175	15055.3	3846.07	1.304	30.64	1.24	26	49.4	32.5	28.7
176	107111.1	14257.72	1.307	58.92	1.712	28	111.6	60.7	45.7
177	9921.6	2857.86	1.28	26.66	1.146	22	35.0	33.8	24.0
178	56096.8	8427.46	1.189	47.49	1.198	28	69.4	54.7	35.3
179	10578.9	2863.81	1.229	27.24	1.167	22	39.0	28.3	23.6
180	37097.7	8556.27	1.591	41.38	3.427	16	116.2	34.9	21.0
181	13254.8	3516.21	1.298	29.36	1.288	20	46.2	34.3	20.9
182	17008.3	4997.97	1.563	31.91	2.805	16	82.3	32.3	15.3
183	15626.7	4105.40	1.358	31.02	1.464	20	51.4	37.1	21.7
184	9095.8	2753.13	1.307	25.90	1.502	18	48.7	25.0	19.2

185	11521.5	3229.53	1.309	28.02	1.314	18	46.8	30.7	24.5
186	17230.4	4163.01	1.29	32.05	1.44	20	58.4	32.5	30.2
187	31484.0	6692.58	1.388	39.18	1.519	20	65.1	56.3	23.3
188	19409.3	4879.81	1.397	33.34	1.858	20	68.4	32.4	21.7
189	32959.8	6393.35	1.286	39.78	1.206	26	58.3	53.9	38.3
190	21056.8	4840.31	1.313	34.26	1.158	24	59.0	39.1	35.5
191	15807.5	4073.62	1.337	31.14	1.394	26	53.0	34.8	24.7
192	18501.0	4570.94	1.351	32.81	1.52	22	61.8	34.4	24.3
193	58057.1	9068.94	1.251	48.04	1.25	22	74.1	55.0	41.0
194	8609.9	2707.05	1.333	25.43	1.535	16	47.5	25.1	21.5
195	10068.5	2938.19	1.303	26.79	1.224	22	40.2	32.1	23.4
196	7775.4	2502.55	1.319	24.58	1.376	12	41.6	29.8	17.9
197	62482.9	10530.05	1.383	49.23	1.648	22	95.8	57.6	37.2
198	11264.3	3065.39	1.261	27.81	1.202	20	43.1	33.1	26.9
199	12626.4	3920.57	1.495	28.89	1.813	22	60.6	32.6	19.0
200	23996.2	5782.94	1.437	35.79	1.674	22	70.8	41.5	21.1

Table B.6 Results of the ∝CT scans of LS038

#	Vol	SA	SA/Saeq	ESD	Tr/Treq	Max	L	W	T
1	11543.2	3276.38	1.326	28.04	1.327	20	45.7	35.1	19.0
2	8428.4	2569.39	1.283	25.25	1.167	24	35.9	29.1	20.6
3	10009.1	2703.84	1.204	26.74	1.267	16	41.1	30.4	20.4
4	13752.6	3464.11	1.248	29.73	1.267	18	42.6	36.3	25.2
5	10889.6	3056.10	1.286	27.50	1.15	22	46.3	32.9	24.4
6	12298.5	3322.24	1.289	28.64	1.392	20	48.9	33.8	21.6
7	15810.8	3728.36	1.224	31.14	1.194	20	49.5	32.9	29.1
8	10341.9	2795.39	1.218	27.03	1.196	16	37.7	27.9	26.7
9	10623.6	2985.29	1.277	27.27	1.182	24	39.0	31.4	22.9
10	14188.4	3454.75	1.219	30.04	1.104	22	41.3	35.6	36.2
11	9022.5	2387.29	1.139	25.83	1.073	16	34.3	27.6	24.9
12	7955.1	2443.09	1.268	24.77	1.058	26	30.3	29.2	22.5
13	19374.6	4115.00	1.18	33.32	1.108	22	45.8	35.6	30.6
14	13332.4	3529.68	1.298	29.42	1.133	22	39.3	35.1	28.1
15	13715.0	3388.08	1.223	29.70	1.141	22	42.6	33.6	28.4
16	8513.9	2572.83	1.276	25.33	1.308	14	39.3	35.1	17.6
17	17820.8	4008.92	1.215	32.41	1.129	24	42.3	39.7	30.2
18	9794.6	2833.54	1.28	26.55	1.346	20	44.3	31.3	22.3
19	9650.3	2971.20	1.355	26.41	1.42	20	44.3	28.1	21.9
20	9741.0	2813.98	1.276	26.50	1.184	22	37.1	34.6	19.8
21	9087.3	2819.38	1.339	25.89	1.408	20	42.6	29.8	19.2
22	8126.1	2543.05	1.301	24.94	1.264	22	37.2	28.9	19.8
23	9007.6	2778.09	1.327	25.81	1.267	20	47.6	29.5	20.5
24	13255.9	3161.71	1.167	29.36	1.107	18	40.7	37.0	24.1
25	9815.8	2849.53	1.285	26.56	1.208	26	39.5	29.6	21.3
26	12886.1	3624.16	1.363	29.09	1.414	22	49.8	37.1	19.5
27	16007.8	3733.81	1.216	31.27	1.108	18	43.7	35.0	34.8
28	11991.1	3249.70	1.283	28.40	1.338	20	54.9	29.7	24.5
29	8576.2	2661.95	1.314	25.40	1.399	20	41.3	30.3	22.4

30	8257.6	2523.96	1.277	25.08	1.504	14	44.3	27.2	18.2
31	8798.4	2677.69	1.299	25.61	1.13	26	36.9	26.5	24.3
32	11100.6	2946.22	1.224	27.68	1.134	24	37.6	34.0	20.9
33	7932.5	2404.29	1.25	24.74	1.306	20	40.0	26.6	17.9
34	8372.1	2516.37	1.262	25.19	1.358	16	40.7	27.4	16.7
35	10785.7	2931.03	1.242	27.41	1.261	18	43.5	29.3	23.2
36	12891.8	3592.42	1.351	29.09	1.615	20	54.5	30.7	16.4
37	10084.0	3087.37	1.368	26.80	1.396	18	40.3	36.2	19.2
38	18322.0	3938.89	1.172	32.71	1.083	24	44.2	36.5	30.8
39	11637.5	3216.56	1.295	28.12	1.111	28	38.6	37.0	23.7
40	9658.2	2873.80	1.31	26.42	1.179	24	38.6	31.0	24.2
41	8913.0	2650.30	1.275	25.72	1.165	22	37.3	27.7	24.7
42	8436.7	2453.84	1.224	25.26	1.17	20	38.0	29.1	21.7
43	10387.7	2892.92	1.257	27.07	1.216	20	39.4	29.8	22.4
44	9064.3	2727.66	1.297	25.87	1.304	20	40.4	27.7	17.3
45	14847.0	4104.85	1.405	30.49	1.437	18	53.4	38.8	23.7
46	8552.3	3018.63	1.493	25.37	1.493	18	48.8	35.0	24.2
47	16588.5	4268.16	1.357	31.64	1.255	22	50.9	42.2	31.0
48	11871.0	3183.13	1.265	28.30	1.257	22	52.5	29.9	25.0
49	14136.8	3473.30	1.228	30.00	1.212	18	43.0	37.2	23.4
50	8830.6	2528.88	1.224	25.64	1.228	18	37.3	30.0	21.1
51	10645.8	3046.66	1.302	27.29	1.158	24	38.1	33.0	24.7
52	8104.8	2523.63	1.293	24.92	1.241	22	42.1	27.3	21.0
53	8413.2	2671.10	1.335	25.23	1.257	18	41.9	36.0	20.5
54	10988.3	2912.54	1.219	27.58	1.131	16	37.4	32.0	24.4
55	10446.2	3000.70	1.298	27.12	1.456	22	47.5	24.5	22.1
56	8780.7	2545.05	1.236	25.60	1.297	18	39.0	26.3	23.0
57	8333.4	2600.40	1.308	25.15	1.258	22	37.1	26.7	22.7
58	8040.0	2500.34	1.288	24.86	1.193	18	34.9	28.8	25.4
59	9776.3	3141.24	1.421	26.53	1.75	18	52.0	30.7	15.2
60	9777.8	2735.18	1.237	26.53	1.263	16	42.1	33.0	19.5
61	21977.1	4717.90	1.243	34.75	1.259	24	49.0	48.5	24.6
62	7857.1	2425.75	1.269	24.67	1.272	18	42.1	28.5	18.8
63	10748.6	3008.85	1.277	27.38	1.332	20	42.4	30.6	20.2
64	9243.8	2632.21	1.236	26.04	1.216	18	41.3	29.8	21.6
65	8005.4	2553.38	1.319	24.82	1.208	20	40.7	30.6	22.4
66	8660.1	2520.07	1.236	25.48	1.161	18	34.3	29.4	25.1
67	17954.3	4232.81	1.277	32.49	1.417	20	57.5	36.8	26.8
68	12019.2	3193.38	1.258	28.42	1.167	20	42.1	30.8	29.4
69	12539.1	3424.28	1.312	28.82	1.517	22	52.2	26.5	23.2
70	11730.6	3101.08	1.242	28.19	1.25	20	42.3	31.2	20.6
71	9315.1	2809.85	1.312	26.11	1.284	22	39.4	30.5	21.7
72	14499.4	3689.39	1.283	30.25	1.151	18	42.7	37.5	33.2
73	16465.7	3798.40	1.214	31.56	1.179	24	45.8	32.5	27.9
74	16982.7	4139.08	1.295	31.89	1.163	28	44.1	40.6	24.4
75	14296.5	3873.03	1.36	30.11	1.381	20	47.1	40.1	25.4

76	11408.2	2905.10	1.185	27.93	1.131	20	38.5	28.7	23.8
77	7784.8	2351.72	1.238	24.59	1.117	18	34.5	25.9	23.8
78	7649.5	2438.38	1.299	24.45	1.593	14	45.6	25.6	16.0
79	11886.1	3049.26	1.211	28.31	1.201	20	41.1	33.1	20.5
80	12663.2	3235.82	1.232	28.92	1.142	22	37.5	32.2	27.1
81	7929.2	2405.78	1.251	24.74	1.237	20	36.3	29.6	18.4
82	11939.4	3313.46	1.312	28.36	1.317	16	49.6	33.0	26.5
83	8133.0	2603.42	1.331	24.95	1.203	18	37.6	29.6	22.7
84	14836.1	3608.03	1.236	30.49	1.142	18	44.5	35.8	31.0
85	15379.1	3798.63	1.27	30.85	1.174	26	41.4	36.1	23.0
86	9686.5	2690.11	1.224	26.45	1.148	22	38.0	29.5	21.7
87	8166.9	2572.83	1.312	24.99	1.486	22	41.7	25.2	16.9
88	14206.5	3796.16	1.338	30.05	1.337	18	51.2	39.2	25.9
89	8345.5	2525.19	1.269	25.17	1.169	18	34.3	32.7	24.3
90	17951.8	4021.17	1.213	32.49	1.126	22	49.8	38.8	26.9
91	10915.2	2983.36	1.254	27.52	1.413	20	44.6	24.2	22.1
92	10957.5	2900.43	1.216	27.56	1.104	20	40.4	29.4	25.2
93	11240.0	3201.10	1.319	27.79	1.379	20	44.0	33.9	21.2
94	9278.0	2736.78	1.282	26.07	1.129	24	36.1	30.2	24.7
95	10805.9	3010.23	1.274	27.43	1.187	24	41.2	32.0	27.4
96	9813.2	2902.38	1.309	26.56	1.246	24	43.6	31.0	23.0
97	10346.5	2858.42	1.245	27.04	1.103	20	35.8	33.3	30.1
98	15806.6	3979.76	1.307	31.14	1.179	18	48.2	39.0	36.6
99	7981.5	2406.06	1.246	24.79	1.241	20	36.2	27.1	20.4
100	9716.7	2845.30	1.292	26.48	1.187	20	46.2	32.0	22.6
101	8523.2	2580.05	1.279	25.34	1.233	18	37.0	29.3	24.4
102	13131.4	3569.25	1.326	29.27	1.246	16	48.3	35.8	32.6
103	12156.0	3238.84	1.267	28.53	1.144	26	40.5	35.1	24.7
104	9568.3	2671.97	1.226	26.34	1.233	18	38.8	25.9	24.0
105	9314.4	2926.00	1.367	26.10	1.247	22	37.0	32.5	23.0
106	10729.9	3060.23	1.301	27.37	1.339	18	43.4	32.4	21.5
107	9824.7	2813.00	1.268	26.57	1.151	20	37.0	34.5	23.6
108	17896.1	3947.76	1.193	32.45	1.125	24	46.0	36.0	28.9
109	13031.5	3412.51	1.274	29.20	1.193	26	41.7	35.5	21.7
110	14116.6	3429.36	1.214	29.99	1.146	22	42.5	34.6	28.6
111	8088.2	2448.36	1.256	24.90	1.206	20	35.9	27.6	21.0
112	8986.9	2581.99	1.235	25.80	1.16	22	37.7	28.9	23.3
113	9078.9	2561.39	1.217	25.88	1.106	20	33.2	32.3	26.1
114	10747.0	3156.69	1.34	27.38	1.286	24	46.4	28.7	23.4
115	9359.3	2650.58	1.234	26.15	1.093	24	33.1	33.7	25.6
116	10417.9	3061.53	1.327	27.10	1.313	14	41.2	33.0	23.7
117	24154.6	4861.66	1.203	35.86	1.184	18	54.9	36.6	31.5
118	7817.3	2495.86	1.31	24.62	1.324	20	40.9	26.3	19.6
119	9032.7	2621.01	1.25	25.84	1.106	22	36.6	31.6	27.3
120	11289.8	2972.13	1.221	27.83	1.123	16	40.1	32.3	26.0
121	11856.6	3372.65	1.341	28.29	1.385	20	46.8	38.4	19.1

122	9679.0	2743.28	1.249	26.44	1.239	18	39.4	33.1	19.2
123	8776.6	2699.18	1.312	25.59	1.245	22	42.8	27.5	21.3
124	9283.1	2754.26	1.289	26.08	1.214	12	39.1	31.4	23.7
125	9525.2	2754.66	1.268	26.30	1.196	14	39.0	34.3	28.9
126	9017.4	2833.24	1.352	25.82	1.354	20	42.2	37.4	18.1
127	14604.3	3723.67	1.289	30.33	1.175	24	47.6	35.7	25.3
128	14320.7	3478.29	1.22	30.13	1.331	20	49.7	27.2	24.0
129	13164.1	3520.97	1.306	29.30	1.268	24	47.7	32.9	24.4
130	9267.9	2803.83	1.314	26.06	1.31	18	41.4	28.6	24.8
131	7910.3	2434.28	1.268	24.72	1.389	20	41.0	23.6	19.3
132	9674.1	2850.73	1.298	26.44	1.366	18	43.6	34.3	17.5
133	8450.0	2607.87	1.3	25.27	1.244	22	40.8	29.4	19.4
134	9010.5	2990.76	1.428	25.82	1.192	22	41.1	29.1	29.2
135	8148.0	2420.69	1.236	24.97	1.174	22	33.7	25.5	20.7
136	12601.8	3588.16	1.37	28.87	1.436	18	55.1	36.8	23.1
137	12175.9	3146.27	1.229	28.54	1.164	22	43.4	31.1	23.2
138	9262.0	2701.20	1.266	26.06	1.136	18	34.4	32.2	27.0
139	8678.5	2488.93	1.219	25.50	1.186	20	38.1	27.0	19.2
140	17439.2	4178.42	1.285	32.17	1.409	22	51.1	33.8	21.2
141	11711.7	3183.63	1.277	28.18	1.127	18	37.6	32.6	30.8
142	8611.6	2687.79	1.323	25.43	1.214	22	42.0	28.5	22.6
143	8248.2	2443.78	1.238	25.07	1.127	18	32.1	30.2	21.1
144	17231.3	4442.14	1.377	32.05	1.229	22	51.8	34.7	34.7
145	10730.1	3162.94	1.344	27.37	1.279	20	40.9	36.3	21.2
146	12733.1	3205.06	1.215	28.97	1.143	22	41.7	34.9	26.7
147	12818.7	3018.91	1.14	29.04	1.048	18	35.0	33.2	32.0
148	18899.5	4265.34	1.243	33.05	1.193	26	49.1	35.3	32.7
149	21585.5	4750.40	1.267	34.55	1.178	20	46.9	41.2	30.7
150	8842.0	2605.03	1.26	25.66	1.173	18	36.8	29.9	22.5
151	11218.0	2904.77	1.199	27.77	1.064	22	37.0	30.7	26.3
152	8766.2	2570.66	1.25	25.58	1.159	22	38.5	27.8	25.4
153	8111.1	2309.26	1.183	24.93	1.098	20	31.4	30.0	24.4
154	9311.8	2798.24	1.307	26.10	1.173	22	37.8	30.8	23.0
155	9643.4	2690.59	1.228	26.41	1.145	22	38.4	31.2	24.0
156	9090.8	2681.50	1.273	25.89	1.319	22	45.5	26.9	21.0
157	10621.2	2968.17	1.27	27.27	1.117	22	36.7	33.2	28.1
158	14463.5	3588.18	1.25	30.23	1.172	20	44.3	38.4	24.5
159	10352.7	2802.10	1.22	27.04	1.179	20	38.5	35.4	23.2
160	11372.2	3149.21	1.288	27.90	1.448	14	48.3	32.3	18.6
161	12621.3	3413.15	1.302	28.89	1.133	24	41.4	38.2	28.5
162	9665.0	2762.74	1.259	26.43	1.16	22	36.5	33.5	21.3
163	10398.6	2786.40	1.209	27.08	1.122	24	38.6	28.9	26.5
164	11167.5	3487.31	1.443	27.73	1.849	16	57.8	37.5	15.3
165	10234.3	3132.05	1.374	26.94	1.351	14	45.6	31.9	24.9
166	8139.3	2555.75	1.306	24.96	1.232	22	37.7	33.7	20.1
167	14134.8	3899.03	1.379	30.00	1.552	20	52.7	33.9	25.1

168	7919.9	2261.14	1.177	24.73	1.158	18	35.4	25.1	20.6
169	8258.1	2337.02	1.183	25.08	1.087	20	33.8	27.0	26.4
170	12982.2	3307.09	1.238	29.16	1.139	22	40.0	36.3	26.1
171	8279.4	2680.05	1.354	25.10	1.505	18	41.4	30.0	15.3
172	10572.0	2993.06	1.285	27.23	1.081	26	35.8	30.4	24.7
173	11652.8	3148.77	1.267	28.13	1.1	26	39.3	32.1	29.7
174	21073.4	4714.53	1.278	34.27	1.197	20	56.1	43.9	28.9
175	13112.3	3439.84	1.279	29.26	1.328	24	47.6	31.1	25.0
176	8057.4	2524.69	1.299	24.87	1.295	20	36.9	37.0	17.4
177	8258.7	2467.65	1.249	25.08	1.11	22	38.3	28.3	23.3
178	11962.4	3119.23	1.233	28.38	1.119	20	37.9	32.6	24.7
179	7860.8	2359.52	1.234	24.67	1.148	22	34.9	26.4	22.0
180	12422.1	3036.29	1.171	28.73	1.09	18	37.0	34.3	29.8
181	8901.6	2865.01	1.379	25.71	1.407	24	46.1	25.7	19.9
182	9930.0	3039.53	1.36	26.67	1.304	24	39.0	38.8	21.7
183	8147.1	3075.18	1.571	24.97	2.384	18	53.2	25.7	15.2
184	14403.7	3690.92	1.289	30.19	1.256	24	44.8	37.8	20.5
185	7859.5	2613.83	1.367	24.67	1.447	20	41.4	25.6	20.5
186	9377.5	2794.86	1.3	26.16	1.136	22	37.1	29.6	30.1
187	7732.1	2423.59	1.282	24.53	1.425	16	42.8	23.1	18.7
188	9349.1	2876.71	1.34	26.14	1.35	20	40.3	36.4	20.7
189	19455.1	4375.04	1.251	33.37	1.195	28	50.3	36.8	27.1
190	12686.4	3450.87	1.312	28.94	1.634	14	51.6	33.5	19.1
191	9403.2	2740.80	1.272	26.19	1.232	22	38.9	27.6	22.7
192	13167.3	3535.05	1.311	29.30	1.314	22	43.9	35.8	19.0
193	8635.9	2576.73	1.266	25.45	1.165	22	38.2	27.2	21.5
194	8174.0	2580.31	1.315	24.99	1.261	24	36.8	26.5	22.1
195	8220.6	2786.88	1.415	25.04	1.598	18	45.0	30.3	16.3
196	7869.2	2425.45	1.268	24.68	1.151	20	34.9	30.7	20.2
197	14798.8	3599.66	1.235	30.46	1.197	20	48.5	35.5	25.9
198	10063.4	2862.08	1.27	26.79	1.12	24	38.9	33.9	25.0
199	9485.3	2597.39	1.199	26.26	1.176	16	37.0	30.9	23.1
200	11076.5	2911.90	1.212	27.66	1.132	22	35.9	31.1	22.9

Table B.7 Results of the ∝CT scans of LS3875

#	Vol	SA	SA/Saeq	ESD	Tr/Treq	Max	L	W	T
1	14216.2	3595.19	1.267	30.06	1.116	18	38.7	36.0	34.8
2	10905.8	3411.15	1.434	27.51	1.396	16	47.4	35.1	23.1
3	10008.8	3118.27	1.388	26.74	1.267	22	43.6	30.5	26.4
4	10412.1	3077.62	1.335	27.09	1.421	18	46.1	31.9	17.1
5	12748.2	3831.51	1.452	28.98	1.346	18	48.7	35.9	27.0
6	9014.9	2658.68	1.269	25.82	1.08	26	32.2	32.7	26.0
7	21651.3	5194.44	1.383	34.58	1.25	22	57.3	42.8	36.6
8	17082.3	4145.93	1.293	31.95	1.326	20	50.8	38.9	26.1
9	9124.8	2889.55	1.368	25.93	1.27	22	43.0	29.6	25.3

10	12089.7	3247.58	1.275	28.48	1.088	28	39.2	35.8	26.4
11	22930.7	5399.13	1.383	35.25	1.492	22	69.2	43.9	33.5
12	10703.8	2962.53	1.261	27.34	1.279	20	42.8	35.0	18.8
13	10923.3	3025.32	1.271	27.53	1.242	16	40.1	32.6	26.5
14	9028.2	2921.68	1.393	25.83	1.265	24	41.6	35.9	23.0
15	9445.8	3018.00	1.397	26.23	1.372	16	48.7	33.6	24.2
16	8609.8	2709.21	1.334	25.43	1.283	20	43.9	27.2	24.3
17	9295.3	3161.52	1.479	26.09	1.432	20	46.1	31.8	26.9
18	10935.0	3722.93	1.563	27.54	1.648	22	56.3	33.9	33.8
19	7904.1	2580.75	1.345	24.71	1.422	12	42.1	34.3	24.4
20	28562.9	6034.07	1.335	37.93	1.303	20	66.0	42.1	37.4
21	10427.6	2837.71	1.229	27.11	1.133	14	37.5	33.1	30.5
22	11319.5	3120.42	1.28	27.86	1.149	24	42.5	30.3	24.6
23	12034.6	3326.18	1.31	28.43	1.251	18	44.9	30.7	28.5
24	10555.8	2936.41	1.262	27.22	1.375	18	47.0	29.7	21.1
25	18280.8	4837.45	1.441	32.68	1.44	18	59.1	44.6	31.3
26	13280.8	3685.96	1.359	29.38	1.301	14	50.0	31.9	30.2
27	8468.5	2631.15	1.31	25.29	1.284	20	42.1	29.6	25.9
28	7855.1	2539.83	1.329	24.66	1.376	22	42.8	25.7	20.4
29	7958.9	2816.55	1.461	24.77	1.608	16	48.7	32.8	22.4
30	7846.7	2544.81	1.333	24.65	1.475	16	46.4	24.8	22.5
31	7609.9	2488.72	1.33	24.40	1.495	14	40.0	32.4	13.8
32	17920.4	4197.06	1.267	32.47	1.155	24	45.7	35.5	28.7
33	9854.5	3213.12	1.446	26.60	1.445	22	51.6	27.6	24.1
34	8076.1	2723.15	1.399	24.89	1.508	18	51.4	28.1	22.3
35	12406.8	3433.49	1.325	28.72	1.318	20	46.3	33.6	29.4
36	10231.8	3226.90	1.416	26.94	1.623	16	47.4	32.3	16.4
37	10631.2	3352.73	1.434	27.28	1.683	16	55.8	30.9	24.4
38	9188.6	2854.07	1.345	25.99	1.41	16	46.9	28.7	20.8
39	10916.4	2890.53	1.215	27.52	1.266	16	42.6	29.0	23.9
40	10702.6	3247.45	1.383	27.34	1.479	14	47.4	32.8	22.5
41	12819.8	3671.86	1.386	29.04	1.282	24	44.2	42.3	23.4
42	10155.6	2884.73	1.272	26.87	1.188	16	40.0	28.6	26.6
43	9215.5	2851.14	1.341	26.01	1.447	14	46.0	34.0	21.9
44	7665.1	2555.46	1.359	24.46	1.41	16	39.8	29.0	17.6
45	8192.2	2502.11	1.273	25.01	1.177	22	38.1	31.1	23.7
46	12059.7	3011.54	1.184	28.45	1.276	14	44.8	34.4	18.0
47	8145.6	2617.61	1.337	24.96	1.366	16	40.1	34.0	24.3
48	10227.2	2844.97	1.249	26.93	1.142	22	40.3	30.0	22.8
49	7838.6	2893.44	1.516	24.65	1.492	22	44.9	35.2	19.1
50	9788.4	2928.30	1.323	26.54	1.226	26	40.5	27.0	25.3
51	9878.4	3151.73	1.416	26.62	1.982	22	56.5	22.6	19.1
52	8318.9	2672.37	1.346	25.14	1.536	20	46.2	28.4	17.3
53	22167.1	5175.00	1.356	34.85	1.949	18	75.9	31.1	25.7
54	10700.4	3112.52	1.325	27.34	1.43	20	46.7	28.4	21.9
55	8934.5	2745.01	1.318	25.74	1.219	20	43.0	28.2	24.6
56	8580.3	2582.62	1.274	25.40	1.142	22	34.9	29.1	22.9
57	13132.1	3374.73	1.254	29.27	1.189	22	45.0	34.6	25.1

58	10670.1	2865.16	1.222	27.31	1.112	22	36.9	29.3	26.0
59	8617.1	2675.29	1.316	25.44	1.186	18	37.3	30.2	27.7
60	8806.9	2741.76	1.329	25.62	1.154	20	36.3	31.5	26.7
61	8631.9	2825.71	1.389	25.45	1.438	18	47.1	30.4	25.1
62	7748.6	2708.72	1.43	24.55	1.259	18	38.0	28.5	24.4
63	9188.2	2732.10	1.288	25.99	1.286	20	42.6	31.1	19.2
64	8302.8	2461.09	1.241	25.12	1.306	16	40.0	30.5	16.8
65	8664.1	2701.89	1.324	25.48	1.657	12	48.7	25.7	22.5
66	9918.6	2667.49	1.195	26.66	1.132	20	36.5	33.7	23.4
67	9080.0	2563.36	1.218	25.88	1.094	22	34.3	28.9	24.6
68	10919.4	2923.29	1.228	27.53	1.241	20	41.1	34.4	21.2
69	9640.0	3272.64	1.494	26.41	1.369	18	44.6	30.1	26.1
70	14716.2	3558.54	1.225	30.40	1.108	26	40.2	33.9	28.2
71	16952.8	3740.21	1.172	31.87	1.148	24	47.6	32.6	27.4
72	7875.8	2925.65	1.528	24.68	1.635	22	50.7	28.1	22.2
73	7678.1	2577.78	1.37	24.48	1.385	14	41.5	31.2	25.6
74	10444.0	3107.64	1.345	27.12	1.288	20	49.2	32.6	26.8
75	10625.2	3114.30	1.332	27.28	1.142	22	40.7	31.9	27.9
76	8671.4	2443.27	1.197	25.49	1.066	18	35.3	28.6	25.7
77	10421.7	3332.28	1.444	27.10	1.418	18	49.7	32.4	27.7
78	8392.0	2866.35	1.435	25.21	1.368	20	41.2	30.9	23.8
79	13099.1	3664.35	1.364	29.25	1.52	20	50.9	33.7	16.9
80	8967.7	2531.94	1.213	25.78	1.3	18	38.9	29.1	18.0
81	14837.8	3867.24	1.324	30.49	1.398	16	50.3	35.3	31.6
82	12797.3	3452.94	1.305	29.02	1.274	20	45.9	32.0	26.3
83	11929.6	3797.27	1.504	28.35	1.757	22	57.1	38.3	23.5
84	11811.9	3470.45	1.384	28.26	1.535	16	51.4	34.8	23.1
85	7896.8	2611.18	1.362	24.71	1.558	16	46.5	24.2	22.0
86	21110.1	5027.98	1.361	34.29	1.484	16	60.5	37.6	28.6
87	15299.7	4068.03	1.365	30.80	1.198	20	47.3	36.8	29.7
88	16538.9	4363.11	1.39	31.61	1.541	22	59.0	29.8	25.0
89	9945.9	3113.49	1.392	26.68	1.241	20	42.5	34.1	23.3
90	11767.0	3437.57	1.374	28.22	1.556	18	53.8	38.6	21.0
91	9904.2	3198.43	1.434	26.64	1.629	14	52.1	39.3	19.0
92	8783.7	2938.22	1.427	25.60	1.652	24	49.3	28.6	15.7
93	9561.3	2871.66	1.318	26.33	1.36	16	43.9	31.2	23.3
94	8845.3	2683.10	1.297	25.66	1.159	20	37.3	31.3	26.4
95	13914.5	3358.55	1.2	29.84	1.104	20	40.2	35.8	30.7
96	8373.5	2989.22	1.499	25.19	1.644	20	48.1	33.3	23.6
97	11510.6	3094.93	1.255	28.01	1.177	18	42.7	30.2	24.7
98	11096.5	3106.82	1.291	27.67	1.385	18	50.0	30.5	24.2
99	12460.7	3424.44	1.317	28.76	1.166	22	41.2	32.5	30.0
100	9179.2	2827.88	1.334	25.98	1.463	18	41.6	35.4	14.7
101	9040.7	2791.09	1.33	25.85	1.446	18	42.2	30.9	18.0
102	7688.7	2568.32	1.363	24.49	1.443	14	38.6	33.6	17.5
103	10717.1	3410.63	1.451	27.35	1.441	16	50.9	32.5	22.5
104	11903.3	3607.82	1.431	28.33	1.424	22	49.1	32.9	24.4
105	12125.0	3169.15	1.242	28.50	1.17	22	42.4	34.2	25.7

106	27689.2	5421.48	1.225	37.54	1.103	20	49.7	45.5	37.0
107	10375.2	3156.61	1.372	27.06	1.222	24	44.6	33.0	26.6
108	8363.5	2620.99	1.315	25.18	1.434	14	44.1	29.6	21.3
109	10618.7	3222.11	1.379	27.27	1.255	20	43.6	38.5	25.3
110	8127.9	2495.21	1.276	24.95	1.219	22	36.2	28.9	18.7
111	10019.0	2816.22	1.253	26.75	1.166	22	38.1	26.4	25.8
112	10119.6	2839.62	1.255	26.84	1.224	22	42.0	27.7	23.5
113	8584.0	2405.88	1.187	25.40	1.063	20	32.5	26.2	25.0
114	21939.1	4750.09	1.253	34.73	1.187	20	57.0	41.1	32.6
115	8307.6	2660.21	1.341	25.13	1.613	16	49.5	25.6	19.2
116	9508.1	2910.02	1.341	26.28	1.492	20	48.8	32.9	16.0
117	9143.9	2590.42	1.225	25.94	1.093	22	34.9	26.8	25.2
118	10662.5	3092.20	1.32	27.31	1.251	24	42.9	28.5	25.7
119	9175.5	2815.49	1.328	25.97	1.594	20	48.4	24.9	17.5
120	8019.0	2341.83	1.209	24.83	1.16	18	36.1	29.0	19.2
121	10045.9	2994.67	1.33	26.77	1.343	16	45.6	32.7	22.3
122	9079.8	2812.39	1.336	25.88	1.331	18	43.5	28.8	24.1
123	11948.0	3452.86	1.366	28.36	1.263	26	51.3	29.9	27.8
124	10742.8	3106.09	1.319	27.38	1.23	20	44.3	32.7	29.1
125	10298.8	3184.16	1.391	26.99	1.884	18	56.8	27.6	18.7
126	12610.0	3480.18	1.328	28.88	1.383	20	53.6	35.9	22.8
127	8155.6	2745.34	1.401	24.97	1.515	16	42.1	33.6	23.3
128	10397.5	3078.85	1.336	27.08	1.313	20	43.2	26.7	25.1
129	8657.7	3134.81	1.537	25.48	2.46	20	61.3	23.6	17.4
130	8207.7	2997.72	1.523	25.03	1.521	20	48.2	33.9	26.8
131	9730.3	2829.92	1.284	26.49	1.2	18	40.8	33.7	25.3
132	7539.0	2662.41	1.432	24.33	1.421	14	42.8	32.1	21.4
133	8029.8	2630.04	1.356	24.84	1.264	18	42.3	31.5	21.0
134	11781.7	3263.02	1.303	28.23	1.244	20	42.3	32.7	30.1
135	7740.2	2648.05	1.399	24.54	1.531	14	38.5	32.1	20.7
136	7570.4	2695.74	1.446	24.36	1.487	18	42.5	28.7	21.7
137	9574.8	2986.27	1.369	26.35	1.288	20	40.9	32.7	25.3
138	8413.3	2507.84	1.254	25.23	1.416	18	46.4	24.2	19.3
139	8296.9	2396.90	1.209	25.12	1.179	20	37.9	26.9	23.3
140	10462.1	2997.70	1.296	27.14	1.174	22	38.1	34.0	26.8
141	8618.4	2766.94	1.361	25.44	1.289	24	39.4	33.1	21.7
142	9436.3	2810.58	1.301	26.22	1.442	22	46.8	26.8	20.4
143	8021.5	2593.50	1.338	24.84	1.43	20	45.0	25.1	20.8
144	20056.7	4305.07	1.206	33.71	1.139	20	48.7	38.1	29.9
145	8020.4	2717.20	1.402	24.84	1.824	16	49.5	28.7	14.2
146	14602.0	4188.83	1.45	30.33	1.366	16	46.2	36.6	27.7
147	14018.6	3648.49	1.298	29.92	1.242	20	52.4	34.2	31.7
148	10179.8	2911.44	1.282	26.89	1.297	16	44.1	31.8	23.7
149	10721.8	2990.60	1.272	27.36	1.178	24	38.0	33.6	23.7
150	8131.9	2337.85	1.195	24.95	1.124	22	33.3	28.7	21.7
151	12714.0	3617.94	1.373	28.96	1.408	12	44.3	42.1	26.2
152	14313.7	4097.80	1.437	30.12	1.627	14	56.5	34.0	27.4
153	9730.1	2711.59	1.23	26.49	1.185	24	38.8	25.3	23.8

154	8530.7	2851.89	1.413	25.35	1.919	18	51.0	27.1	13.4
155	11144.3	3371.49	1.397	27.71	1.241	26	46.4	32.4	26.0
156	8229.3	2894.84	1.469	25.05	1.974	14	53.3	33.1	15.9
157	8115.4	2757.70	1.412	24.93	1.482	22	47.1	30.0	22.0
158	16451.7	4024.98	1.287	31.56	1.424	16	53.3	35.5	25.6
159	14646.4	3806.78	1.315	30.36	1.584	16	59.1	31.6	23.7
160	8377.3	2414.12	1.21	25.20	1.241	18	36.9	29.0	17.7
161	15354.7	3981.16	1.333	30.84	1.391	20	57.2	38.1	28.7
162	9826.1	2892.99	1.304	26.57	1.31	18	43.7	29.3	25.4
163	10585.3	2981.45	1.279	27.24	1.29	12	38.1	34.3	29.1
164	29854.2	6088.26	1.308	38.49	1.201	20	52.6	54.6	38.1
165	8269.5	2516.08	1.272	25.09	1.095	24	35.0	29.6	24.6
166	11530.0	3281.98	1.33	28.03	1.563	18	50.3	29.3	19.1
167	14599.8	3893.65	1.348	30.32	1.335	24	57.0	38.6	24.7
168	8887.9	2629.42	1.267	25.70	1.227	22	37.4	32.4	18.6
169	10871.0	3360.81	1.416	27.48	1.634	12	52.8	32.2	18.9
170	15617.2	4143.25	1.371	31.01	1.318	16	46.7	42.1	31.4
171	9779.3	3051.29	1.38	26.53	1.35	20	44.2	30.1	20.2
172	11438.4	3027.47	1.233	27.95	1.194	20	39.2	32.0	23.3
173	13059.4	3273.70	1.221	29.22	1.15	24	42.4	31.8	24.7
174	16173.0	4385.24	1.418	31.38	1.309	28	49.5	39.8	28.5
175	10575.7	3034.20	1.302	27.23	1.21	18	38.5	32.7	28.3
176	16789.0	4118.34	1.299	31.77	1.402	12	53.5	32.0	28.9
177	21421.9	4917.21	1.318	34.46	1.267	20	58.5	36.2	35.7
178	22891.2	5385.30	1.381	35.23	1.258	20	53.8	58.4	36.1
179	8593.8	2622.63	1.293	25.41	1.249	22	38.0	32.8	19.3
180	7912.0	2669.96	1.39	24.72	1.352	18	45.4	35.0	24.0
181	17532.8	4079.24	1.25	32.23	1.237	24	43.9	37.6	27.6
182	9750.4	3039.80	1.377	26.51	1.249	24	41.2	30.2	23.4
183	8521.6	2531.64	1.255	25.34	1.12	20	34.6	28.7	25.2
184	19530.2	4838.67	1.38	33.41	1.256	26	52.1	44.5	29.2
185	8463.6	2642.51	1.316	25.28	1.539	12	43.4	29.1	15.6
186	11205.7	2891.00	1.194	27.76	1.073	22	35.0	34.3	27.4
187	8326.4	2587.96	1.303	25.15	1.189	22	37.9	26.7	26.2
188	8606.8	2649.08	1.304	25.43	1.393	22	40.6	31.1	15.3
189	7907.3	2614.42	1.362	24.72	1.394	18	42.1	33.5	19.9
190	9558.8	2735.03	1.256	26.33	1.203	18	39.5	28.6	24.6
191	8520.2	2565.61	1.272	25.34	1.482	14	43.1	27.7	17.2
192	15523.6	3776.29	1.255	30.95	1.155	20	49.6	35.1	27.8
193	15453.5	4032.71	1.344	30.90	1.265	24	53.5	34.1	27.0
194	7756.5	2387.58	1.26	24.56	1.093	22	31.7	27.9	26.1
195	11411.6	3363.50	1.372	27.93	1.455	24	52.9	29.8	18.5
196	17715.2	3910.77	1.19	32.34	1.143	24	45.1	33.5	28.9
197	12838.0	3514.01	1.325	29.05	1.318	20	51.5	30.8	24.2
198	10945.3	3444.49	1.445	27.55	1.328	18	46.8	34.3	31.8
199	7952.4	2736.78	1.42	24.76	1.497	22	43.7	33.0	19.0
200	8681.1	2678.68	1.311	25.50	1.173	20	34.2	33.6	25.1

Table B.8 Results of the ∝CT scans of MA038

#	Vol	SA	SA/Saeq	ESD	Tr/Treq	Max	L	W	T
1	15068.2	3679.78	1.247	30.6	1.262	16	47.6	41.0	22.2
2	8109.0	2637.29	1.351	24.9	1.198	18	42.0	31.2	28.8
3	11906.5	3498.61	1.387	28.3	1.354	16	42.0	39.5	21.6
4	10384.9	3092.60	1.343	27.1	1.519	16	47.5	33.2	22.2
5	14740.4	3711.39	1.277	30.4	1.247	22	45.4	38.2	21.5
6	11272.3	3149.38	1.295	27.8	1.309	20	46.1	34.7	20.7
7	27280.7	5390.44	1.23	37.3	1.19	20	52.9	54.8	30.6
8	13970.9	3613.39	1.288	29.9	1.252	22	47.4	35.1	24.9
9	7849.6	2861.98	1.498	24.7	1.257	20	35.5	36.5	28.5
10	9465.2	2916.82	1.348	26.2	1.32	16	39.9	37.6	21.3
11	10596.1	3143.57	1.347	27.3	1.43	20	47.0	30.6	24.1
12	23992.5	5481.60	1.363	35.8	1.231	22	51.5	49.8	35.8
13	15144.8	3693.37	1.248	30.7	1.229	18	46.1	37.0	28.2
14	9380.0	2736.07	1.272	26.2	1.208	18	40.7	28.3	24.5
15	8547.3	2918.58	1.444	25.4	1.547	22	47.5	30.6	18.0
16	8068.8	2476.23	1.273	24.9	1.382	14	41.3	25.4	19.3
17	11079.0	3014.28	1.254	27.7	1.178	22	39.1	34.2	23.2
18	15724.0	3861.43	1.272	31.1	1.531	14	57.5	32.5	20.6
19	8185.1	2800.03	1.426	25.0	2.059	16	59.8	22.1	20.5
20	13389.3	3283.21	1.204	29.5	1.163	22	42.9	34.7	24.7
21	18728.9	4515.79	1.324	32.9	1.38	22	56.8	35.7	26.3
22	10844.6	3070.58	1.296	27.5	1.232	20	45.3	29.1	22.8
23	9054.1	2764.54	1.316	25.9	1.484	16	46.6	27.3	18.4
24	10870.3	3037.72	1.28	27.5	1.169	20	41.1	32.4	26.2
25	10012.8	2840.08	1.264	26.7	1.184	20	37.3	34.3	23.1
26	10409.5	3068.67	1.331	27.1	1.322	18	42.0	32.4	17.1
27	8451.1	2686.80	1.339	25.3	1.274	20	38.9	33.3	21.5
28	17467.3	4116.12	1.264	32.2	1.305	14	47.1	44.0	26.9
29	9413.2	2818.10	1.307	26.2	1.163	22	38.8	37.2	23.7
30	10263.3	2965.36	1.298	27.0	1.285	20	41.9	28.8	25.7
31	15805.4	4073.49	1.337	31.1	1.62	12	64.4	30.2	26.0
32	7894.5	2602.06	1.357	24.7	1.316	24	40.3	25.6	19.7
33	18303.9	5100.14	1.518	32.7	1.823	18	68.3	40.6	30.0
34	8790.4	2726.91	1.324	25.6	1.233	22	38.6	30.7	21.6
35	8294.4	2809.04	1.418	25.1	1.351	16	40.7	30.2	19.1
36	10903.8	3197.10	1.344	27.5	1.463	12	46.9	35.8	20.5
37	8321.1	2393.52	1.205	25.1	1.193	12	37.9	28.2	22.2
38	10143.4	2917.86	1.288	26.9	1.127	20	38.4	31.2	29.6
39	15950.5	4294.04	1.401	31.2	1.22	22	46.2	40.8	32.9
40	8606.0	2679.86	1.32	25.4	1.435	16	47.8	27.0	20.7
41	8483.8	2964.84	1.474	25.3	2.129	14	59.0	27.8	13.4
42	7627.2	2226.60	1.188	24.4	1.197	12	34.4	31.5	19.2
43	11553.9	3189.92	1.291	28.0	1.371	16	44.5	35.8	17.2
44	8729.8	2564.18	1.251	25.5	1.089	20	33.7	29.7	24.0
45	8543.2	2669.79	1.321	25.4	1.197	20	38.3	28.7	26.2
46	10534.6	3190.69	1.373	27.2	1.31	20	43.5	32.7	26.1
47	16047.8	4144.45	1.347	31.3	1.19	26	50.2	35.2	32.6
48	8068.9	2558.16	1.315	24.9	1.28	18	40.5	28.4	21.6
49	8617.1	2990.92	1.471	25.4	2.203	16	58.8	23.4	14.4
50	8628.9	2981.18	1.465	25.4	1.711	18	52.6	35.7	14.6
51	9931.1	3116.85	1.395	26.7	1.597	14	47.4	29.9	17.3
52	14995.8	3897.86	1.325	30.6	1.268	28	47.6	32.1	24.0
53	8154.7	2501.20	1.277	25.0	1.192	20	35.6	25.9	23.9

54	12192.0	3416.45	1.334	28.6	1.286	20	46.7	32.6	28.5
55	8996.9	2796.73	1.337	25.8	1.188	18	39.0	30.4	25.1
56	17160.9	4051.43	1.259	32.0	1.097	20	42.1	40.3	36.8
57	8153.5	2927.25	1.494	25.0	1.609	20	46.4	28.6	21.1
58	10612.3	3079.49	1.319	27.3	1.263	24	41.0	38.5	16.8
59	11845.2	3312.44	1.318	28.3	1.343	18	46.2	35.4	21.4
60	14775.7	3809.41	1.308	30.4	1.188	26	46.1	34.7	23.9
61	9128.3	2858.65	1.353	25.9	1.295	20	41.0	35.7	17.7
62	8833.0	2749.76	1.331	25.6	1.183	22	44.2	30.8	24.8
63	9202.2	2962.36	1.395	26.0	1.553	18	44.5	33.1	16.3
64	12237.3	3279.74	1.277	28.6	1.192	22	41.0	32.6	23.1
65	16304.7	4091.39	1.316	31.5	1.503	22	57.2	32.4	27.2
66	8466.7	2771.39	1.38	25.3	1.545	20	50.1	25.4	20.8
67	10459.3	3148.18	1.361	27.1	1.327	18	47.5	34.2	27.5
68	15147.3	3871.96	1.308	30.7	1.398	18	48.4	34.5	23.1
69	8584.9	2525.39	1.246	25.4	1.269	18	39.9	27.2	19.8
70	9266.0	3076.09	1.442	26.1	1.216	24	39.7	32.1	27.3
71	16314.3	4160.56	1.337	31.5	1.566	22	57.7	32.7	24.7
72	14828.7	3838.69	1.315	30.5	1.337	18	50.7	34.9	23.0
73	8536.2	2503.91	1.24	25.4	1.115	18	35.2	30.5	25.9
74	9691.5	2827.43	1.286	26.5	1.353	18	44.6	25.7	24.6
75	8325.7	2689.96	1.354	25.1	1.202	20	37.6	32.2	24.8
76	8600.1	3059.62	1.507	25.4	1.801	20	49.9	30.8	14.6
77	8046.8	2487.50	1.281	24.9	1.215	22	40.5	28.2	21.1
78	9747.1	2868.22	1.3	26.5	1.199	20	38.2	34.1	21.6
79	8000.4	2664.58	1.377	24.8	1.304	22	41.2	24.7	24.3
80	11097.8	3358.22	1.396	27.7	1.219	26	43.3	35.2	20.7
81	19932.3	4724.71	1.329	33.6	1.307	24	57.1	38.0	29.7
82	9587.5	2893.84	1.326	26.4	1.388	18	45.2	27.0	23.1
83	12981.7	3446.59	1.29	29.2	1.235	20	46.6	32.8	27.3
84	8070.6	2277.98	1.171	24.9	1.071	18	32.6	29.2	23.5
85	11832.2	3267.32	1.301	28.3	1.324	20	47.4	29.3	22.5
86	10824.9	3181.67	1.344	27.4	1.308	18	45.0	37.3	22.5
87	8744.8	2750.63	1.34	25.6	1.271	20	40.8	28.8	24.8
88	10512.8	2941.29	1.267	27.2	1.393	16	46.5	27.3	18.5
89	11795.2	3251.33	1.297	28.2	1.292	16	42.9	36.5	21.6
90	12665.9	3316.40	1.262	28.9	1.205	20	42.9	35.2	24.0
91	9461.5	2926.36	1.353	26.2	1.618	18	51.4	23.6	23.3
92	7893.4	3003.46	1.567	24.7	1.911	16	50.9	35.7	23.8
93	12114.8	3381.21	1.325	28.5	1.37	18	48.7	31.3	22.7
94	8951.0	2704.61	1.297	25.8	1.357	16	43.6	30.1	19.4
95	7989.5	2557.79	1.323	24.8	1.261	18	38.9	34.1	18.4
96	9087.8	2794.72	1.327	25.9	1.328	20	42.8	32.0	18.9
97	8862.7	2824.37	1.364	25.7	1.391	16	41.4	37.1	20.0
98	19579.5	4814.68	1.371	33.4	1.254	24	61.0	43.9	25.9
99	9858.7	2831.64	1.274	26.6	1.241	20	41.4	29.4	22.4
100	10410.7	3453.07	1.498	27.1	1.304	18	41.0	36.4	26.8
101	8161.4	2558.83	1.305	25.0	1.125	22	34.5	31.2	23.5
102	8117.8	2579.29	1.32	24.9	1.347	14	38.4	31.5	17.9
103	16441.8	4057.38	1.298	31.5	1.298	20	56.4	36.3	25.6
104	8166.2	2635.31	1.344	25.0	1.453	16	40.7	30.7	17.3
105	16725.0	4085.85	1.292	31.7	1.153	28	47.7	35.2	33.6
106	10505.0	3301.81	1.423	27.2	1.556	22	46.3	36.9	17.7
107	9378.1	2888.94	1.343	26.2	1.619	22	52.9	24.1	22.1
108	10042.4	2882.50	1.281	26.8	1.252	20	44.4	32.5	23.8
109	8035.3	2654.73	1.368	24.9	1.613	16	44.9	30.0	15.0

110	8900.6	2587.90	1.246	25.7	1.296	16	40.8	30.5	20.2
111	7497.3	2317.21	1.251	24.3	1.21	12	34.8	27.3	23.3
112	18976.9	4584.87	1.333	33.1	1.175	28	52.3	43.1	28.1
113	18121.0	4145.72	1.243	32.6	1.16	26	44.2	38.8	30.6
114	11656.3	3233.19	1.3	28.1	1.468	18	52.1	28.6	21.4
115	9154.4	2821.20	1.333	26.0	1.18	22	36.8	33.6	23.8
116	9877.1	3219.97	1.446	26.6	1.441	20	43.2	35.8	22.1
117	9098.6	2614.01	1.24	25.9	1.112	18	34.7	32.3	24.8
118	9728.8	2933.03	1.331	26.5	1.491	14	44.7	36.8	15.8
119	8135.9	2647.47	1.353	25.0	1.288	20	39.2	33.0	19.3
120	9549.8	2736.05	1.257	26.3	1.213	20	40.1	27.8	25.9
121	8952.4	2554.93	1.225	25.8	1.105	16	33.0	32.0	25.5
122	10804.6	3259.45	1.379	27.4	1.566	18	53.5	30.3	17.5
123	8255.3	2509.55	1.27	25.1	1.119	20	34.5	30.5	23.9
124	10917.6	2999.13	1.26	27.5	1.291	18	40.0	34.9	19.1
125	17152.4	4139.88	1.287	32.0	1.112	26	43.6	36.8	31.5
126	11694.4	3478.45	1.396	28.2	1.292	22	41.7	38.5	23.9
127	17740.2	4268.12	1.298	32.4	1.111	28	43.5	40.8	29.9
128	9997.7	3134.32	1.397	26.7	1.361	20	42.0	38.3	19.7
129	14755.4	3988.40	1.371	30.4	1.296	20	53.0	32.8	32.4
130	12987.1	3500.70	1.31	29.2	1.535	22	53.4	27.6	23.4
131	8448.3	2945.89	1.469	25.3	1.918	16	56.8	26.1	16.6
132	8509.9	3113.27	1.544	25.3	1.72	16	47.4	32.9	23.3
133	13192.8	3434.89	1.272	29.3	1.259	24	50.0	30.2	25.9
134	8663.4	2443.88	1.198	25.5	1.122	18	37.9	26.8	24.3
135	11092.3	2845.05	1.183	27.7	1.119	18	35.9	32.3	23.2
136	12603.1	3385.52	1.293	28.9	1.303	20	45.2	32.8	26.4
137	10375.6	3266.48	1.42	27.1	1.336	24	43.3	38.1	23.1
138	11088.9	2975.79	1.237	27.7	1.087	24	36.2	32.5	26.8
139	14875.5	4028.93	1.377	30.5	1.858	16	69.7	29.2	22.4
140	10056.4	3102.03	1.377	26.8	1.615	22	51.7	27.9	18.7
141	10293.1	2979.47	1.302	27.0	1.315	16	45.4	33.5	24.4
142	9294.6	2824.16	1.321	26.1	1.241	18	38.8	31.1	20.7
143	14393.5	3728.96	1.303	30.2	1.526	22	55.6	27.5	26.2
144	9115.7	3049.37	1.445	25.9	1.581	22	49.9	33.9	16.3
145	12438.8	3456.04	1.331	28.7	1.188	24	41.7	36.8	25.5
146	9598.2	3086.49	1.413	26.4	1.702	16	49.0	28.0	20.7
147	11714.1	3354.53	1.345	28.2	1.243	20	46.0	36.1	27.1
148	8148.7	2722.51	1.39	25.0	1.757	18	52.7	29.4	15.3
149	13349.7	3451.88	1.268	29.4	1.193	20	42.3	33.9	26.9
150	10717.4	3182.76	1.354	27.4	1.253	20	46.1	33.2	25.7
151	9258.2	2877.18	1.349	26.1	1.36	20	40.5	25.5	24.2
152	11025.3	3141.44	1.311	27.6	1.335	18	45.5	29.2	23.3
153	14027.6	3686.26	1.311	29.9	1.318	20	53.7	37.7	22.7
154	9082.0	2723.63	1.294	25.9	1.318	20	39.3	32.5	19.2
155	9135.2	3007.26	1.423	25.9	1.295	22	43.3	34.7	20.9
156	16010.4	3646.84	1.187	31.3	1.1	22	40.8	34.9	30.2
157	18608.1	4196.51	1.236	32.9	1.206	22	48.7	40.0	25.3
158	17681.8	4238.50	1.291	32.3	1.33	20	55.0	32.3	28.5
159	10568.1	3136.13	1.347	27.2	1.405	16	48.2	28.6	24.0
160	18116.0	4198.18	1.259	32.6	1.2	24	47.9	34.2	29.6
161	9052.0	2848.77	1.356	25.9	1.317	20	42.9	27.1	24.9
162	9754.9	3085.99	1.398	26.5	1.433	16	49.0	31.3	25.3
163	10237.8	3137.40	1.376	26.9	1.518	18	48.2	32.0	21.1
164	11376.0	3481.09	1.423	27.9	1.327	24	50.0	32.0	32.2
165	26743.5	7061.20	1.633	37.1	1.653	18	68.5	53.3	36.4

166	8972.1	2763.18	1.323	25.8	1.334	20	40.7	28.1	24.2
167	10133.1	3291.76	1.454	26.8	2.029	16	55.9	26.8	15.1
168	11162.0	3007.29	1.245	27.7	1.125	22	37.7	33.3	26.4
169	9096.1	2683.99	1.274	25.9	1.337	16	41.0	30.1	16.6
170	14745.5	3479.66	1.197	30.4	1.23	20	43.4	31.9	26.8
171	8067.0	2690.85	1.383	24.9	1.546	16	41.7	34.7	18.0
172	10216.5	3097.32	1.36	26.9	1.353	14	41.0	36.5	21.5
173	7876.0	2707.09	1.414	24.7	1.34	16	40.7	30.3	23.8
174	17503.4	4037.90	1.239	32.2	1.196	22	48.3	39.0	24.2
175	16899.7	4059.17	1.275	31.8	1.175	24	45.8	40.2	32.5
176	11202.6	3095.83	1.279	27.8	1.203	22	43.5	29.6	25.6
177	9562.5	2954.12	1.356	26.3	1.339	20	39.2	39.2	16.0
178	13071.5	3473.32	1.294	29.2	1.271	14	43.9	37.4	30.0
179	27356.1	5782.62	1.317	37.4	1.477	28	66.6	37.6	28.7
180	14721.0	3688.23	1.27	30.4	1.431	18	52.5	32.2	25.2
181	7770.4	2303.41	1.214	24.6	1.266	14	34.2	34.1	16.2
182	7755.5	2946.08	1.555	24.6	2.375	12	55.5	27.4	12.8
183	9427.9	2899.46	1.343	26.2	1.428	18	45.6	30.4	20.8
184	9119.9	3270.84	1.549	25.9	1.55	18	45.4	34.2	24.2
185	17652.3	4261.43	1.3	32.3	1.248	26	49.6	37.2	25.1
186	11295.6	3237.17	1.33	27.8	1.603	20	51.7	27.8	16.4
187	7720.6	2412.73	1.277	24.5	1.288	18	40.8	27.1	22.5
188	7734.2	2703.81	1.43	24.5	1.685	18	47.8	24.6	24.4
189	8021.6	2534.17	1.308	24.8	1.285	20	40.9	24.1	21.0
190	8660.2	2829.41	1.387	25.5	1.74	18	46.5	26.7	17.0
191	17963.6	4198.88	1.266	32.5	1.116	24	45.3	37.3	29.9
192	10315.1	2998.41	1.308	27.0	1.346	18	45.0	30.5	18.7
193	10344.8	2774.51	1.208	27.0	1.252	12	37.8	33.5	22.1
194	7791.3	2537.25	1.335	24.6	1.337	18	41.1	28.8	20.7
195	10589.7	3059.34	1.312	27.2	1.47	18	48.4	30.5	20.2
196	19870.2	4608.79	1.299	33.6	1.297	18	47.2	42.5	23.3
197	8668.4	2753.09	1.349	25.5	1.2	20	40.7	31.9	24.6
198	8270.0	2486.93	1.258	25.1	1.201	16	36.6	29.3	20.4
199	8098.1	2550.46	1.308	24.9	1.233	22	37.6	27.9	21.9
200	9007.0	2968.52	1.418	25.8	1.6	14	43.0	34.3	15.5

Table B.9 Results of the ∝CT scans of MA3875

#	Vol	SA	SA/Saeq	ESD	Tr/Treq	Max	L	W	T
1	11765.1	3172.89	1.268	28.22	1.23	20	44.9	33.4	26.2
2	7882.9	2520.67	1.316	24.69	1.494	20	44.5	22.8	19.7
3	62087.6	9556.42	1.26	49.13	1.211	26	69.9	62.1	39.2
4	41634.0	7521.81	1.295	43.00	1.326	20	68.2	52.1	33.4
5	39496.8	6992.35	1.247	42.25	1.282	26	66.3	42.9	36.9
6	26807.2	5763.38	1.331	37.13	1.36	28	61.0	40.9	30.8
7	8094.6	2745.83	1.408	24.91	1.685	18	49.3	27.9	16.1
8	11541.6	3749.65	1.518	28.04	2.883	16	71.8	25.1	14.0
9	12039.9	3439.56	1.354	28.44	1.58	20	48.9	36.3	16.9
10	38844.3	6840.46	1.233	42.02	1.207	20	64.2	50.4	34.4
11	34992.7	6511.70	1.259	40.58	1.26	26	60.2	43.8	34.6
12	7824.9	2340.69	1.228	24.63	1.155	20	34.9	29.5	23.2
13	14774.9	3548.98	1.219	30.44	1.216	20	45.7	31.1	24.8
14	22214.1	4852.49	1.27	34.88	1.279	20	52.5	44.4	22.5
15	31495.7	6346.99	1.316	39.18	1.341	24	64.7	47.3	30.7

16	8439.5	2371.50	1.183	25.26	1.122	18	34.9	29.3	22.0
17	67535.5	10920.62	1.362	50.53	1.537	26	89.6	56.1	40.1
18	28585.0	5755.84	1.273	37.94	1.156	28	56.4	39.3	39.4
19	15356.5	3669.82	1.228	30.84	1.191	24	44.8	35.3	23.5
20	9499.2	2830.89	1.305	26.28	1.194	22	39.9	32.6	23.3
21	42766.0	7230.06	1.223	43.39	1.213	26	62.6	53.8	30.7
22	22647.2	4811.20	1.243	35.10	1.333	18	58.3	44.4	25.3
23	9498.0	2802.13	1.292	26.28	1.394	18	47.7	25.5	20.9
24	8740.7	2636.38	1.285	25.56	1.35	20	42.5	25.1	22.6
25	12031.7	3484.68	1.372	28.43	1.716	20	57.7	25.5	23.1
26	32255.3	6079.28	1.241	39.49	1.164	26	52.6	45.7	39.6
27	13252.4	3695.51	1.365	29.36	1.472	18	55.4	40.0	20.5
28	40704.2	7536.68	1.317	42.68	1.305	24	69.2	63.6	27.9
29	10645.1	3115.60	1.331	27.29	1.449	18	48.7	30.7	18.8
30	17855.5	4490.05	1.359	32.43	1.7	20	57.8	35.4	26.9
31	11214.4	2947.92	1.217	27.77	1.241	18	42.8	31.3	21.2
32	16715.5	4643.39	1.469	31.72	2.387	12	69.9	34.9	19.6
33	13381.7	3493.60	1.282	29.46	1.295	22	46.4	31.8	22.9
34	25525.3	5554.10	1.325	36.53	1.31	24	55.6	41.3	34.0
35	11436.0	3441.62	1.402	27.95	1.666	20	56.6	34.4	19.1
36	50050.7	8167.76	1.244	45.72	1.175	26	68.2	54.1	46.2
37	15704.0	4407.17	1.453	31.07	1.656	18	52.2	44.9	15.7
38	11444.5	3477.61	1.416	27.96	1.747	16	55.8	34.5	16.5
39	11071.7	3199.56	1.332	27.65	1.165	24	39.8	33.2	23.5
40	7677.6	2582.03	1.372	24.48	1.569	18	41.6	32.8	13.6
41	12646.7	3358.96	1.28	28.91	1.354	16	46.8	39.4	16.5
42	7874.5	2449.38	1.28	24.68	1.293	18	38.7	25.9	21.5
43	98135.4	13865.17	1.348	57.23	1.447	24	102.2	70.1	36.6
44	26464.1	5474.52	1.275	36.97	1.143	26	50.7	45.1	41.6
45	17343.3	4478.45	1.382	32.12	1.988	14	70.9	28.0	24.6
46	23069.1	5123.21	1.307	35.32	1.111	22	48.9	44.4	35.5
47	20191.5	4632.95	1.292	33.78	1.19	20	53.0	45.5	29.9
48	32388.6	6627.27	1.349	39.55	1.374	26	72.8	42.8	29.7
49	19890.7	4573.26	1.288	33.62	1.396	24	59.8	33.8	33.7
50	9563.9	2832.14	1.3	26.34	1.117	22	37.4	28.2	23.7
51	22939.1	5288.78	1.355	35.25	1.462	20	65.1	43.2	26.6
52	27879.1	5501.13	1.237	37.62	1.142	24	48.8	44.7	38.3
53	22548.4	5468.37	1.417	35.05	1.991	20	77.3	32.0	19.7
54	17518.9	4175.85	1.28	32.22	1.214	24	53.3	37.3	28.9
55	14465.9	3781.07	1.317	30.23	1.476	22	54.3	29.0	25.2
56	17515.5	4176.21	1.28	32.22	1.122	24	47.0	38.9	34.7
57	41336.7	8083.50	1.398	42.90	1.673	22	86.0	43.4	32.7
58	17759.7	4438.23	1.348	32.37	1.449	24	54.1	43.6	21.7
59	20264.7	4981.88	1.386	33.83	1.631	20	61.2	36.6	25.0
60	17745.5	4437.48	1.349	32.36	1.242	22	48.2	37.5	30.3
61	28832.3	5887.77	1.295	38.04	1.381	24	66.4	39.9	30.5
62	8757.4	2711.40	1.32	25.57	1.29	22	41.3	30.3	22.7
63	30989.0	6083.99	1.275	38.97	1.337	22	57.4	52.0	23.0
64	20300.9	5020.48	1.395	33.85	1.736	24	68.6	40.1	20.3
65	175190.1	20216.41	1.335	69.42	1.494	26	120.7	72.1	61.3
66	72669.1	10500.79	1.247	51.77	1.194	20	80.4	59.9	46.2
67	31994.9	6029.89	1.237	39.39	1.263	24	58.5	52.7	27.8
68	54574.2	9672.21	1.39	47.06	1.702	20	90.8	54.7	27.9

69	10704.1	3182.93	1.355	27.34	1.451	16	45.7	33.6	21.5
70	7896.3	2704.84	1.411	24.71	2.234	18	51.8	21.7	15.9
71	14562.7	3657.24	1.268	30.30	1.199	22	45.1	39.9	27.8
72	8359.1	2476.87	1.244	25.18	1.176	20	37.8	26.1	22.0
73	10925.7	3074.74	1.291	27.53	1.423	18	42.9	32.4	17.6
74	11562.2	3231.78	1.307	28.06	1.512	20	53.0	27.1	25.2
75	8616.1	2615.35	1.287	25.44	1.2	22	37.6	30.1	21.8
76	25034.6	5306.72	1.282	36.30	1.334	18	58.5	38.7	28.5
77	43305.1	7593.90	1.273	43.57	1.291	28	75.2	53.3	29.7
78	18833.2	4783.18	1.397	33.01	1.46	18	52.1	39.9	30.5
79	9147.3	2788.64	1.318	25.95	1.279	18	41.4	28.0	23.3
80	12851.7	3603.79	1.358	29.06	1.32	24	48.4	38.5	21.3
81	14826.8	3620.50	1.24	30.48	1.165	24	44.6	33.8	27.1
82	32760.8	5999.46	1.212	39.70	1.151	18	56.6	48.3	33.8
83	16773.9	4695.63	1.482	31.76	1.784	20	67.0	40.0	19.0
84	12154.5	3594.26	1.406	28.53	1.662	18	54.8	36.8	14.0
85	9211.7	2610.69	1.229	26.01	1.218	18	36.6	32.5	20.3
86	23029.1	4763.35	1.217	35.30	1.235	18	50.7	46.2	25.5
87	8395.9	2524.22	1.264	25.22	1.297	18	40.1	31.0	20.1
88	10906.8	3221.21	1.354	27.51	1.37	20	42.6	39.8	18.2
89	34935.0	6442.41	1.247	40.56	1.332	18	65.7	47.2	28.4
90	11201.3	3160.35	1.305	27.76	1.236	22	42.6	36.6	20.2
91	30942.2	6327.57	1.328	38.95	1.494	20	70.3	47.3	27.9
92	20637.2	5181.05	1.424	34.03	1.9	20	70.2	37.5	16.8
93	7721.6	2535.16	1.342	24.52	1.314	22	40.7	26.1	20.3
94	10143.0	2882.54	1.272	26.86	1.356	18	42.9	32.0	17.5
95	8230.1	2715.30	1.377	25.05	1.575	18	48.9	26.6	20.3
96	16755.5	4204.34	1.328	31.75	1.333	22	54.0	36.8	28.1
97	7775.9	2507.68	1.321	24.58	1.112	26	34.2	26.8	25.5
98	8020.9	2636.84	1.361	24.84	1.486	20	47.7	24.5	22.2
99	7974.5	2493.53	1.292	24.79	1.453	18	43.4	25.0	20.2
100	44122.0	8192.50	1.357	43.84	1.342	16	67.6	60.3	36.8
101	26801.7	5469.46	1.263	37.13	1.193	28	54.0	44.3	29.0
102	8405.6	2597.37	1.299	25.23	1.255	20	40.8	31.4	20.2
103	55443.0	9229.60	1.313	47.31	1.405	28	79.2	59.3	29.4
104	29959.7	5949.01	1.275	38.53	1.182	24	51.7	51.2	32.5
105	34650.2	6785.63	1.32	40.45	1.552	20	70.3	51.2	20.0
106	25239.6	5437.47	1.307	36.39	1.274	22	61.0	45.3	30.4
107	20542.1	4860.12	1.34	33.98	1.409	22	54.9	39.3	28.7
108	8371.9	2611.97	1.31	25.19	1.32	20	37.6	31.9	18.3
109	19214.9	4285.73	1.235	33.23	1.278	22	53.1	39.9	22.3
110	27171.1	5807.82	1.329	37.30	1.449	22	66.5	43.6	28.6
111	16820.6	4096.38	1.29	31.79	1.361	20	48.8	39.0	22.4
112	17409.3	3886.88	1.197	32.16	1.133	18	43.3	39.7	29.5
113	24662.8	5298.95	1.293	36.11	1.332	22	55.6	54.5	25.7
114	8801.6	2948.42	1.43	25.62	1.968	12	52.3	29.0	13.2
115	24863.7	5417.54	1.315	36.21	1.383	24	58.9	41.4	29.4
116	15743.5	4363.08	1.436	31.10	1.635	18	52.6	44.6	17.6
117	27011.3	5739.49	1.318	37.23	1.267	26	56.6	43.4	28.9
118	8240.9	2546.08	1.29	25.06	1.286	20	39.4	30.2	18.2
119	29956.2	5704.60	1.223	38.53	1.197	22	56.4	49.6	32.3
120	23851.9	4878.63	1.217	35.71	1.145	20	47.2	45.2	27.8
121	18055.3	4132.85	1.242	32.55	1.214	26	46.5	36.9	27.3

122	9997.8	3004.75	1.339	26.73	1.439	20	45.0	31.9	19.9
123	11591.5	3392.33	1.37	28.08	1.449	16	49.2	35.2	28.5
124	31343.9	6187.89	1.287	39.12	1.271	16	58.0	49.4	30.8
125	13937.2	3595.60	1.284	29.86	1.15	26	40.9	34.3	23.1
126	7802.5	2409.41	1.266	24.61	1.264	18	39.1	28.3	21.1
127	33376.4	6111.56	1.219	39.95	1.19	26	58.7	39.8	36.0
128	8036.3	2561.68	1.32	24.85	1.209	12	34.2	31.4	21.1
129	9285.5	2680.80	1.255	26.08	1.272	18	38.7	30.2	19.4
130	15199.8	3752.91	1.265	30.73	1.317	22	50.9	36.2	24.4
131	28908.2	5312.91	1.166	38.08	1.157	22	56.5	44.9	34.7
132	10815.9	3401.20	1.438	27.44	1.884	14	56.3	35.9	13.5
133	14569.4	3902.27	1.353	30.30	1.423	22	50.9	40.1	19.5
134	40710.8	7387.82	1.291	42.68	1.28	28	70.9	52.7	38.4
135	34775.0	6725.11	1.305	40.50	1.269	22	61.1	53.7	31.0
136	41341.1	7655.66	1.324	42.90	1.269	26	67.0	51.2	37.0
137	17053.9	4263.84	1.331	31.94	1.304	20	51.6	39.8	22.5
138	30048.2	5845.33	1.251	38.57	1.131	28	52.8	50.8	38.5
139	8385.8	2759.07	1.382	25.21	1.259	22	39.1	27.6	27.9
140	87753.3	12260.24	1.284	55.13	1.335	14	87.7	66.5	45.4
141	8756.5	2585.39	1.258	25.57	1.228	20	41.6	30.8	19.5
142	9150.2	2955.33	1.397	25.95	1.36	16	39.3	33.5	31.2
143	15916.5	3965.14	1.296	31.21	1.223	20	48.5	35.6	31.3
144	34235.1	6606.14	1.296	40.29	1.357	24	63.7	46.8	27.2
145	14933.7	4218.71	1.439	30.55	1.664	18	59.5	42.4	16.7
146	39431.5	7161.42	1.278	42.23	1.254	20	61.5	57.9	30.0
147	11948.2	3339.32	1.321	28.36	1.195	28	39.5	35.3	21.4
148	12237.4	3722.18	1.449	28.59	1.781	14	55.5	44.4	13.2
149	10484.1	3010.36	1.3	27.15	1.386	18	49.7	31.2	19.9
150	25509.7	5342.41	1.275	36.52	1.32	24	57.8	46.5	25.6
151	13158.1	4368.94	1.621	29.29	3.639	18	93.0	24.6	16.5
152	17042.3	4262.43	1.331	31.93	1.481	22	60.9	32.5	23.2
153	13377.9	3457.54	1.269	29.45	1.399	18	43.5	35.7	18.4
154	28571.8	5585.66	1.236	37.93	1.193	26	55.4	45.8	33.0
155	13840.7	3762.87	1.35	29.79	1.591	14	47.4	40.8	13.3
156	26577.9	6056.82	1.406	37.03	1.528	24	61.9	50.8	19.0
157	39177.8	7077.20	1.269	42.14	1.356	20	63.1	53.2	25.2
158	24019.2	5403.00	1.342	35.80	1.155	24	54.2	43.3	33.3
159	7891.1	2730.12	1.424	24.70	1.564	16	42.0	33.8	13.7
160	24812.8	6012.33	1.461	36.19	2.265	12	79.8	40.7	25.6
161	12040.6	3189.93	1.256	28.44	1.258	22	43.0	32.6	20.0
162	27284.0	5438.58	1.241	37.35	1.173	24	52.0	49.2	36.0
163	33411.0	6685.18	1.333	39.96	1.382	24	62.9	55.0	27.1
164	53227.9	10299.31	1.505	46.67	2.062	24	98.2	46.1	30.8
165	39072.5	6829.70	1.227	42.10	1.224	22	68.8	45.7	38.2
166	11105.0	3285.23	1.365	27.68	1.773	16	57.2	26.2	22.3
167	17830.3	4412.16	1.337	32.41	1.399	24	57.9	38.0	23.1
168	33219.6	7077.37	1.416	39.88	1.733	16	79.3	46.9	20.4
169	60735.5	9354.31	1.252	48.77	1.18	28	71.4	60.9	47.5
170	22984.3	5356.09	1.37	35.28	1.512	16	58.4	47.4	21.7
171	34559.3	6738.43	1.313	40.41	1.601	18	71.1	43.4	29.9
172	21514.0	4671.93	1.249	34.51	1.15	26	47.9	41.3	32.9
173	65365.1	9966.74	1.27	49.98	1.278	20	74.7	66.9	39.1
174	10894.7	3026.29	1.273	27.50	1.141	22	38.3	34.5	31.0

175	29226.4	6195.44	1.35	38.22	1.518	24	70.4	42.4	26.7
176	18913.0	4283.41	1.248	33.06	1.3	12	49.0	43.0	22.6
177	18238.6	4388.81	1.31	32.66	1.535	22	61.4	35.6	21.6
178	12425.5	3338.68	1.287	28.74	1.264	18	45.9	34.3	24.7
179	21805.9	5188.19	1.375	34.66	1.459	22	63.9	37.3	25.0
180	25733.7	5538.70	1.314	36.63	1.439	28	64.1	36.8	27.2
181	58631.2	9113.06	1.249	48.20	1.304	26	77.6	49.4	41.1
182	21645.4	4744.56	1.263	34.58	1.125	26	46.4	45.2	29.4
183	10714.2	3144.35	1.338	27.35	1.67	20	54.1	29.0	19.4
184	12393.5	3624.85	1.4	28.71	1.562	24	53.5	33.7	19.5
185	15088.1	3825.60	1.296	30.66	1.291	20	50.2	39.9	22.0
186	9404.0	2688.59	1.248	26.19	1.207	22	41.7	28.7	23.0
187	27270.8	5176.23	1.181	37.35	1.088	28	49.6	37.2	32.9
188	33152.6	7028.99	1.408	39.86	1.461	20	70.2	55.0	33.6
189	69187.7	10311.06	1.265	50.93	1.189	26	81.0	62.7	44.9
190	22752.7	5403.88	1.392	35.16	1.754	20	64.9	41.3	20.2
191	27267.6	5418.04	1.237	37.34	1.314	22	59.2	36.4	33.9
192	8969.2	2889.78	1.384	25.78	1.27	28	42.4	30.2	19.4
193	21251.9	4586.05	1.236	34.37	1.147	26	47.8	38.0	34.6
194	14875.8	3469.83	1.186	30.51	1.118	16	40.9	36.5	33.3
195	11258.6	3054.12	1.257	27.81	1.246	22	43.3	29.2	24.7
196	23436.8	5417.30	1.368	35.51	1.462	24	63.4	33.3	35.3
197	12559.7	3122.85	1.195	28.84	1.146	20	42.4	30.1	29.5
198	18601.2	4161.39	1.226	32.87	1.257	16	51.0	38.6	25.0
199	87000.8	11966.79	1.26	54.98	1.357	22	98.7	55.7	46.0
200	10705.9	3217.71	1.37	27.34	1.455	20	45.1	35.5	16.8

Table B.10 Results of the ∝CT scans of NS038

#	Vol	SA	SA/Saeq	ESD	Tr/Treq	Max	L	W	T
1	7919.3	2881.29	1.5	24.73	1.576	20	41.2	39.4	17.2
2	9669.2	2768.79	1.261	26.43	1.161	24	37.3	32.0	21.5
3	10722.1	3039.56	1.293	27.36	1.181	24	43.5	29.5	26.1
4	10094.9	3053.12	1.352	26.81	1.715	18	50.9	29.2	14.3
5	14204.6	3553.14	1.253	30.05	1.257	22	43.0	37.4	20.7
6	8352.3	2489.05	1.25	25.17	1.116	22	32.1	30.5	23.7
7	15742.4	3496.08	1.151	31.10	1.096	22	38.5	39.4	26.1
8	11112.6	3120.36	1.296	27.69	1.24	24	41.9	34.1	20.6
9	21988.6	4442.21	1.17	34.76	1.076	22	44.9	41.7	34.4
10	10670.3	2890.68	1.233	27.31	1.166	22	39.1	30.7	25.1
11	10088.2	2990.53	1.325	26.81	1.427	12	39.1	36.0	15.9
12	12734.1	3459.58	1.312	28.97	1.233	18	45.8	32.6	24.9
13	8353.6	2743.57	1.378	25.17	1.624	16	41.3	35.4	12.4
14	10657.9	3128.24	1.336	27.30	1.392	18	45.7	32.7	18.3
15	21426.7	4933.26	1.322	34.46	1.471	26	59.1	42.1	24.3
16	8777.5	2492.59	1.211	25.59	1.136	18	38.3	28.4	23.0
17	10694.6	2961.71	1.262	27.34	1.207	24	39.9	31.1	25.5
18	13165.0	3353.16	1.244	29.30	1.318	22	46.4	31.5	21.8
19	10586.8	2922.09	1.253	27.24	1.245	22	41.8	28.2	25.0
20	14653.7	3736.97	1.29	30.36	1.398	18	48.6	37.1	20.8
21	13582.1	3508.67	1.275	29.60	1.441	20	47.4	33.3	18.4
22	20286.9	4925.36	1.369	33.84	1.224	22	49.2	46.9	39.3

23	14074.0	3430.47	1.217	29.96	1.116	24	39.9	34.0	29.3
24	14156.6	3395.37	1.2	30.01	1.187	18	43.8	30.6	30.7
25	8573.6	2816.33	1.39	25.39	1.555	24	47.0	30.2	16.7
26	8043.5	2611.76	1.345	24.86	1.349	22	40.4	33.4	17.7
27	11371.9	2957.45	1.209	27.90	1.114	22	38.3	32.2	26.2
28	20624.8	4560.55	1.254	34.02	1.479	18	55.9	38.0	19.7
29	11022.1	3377.29	1.41	27.61	1.465	18	49.0	41.1	17.9
30	10696.9	2816.34	1.2	27.34	1.206	20	42.1	28.6	21.2
31	8850.9	2739.40	1.324	25.66	1.205	24	37.6	34.3	20.7
32	22822.5	4922.69	1.265	35.19	1.226	22	53.5	40.8	29.4
33	10933.2	3063.15	1.286	27.54	1.286	18	43.3	31.5	23.7
34	20045.4	4908.43	1.375	33.70	1.246	24	51.6	37.7	34.0
35	7803.2	2283.16	1.2	24.61	1.099	20	33.0	29.5	23.2
36	9996.0	2973.58	1.325	26.73	1.728	18	52.4	27.4	15.6
37	8048.6	2315.55	1.192	24.86	1.236	16	37.4	26.4	18.8
38	9242.7	2511.86	1.179	26.04	1.089	20	35.0	28.4	25.2
39	9809.6	2802.42	1.265	26.56	1.091	26	34.3	30.5	26.1
40	11701.9	3306.54	1.327	28.17	1.462	12	47.3	34.5	19.7
41	8168.7	2394.88	1.221	24.99	1.158	18	34.5	27.3	23.1
42	11594.5	3144.58	1.269	28.08	1.273	20	41.8	36.9	20.2
43	8443.6	2733.81	1.363	25.26	1.184	26	44.5	30.6	21.8
44	10087.9	2893.16	1.281	26.81	1.146	22	40.2	30.9	26.6
45	11463.4	3057.34	1.244	27.98	1.149	24	40.6	36.7	24.1
46	10563.8	3050.94	1.31	27.22	1.234	24	41.7	30.5	24.6
47	7903.2	2355.30	1.228	24.71	1.262	18	37.8	30.2	16.7
48	8496.3	2774.60	1.378	25.32	1.923	22	52.6	24.7	17.5
49	10476.9	3107.32	1.342	27.15	1.199	20	40.3	30.2	28.6
50	18780.1	4231.46	1.238	32.98	1.372	16	59.7	33.2	28.4
51	11859.9	3296.41	1.311	28.29	1.226	28	41.5	35.5	20.7
52	11532.4	3101.62	1.256	28.03	1.112	22	39.6	32.5	27.7
53	10536.2	3054.28	1.314	27.20	1.292	26	43.8	30.0	20.9
54	15330.6	3940.75	1.32	30.82	1.288	18	47.6	35.3	32.7
55	8653.3	2763.31	1.356	25.47	1.468	16	42.1	33.6	16.3
56	12602.5	3662.60	1.399	28.87	2.084	22	60.3	26.7	17.8
57	17303.5	4219.69	1.304	32.09	1.279	24	50.8	37.7	31.6
58	14207.5	3973.84	1.401	30.05	1.372	22	50.5	41.0	21.1
59	8886.3	2808.20	1.354	25.70	1.452	18	44.9	30.1	16.7
60	9546.6	2822.31	1.297	26.32	1.376	16	45.0	30.2	21.8
61	7475.9	2295.98	1.242	24.26	1.379	12	35.9	24.0	22.0
62	8789.4	2556.52	1.241	25.60	1.367	18	42.8	29.1	15.6
63	22419.5	5128.85	1.334	34.98	1.331	28	58.3	36.4	30.4
64	19600.7	4743.26	1.349	33.45	1.449	24	62.2	34.8	25.6
65	10056.8	2823.40	1.253	26.78	1.223	22	41.4	30.0	23.5
66	24583.6	5328.19	1.303	36.08	1.314	26	56.9	42.1	27.2
67	16410.1	3722.81	1.192	31.53	1.079	26	38.9	35.6	28.4
68	7924.5	2425.37	1.262	24.74	1.272	18	37.1	33.0	18.1
69	7708.8	2515.68	1.333	24.51	1.405	16	35.9	34.7	15.7
70	13248.6	3675.24	1.357	29.36	1.587	20	58.3	29.9	25.2
71	20937.5	4554.99	1.24	34.20	1.193	26	49.2	40.5	27.8
72	12142.7	3150.05	1.233	28.52	1.141	26	40.6	31.0	25.1
73	14679.3	3609.93	1.245	30.38	1.161	26	41.6	37.3	25.1
74	48907.7	9361.84	1.448	45.37	1.411	18	80.3	50.0	34.3

75	11396.7	2965.13	1.211	27.92	1.172	20	39.9	32.8	22.4
76	8194.9	2414.48	1.228	25.01	1.167	18	31.9	30.4	22.4
77	8487.2	2660.36	1.322	25.31	1.341	20	42.1	27.0	20.1
78	9381.4	2913.39	1.354	26.17	1.412	24	43.4	30.6	19.4
79	8888.2	2559.24	1.233	25.70	1.081	22	33.1	30.8	27.7
80	20239.6	4124.44	1.148	33.81	1.077	24	44.4	37.0	32.6
81	14693.5	3914.16	1.349	30.39	1.693	22	56.3	27.6	24.0
82	8187.7	2437.43	1.241	25.01	1.124	16	33.0	28.4	23.7
83	11492.9	3082.88	1.252	28.00	1.112	24	38.7	34.3	27.6
84	8046.5	2375.77	1.223	24.86	1.145	18	37.4	27.4	23.3
85	9090.8	2790.06	1.325	25.89	1.349	14	42.1	28.6	21.6
86	11698.6	2992.59	1.201	28.17	1.132	24	39.2	32.1	23.7
87	13756.9	3442.18	1.24	29.73	1.196	24	40.2	35.1	23.2
88	8149.8	2562.85	1.309	24.97	1.294	20	38.7	27.9	18.1
89	20415.8	4417.39	1.223	33.91	1.134	28	45.9	38.8	29.2
90	9924.2	2836.70	1.27	26.66	1.359	18	42.5	29.1	20.9
91	9363.4	2720.11	1.266	26.15	1.371	16	47.0	28.3	17.5
92	38674.9	7332.36	1.326	41.96	1.227	26	65.6	46.4	40.0
93	8759.1	2634.27	1.282	25.58	1.17	22	36.6	30.7	21.2
94	13655.7	3580.26	1.296	29.66	1.255	22	47.4	36.2	27.1
95	9810.0	3228.50	1.457	26.56	1.514	24	45.6	30.7	20.2
96	34794.6	6624.26	1.285	40.50	1.404	28	68.9	41.1	31.9
97	21495.0	4454.50	1.191	34.50	1.156	20	49.1	34.7	30.3
98	13841.0	3526.44	1.265	29.79	1.186	20	43.0	33.2	24.7
99	8963.0	2990.55	1.433	25.77	1.689	22	50.3	31.4	15.7
100	12285.6	3385.00	1.315	28.63	1.43	12	52.4	31.7	25.6
101	26346.5	5475.59	1.279	36.92	1.159	26	53.6	43.8	36.7
102	10891.7	2808.36	1.182	27.50	1.124	20	38.0	29.6	25.7
103	7728.3	2411.86	1.276	24.53	1.27	18	42.5	28.2	22.2
104	14998.2	3613.45	1.229	30.60	1.235	22	46.1	31.1	23.6
105	10204.5	2817.84	1.239	26.91	1.163	22	36.5	33.1	21.6
106	7792.4	2475.91	1.303	24.60	1.451	16	42.3	29.4	15.6
107	8121.4	2616.54	1.339	24.94	1.158	26	34.1	29.1	21.1
108	9401.1	2937.84	1.364	26.19	1.477	16	46.7	35.7	17.1
109	8292.1	2544.11	1.284	25.11	1.37	16	40.3	28.8	16.6
110	11297.3	3096.10	1.272	27.84	1.343	14	43.3	33.7	20.6
111	14189.1	4012.80	1.416	30.04	1.785	18	55.1	36.6	24.8
112	10745.5	3136.63	1.332	27.38	1.155	26	38.0	33.8	27.4
113	14403.5	3654.21	1.276	30.19	1.494	14	52.2	30.3	24.4
114	8260.5	2679.73	1.356	25.08	1.296	20	41.0	32.5	18.0
115	8202.7	2432.03	1.236	25.02	1.22	18	34.6	33.9	21.9
116	12229.7	3203.14	1.248	28.59	1.181	18	42.6	29.0	26.3
117	16211.5	3972.94	1.283	31.40	1.237	22	45.8	37.9	29.9
118	10182.7	2961.79	1.304	26.89	1.252	22	40.7	36.0	19.5
119	11507.1	3086.07	1.252	28.01	1.231	24	38.7	31.0	20.6
120	9584.1	2804.15	1.285	26.35	1.296	22	38.9	38.1	18.8
121	8350.4	2427.50	1.22	25.17	1.093	18	31.2	29.5	22.7
122	14980.1	3980.22	1.354	30.58	1.564	14	53.1	42.3	18.0
123	26978.7	5227.48	1.202	37.21	1.101	28	47.1	44.3	39.0
124	12528.7	3212.52	1.231	28.82	1.19	20	41.2	36.0	23.2
125	13795.7	3411.90	1.227	29.76	1.198	16	45.4	35.2	28.3
126	13637.3	3494.55	1.266	29.64	1.126	18	39.7	34.6	29.8

127	14646.4	3736.95	1.291	30.36	1.324	20	50.2	35.8	26.7
128	11458.4	3705.13	1.507	27.97	1.762	16	46.5	46.1	16.0
129	10202.7	3005.93	1.321	26.91	1.64	20	49.6	27.0	17.6
130	12359.7	3588.14	1.388	28.69	1.494	24	47.8	39.5	19.7
131	13959.7	3588.25	1.28	29.87	1.365	20	50.2	36.9	22.8
132	10820.3	2812.92	1.189	27.44	1.045	24	35.1	32.0	26.8
133	14865.5	4224.35	1.445	30.51	1.711	18	58.9	33.3	20.3
134	11238.6	3281.71	1.353	27.79	1.842	14	52.6	28.6	14.3
135	8803.8	2771.87	1.344	25.62	1.494	22	45.7	26.4	21.6
136	13304.7	3336.92	1.229	29.40	1.179	22	40.7	34.0	25.8
137	12113.5	3188.67	1.25	28.49	1.086	26	37.5	31.5	26.7
138	8239.8	2660.38	1.348	25.06	1.526	14	42.9	33.4	13.3
139	9038.2	2681.45	1.278	25.84	1.173	22	35.8	27.3	24.8
140	7861.2	2754.93	1.441	24.67	1.698	20	41.9	35.1	12.8
141	8425.4	2649.77	1.323	25.25	1.243	22	39.0	29.2	20.7
142	10356.8	2844.67	1.238	27.04	1.294	16	42.3	30.5	19.9
143	10262.6	2773.92	1.215	26.96	1.258	18	40.3	30.9	22.3
144	10814.9	2954.06	1.249	27.44	1.134	22	39.0	30.6	27.1
145	8574.3	2548.64	1.258	25.39	1.164	20	34.5	32.7	21.0
146	28740.1	5583.87	1.231	38.00	1.157	24	57.5	41.4	36.8
147	10892.0	3262.71	1.373	27.50	1.418	16	45.7	37.3	19.7
148	10038.3	2934.94	1.304	26.76	1.296	18	42.3	30.3	23.4
149	9032.9	2770.76	1.321	25.84	1.153	26	35.0	34.8	23.8
150	16703.6	4319.75	1.367	31.72	1.617	14	53.0	46.0	16.2
151	10674.2	3007.14	1.283	27.32	1.172	20	37.3	33.9	28.5
152	10856.3	2800.51	1.181	27.47	1.112	18	38.6	29.4	27.0
153	9816.1	2718.80	1.226	26.57	1.191	22	38.2	26.1	23.5
154	8910.6	2542.54	1.223	25.72	1.131	16	35.5	33.8	23.3
155	7827.3	2409.02	1.264	24.63	1.349	14	38.5	28.2	18.5
156	13257.7	3477.23	1.284	29.36	1.295	18	49.7	30.1	30.2
157	11254.5	2965.46	1.221	27.80	1.148	22	36.7	35.9	25.4
158	13140.3	3279.19	1.218	29.28	1.212	20	44.9	32.2	26.1
159	12326.3	3372.67	1.307	28.66	1.528	16	51.1	32.9	18.0
160	9876.1	2635.37	1.184	26.62	1.146	20	36.7	28.3	22.8
161	12341.3	3282.66	1.271	28.67	1.099	24	38.9	36.0	26.1
162	13034.4	3428.94	1.28	29.20	1.215	24	44.6	39.5	23.0
163	9779.9	2875.96	1.3	26.53	1.331	20	46.8	27.3	22.5
164	9087.9	2569.25	1.22	25.89	1.148	22	35.1	29.8	24.2
165	8300.0	2340.25	1.18	25.12	1.088	20	31.5	30.4	21.4
166	9089.4	2816.88	1.337	25.89	1.363	16	40.2	33.4	18.0
167	7746.9	2564.00	1.354	24.55	1.535	22	44.3	28.3	15.9
168	14884.2	3883.33	1.327	30.52	1.459	18	48.3	38.4	18.0
169	10426.0	2837.18	1.229	27.10	1.303	18	40.5	36.3	19.9
170	22798.1	4762.14	1.225	35.18	1.184	22	49.9	46.7	28.3
171	13532.4	3845.67	1.4	29.57	1.48	20	58.4	30.1	26.6
172	14547.2	4038.41	1.401	30.29	1.725	20	57.5	39.0	17.8
173	10665.9	2900.14	1.238	27.31	1.18	20	39.3	32.2	23.2
174	12335.0	3658.90	1.417	28.67	1.573	18	53.6	34.7	17.3
175	12522.4	3466.83	1.329	28.81	1.533	24	55.2	29.4	22.8
176	11307.1	3199.66	1.313	27.85	1.393	22	45.8	30.3	24.8
177	11164.9	2942.05	1.218	27.73	1.114	24	35.5	33.5	24.8
178	7790.9	2367.23	1.246	24.60	1.111	20	32.1	30.2	25.0

179	9469.5	2814.75	1.3	26.25	1.25	22	39.5	29.4	23.6
180	8733.2	2672.17	1.303	25.55	1.239	20	37.0	36.7	20.0
181	20909.1	4570.27	1.245	34.18	1.212	22	52.3	40.5	29.0
182	13665.4	3338.12	1.208	29.66	1.263	20	47.4	32.2	25.3
183	7949.0	2467.25	1.281	24.76	1.273	16	38.6	28.4	22.5
184	13699.1	3391.39	1.225	29.69	1.243	16	44.3	36.7	24.0
185	12858.4	3239.38	1.22	29.07	1.149	24	41.1	33.2	24.2
186	10916.4	2844.33	1.195	27.52	1.136	20	39.5	33.7	23.2
187	15169.7	3585.85	1.21	30.71	1.08	24	40.0	38.0	26.8
188	11234.6	3195.17	1.317	27.79	1.32	22	44.0	29.0	26.1
189	14754.4	3884.08	1.335	30.43	1.394	22	46.9	37.8	18.4
190	10778.7	2943.10	1.247	27.41	1.468	12	50.6	29.2	18.3
191	11805.9	3272.48	1.305	28.25	1.169	24	40.4	32.9	25.9
192	7687.7	2294.08	1.218	24.49	1.135	12	32.9	29.7	24.9
193	11141.6	3265.79	1.354	27.71	1.41	12	43.8	36.1	19.8
194	8673.3	2402.95	1.177	25.49	1.125	20	34.9	27.6	21.4
195	15134.4	3914.24	1.323	30.69	1.309	26	48.1	39.1	21.6
196	8900.6	2548.99	1.227	25.71	1.129	20	37.1	29.3	24.5
197	8503.7	2576.56	1.279	25.32	1.485	16	43.2	32.1	14.4
198	11906.4	3007.73	1.193	28.33	1.167	16	37.1	35.2	24.9
199	12563.6	3404.90	1.303	28.84	1.486	22	52.4	27.5	22.6
200	8763.4	2618.29	1.274	25.58	1.067	26	33.4	26.6	24.6

Table B.11 Results of the ∝CT scans of NS3875

#	Vol	SA	SA/Saeq	ESD	Tr/Treq	Max	L	W	T
1	49019.1	8553.23	1.32	45.41	1.5	20	80.5	53.6	26.5
2	28273.7	6239.01	1.39	37.80	1.344	22	64.5	54.2	25.0
3	22608.3	5100.34	1.319	35.08	1.435	18	58.7	39.7	25.0
4	15166.7	4289.19	1.448	30.71	1.639	20	54.8	43.3	16.8
5	10443.2	2981.39	1.29	27.12	1.161	12	37.3	32.5	31.1
6	15615.9	3959.67	1.311	31.01	1.19	26	43.9	38.8	24.2
7	28580.5	5954.87	1.317	37.93	1.423	20	65.4	39.5	28.3
8	14431.9	3791.93	1.323	30.21	1.229	16	50.2	32.3	28.9
9	8719.8	2541.91	1.241	25.54	1.141	16	35.6	30.9	23.3
10	41230.2	7970.98	1.381	42.86	1.315	24	70.9	53.5	35.9
11	19811.6	4342.72	1.226	33.57	1.279	16	48.7	41.0	24.5
12	60293.5	9641.39	1.297	48.65	1.167	20	67.5	62.4	44.1
13	80233.3	10755.53	1.196	53.51	1.173	18	78.6	68.8	44.1
14	28189.3	5602.99	1.251	37.76	1.314	18	61.7	41.0	30.3
15	18045.3	4393.87	1.321	32.54	1.702	14	66.6	35.1	18.5
16	34274.9	6721.33	1.317	40.30	1.344	20	70.8	48.2	31.8
17	59219.8	9134.84	1.243	48.36	1.293	22	75.9	48.9	39.0
18	7975.7	2553.23	1.323	24.79	1.377	18	41.7	29.0	20.7
19	22427.0	5190.24	1.35	34.99	1.805	14	72.8	34.5	23.9
20	11657.5	3250.03	1.307	28.13	1.199	20	42.0	36.8	25.7
21	40880.9	7680.13	1.338	42.74	1.526	14	75.5	50.6	25.4
22	11549.6	3262.93	1.321	28.05	1.369	14	44.0	37.8	22.5
23	15540.4	4229.52	1.404	30.96	1.332	18	47.1	43.6	22.9
24	39209.0	7151.42	1.281	42.15	1.278	26	65.1	44.8	31.4
25	12188.8	3328.72	1.3	28.55	1.314	16	43.1	32.3	18.5
26	39939.2	8120.54	1.437	42.41	1.402	22	78.6	50.8	35.1

27	8690.6	2570.40	1.257	25.51	1.204	18	38.2	29.5	21.8
28	30398.8	6046.78	1.284	38.72	1.238	22	56.5	42.4	29.6
29	15523.2	3708.09	1.232	30.95	1.159	22	40.2	40.3	23.8
30	9068.2	2709.42	1.288	25.87	1.344	20	42.4	27.0	19.3
31	29409.4	5946.38	1.291	38.30	1.341	14	56.6	49.2	22.8
32	34484.0	6648.56	1.298	40.38	1.207	28	58.3	53.9	31.8
33	48904.1	8603.93	1.33	45.37	1.349	24	72.8	62.3	29.5
34	18512.2	4802.47	1.419	32.82	1.489	20	63.0	38.2	23.4
35	18474.6	4347.37	1.286	32.80	1.525	12	55.1	33.4	27.4
36	80609.2	10670.94	1.182	53.60	1.107	28	70.0	67.2	43.3
37	64832.9	9434.49	1.209	49.84	1.157	22	74.7	52.7	47.6
38	18031.0	4285.68	1.289	32.53	1.353	20	49.5	46.9	19.8
39	65299.9	9871.21	1.259	49.96	1.288	18	77.7	51.6	48.4
40	108554.4	14133.62	1.284	59.19	1.298	28	89.0	75.4	52.3
41	24425.7	5035.21	1.237	36.00	1.129	18	51.6	38.4	36.1
42	58169.4	9587.82	1.321	48.07	1.147	20	66.9	61.8	54.5
43	34864.9	6803.27	1.318	40.53	1.369	22	69.3	50.2	32.2
44	11140.5	3310.90	1.373	27.71	1.428	22	48.2	31.3	22.3
45	14756.3	3810.93	1.31	30.43	1.364	16	54.5	34.1	24.1
46	21963.8	5235.00	1.38	34.75	1.412	26	56.2	40.6	23.6
47	17793.0	4311.30	1.308	32.39	1.183	20	50.3	39.0	32.5
48	48419.1	8145.71	1.268	45.22	1.176	28	66.6	54.7	40.8
49	35017.9	6507.89	1.257	40.59	1.205	20	61.0	45.1	33.2
50	31867.3	6281.82	1.292	39.34	1.263	22	75.3	42.3	33.2
51	33289.2	6555.60	1.31	39.91	1.256	20	60.2	58.6	32.5
52	7916.3	2456.39	1.279	24.73	1.352	16	38.2	28.8	18.8
53	18402.5	4206.98	1.248	32.76	1.113	22	43.0	39.6	28.3
54	33456.2	6571.86	1.309	39.98	1.227	18	59.4	56.6	33.6
55	24439.0	5184.45	1.273	36.00	1.235	16	52.0	49.6	32.3
56	26495.0	5497.85	1.279	36.99	1.185	16	55.8	41.4	32.0
57	22302.6	5099.14	1.331	34.92	1.402	22	54.1	44.3	23.5
58	17594.8	4737.20	1.448	32.27	1.668	20	61.1	40.4	19.6
59	10827.9	3109.57	1.314	27.45	1.34	20	44.9	33.9	20.6
60	12704.9	3216.62	1.222	28.95	1.192	14	41.8	40.4	23.7
61	18025.0	4186.51	1.259	32.53	1.144	22	46.8	39.9	31.8
62	31632.3	6575.44	1.359	39.24	1.365	20	63.2	55.2	34.1
63	55420.8	9086.89	1.293	47.30	1.326	24	71.8	64.1	30.4
64	61970.5	9306.45	1.229	49.10	1.244	18	72.0	58.9	35.8
65	20075.5	5103.22	1.429	33.72	1.789	18	68.6	39.7	23.7
66	17861.8	4648.61	1.407	32.43	1.452	18	54.7	39.6	21.4
67	48714.4	8413.26	1.304	45.31	1.362	28	79.8	55.2	32.6
68	29010.7	5957.58	1.305	38.12	1.472	16	66.8	42.3	24.7
69	14235.4	3999.10	1.408	30.07	1.476	22	55.2	35.6	23.8
70	101484.2	13586.40	1.291	57.87	1.306	24	93.0	59.9	44.3
71	7974.6	2566.74	1.33	24.79	1.532	16	44.3	29.5	17.2
72	121208.0	15163.68	1.28	61.40	1.254	16	90.5	78.5	44.0
73	13818.6	3659.94	1.314	29.77	1.253	22	46.2	37.6	23.1
74	12676.4	3839.12	1.46	28.93	1.622	16	62.6	31.9	26.9
75	7653.3	2560.38	1.363	24.45	1.603	18	45.3	25.6	16.8
76	112309.1	14017.64	1.245	59.86	1.417	12	92.3	63.8	41.8
77	51060.8	9474.03	1.423	46.03	1.585	26	84.4	70.9	26.7
78	28096.0	5849.36	1.309	37.72	1.186	20	50.4	43.5	38.0
79	17432.5	4137.23	1.272	32.17	1.334	24	50.5	39.2	21.6

80	14664.5	4374.19	1.51	30.37	1.22	26	53.2	43.9	31.2
81	34053.6	6745.08	1.328	40.21	1.363	16	64.4	55.2	30.9
82	14918.3	3978.22	1.357	30.54	1.32	20	49.1	38.9	26.6
83	9948.5	3156.00	1.411	26.68	1.376	20	41.6	36.3	22.6
84	41347.8	8136.34	1.407	42.90	1.727	20	86.8	43.3	30.9
85	13622.3	3687.06	1.337	29.63	1.468	18	49.3	37.4	20.1
86	13523.4	3615.77	1.317	29.56	1.263	22	48.5	32.9	26.8
87	39972.9	7739.22	1.369	42.42	1.436	28	77.7	47.9	35.0
88	18472.2	4867.26	1.44	32.80	1.683	16	60.3	45.1	18.5
89	10206.0	3246.09	1.427	26.91	1.524	20	46.6	38.9	17.3
90	12261.2	3557.76	1.384	28.61	1.513	16	49.4	32.6	18.6
91	21053.1	4773.79	1.295	34.26	1.234	22	50.0	45.7	26.3
92	20288.3	4533.79	1.26	33.84	1.177	28	50.3	35.9	29.2
93	8547.2	2629.93	1.301	25.37	1.294	22	38.5	33.1	16.4
94	48788.4	8027.00	1.243	45.34	1.289	20	79.6	48.0	35.7
95	36291.9	7137.32	1.346	41.08	1.306	18	62.7	53.0	29.1
96	40472.0	7300.75	1.281	42.60	1.288	26	67.5	53.4	31.9
97	9661.3	3065.37	1.397	26.42	1.536	16	43.7	34.1	17.3
98	13063.0	3728.26	1.39	29.22	1.449	20	46.1	40.3	17.1
99	12472.1	3443.05	1.324	28.77	1.357	16	48.2	34.5	22.8
100	14195.1	3837.52	1.354	30.04	1.383	18	50.7	38.5	20.5
101	61961.8	10356.26	1.368	49.10	1.755	12	89.0	57.3	26.6
102	40903.7	7556.34	1.316	42.75	1.268	20	67.9	54.8	37.7
103	97635.0	12908.32	1.259	57.13	1.176	18	82.9	68.3	55.4
104	19045.6	4572.95	1.326	33.13	1.227	22	48.1	42.4	30.4
105	18499.7	4340.32	1.283	32.81	1.183	16	46.8	42.6	31.8
106	26624.9	5673.30	1.316	37.05	1.152	24	57.3	41.2	32.4
107	11795.7	3544.04	1.414	28.24	1.463	24	53.2	34.1	20.0
108	7973.4	2617.55	1.356	24.79	1.464	16	42.1	35.4	14.2
109	21290.6	4736.65	1.275	34.39	1.209	14	49.5	42.1	34.4
110	10809.8	3067.17	1.297	27.43	1.182	18	41.7	33.8	24.8
111	28048.9	5757.82	1.29	37.70	1.257	18	55.5	48.3	36.1
112	53592.1	8357.93	1.216	46.78	1.117	20	61.8	61.6	42.7
113	46079.8	7827.42	1.259	44.48	1.186	20	61.4	50.9	37.0
114	93159.9	11959.71	1.203	56.24	1.124	12	78.2	68.2	54.2
115	11233.4	3393.65	1.399	27.79	1.647	18	53.5	36.3	16.0
116	72570.0	10847.15	1.289	51.75	1.185	28	79.3	64.4	52.7
117	18772.4	4507.23	1.32	32.97	1.41	20	53.6	39.2	22.3
118	23712.6	5112.03	1.281	35.64	1.48	16	59.7	40.2	24.2
119	8794.7	2887.84	1.402	25.61	1.623	20	47.5	28.5	18.3
120	47664.6	9603.93	1.511	44.98	2.714	24	114.8	41.6	26.4
121	11336.2	3264.91	1.338	27.87	1.32	22	47.2	28.2	24.7
122	21821.2	4966.51	1.315	34.67	1.124	24	49.7	41.4	36.2
123	50235.0	8563.48	1.301	45.78	1.251	14	72.9	58.3	36.0
124	43725.4	7604.19	1.267	43.71	1.332	18	66.7	51.0	32.4
125	8400.4	2567.58	1.285	25.22	1.394	16	42.4	26.2	23.0
126	7987.0	2762.90	1.43	24.80	1.869	12	47.6	29.2	12.9
127	80621.6	11889.60	1.317	53.60	1.363	24	89.3	61.4	40.1
128	7656.7	2380.58	1.267	24.45	1.118	18	33.9	30.0	21.3
129	33692.5	6476.15	1.284	40.07	1.218	18	60.0	54.0	30.0
130	59120.0	8863.21	1.208	48.33	1.112	22	61.8	57.3	43.5
131	47619.4	8433.70	1.327	44.97	1.58	20	79.6	54.0	25.7
132	16964.8	4066.94	1.274	31.88	1.148	16	42.6	37.1	35.4

133	9104.5	2683.83	1.273	25.91	1.183	12	36.3	29.0	25.8
134	8095.3	2734.78	1.403	24.91	1.75	14	47.6	28.1	20.1
135	8272.8	2772.99	1.402	25.09	1.556	16	44.7	30.5	21.2
136	23513.6	4982.98	1.255	35.54	1.241	16	58.2	40.9	29.1
137	70125.3	11084.56	1.348	51.16	1.289	28	83.5	64.0	39.8
138	92956.3	11499.85	1.159	56.20	1.093	28	80.4	58.0	54.4
139	43603.5	8182.41	1.366	43.67	1.368	22	76.6	44.0	40.6
140	23794.9	5326.71	1.331	35.69	1.676	12	65.8	41.4	24.4
141	7505.6	2548.47	1.375	24.29	1.275	16	36.3	31.5	18.4
142	30738.2	6169.95	1.3	38.87	1.324	26	64.7	38.1	36.3
143	36637.9	6892.00	1.292	41.21	1.232	20	60.2	47.4	35.0
144	42804.7	7461.57	1.261	43.40	1.281	24	66.4	48.9	32.0
145	22807.6	4945.00	1.271	35.19	1.16	24	52.0	46.4	29.1
146	10728.9	3192.31	1.357	27.36	1.538	22	55.0	28.6	19.7
147	8445.6	2640.03	1.316	25.27	1.122	20	35.8	30.5	26.9
148	17496.7	4011.34	1.231	32.21	1.166	18	45.3	39.8	32.5
149	15623.7	4263.63	1.411	31.02	1.396	18	48.8	46.1	27.7
150	12435.3	3461.27	1.333	28.74	1.242	22	46.9	30.1	28.9
151	19070.1	4468.81	1.295	33.15	1.232	18	49.7	38.8	29.7
152	11774.6	3449.16	1.378	28.23	1.498	16	49.4	31.0	19.6
153	49287.9	8644.60	1.33	45.49	1.28	28	75.0	47.1	43.2
154	41975.6	7106.35	1.217	43.12	1.167	16	60.4	47.5	39.0
155	39567.4	8262.55	1.471	42.28	1.74	16	73.0	58.1	25.0
156	34778.9	6528.10	1.267	40.50	1.28	18	61.6	58.4	33.7
157	23354.2	5244.45	1.327	35.46	1.273	20	53.1	48.5	26.5
158	9722.2	3294.32	1.495	26.48	1.583	18	49.2	42.5	20.1
159	23657.3	4968.16	1.247	35.62	1.318	16	56.1	43.9	26.1
160	9181.3	2974.19	1.403	25.98	1.301	24	39.0	39.1	19.1
161	29892.9	6357.79	1.365	38.51	1.323	28	59.0	54.6	28.7
162	57369.3	8775.32	1.22	47.85	1.358	16	86.1	46.6	41.5
163	90666.3	12118.45	1.242	55.74	1.251	22	88.1	68.3	43.0
164	15188.8	4288.51	1.446	30.73	1.578	12	52.1	47.7	18.9
165	9625.8	2764.83	1.263	26.39	1.241	18	37.2	32.7	20.9
166	25551.5	5424.07	1.293	36.54	1.312	24	59.9	43.8	27.3
167	15411.9	4274.18	1.427	30.88	1.493	18	60.4	41.6	25.7
168	32225.8	5942.68	1.213	39.48	1.17	24	57.6	45.7	38.1
169	22908.5	5134.93	1.316	35.24	1.281	22	56.5	44.2	29.5
170	30456.6	6232.56	1.321	38.75	1.403	16	66.0	48.7	31.8
171	22778.9	5164.72	1.329	35.17	1.542	16	65.2	39.1	20.9
172	33624.1	6905.31	1.371	40.05	1.339	18	68.3	45.4	36.6
173	8285.1	2580.87	1.303	25.11	1.328	16	37.8	30.7	18.1
174	21725.2	5056.40	1.343	34.62	1.322	22	58.9	40.5	29.0
175	27664.8	5779.46	1.307	37.52	1.269	20	57.9	45.7	31.5
176	75408.9	11075.68	1.283	52.42	1.217	26	81.2	70.4	41.3
177	27169.8	6061.69	1.387	37.30	1.221	18	53.4	51.5	38.4
178	23174.8	5073.30	1.291	35.37	1.173	26	53.1	39.2	33.8
179	12277.3	3514.89	1.366	28.62	1.342	14	43.6	36.7	22.3
180	30518.5	5731.20	1.214	38.77	1.138	20	50.7	44.7	33.6
181	20934.1	4441.39	1.209	34.19	1.129	12	44.5	39.5	34.4
182	9996.2	2989.29	1.332	26.73	1.32	20	42.4	33.4	18.4
183	28353.7	5754.14	1.28	37.83	1.202	24	53.3	52.3	29.1
184	22299.1	4958.88	1.294	34.92	1.219	20	53.6	50.7	27.2
185	23687.8	4856.61	1.218	35.63	1.105	24	49.8	43.5	29.5

186	25237.6	5414.50	1.301	36.39	1.264	14	58.0	38.6	32.3
187	110537.6	15200.06	1.365	59.54	1.414	18	93.6	65.6	57.2
188	29911.9	6293.25	1.351	38.51	1.326	24	58.4	54.9	30.0
189	41507.7	7741.44	1.335	42.96	1.253	24	64.9	55.2	38.3
190	11107.5	3161.62	1.313	27.68	1.309	18	46.9	29.7	24.4
191	14128.1	3517.30	1.245	29.99	1.199	18	46.7	33.3	29.5
192	8331.8	2708.70	1.363	25.15	1.221	18	38.7	34.3	26.0
193	50140.8	8477.96	1.289	45.75	1.362	12	75.8	56.3	38.8
194	9264.2	2695.77	1.264	26.06	1.202	20	44.4	27.7	22.9
195	19985.7	4623.94	1.298	33.67	1.343	20	57.7	38.5	27.7
196	84824.5	11980.35	1.283	54.51	1.183	24	79.3	70.0	45.9
197	18303.0	4608.33	1.372	32.70	1.588	22	59.0	38.6	21.0
198	13662.8	3607.54	1.305	29.66	1.529	20	54.7	30.9	22.8
199	13308.4	3836.27	1.413	29.40	1.534	20	51.1	36.2	21.1
200	45853.4	7910.11	1.277	44.41	1.222	26	69.0	52.0	38.7

Table B.12 Results of the ∝CT scans of PF038

#	Vol	SA	SA/Saeq	ESD	Tr/Treq	Max	L	W	T
1	12328.3	3252.44	1.26	28.66	1.173	22	41.8	33.5	22.5
2	9334.9	2841.88	1.326	26.12	1.291	16	37.3	34.1	19.6
3	8190.2	2576.47	1.311	25.01	1.258	20	37.8	29.8	20.7
4	9729.2	2801.15	1.271	26.49	1.249	22	39.4	29.5	21.6
5	7964.2	2381.16	1.235	24.78	1.055	22	30.6	28.9	25.5
6	11425.6	3147.22	1.283	27.94	1.333	16	46.7	29.4	26.3
7	10390.4	2965.43	1.288	27.07	1.12	26	41.0	29.3	26.7
8	12178.7	3409.76	1.332	28.55	1.409	18	52.7	35.5	20.1
9	10113.6	2973.51	1.315	26.83	1.224	18	39.8	29.8	25.1
10	13306.2	3450.67	1.271	29.40	1.136	22	40.2	36.7	28.3
11	14300.4	3712.58	1.303	30.12	1.299	24	47.7	35.2	22.8
12	11299.4	3292.14	1.352	27.84	1.186	18	41.0	35.6	26.0
13	14061.5	3564.52	1.265	29.95	1.18	22	44.1	35.5	25.8
14	8366.9	3117.98	1.564	25.19	1.486	24	47.0	32.2	19.0
15	9933.8	2834.85	1.269	26.67	1.359	12	42.5	34.9	17.8
16	9282.1	2873.99	1.346	26.07	1.625	20	45.8	25.8	19.2
17	13910.8	3801.94	1.359	29.84	1.427	22	56.4	34.5	22.8
18	9280.2	2934.69	1.374	26.07	1.671	18	52.2	28.0	20.1
19	9725.5	2965.70	1.346	26.48	1.309	20	40.1	35.9	18.1
20	11227.8	3325.50	1.371	27.78	1.691	20	57.2	25.1	22.0
21	9534.8	2758.27	1.268	26.31	1.355	20	44.2	24.8	19.5
22	7809.9	2535.25	1.332	24.62	1.235	20	36.9	28.8	23.0
23	12401.1	3090.54	1.193	28.72	1.154	22	40.4	30.8	25.3
24	12257.7	3040.62	1.183	28.61	1.081	18	35.5	35.3	29.0
25	12436.0	3391.79	1.307	28.74	1.304	16	44.2	38.4	22.0
26	8434.8	2415.85	1.206	25.26	1.104	16	34.6	32.3	25.1
27	10559.8	3111.94	1.337	27.22	1.314	22	41.1	35.5	23.8
28	11718.7	3344.27	1.34	28.18	1.588	18	49.5	31.0	21.3
29	10626.4	3274.29	1.401	27.28	1.806	20	55.3	30.1	16.7
30	13747.8	3384.20	1.219	29.72	1.101	24	42.1	32.3	30.3
31	48473.0	8931.91	1.389	45.24	1.374	18	81.1	54.0	44.2
32	8965.2	2673.70	1.281	25.77	1.121	20	38.0	33.0	24.9
33	8408.0	2732.60	1.367	25.23	1.281	20	41.0	29.4	22.6

34	11803.5	2994.75	1.195	28.25	1.109	20	39.0	36.4	28.4
35	11871.1	3244.02	1.289	28.30	1.486	16	50.6	29.8	19.4
36	13892.3	4080.12	1.46	29.83	1.651	14	54.2	41.6	20.6
37	8658.0	3014.12	1.478	25.48	1.516	20	44.3	40.0	19.8
38	10248.8	2857.52	1.252	26.95	1.245	16	38.7	30.5	22.5
39	12113.2	3142.07	1.232	28.49	1.14	18	41.5	33.4	25.2
40	9300.1	2681.91	1.254	26.09	1.12	22	36.9	32.0	25.3
41	8396.6	2680.11	1.342	25.22	1.281	16	42.4	29.3	21.8
42	12298.1	3195.55	1.24	28.64	1.208	24	42.3	31.0	22.0
43	8959.3	2854.32	1.368	25.77	1.331	16	43.0	35.1	21.0
44	16952.9	3883.21	1.217	31.87	1.174	16	47.2	36.9	34.4
45	8818.4	2651.24	1.284	25.63	1.229	22	40.1	27.6	24.8
46	8560.7	2664.90	1.317	25.38	1.166	22	35.1	30.5	27.5
47	10285.1	3033.07	1.326	26.98	1.159	24	39.8	31.0	25.1
48	9268.1	2713.64	1.272	26.06	1.239	16	37.0	36.1	20.6
49	14753.3	3730.42	1.282	30.43	1.258	18	50.2	36.6	27.3
50	10661.8	3029.17	1.293	27.31	1.151	24	38.6	30.6	29.4
51	14990.6	3986.09	1.356	30.59	1.414	20	51.9	34.8	28.8
52	8594.5	2653.03	1.308	25.41	1.323	18	40.7	26.4	19.8
53	9935.0	3020.09	1.351	26.67	1.201	28	38.0	35.0	20.7
54	8850.9	3048.87	1.473	25.66	1.65	16	45.8	39.3	13.1
55	7963.6	2611.55	1.354	24.78	1.299	18	35.0	32.3	22.6
56	9715.5	2671.36	1.213	26.47	1.208	18	38.5	30.3	20.2
57	11802.8	3463.89	1.382	28.25	1.324	24	43.4	32.3	25.6
58	8265.0	2325.26	1.176	25.09	1.091	16	32.4	31.5	23.4
59	9113.6	2717.53	1.288	25.92	1.372	14	45.2	30.0	19.1
60	10963.9	3090.65	1.295	27.56	1.24	22	45.3	29.6	22.9
61	12871.2	3822.31	1.439	29.08	1.404	14	45.8	39.6	31.0
62	10746.8	3286.92	1.396	27.38	1.462	22	43.3	33.0	17.1
63	8433.5	2451.44	1.223	25.25	1.095	20	34.6	28.0	24.0
64	7900.6	2537.91	1.323	24.71	1.312	18	38.9	30.2	18.8
65	11755.6	3344.32	1.338	28.21	1.209	22	45.1	36.0	26.5
66	7951.2	2534.95	1.316	24.76	1.084	20	34.2	30.8	26.5
67	8831.4	2640.14	1.278	25.65	1.294	18	38.6	26.5	22.9
68	14061.8	3727.80	1.323	29.95	1.101	24	40.5	38.4	28.5
69	9190.6	2738.05	1.29	25.99	1.23	22	39.0	33.1	20.7
70	10904.2	3025.86	1.272	27.51	1.223	22	42.5	32.2	24.4
71	17251.3	4245.16	1.315	32.06	1.168	22	45.5	40.0	30.5
72	9559.3	2830.09	1.299	26.33	1.484	14	47.7	34.9	16.6
73	12012.5	3285.83	1.295	28.41	1.274	22	42.3	40.0	20.3
74	8862.9	2649.92	1.279	25.68	1.222	22	37.9	29.0	18.3
75	10226.9	3028.07	1.329	26.93	1.437	16	45.3	31.1	17.9
76	9559.7	3056.43	1.403	26.33	1.355	22	41.7	35.4	19.3
77	7860.0	2457.74	1.286	24.67	1.112	18	34.4	28.1	25.2
78	9239.9	2574.14	1.209	26.03	1.05	24	31.9	29.6	27.5
79	8804.5	2722.91	1.321	25.62	1.141	24	37.2	36.0	24.2
80	8416.3	2561.91	1.28	25.24	1.077	24	33.3	27.3	23.3
81	9803.1	2843.18	1.284	26.55	1.303	18	38.8	40.8	18.5
82	11347.0	3003.01	1.23	27.88	1.107	24	38.5	32.4	24.7
83	8684.6	2592.09	1.269	25.50	1.214	20	38.3	26.1	21.3
84	14366.7	3420.75	1.197	30.16	1.097	20	41.3	33.8	27.9
85	7961.2	2530.64	1.312	24.77	1.216	18	37.2	31.9	24.5

86	11025.2	2988.87	1.248	27.61	1.139	22	40.0	32.3	24.3
87	13128.4	3641.51	1.353	29.27	1.608	16	51.7	38.6	15.3
88	20320.1	4574.70	1.27	33.86	1.182	26	54.5	40.5	33.3
89	10758.5	3062.92	1.3	27.39	1.265	16	43.0	33.3	24.7
90	9317.2	2840.24	1.326	26.11	1.384	16	45.5	30.6	25.9
91	10623.5	2847.48	1.218	27.27	1.145	18	38.9	32.8	26.3
92	11047.4	3442.13	1.435	27.63	1.58	16	46.7	39.1	20.2
93	12630.9	3561.07	1.358	28.89	1.19	26	45.8	33.1	28.3
94	7929.1	2474.07	1.287	24.74	1.171	22	33.4	32.6	21.3
95	9413.9	2725.05	1.264	26.20	1.241	20	45.3	31.0	18.2
96	9988.8	2725.94	1.215	26.72	1.193	18	39.2	30.4	26.6
97	10380.5	3117.88	1.355	27.06	1.375	20	41.5	36.2	19.5
98	12829.6	3456.70	1.304	29.05	1.223	26	46.6	34.8	22.7
99	7724.6	2537.98	1.343	24.53	1.255	20	41.0	30.2	20.6
100	9086.8	2741.98	1.302	25.89	1.191	20	38.8	28.4	25.1
101	14889.8	3805.78	1.3	30.52	1.17	26	48.3	35.3	25.8
102	21549.5	5483.86	1.464	34.53	1.62	18	77.1	38.9	33.3
103	14577.5	3644.49	1.263	30.31	1.137	24	41.7	38.3	26.8
104	10300.0	3126.38	1.366	26.99	1.414	18	43.0	38.7	16.0
105	12191.2	3299.09	1.288	28.56	1.259	22	42.2	34.1	22.6
106	10364.3	3022.54	1.315	27.05	1.438	20	46.6	25.2	23.0
107	8513.6	2813.62	1.395	25.33	1.646	20	50.7	25.2	17.3
108	7691.8	2530.79	1.343	24.49	1.141	24	32.4	26.8	24.2
109	9042.2	2607.53	1.242	25.85	1.22	18	38.0	33.0	21.9
110	9794.0	2784.15	1.258	26.55	1.163	20	36.2	28.3	26.3
111	14920.8	3832.88	1.308	30.54	1.567	16	57.8	34.4	20.0
112	13013.6	3421.21	1.279	29.18	1.474	18	47.6	30.5	21.7
113	11638.8	3392.66	1.366	28.12	1.404	20	46.5	35.5	19.5
114	10118.7	3033.65	1.341	26.84	1.316	24	41.0	31.4	21.6
115	11809.7	3330.67	1.328	28.25	1.248	18	44.1	30.8	23.6
116	12367.0	3720.14	1.438	28.69	1.655	26	51.3	29.6	20.1
117	11317.0	3497.29	1.435	27.86	1.532	26	47.4	34.7	19.3
118	14375.2	3848.58	1.346	30.17	1.248	20	47.2	38.3	23.4
119	8106.8	2418.66	1.239	24.92	1.461	16	41.2	26.7	19.1
120	9558.7	2757.51	1.266	26.33	1.213	22	40.5	27.4	24.1
121	9714.0	2947.20	1.339	26.47	1.677	18	51.4	26.7	19.2
122	11694.0	3011.57	1.209	28.16	1.179	18	38.7	31.5	25.5
123	9455.6	2872.69	1.328	26.24	1.147	26	37.1	31.6	24.0
124	9048.6	2641.87	1.258	25.85	1.248	18	38.8	29.4	20.2
125	9047.9	2729.30	1.3	25.85	1.301	18	44.6	30.5	19.5
126	11523.0	3203.81	1.299	28.02	1.139	22	40.3	35.4	28.9
127	7693.1	2410.06	1.279	24.49	1.294	14	37.0	33.7	21.0
128	9771.1	2955.16	1.337	26.52	1.153	20	35.9	30.3	29.7
129	14308.3	3554.56	1.247	30.12	1.122	22	40.2	35.1	27.3
130	8896.4	2804.50	1.351	25.71	1.427	22	44.5	28.1	18.1
131	8150.6	2636.98	1.346	24.97	1.454	18	41.5	29.9	15.0
132	11256.3	3272.42	1.347	27.81	1.416	18	43.6	37.7	20.2
133	8617.9	2635.19	1.296	25.44	1.212	20	42.0	31.0	22.8
134	8025.0	2334.81	1.204	24.84	1.17	16	36.9	28.5	22.2
135	11835.9	3426.03	1.364	28.27	1.537	18	48.6	32.7	19.2
136	8882.2	2718.18	1.311	25.69	1.285	22	36.7	35.2	17.8
137	9660.3	2675.24	1.22	26.42	1.218	16	40.5	26.3	23.1

138	9337.8	2664.86	1.243	26.13	1.113	18	37.0	29.4	28.6
139	8379.8	2765.13	1.386	25.20	1.136	22	36.3	29.3	27.2
140	12285.0	3095.52	1.202	28.63	1.139	18	40.0	31.8	25.2
141	14906.2	3629.12	1.239	30.53	1.119	22	41.7	35.8	28.0
142	9769.7	2859.59	1.294	26.52	1.194	18	39.8	29.0	24.9
143	17569.3	4086.36	1.25	32.25	1.231	16	49.6	34.3	30.7
144	13703.2	3644.35	1.316	29.69	1.171	22	42.6	35.5	29.8
145	9425.9	2845.25	1.319	26.21	1.378	16	42.2	28.3	24.6
146	8769.3	2521.35	1.226	25.59	1.23	16	35.1	31.8	17.3
147	9920.7	2822.90	1.264	26.66	1.173	20	38.0	31.1	28.7
148	7759.7	2400.20	1.266	24.56	1.255	16	38.1	29.9	19.4
149	9433.0	2811.58	1.302	26.22	1.214	20	38.5	33.6	24.6
150	11229.1	3160.75	1.303	27.78	1.205	24	44.0	33.1	23.0
151	9259.4	3085.48	1.447	26.05	1.289	24	40.7	36.7	18.5
152	8328.1	2495.22	1.256	25.15	1.239	18	36.9	32.1	20.7
153	14218.0	3946.85	1.391	30.06	1.275	20	45.7	39.3	27.6
154	12008.1	3441.98	1.357	28.41	1.309	22	47.1	29.4	25.8
155	9607.2	2754.71	1.26	26.38	1.185	20	39.1	29.8	25.6
156	9098.3	2421.18	1.149	25.90	1.083	18	33.1	27.8	24.5
157	12300.4	3297.91	1.28	28.64	1.121	26	41.4	32.1	28.2
158	9400.5	2806.08	1.303	26.18	1.241	18	38.6	29.9	23.3
159	10300.5	2907.50	1.27	27.00	1.253	20	41.6	27.6	23.8
160	11977.1	3408.79	1.347	28.39	1.557	14	46.2	37.2	16.5
161	16831.1	3935.80	1.239	31.80	1.117	26	45.8	36.2	31.8
162	9507.7	2754.21	1.269	26.28	1.158	22	35.4	32.4	23.6
163	15605.6	3905.95	1.293	31.00	1.218	22	47.6	35.3	27.9
164	9639.0	2814.73	1.285	26.40	1.397	18	42.2	33.3	17.0
165	10328.8	3159.64	1.378	27.02	1.336	18	40.4	38.9	18.8
166	11441.2	3237.66	1.319	27.96	1.196	22	42.7	35.2	24.0
167	9198.1	2572.74	1.212	26.00	1.131	20	36.5	29.2	22.3
168	9090.7	2829.66	1.343	25.89	1.224	24	37.6	29.8	23.3
169	10231.4	2801.86	1.229	26.93	1.19	14	36.6	31.3	25.8
170	13066.9	3595.57	1.34	29.22	1.4	22	48.8	32.6	24.6
171	8184.9	2598.10	1.323	25.00	1.235	22	35.9	33.6	21.1
172	7749.4	2480.48	1.31	24.55	1.295	20	38.3	30.6	18.5
173	15525.7	3732.32	1.24	30.95	1.143	24	49.0	34.9	29.8
174	7706.2	2624.55	1.391	24.51	1.268	22	39.4	29.3	22.9
175	12494.0	3876.00	1.489	28.79	1.765	18	58.0	42.7	15.7
176	8756.9	2816.87	1.371	25.57	1.392	22	44.9	29.6	18.1
177	10377.6	2743.18	1.192	27.06	1.191	16	36.9	31.0	23.9
178	10584.0	2998.84	1.286	27.24	1.074	24	33.8	33.3	29.9
179	13112.2	3345.72	1.244	29.26	1.134	22	40.8	31.0	29.7
180	10539.6	3148.33	1.354	27.20	1.532	16	48.1	30.4	19.7
181	14120.2	3910.71	1.384	29.99	1.291	26	48.6	38.3	22.2
182	7985.5	2645.47	1.369	24.80	1.09	24	31.8	31.7	27.9
183	8794.8	2793.69	1.356	25.61	1.524	20	47.3	27.0	17.0
184	8033.1	2751.51	1.419	24.85	1.316	18	40.1	30.2	22.2
185	7729.0	2511.04	1.328	24.53	1.704	16	47.3	23.7	18.5
186	9043.5	2730.25	1.301	25.85	1.228	24	40.6	26.3	24.1
187	9649.1	2954.59	1.348	26.41	1.501	16	47.9	36.0	17.3
188	8294.7	2874.69	1.451	25.12	2.309	16	57.0	23.3	15.5
189	8334.1	2657.96	1.337	25.15	1.127	28	37.4	27.6	26.1

190	13396.2	3598.31	1.319	29.47	1.475	18	58.0	30.7	24.9
191	8068.6	2556.18	1.314	24.88	1.258	18	39.5	26.4	24.3
192	15414.3	3812.00	1.273	30.88	1.165	26	44.0	32.7	30.4
193	9793.6	2977.35	1.345	26.54	1.316	22	38.4	38.6	18.5
194	9425.8	2860.04	1.325	26.21	1.549	22	46.9	28.0	19.0
195	8549.8	2723.03	1.347	25.37	1.244	22	39.0	32.0	20.7
196	9419.4	2973.08	1.378	26.20	1.653	22	51.7	27.1	17.9
197	12772.5	3436.64	1.301	29.00	1.201	14	38.8	36.3	28.7
198	7725.2	2644.42	1.399	24.53	1.463	18	41.2	30.6	20.3
199	13290.8	3506.79	1.292	29.39	1.143	22	42.3	34.2	26.1
200	8822.2	2668.54	1.292	25.64	1.407	16	40.4	26.1	21.7

Table B.13 Results of the ∝CT scans of PF3875

#	Vol	SA	SA/Saeq	ESD	Tr/Treq	Max	L	W	T
1	11764.7	3265.01	1.305	28.22	1.142	26	38.2	32.3	31.2
2	17723.8	4070.60	1.238	32.35	1.128	22	44.6	36.3	33.5
3	38935.3	7130.54	1.284	42.05	1.248	28	65.5	45.4	38.1
4	39040.0	7675.82	1.379	42.09	1.585	22	70.3	56.6	26.1
5	29803.9	5767.60	1.241	38.47	1.228	18	55.9	48.4	37.8
6	18611.4	4694.31	1.382	32.88	1.389	22	57.8	43.8	23.8
7	8684.0	2873.51	1.406	25.50	1.614	16	45.2	31.2	15.8
8	12730.6	3543.06	1.344	28.97	1.204	26	45.1	39.9	26.9
9	19373.1	4621.35	1.325	33.32	1.422	20	51.9	49.2	18.9
10	13077.7	3401.64	1.267	29.23	1.4	20	46.4	28.8	23.8
11	18658.2	4761.81	1.4	32.91	1.423	22	54.7	45.1	26.4
12	39746.0	7067.37	1.255	42.34	1.168	28	60.2	55.0	33.3
13	8516.5	2768.56	1.373	25.34	1.37	18	44.4	29.2	23.5
14	18813.4	4680.25	1.368	33.00	1.837	16	63.7	32.0	19.7
15	22159.3	4631.09	1.214	34.85	1.108	28	45.1	42.9	32.3
16	7954.1	2410.04	1.251	24.77	1.167	20	35.2	28.6	23.7
17	17684.7	4173.59	1.271	32.32	1.136	24	44.0	37.5	30.4
18	43472.1	6962.03	1.164	43.63	1.118	24	57.4	47.4	40.4
19	11005.6	2937.71	1.228	27.60	1.083	22	38.3	31.4	27.3
20	11268.6	3361.51	1.383	27.82	1.596	14	45.4	41.3	15.0
21	26385.6	5641.36	1.316	36.94	1.306	24	62.9	48.2	25.2
22	9606.0	2834.65	1.297	26.37	1.307	18	42.6	28.1	22.9
23	13090.2	3604.19	1.342	29.24	1.402	18	47.0	35.7	20.9
24	46503.9	7546.65	1.207	44.62	1.181	22	60.4	53.8	40.1
25	40504.1	7274.16	1.275	42.61	1.225	26	65.5	55.9	35.4
26	45107.1	7940.93	1.296	44.17	1.313	24	69.4	57.2	31.9
27	9582.6	2943.20	1.349	26.35	1.674	20	47.8	30.1	17.4
28	19731.3	4968.97	1.407	33.53	1.563	24	59.1	47.1	19.7
29	9777.9	2879.32	1.302	26.53	1.131	26	36.5	31.7	23.3
30	8434.3	2918.12	1.456	25.26	1.769	20	47.5	30.3	14.0
31	17890.6	4334.98	1.31	32.45	1.421	18	51.8	31.9	22.7
32	10100.4	3148.57	1.393	26.82	1.279	24	40.9	34.0	20.8
33	22100.1	4530.55	1.19	34.82	1.158	14	48.7	44.9	25.9
34	9044.0	2816.53	1.342	25.85	1.36	20	37.7	36.5	16.2
35	8103.2	2926.79	1.5	24.92	1.828	20	53.3	34.3	14.0
36	31218.4	6326.73	1.32	39.07	1.346	18	68.9	52.8	36.8

37	17785.4	4190.22	1.272	32.39	1.205	24	50.5	40.8	30.6
38	19814.7	5100.81	1.44	33.57	1.782	14	67.6	41.7	20.3
39	34341.8	6255.74	1.224	40.33	1.181	22	59.2	52.2	32.6
40	30814.2	6705.39	1.411	38.90	1.608	22	79.8	43.7	30.6
41	18780.2	4206.00	1.231	32.98	1.147	24	48.5	43.6	27.9
42	18658.2	4307.81	1.266	32.91	1.174	26	48.7	39.2	29.5
43	10079.4	3144.64	1.394	26.80	1.687	24	52.2	24.4	21.0
44	12521.6	3697.57	1.418	28.81	1.332	24	47.4	35.0	28.1
45	27225.2	5496.89	1.256	37.32	1.23	20	57.8	47.7	26.9
46	13773.8	3577.83	1.288	29.74	1.302	22	45.0	35.8	22.6
47	15135.9	3840.96	1.298	30.69	1.36	22	51.4	31.6	23.6
48	12537.5	3477.60	1.332	28.82	1.407	22	49.6	35.4	20.6
49	18805.6	4471.60	1.308	32.99	1.256	28	53.5	36.2	30.9
50	9249.6	2804.17	1.316	26.04	1.259	24	39.7	29.9	20.4
51	18305.8	4643.64	1.382	32.70	1.493	20	61.4	34.5	24.5
52	33580.2	7578.35	1.506	40.03	1.651	16	72.8	58.7	31.4
53	11918.7	3116.88	1.235	28.34	1.272	20	43.1	30.1	22.2
54	11628.9	2990.65	1.205	28.11	1.092	20	36.8	32.3	28.9
55	14712.1	3774.18	1.3	30.40	1.132	24	43.4	37.3	28.1
56	17542.5	3847.35	1.178	32.24	1.052	26	39.9	35.2	34.2
57	22623.3	5442.08	1.407	35.09	1.528	18	65.2	40.2	30.3
58	16346.2	3780.53	1.214	31.49	1.185	22	45.6	38.8	23.1
59	45384.9	7982.32	1.297	44.26	1.274	28	73.6	52.6	39.9
60	16064.9	4173.61	1.356	31.31	1.451	20	52.6	37.8	20.0
61	11956.3	3345.91	1.323	28.37	1.375	20	43.8	41.2	16.5
62	10183.2	3023.69	1.331	26.89	1.235	22	37.1	36.8	23.1
63	18090.8	4261.90	1.279	32.57	1.246	26	54.2	32.9	30.4
64	11107.2	3096.09	1.286	27.68	1.185	22	40.0	30.9	25.5
65	7841.2	2568.33	1.346	24.65	1.298	20	38.2	33.4	18.5
66	8137.0	2506.07	1.281	24.95	1.143	20	38.3	28.5	25.4
67	10005.1	3265.29	1.454	26.73	1.475	24	46.0	27.9	23.3
68	12361.9	3226.82	1.248	28.69	1.352	20	48.4	31.1	21.3
69	17994.1	4006.63	1.207	32.51	1.079	26	44.4	38.3	31.5
70	24233.9	5137.77	1.269	35.90	1.261	26	53.8	45.4	26.3
71	11546.2	3129.69	1.267	28.04	1.322	16	45.4	35.3	19.6
72	11402.8	3411.59	1.393	27.93	1.333	22	47.0	34.6	22.0
73	19707.4	4326.02	1.226	33.51	1.219	18	50.9	38.0	28.9
74	18636.2	4501.18	1.324	32.89	1.648	18	59.5	34.2	19.4
75	9163.5	3183.61	1.503	25.96	1.582	18	46.2	38.4	17.7
76	9116.0	2717.94	1.288	25.92	1.242	22	42.1	28.4	21.9
77	7760.2	2462.59	1.299	24.56	1.159	24	37.0	27.0	23.4
78	18218.6	4524.34	1.351	32.65	1.295	28	50.6	35.3	23.2
79	24539.3	5594.28	1.37	36.05	1.697	20	72.8	37.1	21.6
80	15762.5	4283.15	1.409	31.11	1.521	20	56.5	36.5	23.7
81	14402.6	3640.27	1.272	30.19	1.228	20	42.5	38.8	23.0
82	17053.8	4162.80	1.299	31.94	1.249	22	49.3	35.1	29.6
83	36693.1	6546.11	1.226	41.23	1.28	22	63.7	44.0	34.7
84	10522.1	2913.73	1.255	27.19	1.367	16	44.6	27.8	22.9
85	34326.1	6304.07	1.234	40.32	1.22	24	61.1	48.5	35.0
86	17378.9	4014.25	1.237	32.14	1.152	22	43.6	40.1	26.9
87	11267.5	2951.37	1.214	27.81	1.098	22	37.3	32.4	28.8

88	13135.6	3406.50	1.265	29.27	1.101	28	39.1	38.0	25.8
89	20036.4	4710.04	1.32	33.70	1.382	16	59.2	40.0	26.2
90	28294.6	5291.61	1.178	37.81	1.055	26	45.3	40.6	39.9
91	9002.6	2663.04	1.272	25.81	1.146	26	38.0	26.8	22.9
92	9541.4	2808.38	1.291	26.32	1.338	18	44.1	26.0	22.3
93	10843.3	2900.01	1.224	27.46	1.064	24	33.9	31.5	27.7
94	7936.1	2479.41	1.289	24.75	1.214	20	35.1	29.8	22.2
95	8819.0	2745.72	1.33	25.63	1.524	20	44.5	25.9	18.5
96	69331.5	10544.68	1.292	50.97	1.304	28	83.4	58.8	45.1
97	28618.7	5540.27	1.224	37.95	1.115	28	54.2	40.0	36.1
98	60128.7	9413.49	1.268	48.61	1.214	26	75.5	56.1	42.4
99	9635.7	2678.20	1.223	26.40	1.075	22	34.8	31.7	28.7
100	10068.2	2766.69	1.227	26.79	1.099	22	35.0	33.0	25.1
101	8034.9	2415.59	1.245	24.85	1.089	24	32.4	28.7	24.9
102	9881.3	2855.41	1.282	26.62	1.324	24	43.0	27.7	19.4
103	19521.7	4832.94	1.378	33.41	1.221	28	54.6	45.5	32.9
104	8085.4	2683.66	1.378	24.90	1.239	24	36.2	34.3	18.0
105	17305.2	4155.63	1.284	32.09	1.204	22	45.3	36.0	33.7
106	14345.2	3852.64	1.349	30.15	1.233	22	45.5	37.1	26.3
107	13052.4	3424.35	1.277	29.21	1.308	18	45.9	31.4	26.7
108	10127.7	3170.12	1.4	26.84	1.437	14	45.3	34.9	20.8
109	13564.7	3603.23	1.31	29.59	1.151	28	41.7	36.8	26.6
110	12742.4	3614.19	1.37	28.98	1.466	18	50.7	32.1	23.2
111	11907.6	3190.47	1.265	28.33	1.154	22	41.4	35.3	27.5
112	23528.1	4927.64	1.241	35.55	1.197	26	55.7	44.6	30.8
113	7728.2	2566.17	1.358	24.53	1.349	20	39.6	29.6	20.4
114	9632.2	2725.73	1.245	26.40	1.16	18	39.0	34.4	23.9
115	26370.1	5822.28	1.359	36.93	1.394	26	63.7	41.2	32.8
116	10289.5	3164.16	1.383	26.99	1.923	22	55.6	23.6	16.4
117	15621.7	3627.28	1.2	31.02	1.111	22	47.7	34.4	30.7
118	9975.4	3014.20	1.345	26.71	1.265	24	41.6	29.8	20.1
119	12551.6	3325.01	1.273	28.83	1.246	22	46.1	33.1	24.7
120	18160.0	4314.04	1.291	32.61	1.127	26	45.6	37.2	32.9
121	15856.3	4397.08	1.441	31.17	1.581	20	58.9	30.4	24.0
122	30555.0	5844.84	1.237	38.79	1.199	16	61.1	44.0	34.3
123	19450.1	4347.04	1.243	33.37	1.254	20	49.3	45.5	25.2
124	9663.4	2882.27	1.314	26.43	1.144	26	35.5	29.3	27.2
125	11075.7	3134.43	1.304	27.66	1.329	14	44.3	31.5	24.5
126	23677.9	5519.41	1.384	35.63	1.504	22	62.2	42.9	21.3
127	11984.4	3259.27	1.287	28.39	1.287	18	43.8	35.5	20.1
128	53091.5	8353.43	1.223	46.63	1.125	28	64.9	52.1	43.6
129	20332.1	4642.63	1.289	33.86	1.184	28	49.5	42.4	28.8
130	36406.9	7244.02	1.364	41.12	1.258	24	66.6	58.5	35.0
131	9519.6	2957.17	1.361	26.29	1.628	14	46.1	39.9	12.6
132	21569.4	4763.30	1.271	34.54	1.197	22	49.7	41.5	27.3
133	33246.7	6439.08	1.288	39.89	1.388	24	65.8	42.0	30.0
134	50658.1	8400.36	1.269	45.91	1.269	28	66.4	62.3	33.6
135	24786.1	5121.81	1.246	36.17	1.188	28	51.0	43.3	27.4
136	9063.8	2574.43	1.225	25.87	1.205	16	37.8	31.7	21.8
137	11328.1	3389.97	1.39	27.86	1.524	16	48.9	40.5	14.8
138	21153.9	4889.64	1.322	34.31	1.282	26	55.0	37.3	32.1

139	10481.2	2739.06	1.183	27.15	1.105	18	36.0	34.2	23.3
140	12919.6	3273.51	1.229	29.11	1.082	24	38.7	35.9	26.7
141	19700.1	4471.77	1.268	33.51	1.456	22	60.6	35.5	22.2
142	21903.5	4724.01	1.248	34.71	1.173	24	52.2	44.6	28.4
143	8685.3	2618.50	1.281	25.50	1.2	22	36.1	29.0	20.9
144	11512.1	3548.63	1.439	28.01	1.682	18	53.3	37.2	15.1
145	15961.9	4225.25	1.378	31.24	1.609	20	61.6	29.9	25.3
146	15472.1	3749.90	1.249	30.92	1.091	26	43.4	38.0	28.1
147	21068.2	4691.78	1.272	34.27	1.297	22	50.1	37.3	28.3
148	42728.1	7774.80	1.315	43.37	1.31	20	66.2	57.2	31.8
149	21145.1	4854.32	1.313	34.31	1.115	28	46.1	43.4	35.6
150	13736.0	3854.37	1.39	29.71	1.773	16	59.5	36.5	16.8
151	11808.0	3619.45	1.443	28.25	1.678	18	54.5	40.9	15.8
152	43099.7	7405.96	1.246	43.50	1.35	20	76.3	51.6	33.0
153	79439.9	12308.94	1.377	53.34	1.705	26	98.8	59.1	30.6
154	21923.7	4916.00	1.298	34.72	1.215	28	53.9	37.7	30.9
155	16459.2	3933.43	1.257	31.56	1.15	24	44.4	33.8	32.8
156	47745.5	7455.99	1.171	45.01	1.15	26	58.3	47.1	39.8
157	15911.5	4454.66	1.456	31.21	2.772	12	73.3	26.7	15.9
158	10857.2	2970.08	1.253	27.47	1.181	18	42.0	33.0	28.4
159	11400.0	2956.55	1.207	27.92	1.202	16	39.0	33.0	23.6
160	7929.2	2661.89	1.384	24.74	1.247	24	37.9	29.6	23.6
161	24386.4	4896.52	1.204	35.98	1.163	22	55.1	36.8	37.3
162	10091.3	2894.00	1.281	26.81	1.275	22	43.0	30.0	24.9
163	18328.5	4260.79	1.267	32.71	1.113	28	41.5	38.9	33.8
164	10421.7	2999.50	1.3	27.10	1.246	24	43.2	30.0	22.2
165	24708.2	5231.93	1.275	36.14	1.385	20	61.2	42.8	24.9
166	17817.5	4075.31	1.235	32.41	1.258	18	50.3	40.4	26.3
167	16834.7	4133.48	1.301	31.80	1.146	26	46.2	41.5	31.3
168	8848.3	2564.16	1.239	25.66	1.169	22	36.7	28.0	20.9
169	9368.9	2957.11	1.376	26.16	1.417	22	47.2	31.2	16.8
170	9645.5	3044.76	1.389	26.41	1.381	16	43.2	37.0	18.7
171	17283.4	4251.22	1.315	32.08	1.31	26	53.4	33.5	24.9
172	10250.3	3140.54	1.376	26.95	1.183	24	41.0	34.5	26.2
173	8349.3	2694.06	1.354	25.17	1.27	20	45.0	27.1	23.3
174	8620.7	2779.63	1.367	25.44	1.245	28	37.8	27.6	23.0
175	8780.5	2560.53	1.244	25.60	1.172	20	35.7	30.0	21.1
176	28753.8	5696.87	1.255	38.01	1.155	24	51.7	47.7	32.5
177	18564.3	4416.84	1.303	32.85	1.215	16	48.1	40.2	31.7
178	16306.6	3999.36	1.286	31.46	1.47	20	54.5	29.4	27.3
179	9625.1	2789.47	1.275	26.39	1.248	20	37.9	30.3	23.7
180	49146.9	7940.90	1.224	45.45	1.147	28	62.5	54.9	42.4
181	40149.7	7299.87	1.287	42.48	1.294	22	65.9	52.6	35.7
182	26096.2	4969.18	1.168	36.80	1.188	20	55.7	39.1	36.2
183	8788.3	2584.89	1.255	25.60	1.254	16	36.7	36.2	18.2
184	29572.0	5753.44	1.244	38.37	1.271	26	58.0	50.3	28.2
185	21911.2	4867.77	1.285	34.72	1.122	24	46.2	44.0	33.0
186	23492.8	5591.64	1.41	35.53	1.736	18	65.3	45.8	16.6
187	8472.2	2790.00	1.388	25.29	1.397	22	45.7	24.6	22.4
188	45326.5	7567.61	1.231	44.24	1.127	28	62.1	55.7	40.3
189	8575.4	2871.47	1.417	25.40	1.377	18	41.2	29.9	19.6

190	12802.0	3482.35	1.316	29.02	1.403	16	46.7	38.5	21.3
191	12839.8	3784.15	1.427	29.05	1.435	20	52.4	36.7	23.9
192	19217.5	5040.46	1.453	33.23	1.729	22	67.1	35.5	27.3
193	22842.6	4918.74	1.263	35.20	1.144	28	48.8	42.2	28.9
194	25051.0	5054.06	1.221	36.30	1.142	24	49.4	42.2	36.2
195	12052.3	3399.75	1.337	28.45	1.195	24	41.8	34.1	31.1
196	28924.8	5615.59	1.232	38.09	1.247	24	54.0	50.4	26.7
197	12783.8	3474.32	1.314	29.01	1.646	20	53.4	27.0	20.4
198	9264.6	2881.67	1.351	26.06	1.424	18	42.7	32.4	18.2
199	9370.1	2751.59	1.28	26.16	1.159	22	38.9	32.7	25.6
200	57795.5	8878.91	1.228	47.97	1.163	26	69.7	68.8	40.5

Table B.14 Results of the ∝CT scans of TR038

#	Vol	SA	SA/Saeq	ESD	Tr/Treq	Max	L	W	T
1	9397.8	2438.68	1.132	26.18	1.03	20	31.3	28.4	28.2
2	10522.2	2681.17	1.155	27.19	1.029	20	36.6	27.7	27.6
3	12342.3	3129.72	1.212	28.67	1.012	28	34.5	31.2	29.5
4	8736.4	2382.89	1.162	25.55	1.017	22	32.3	27.3	26.6
5	11307.6	2931.01	1.203	27.85	1.02	26	36.4	31.1	28.8
6	8013.4	2266.03	1.17	24.83	1.012	24	29.7	26.5	26.4
7	15178.7	3852.01	1.299	30.72	1.374	20	53.2	34.0	27.1
8	17092.4	3523.25	1.098	31.96	1.006	24	37.0	33.4	33.2
9	15888.1	3888.83	1.272	31.19	1.166	20	47.4	35.2	28.2
10	8136.0	2180.81	1.115	24.95	1.009	20	27.2	27.1	26.6
11	9579.8	2716.15	1.245	26.35	1.037	26	32.4	29.6	27.7
12	7807.8	2307.13	1.212	24.61	1.013	26	27.5	26.6	26.3
13	8036.6	2289.34	1.18	24.85	1.012	24	27.9	26.8	26.3
14	12372.1	2826.96	1.093	28.70	1.01	22	32.2	29.9	28.5
15	12913.0	3328.04	1.25	29.11	1.277	22	45.1	34.0	20.0
16	13847.7	3382.43	1.213	29.79	1.228	16	47.1	30.3	29.2
17	7631.0	2646.25	1.412	24.43	1.524	14	45.4	25.2	21.3
18	17981.7	3690.39	1.112	32.50	1.015	24	41.5	35.4	33.1
19	9070.8	2528.56	1.202	25.88	1.053	22	34.5	30.0	26.6
20	9756.1	2504.15	1.134	26.51	1.021	22	34.8	28.3	28.3
21	20976.9	4603.22	1.251	34.22	1.219	24	51.2	38.3	31.5
22	9590.8	2616.78	1.199	26.36	1.107	20	40.2	28.6	26.0
23	8578.0	2394.21	1.181	25.40	1.01	26	29.5	27.6	26.9
24	11544.7	2755.98	1.116	28.04	1.007	24	30.0	30.0	28.9
25	11962.1	2833.48	1.12	28.38	1.011	22	35.4	29.5	29.0
26	10011.0	2746.44	1.223	26.74	1.011	28	29.9	28.8	26.9
27	17701.9	3992.57	1.216	32.34	1.127	18	51.4	43.5	32.6
28	10077.5	2699.22	1.196	26.80	1.011	28	29.6	29.2	28.0
29	7745.1	2442.97	1.29	24.55	1.097	22	39.6	27.2	25.9
30	11858.6	2832.63	1.126	28.29	1.016	22	36.5	29.9	28.8
31	12582.1	2933.52	1.121	28.86	1.023	22	31.7	32.3	29.5
32	9500.6	2537.58	1.17	26.28	1.015	24	31.0	28.1	27.0
33	9610.0	2648.13	1.211	26.38	1.065	24	37.5	28.1	26.2
34	11314.0	2855.29	1.172	27.85	1.009	26	30.3	29.7	28.3
35	8623.3	2471.14	1.215	25.44	1.026	24	28.7	27.5	26.5
36	11742.5	2964.42	1.187	28.20	1.072	22	38.7	30.5	29.0
37	14847.4	3197.64	1.095	30.49	1.007	24	33.6	32.3	31.7
38	12623.9	3108.95	1.186	28.89	1.036	26	37.2	30.5	28.9

39	12051.5	2834.96	1.115	28.45	1.008	24	31.1	31.2	29.1
40	8202.7	2294.23	1.166	25.02	1.014	22	31.8	27.4	26.0
41	7825.1	2139.45	1.122	24.63	1.012	20	29.4	26.2	25.9
42	11994.1	2929.19	1.156	28.40	1.048	22	35.1	32.7	25.9
43	10074.0	2786.01	1.235	26.80	1.033	24	36.3	32.1	26.2
44	8982.1	2629.83	1.259	25.79	1.227	20	40.6	27.2	23.2
45	8226.2	2290.21	1.162	25.05	1.02	20	32.5	27.4	26.6
46	25043.0	4834.74	1.168	36.30	1.044	28	42.8	37.4	34.3
47	7959.8	2263.02	1.174	24.77	1.014	24	29.6	26.7	25.5
48	12193.4	3019.38	1.179	28.56	1.07	16	34.8	31.5	30.8
49	12219.4	2972.06	1.158	28.58	1.022	24	35.2	30.8	29.7
50	9358.3	2442.34	1.137	26.15	1.015	22	29.4	28.2	27.9
51	9194.4	2548.93	1.201	25.99	1.019	26	28.7	29.1	27.2
52	10185.2	2609.65	1.148	26.89	1.014	24	33.1	29.7	26.9
53	17790.1	4539.53	1.377	32.39	1.356	20	51.0	43.7	31.0
54	12687.6	3223.28	1.225	28.94	1.029	28	39.0	29.7	29.8
55	8672.2	2473.07	1.212	25.49	1.011	28	28.4	27.9	26.5
56	8090.9	2205.47	1.132	24.91	1.014	20	29.6	27.3	25.9
57	7977.4	2208.85	1.144	24.79	1.019	20	27.2	26.7	25.0
58	13836.8	3118.62	1.119	29.79	1.019	22	39.4	31.6	30.1
59	8129.8	2265.87	1.159	24.95	1.016	22	28.0	26.6	25.8
60	15120.1	3288.64	1.112	30.68	1.01	24	34.7	33.8	29.7
61	13450.2	3664.80	1.34	29.51	1.208	20	43.0	37.3	26.1
62	8903.8	2433.06	1.171	25.72	1.011	24	27.9	27.3	26.8
63	9862.9	2606.02	1.172	26.61	1.011	26	29.0	28.2	27.5
64	18805.1	4362.92	1.276	32.99	1.166	28	44.0	37.3	32.7
65	16212.1	3377.20	1.09	31.40	1.006	24	36.0	33.3	32.2
66	11137.0	2781.18	1.153	27.71	1.061	20	36.3	32.2	31.7
67	20535.7	3960.75	1.092	33.98	1.014	26	38.8	34.5	34.6
68	8266.8	2371.20	1.199	25.09	1.426	14	37.9	23.6	20.7
69	8919.0	2445.74	1.176	25.73	1.052	22	33.3	28.8	26.3
70	18733.3	4047.06	1.186	32.95	1.048	24	44.0	36.3	37.1
71	9041.7	2353.93	1.122	25.85	1.028	16	29.5	29.3	27.0
72	7997.8	2314.23	1.197	24.81	1.103	18	35.3	24.8	24.4
73	10486.3	2591.51	1.119	27.16	1.008	24	29.8	28.7	28.3
74	7821.2	2194.20	1.152	24.63	1.035	18	33.7	26.1	24.2
75	8351.6	2648.35	1.33	25.17	1.212	20	37.9	35.9	20.8
76	7904.3	2164.39	1.128	24.71	1.021	20	30.0	26.1	24.9
77	10782.0	2877.52	1.219	27.41	1.107	22	40.9	29.1	28.5
78	18184.0	3774.20	1.129	32.63	1.006	28	35.3	33.9	33.8
79	8740.8	2408.21	1.174	25.56	1.032	22	35.5	27.5	25.4
80	8786.0	2513.60	1.221	25.60	1.125	18	35.5	27.6	24.5
81	17624.4	3666.19	1.119	32.29	1.008	26	35.3	34.8	34.1
82	11161.3	2925.65	1.211	27.73	1.445	14	40.5	27.1	23.7
83	9086.0	2501.45	1.188	25.89	1.024	24	29.1	28.0	26.6
84	8098.2	2481.60	1.272	24.92	1.089	20	29.5	27.0	27.6
85	8398.1	2420.67	1.212	25.22	1.011	26	29.2	27.4	25.7
86	8272.3	2266.15	1.146	25.09	1.016	22	31.3	26.4	26.2
87	10293.9	2738.10	1.197	26.99	1.047	20	33.2	30.1	27.4
88	8972.7	2357.23	1.129	25.78	1.019	20	28.3	27.6	26.7
89	7894.1	2627.33	1.37	24.70	1.331	22	40.3	28.8	22.6
90	10533.2	2648.53	1.14	27.20	1.014	24	31.7	28.6	27.1
91	10983.7	2771.13	1.16	27.58	1.017	24	32.2	29.0	28.0
92	18231.3	3571.08	1.066	32.65	1.01	18	41.5	33.7	33.0

93	19424.1	3847.31	1.101	33.35	1.006	26	37.4	35.5	34.0
94	8680.5	2414.72	1.182	25.50	1.011	26	28.2	27.3	26.0
95	13818.6	3829.42	1.375	29.77	1.509	20	52.4	35.1	27.4
96	12677.9	2852.30	1.085	28.93	1.007	22	31.2	30.3	29.8
97	14371.4	3194.67	1.118	30.16	1.022	20	35.7	31.8	30.6
98	9017.3	2530.06	1.208	25.82	1.011	26	30.7	27.5	27.0
99	7968.3	2179.58	1.13	24.78	1.016	20	30.7	27.8	25.7
100	11403.4	2739.30	1.118	27.93	1.009	24	30.6	29.6	29.3
101	8718.4	2641.29	1.289	25.54	1.309	20	41.4	30.6	22.7
102	12332.6	2874.31	1.113	28.67	1.006	24	31.4	30.2	29.3
103	10975.5	2717.64	1.138	27.57	1.012	24	30.2	29.6	29.3
104	11552.0	2698.54	1.092	28.05	1.006	22	30.8	29.8	28.7
105	8655.1	2335.91	1.146	25.47	1.019	22	30.5	26.8	26.7
106	16230.9	3479.09	1.122	31.41	1.006	26	33.7	33.2	32.8
107	8294.3	2394.55	1.208	25.11	1.011	26	28.1	27.2	26.1
108	12874.1	3038.94	1.144	29.08	1.013	26	34.1	33.8	29.5
109	8048.1	2389.88	1.231	24.86	1.018	26	28.5	26.4	25.8
110	14154.0	3428.19	1.212	30.01	1.054	26	35.6	32.6	29.9
111	12349.4	3401.82	1.317	28.68	1.312	18	46.8	37.3	25.4
112	8261.2	2220.01	1.123	25.08	1.022	20	30.3	27.5	24.9
113	8077.6	2340.38	1.202	24.89	1.018	26	27.7	26.9	25.3
114	22673.0	4452.20	1.149	35.12	1.126	16	52.9	35.1	33.6
115	8137.2	2376.33	1.215	24.96	1.015	26	27.8	26.9	25.7
116	9347.9	2613.19	1.218	26.14	1.135	22	36.9	27.7	25.1
117	8794.1	2455.96	1.192	25.61	1.023	24	31.2	28.4	26.0
118	11844.2	3212.29	1.278	28.28	1.344	18	49.3	30.2	26.7
119	20308.2	3872.88	1.076	33.85	1.008	22	42.4	35.4	35.0
120	13205.4	3038.97	1.125	29.33	1.007	24	31.4	30.8	31.7
121	9336.5	2559.78	1.194	26.13	1.009	26	28.8	28.1	27.6
122	7930.7	2200.70	1.144	24.74	1.01	22	27.2	27.0	25.0
123	9425.5	2364.73	1.096	26.21	1.008	20	29.5	28.0	27.0
124	8132.0	2225.20	1.138	24.95	1.044	22	32.1	26.3	23.5
125	14063.3	3484.19	1.237	29.95	1.172	24	43.0	31.3	28.7
126	13452.0	3251.88	1.189	29.51	1.027	24	40.8	31.7	29.7
127	8213.6	2335.79	1.186	25.03	1.069	22	30.4	28.3	25.5
128	8428.7	2485.73	1.241	25.25	1.023	26	33.2	27.5	26.1
129	14201.3	3622.09	1.277	30.05	1.266	18	45.3	35.6	33.2
130	15569.0	3630.15	1.204	30.98	1.085	24	45.8	32.6	29.1
131	8786.2	2413.73	1.172	25.60	1.045	20	34.2	29.8	25.7
132	8498.0	2528.02	1.255	25.32	1.068	24	34.4	28.3	24.9
133	8474.8	2302.94	1.146	25.30	1.009	22	27.4	27.1	26.5
134	8422.6	2468.26	1.233	25.24	1.101	16	30.1	28.8	22.5
135	9102.9	2406.63	1.141	25.91	1.042	18	32.6	31.2	25.3
136	7880.6	2151.75	1.124	24.69	1.008	22	27.9	26.3	26.4
137	8717.0	2458.60	1.2	25.53	1.041	22	29.9	29.4	26.0
138	8363.9	2327.89	1.168	25.18	1.018	24	28.5	26.9	26.0
139	12634.3	2910.06	1.109	28.90	1.008	22	34.6	32.7	29.0
140	8221.8	2754.32	1.398	25.04	1.32	18	40.1	30.3	29.2
141	9636.5	2677.89	1.223	26.40	1.017	28	32.0	28.8	26.9
142	10823.7	2789.12	1.179	27.44	1.054	22	34.2	29.2	24.7
143	8166.0	2343.89	1.195	24.98	1.014	24	27.6	26.7	25.5
144	11642.0	2830.15	1.139	28.12	1.027	24	33.9	31.4	28.8
145	9594.8	2529.79	1.159	26.36	1.009	24	30.5	27.9	27.3
146	13875.7	3143.48	1.126	29.81	1.006	26	31.5	31.5	31.1

147	11362.1	2874.10	1.176	27.89	1.013	22	30.5	30.5	28.8
148	12663.1	3088.22	1.175	28.92	1.008	28	31.2	30.7	29.0
149	10536.6	2635.86	1.134	27.20	1.021	18	29.3	28.9	28.3
150	8810.9	2622.88	1.271	25.63	1.052	26	31.3	29.5	27.2
151	10312.4	2628.43	1.147	27.01	1.009	24	33.5	28.4	28.4
152	9416.9	2781.48	1.29	26.20	1.735	16	48.2	23.1	22.0
153	11982.8	2938.71	1.16	28.39	1.01	26	31.0	31.0	29.6
154	13471.2	3119.16	1.139	29.52	1.006	26	31.8	31.7	30.6
155	7786.8	2347.95	1.236	24.59	1.044	26	32.2	27.5	25.1
156	7998.4	2269.10	1.173	24.81	1.014	24	27.3	27.1	24.6
157	12539.3	2835.24	1.086	28.82	1.006	22	31.3	30.6	29.6
158	16372.0	3853.66	1.236	31.50	1.214	22	49.3	31.6	29.9
159	8826.6	2939.87	1.423	25.64	1.811	16	48.5	37.0	20.9
160	11996.3	2868.11	1.132	28.40	1.011	24	31.3	31.6	28.2
161	10969.4	3118.86	1.306	27.57	1.119	28	36.2	32.7	30.7
162	8920.7	2325.23	1.118	25.73	1.011	22	28.2	27.4	26.2
163	7734.1	2183.11	1.154	24.54	1.123	16	38.2	25.8	24.0
164	13679.4	3082.08	1.114	29.67	1.005	24	31.9	31.2	30.5
165	9559.7	2584.69	1.187	26.33	1.077	12	31.7	31.1	27.3
166	11080.0	2775.66	1.155	27.66	1.012	24	30.4	30.0	29.3
167	17711.5	3578.65	1.089	32.34	1.005	24	35.1	34.1	33.2
168	13634.9	3403.79	1.233	29.64	1.151	22	44.4	34.5	28.5
169	9275.1	2584.94	1.211	26.07	1.013	26	28.6	28.9	26.8
170	14585.4	3240.12	1.122	30.31	1.007	24	32.9	32.5	31.2
171	12423.8	2941.86	1.134	28.74	1.011	24	31.4	30.7	28.4
172	11504.6	2880.10	1.169	28.01	1.008	28	30.8	29.4	29.2
173	9231.1	2541.52	1.194	26.03	1.143	22	36.4	27.8	21.8
174	15990.2	3752.71	1.223	31.26	1.072	26	41.6	33.1	31.0
175	13858.6	3199.28	1.147	29.80	1.086	22	37.9	31.5	29.3
176	9063.3	2506.83	1.192	25.87	1.039	22	32.3	31.8	25.7
177	11726.3	2887.72	1.157	28.19	1.04	22	34.0	28.6	28.2
178	7978.8	2435.65	1.261	24.79	1.485	16	41.3	24.2	22.8
179	8659.2	2459.50	1.206	25.48	1.243	18	37.3	29.1	18.1
180	11914.8	2823.22	1.119	28.34	1.01	24	33.4	30.1	28.6
181	8283.9	2291.75	1.158	25.10	1.059	12	28.9	26.5	24.0
182	8593.8	2550.09	1.257	25.41	1.053	20	30.4	29.8	27.8
183	8652.3	2409.80	1.182	25.47	1.074	22	32.6	27.1	26.6
184	14488.1	3171.44	1.103	30.25	1.006	24	32.5	32.0	31.9
185	9011.3	2429.69	1.16	25.82	1.009	24	28.2	28.7	27.6
186	8996.6	2403.00	1.149	25.80	1.01	24	29.2	27.9	27.0
187	10894.1	2719.88	1.144	27.50	1.011	24	30.0	29.1	28.1
188	12053.2	2846.14	1.12	28.45	1.015	22	34.4	30.7	29.1
189	8368.8	2325.12	1.166	25.19	1.012	22	29.5	26.6	25.8
190	15804.6	3405.56	1.118	31.14	1.008	26	33.6	33.2	32.5
191	7887.1	2375.74	1.24	24.70	1.024	26	30.8	26.3	24.8
192	10949.2	2704.14	1.134	27.55	1.047	22	35.1	28.3	25.6
193	11609.8	2854.09	1.151	28.09	1.006	26	30.2	30.0	29.5
194	7648.1	2497.40	1.33	24.44	1.056	24	29.5	26.9	26.6
195	17893.4	3539.11	1.07	32.45	1.005	22	35.0	34.0	33.0
196	10805.2	2637.93	1.116	27.43	1.017	20	33.8	29.2	28.7
197	21739.6	4024.35	1.068	34.63	1.007	24	37.1	36.5	34.9
198	13669.5	3341.72	1.209	29.67	1.034	26	43.5	31.0	30.1
199	9196.1	2542.98	1.198	25.99	1.013	26	32.4	27.6	27.2
200	9414.2	2489.84	1.155	26.20	1.009	24	28.6	28.7	26.7

Table B.15 Results of the CT scans of the siliceous river gravel coarse aggregate from Indiana

#	Vol	SA	SA/Saeq	ESD	Tr/Treq	Max	L	W	T
1	1273	740	1.303	13.4	1.457	28	21.94	17.30	9.27
2	2783	1118	1.168	17.5	1.154	16	23.95	19.99	14.73
3	178	203	1.326	7	1.185	30	9.45	7.63	5.44
4	1826	866	1.199	15.2	1.188	12	21.96	18.01	14.25
5	1173	667	1.24	13.1	1.177	30	20.88	14.37	13.67
6	626	451	1.275	10.6	1.495	30	18.65	9.74	8.98
7	234	256	1.395	7.6	1.622	24	13.77	9.33	4.66
8	2970	1278	1.279	17.8	1.446	28	28.72	19.84	12.19
9	2120	1003	1.257	15.9	1.458	28	24.03	21.65	7.98
10	1783	925	1.301	15	1.417	28	23.09	20.59	8.50
11	1904	909	1.224	15.4	1.177	28	21.84	15.57	14.02
12	1384	756	1.259	13.8	1.241	30	20.23	16.14	9.40
13	402	365	1.386	9.2	1.461	24	16.30	12.12	5.72
14	346	334	1.4	8.7	1.743	26	16.76	10.17	4.99
15	136	187	1.461	6.4	1.364	24	9.68	8.15	4.53
16	1573	841	1.286	14.4	1.291	30	23.71	15.42	12.10
17	2841	1310	1.351	17.6	1.515	26	32.57	19.22	11.37
18	149	177	1.305	6.6	1.311	16	10.28	7.79	5.38
19	894	549	1.223	12	1.211	30	15.92	15.07	7.88
20	633	478	1.34	10.7	1.328	28	16.47	13.59	7.22
21	493	418	1.385	9.8	1.732	24	18.94	9.37	6.15
22	213	231	1.34	7.4	1.255	22	9.98	9.89	5.15
23	2444	1029	1.173	16.7	1.14	30	22.75	19.75	14.92
24	165	190	1.304	6.8	1.313	24	10.34	8.12	4.93
25	1156	624	1.171	13	1.148	28	17.79	14.01	11.34
26	1503	775	1.221	14.2	1.221	30	22.83	16.23	12.34
27	231	224	1.231	7.6	1.239	22	11.53	8.26	5.68
28	698	480	1.261	11	1.496	18	20.21	11.11	8.87
29	365	356	1.443	8.9	1.405	30	15.00	10.82	6.46
30	300	282	1.302	8.3	1.253	22	11.48	10.67	7.05
31	960	622	1.321	12.2	1.646	28	24.15	11.87	7.09
32	738	493	1.249	11.2	1.219	30	16.76	14.14	8.47
33	208	215	1.265	7.4	1.097	28	9.55	8.40	6.72
34	851	631	1.452	11.8	1.583	30	21.23	16.31	6.53
35	603	533	1.544	10.5	1.806	26	19.81	14.39	5.78
36	648	480	1.326	10.7	1.58	14	20.67	14.12	7.49
37	622	454	1.288	10.6	1.291	26	16.11	11.29	9.61
38	827	558	1.31	11.6	1.417	30	20.72	11.10	9.72
39	2195	903	1.106	16.1	1.133	30	21.92	17.23	12.26
40	650	436	1.201	10.7	1.106	30	13.88	11.76	9.73
41	1243	679	1.215	13.3	1.188	24	18.50	15.88	12.64
42	503	397	1.297	9.9	1.457	28	16.94	11.52	6.63
43	355	304	1.253	8.8	1.159	30	11.76	11.13	7.53
44	876	624	1.409	11.9	1.727	28	22.19	13.08	6.77
45	5043	1683	1.183	21.3	1.223	26	31.99	23.13	17.32
46	1042	631	1.269	12.6	1.222	30	17.24	16.43	8.78
47	1377	752	1.256	13.8	1.231	30	21.08	15.84	10.64
48	130	167	1.349	6.3	1.203	28	9.41	6.72	5.75

49	1923	945	1.264	15.4	1.646	30	27.58	15.14	7.88
50	929	539	1.171	12.1	1.156	30	16.58	11.79	10.57
51	833	521	1.217	11.7	1.131	30	16.05	13.70	10.22
52	421	359	1.321	9.3	1.362	28	13.70	11.30	5.62
53	1619	815	1.222	14.6	1.371	30	23.60	15.35	10.69
54	2166	1000	1.235	16.1	1.327	20	25.62	16.06	13.11
55	203	215	1.286	7.3	1.34	28	10.85	8.45	4.72
56	2042	929	1.193	15.7	1.199	30	22.25	18.04	15.49
57	386	342	1.335	9	1.425	24	13.70	11.87	5.61
58	8010	2358	1.218	24.8	1.108	30	31.80	29.72	25.32
59	1204	716	1.308	13.2	1.419	18	20.69	20.24	8.27
60	1672	933	1.37	14.7	1.476	28	23.71	20.81	8.59
61	117	158	1.369	6.1	1.248	26	9.24	7.17	5.02
62	573	407	1.221	10.3	1.262	24	14.72	11.19	7.03
63	1027	637	1.294	12.5	1.394	30	21.09	13.49	8.06
64	470	375	1.283	9.6	1.325	30	13.92	12.77	6.16
65	75	106	1.23	5.2	1.108	16	6.99	5.98	4.48
66	2847	1126	1.159	17.6	1.165	28	22.89	20.38	13.78
67	1595	910	1.378	14.5	1.627	28	25.98	17.67	9.64
68	803	560	1.34	11.5	1.519	20	18.24	14.85	6.16
69	319	329	1.457	8.5	1.685	18	14.56	11.86	4.29
70	300	278	1.282	8.3	1.204	26	11.73	9.13	6.93
71	1334	708	1.208	13.7	1.19	30	20.37	14.48	12.40
72	291	325	1.529	8.2	2.009	26	17.64	9.40	3.94
73	613	458	1.312	10.5	1.184	22	14.59	12.73	8.87
74	274	262	1.285	8.1	1.15	30	11.16	8.52	6.54
75	316	280	1.249	8.4	1.206	28	12.34	8.24	7.96
76	2081	831	1.054	15.8	1.093	30	20.03	16.54	12.07
77	369	326	1.311	8.9	1.385	26	14.56	9.11	6.60
78	2826	1297	1.342	17.5	1.582	24	31.85	18.38	13.25
79	538	372	1.162	10.1	1.076	26	13.42	10.43	10.48
80	2083	922	1.169	15.8	1.27	30	23.29	19.40	9.98
81	277	282	1.373	8.1	1.352	14	12.52	10.68	6.17
82	2739	1178	1.244	17.4	1.397	30	25.81	22.62	9.46
83	339	287	1.222	8.6	1.27	28	12.36	11.22	5.35
84	948	613	1.314	12.2	1.442	30	22.07	13.62	7.75
85	264	292	1.469	8	1.457	30	14.00	9.22	5.77
86	2021	939	1.215	15.7	1.221	20	23.05	15.72	13.92
87	833	592	1.382	11.7	1.961	24	24.39	11.83	7.00
88	2929	1182	1.194	17.8	1.337	30	28.17	18.52	12.80
89	186	187	1.185	7.1	1.103	20	8.67	8.25	6.85
90	2089	931	1.178	15.9	1.141	30	20.61	18.45	13.63
91	265	279	1.398	8	1.478	24	12.90	12.36	4.92
92	2203	1037	1.267	16.1	1.312	30	24.32	20.34	10.75
93	2709	1214	1.292	17.3	1.296	22	25.46	21.55	13.91
94	1979	866	1.136	15.6	1.14	30	20.45	18.61	12.01
95	1121	716	1.372	12.9	1.371	24	20.63	18.44	9.56
96	718	473	1.22	11.1	1.167	30	16.06	13.74	8.98
97	531	408	1.287	10	1.49	26	19.17	9.30	8.72
98	776	496	1.215	11.4	1.473	26	18.97	12.47	6.12
99	106	144	1.332	5.9	1.333	28	9.38	6.72	3.88
100	906	521	1.15	12	1.19	30	16.43	13.55	8.35

101	801	518	1.242	11.5	1.44	26	18.51	13.89	6.31
102	5608	1852	1.213	22	1.308	30	36.12	23.30	18.24
103	2930	1263	1.276	17.8	1.318	22	28.90	23.07	13.69
104	6089	1848	1.146	22.7	1.349	30	37.24	21.31	15.88
105	789	570	1.38	11.5	1.493	26	18.62	15.52	6.09
106	835	530	1.236	11.7	1.231	28	16.17	14.63	8.29
107	227	259	1.44	7.6	1.506	24	12.30	10.99	4.36
108	2863	1136	1.165	17.6	1.257	16	25.05	21.66	10.94
109	1140	661	1.253	13	1.186	16	17.76	15.36	11.60
110	150	211	1.543	6.6	1.683	16	12.40	9.80	3.95
111	229	228	1.26	7.6	1.076	30	10.14	8.12	7.98
112	1051	639	1.278	12.6	1.272	30	18.10	16.89	9.61
113	5222	1805	1.24	21.5	1.329	30	33.38	22.87	16.77
114	769	512	1.261	11.4	1.347	30	18.24	11.32	7.66
115	1471	718	1.148	14.1	1.223	22	19.99	15.82	9.06
116	564	443	1.343	10.2	1.613	18	19.60	12.11	6.93
117	180	219	1.418	7	1.538	24	11.86	7.22	4.47
118	393	330	1.271	9.1	1.223	24	12.85	10.39	8.06
119	82	125	1.369	5.4	1.473	24	9.06	6.45	3.41
120	288	274	1.3	8.2	1.239	30	12.36	8.25	6.05
121	4036	1439	1.174	19.8	1.182	26	28.79	21.55	15.27
122	1551	712	1.099	14.4	1.087	30	18.67	14.32	13.54
123	542	386	1.2	10.1	1.173	14	14.19	12.33	8.57
124	773	512	1.257	11.4	1.38	28	16.95	15.16	6.68
125	41	83	1.454	4.3	1.766	12	7.78	6.59	2.29
126	690	510	1.35	11	1.325	26	17.26	13.08	9.89
127	156	187	1.335	6.7	1.306	26	10.81	8.00	5.79
128	2003	857	1.115	15.6	1.086	24	21.45	18.20	12.54
129	480	410	1.382	9.7	1.621	26	17.04	9.33	7.07
130	452	383	1.344	9.5	1.47	30	15.43	11.43	5.34
131	1505	815	1.283	14.2	1.456	26	22.68	19.92	7.37
132	50	90	1.377	4.6	1.35	20	7.36	4.69	4.46
133	105	153	1.419	5.9	1.283	28	8.88	7.11	4.59
134	2022	942	1.218	15.7	1.2	24	22.51	19.93	12.05
135	302	295	1.354	8.3	1.433	26	14.39	9.59	5.49
136	501	393	1.287	9.9	1.253	22	14.03	12.63	6.36
137	1957	920	1.216	15.5	1.252	22	22.21	18.76	10.75
138	1297	824	1.433	13.5	1.704	26	24.03	17.93	6.85
139	718	488	1.259	11.1	1.212	30	16.12	13.03	8.92
140	3768	1419	1.212	19.3	1.24	30	29.33	21.20	15.77
141	5060	1536	1.078	21.3	1.056	30	26.28	22.57	20.07
142	519	412	1.319	10	1.283	30	15.16	12.89	8.30
143	841	528	1.226	11.7	1.125	30	15.50	13.95	11.36
144	159	194	1.366	6.7	1.325	22	10.15	8.81	5.25
145	742	529	1.335	11.2	1.38	18	18.50	14.06	7.96
146	901	535	1.186	12	1.129	30	16.82	13.82	10.85
147	1492	802	1.27	14.2	1.337	30	21.48	15.66	12.04
148	1143	628	1.188	13	1.25	20	18.73	15.14	9.22
149	170	204	1.376	6.9	1.613	26	12.38	7.96	3.91
150	1652	911	1.348	14.7	1.55	28	24.10	21.03	8.05

Table B.16 Results of the CT scans of the siliceous river gravel coarse aggregate from Arizona

#	Vol	SA	SA/Saeq	ESD	Tr/Treq	Max	L	W	T
1	746	515	1.295	11.3	1.408	30	17.39	14.46	6.91
2	486	418	1.399	9.8	1.934	20	21.05	9.09	6.60
3	157	193	1.374	6.7	1.48	18	11.24	9.66	4.11
4	399	349	1.332	9.1	1.43	30	15.20	13.50	6.88
5	135	180	1.416	6.4	1.562	20	11.36	8.00	4.55
6	524	399	1.27	10	1.284	30	16.22	11.39	8.56
7	325	308	1.348	8.5	1.68	26	16.63	8.24	6.13
8	570	462	1.389	10.3	1.516	30	18.66	13.68	6.59
9	278	272	1.32	8.1	1.646	12	16.01	8.32	6.01
10	709	520	1.352	11.1	1.423	30	18.36	12.70	10.92
11	590	429	1.261	10.4	1.28	30	15.60	13.53	7.06
12	751	526	1.317	11.3	1.41	26	19.31	12.35	7.86
13	237	248	1.341	7.7	1.338	28	12.93	8.54	6.07
14	363	344	1.397	8.9	2.013	22	17.71	8.45	7.23
15	241	275	1.468	7.7	1.802	24	15.54	9.98	5.23
16	341	310	1.314	8.7	1.366	30	14.07	9.39	6.23
17	303	259	1.188	8.3	1.188	30	12.20	9.28	7.07
18	336	321	1.373	8.6	1.432	28	13.61	12.49	6.03
19	620	431	1.226	10.6	1.317	20	17.97	11.45	8.88
20	224	225	1.261	7.5	1.216	30	11.05	8.31	7.06
21	1428	854	1.393	14	1.867	30	28.69	13.20	8.16
22	138	186	1.443	6.4	1.782	18	12.23	8.36	3.79
23	136	193	1.509	6.4	1.473	18	11.54	9.26	3.86
24	271	276	1.364	8	1.691	22	15.03	9.07	4.84
25	337	296	1.263	8.6	1.494	30	15.08	9.69	4.93
26	379	286	1.129	9	1.222	30	12.90	9.51	6.41
27	142	194	1.477	6.5	2.183	20	13.98	7.02	3.09
28	520	392	1.254	10	1.255	18	15.02	13.01	8.17
29	40	88	1.565	4.2	1.673	22	8.09	6.44	2.81
30	620	451	1.283	10.6	1.294	26	17.06	13.33	8.68
31	42	83	1.425	4.3	1.756	18	7.68	6.59	2.01
32	1111	609	1.174	12.8	1.203	30	19.22	12.84	10.90
33	630	431	1.213	10.6	1.286	28	16.61	10.94	8.41
34	400	385	1.467	9.1	1.642	30	16.84	14.57	4.70
35	484	340	1.141	9.7	1.281	30	14.85	9.86	6.11
36	192	243	1.51	7.2	2.127	16	15.95	8.07	4.27
37	204	221	1.32	7.3	1.416	26	12.79	7.19	6.15
38	1171	686	1.277	13.1	1.575	30	24.78	13.45	8.70
39	662	504	1.372	10.8	1.438	26	19.54	13.08	9.68
40	512	384	1.241	9.9	1.247	30	14.52	13.01	8.03
41	424	395	1.446	9.3	1.96	18	20.42	10.42	4.78
42	386	322	1.256	9	1.367	30	15.20	9.11	6.70
43	560	385	1.172	10.2	1.142	30	13.58	12.36	8.14
44	216	248	1.424	7.4	1.605	24	15.22	8.20	6.06
45	144	182	1.373	6.5	2.051	18	14.48	5.41	4.69
46	339	302	1.283	8.7	1.342	26	14.19	10.04	5.77
47	1051	540	1.08	12.6	1.095	30	17.49	12.51	12.04
48	325	255	1.116	8.5	1.084	30	10.60	9.26	8.02
49	84	117	1.259	5.4	1.309	26	8.16	6.03	4.41
50	339	287	1.221	8.7	1.293	30	14.14	8.63	7.40
51	598	422	1.229	10.5	1.221	30	15.54	12.12	8.23

52	350	312	1.298	8.7	1.434	30	14.11	10.07	5.84
53	406	320	1.207	9.2	1.316	30	14.33	9.26	7.25
54	280	238	1.149	8.1	1.2	30	11.61	9.27	6.09
55	435	404	1.455	9.4	1.589	26	18.31	12.23	5.53
56	289	281	1.33	8.2	1.421	30	13.13	9.57	5.38
57	389	398	1.544	9.1	2.644	24	22.84	8.62	4.87
58	513	436	1.406	9.9	1.905	24	21.38	10.88	5.96
59	160	226	1.589	6.7	1.939	18	13.84	9.42	3.16
60	113	145	1.282	6	1.301	30	8.82	7.76	3.86
61	994	627	1.302	12.4	1.578	28	22.88	12.68	9.31
62	68	112	1.392	5.1	1.637	22	9.64	5.55	3.36
63	648	467	1.289	10.7	1.253	28	15.73	13.14	9.84
64	907	532	1.174	12	1.117	30	16.03	13.05	11.76
65	285	267	1.275	8.2	1.34	28	12.14	11.45	5.23
66	311	276	1.244	8.4	1.266	30	12.69	10.36	6.15
67	381	326	1.283	9	1.422	28	14.02	12.36	5.80
68	475	415	1.411	9.7	1.757	28	18.33	11.60	4.90
69	336	285	1.219	8.6	1.254	30	12.12	10.41	7.38
70	531	363	1.145	10	1.107	30	14.26	10.28	9.61
71	529	409	1.293	10	1.285	22	16.90	10.55	8.41
72	252	286	1.483	7.8	1.805	24	14.87	10.84	4.91
73	154	184	1.322	6.7	1.418	26	10.65	8.07	4.36
74	795	539	1.298	11.5	1.286	30	17.81	15.28	10.30
75	256	292	1.499	7.9	1.625	26	14.40	11.98	4.88
76	197	194	1.186	7.2	1.208	30	10.81	7.80	5.49
77	162	213	1.481	6.8	1.644	28	11.66	10.41	3.82
78	665	490	1.329	10.8	1.442	30	19.14	11.71	8.46
79	364	278	1.127	8.9	1.112	30	11.06	9.95	7.04
80	145	182	1.362	6.5	1.365	30	10.97	8.25	4.46
81	153	168	1.213	6.6	1.213	28	9.33	8.28	5.48
82	243	262	1.391	7.7	1.542	26	12.74	11.87	4.46
83	162	187	1.304	6.8	1.505	26	12.48	6.39	5.28
84	379	359	1.418	9	1.618	30	15.63	13.27	4.71
85	363	309	1.255	8.9	1.22	30	12.37	10.85	7.94
86	520	437	1.398	10	1.61	30	18.80	11.72	6.43
87	182	229	1.475	7	1.668	24	12.42	10.30	3.44
88	328	284	1.234	8.6	1.248	30	11.87	11.01	5.98
89	377	345	1.367	9	1.616	24	14.90	10.97	4.89
90	166	206	1.409	6.8	1.48	26	11.98	8.78	5.14
91	90	134	1.379	5.6	1.561	22	9.78	6.92	3.37
92	446	368	1.304	9.5	1.392	30	16.44	12.20	6.39
93	72	127	1.517	5.2	1.592	18	9.43	7.80	3.38
94	148	178	1.313	6.6	1.309	28	9.29	8.36	4.17
95	508	365	1.185	9.9	1.265	30	16.07	10.50	8.19
96	650	462	1.273	10.7	1.431	30	18.56	12.53	7.36
97	527	372	1.179	10	1.167	30	13.87	12.09	8.07
98	105	158	1.467	5.9	2.205	20	13.57	5.86	3.76
99	276	277	1.351	8.1	1.456	30	13.16	12.12	5.15
100	293	264	1.239	8.2	1.234	30	11.81	10.40	6.24
101	797	650	1.564	11.5	2.278	28	27.08	15.62	5.83
102	662	518	1.41	10.8	1.65	30	21.32	11.86	7.38
103	984	560	1.17	12.3	1.139	18	16.53	12.64	11.66
104	635	487	1.364	10.7	1.506	30	17.05	14.73	6.14
105	1068	568	1.124	12.7	1.113	30	16.62	12.72	12.10
106	160	222	1.555	6.7	2.86	22	17.34	6.78	3.39
107	550	472	1.455	10.2	2.075	16	22.38	11.65	5.69

108	255	236	1.212	7.9	1.4	28	13.46	8.52	5.05
109	183	219	1.404	7	1.697	24	13.35	8.27	3.57
110	366	291	1.176	8.9	1.329	30	14.38	9.30	6.46
111	781	474	1.156	11.4	1.107	22	14.43	13.24	10.11
112	481	355	1.196	9.7	1.164	30	13.70	12.90	7.74
113	109	165	1.494	5.9	1.782	22	10.62	8.52	2.98
114	305	308	1.407	8.3	1.825	26	16.80	9.14	4.57
115	36	67	1.281	4.1	1.364	18	6.43	4.99	2.54
116	231	255	1.4	7.6	1.713	20	15.11	10.28	3.79
117	492	368	1.222	9.8	1.261	30	15.02	10.78	8.83
118	308	298	1.351	8.4	1.335	30	12.85	12.30	6.08
119	775	508	1.245	11.4	1.345	30	19.70	12.40	9.51
120	148	177	1.31	6.6	1.375	30	11.23	7.45	4.79
121	152	207	1.503	6.6	1.811	24	12.55	10.15	3.22
122	377	310	1.229	9	1.203	30	13.23	9.77	7.09
123	106	151	1.396	5.9	1.732	20	10.38	6.98	3.31
124	655	422	1.157	10.8	1.18	30	14.99	11.33	8.85
125	1101	569	1.103	12.8	1.148	30	18.86	12.96	11.60
126	152	183	1.331	6.6	1.368	22	10.44	8.59	4.97
127	504	405	1.322	9.9	1.386	30	16.01	12.94	7.20
128	1093	655	1.276	12.8	1.502	30	22.79	12.41	9.26
129	298	281	1.302	8.3	1.259	26	12.61	11.98	6.70
130	772	499	1.226	11.4	1.234	30	16.00	15.30	9.74
131	868	566	1.286	11.8	1.279	30	18.31	13.31	12.83
132	561	388	1.18	10.2	1.104	28	13.43	11.38	10.17
133	245	267	1.41	7.8	1.478	16	14.02	10.78	5.79
134	698	473	1.243	11	1.251	30	17.13	13.68	9.07
135	263	245	1.235	7.9	1.228	30	12.46	9.59	7.53
136	302	275	1.264	8.3	1.367	30	13.76	7.48	7.25
137	463	324	1.119	9.6	1.091	28	12.26	11.43	8.48
138	165	192	1.32	6.8	1.68	30	12.78	5.84	5.54
139	415	346	1.285	9.3	1.289	30	14.63	10.36	7.68
140	142	217	1.652	6.5	1.926	22	12.96	10.29	3.03
141	298	274	1.27	8.3	1.264	30	12.68	11.26	6.26
142	471	386	1.319	9.7	1.307	30	15.52	12.09	8.23
143	236	229	1.24	7.7	1.217	30	12.22	8.80	6.73
144	205	233	1.384	7.3	1.601	24	12.91	8.23	4.95
145	697	493	1.297	11	1.492	30	21.28	11.28	7.82
146	133	167	1.325	6.3	1.462	16	10.76	8.86	4.64
147	339	262	1.114	8.7	1.128	24	10.62	10.35	5.87
148	217	224	1.282	7.5	1.313	28	11.94	8.27	6.24
149	586	464	1.37	10.4	1.632	30	18.40	12.70	5.54
150	420	449	1.655	9.3	2.957	26	23.50	9.40	4.94

Table B.17 Results of the CT scans of the granite coarse aggregate

#	Vol	SA	SA/Saeq	ESD	Tr/Treq	Max	L	W	T
1	43	88	1.49	4.3	1.782	22	8.18	4.31	3.48
2	197	234	1.43	7.2	1.396	28	11.95	9.48	5.63
3	924	648	1.41	12.1	1.573	26	20.41	18.35	6.69
4	619	445	1.27	10.6	1.28	24	16.38	12.13	7.82
5	65	112	1.43	5	1.435	20	8.25	6.67	3.18
6	266	254	1.27	8	1.302	18	13.40	8.58	6.06
7	477	359	1.22	9.7	1.148	26	13.51	10.35	9.31

8	803	513	1.23	11.5	1.147	24	14.88	14.12	10.71
9	74	123	1.45	5.2	1.392	14	9.07	5.50	4.78
10	57	94	1.32	4.8	1.225	24	6.50	6.39	3.49
11	31	67	1.39	3.9	1.613	18	7.15	4.83	2.67
12	1328	770	1.32	13.6	1.589	22	24.31	14.16	11.63
13	413	347	1.29	9.2	1.211	24	13.92	10.38	8.62
14	2047	962	1.23	15.8	1.286	18	24.61	16.20	13.50
15	281	273	1.32	8.1	1.42	22	13.29	8.29	6.77
16	71	117	1.41	5.1	1.375	26	8.53	5.35	4.79
17	52	87	1.29	4.6	1.374	20	7.26	6.36	2.98
18	313	305	1.37	8.4	1.777	24	17.60	7.31	6.31
19	287	252	1.20	8.2	1.104	20	10.71	9.37	8.08
20	99	143	1.38	5.7	1.232	22	8.83	7.78	4.72
21	43	89	1.50	4.4	1.377	22	7.54	6.04	3.88
22	366	299	1.21	8.9	1.087	28	11.58	11.14	8.75
23	738	498	1.26	11.2	1.24	12	16.95	14.19	9.90
24	192	215	1.34	7.2	1.335	28	11.82	7.27	6.61
25	269	266	1.32	8	1.198	24	12.25	9.44	7.53
26	312	283	1.27	8.4	1.236	28	12.61	9.50	6.27
27	137	168	1.31	6.4	1.124	26	8.50	7.10	6.66
28	438	367	1.32	9.4	1.382	16	16.62	10.57	8.09
29	154	186	1.34	6.6	1.381	26	10.73	6.81	6.22
30	193	218	1.35	7.2	1.485	26	12.04	7.74	5.19
31	251	245	1.27	7.8	1.169	28	10.70	8.97	7.81
32	501	423	1.39	9.9	1.401	28	15.72	14.33	6.68
33	296	262	1.22	8.3	1.153	28	11.32	9.23	8.26
34	38	89	1.63	4.2	1.444	20	7.06	6.15	3.06
35	353	297	1.23	8.8	1.139	26	11.72	9.55	8.96
36	585	451	1.33	10.4	1.526	24	18.67	11.31	6.69
37	1368	788	1.32	13.8	1.328	28	21.07	17.69	11.10
38	1158	693	1.30	13	1.432	28	22.37	16.16	7.28
39	91	128	1.31	5.6	1.157	22	8.17	6.34	5.04
40	147	184	1.37	6.5	1.335	18	11.84	6.77	6.55
41	176	193	1.27	7	1.201	26	9.73	7.61	6.60
42	678	523	1.40	10.9	1.688	28	20.46	12.14	6.30
43	104	135	1.27	5.8	1.411	24	9.94	5.66	4.75
44	224	229	1.28	7.5	1.253	24	11.16	8.20	6.58
45	102	137	1.30	5.8	1.234	16	8.67	7.87	4.54
46	414	371	1.38	9.2	1.735	28	18.63	10.20	6.51
47	38	73	1.33	4.2	1.321	22	6.97	4.32	3.29
48	1079	663	1.30	12.7	1.372	26	19.41	16.65	8.08
49	667	491	1.33	10.8	1.441	26	19.01	12.16	7.48
50	189	207	1.30	7.1	1.122	28	9.13	8.90	6.90
51	251	244	1.27	7.8	1.345	18	11.92	11.11	4.81
52	234	244	1.33	7.6	1.269	28	13.15	8.32	6.57
53	219	246	1.40	7.5	1.317	24	12.37	9.48	5.70
54	408	363	1.36	9.2	1.329	28	14.32	12.17	6.17
55	494	379	1.26	9.8	1.181	28	13.59	12.52	7.37
56	29	62	1.36	3.8	1.173	20	5.69	4.43	3.47
57	123	163	1.36	6.2	1.485	24	11.29	5.90	5.40
58	413	337	1.26	9.2	1.37	26	16.01	8.42	8.06

59	762	495	1.23	11.3	1.226	28	16.44	12.90	9.78
60	91	143	1.46	5.6	1.359	26	9.84	6.25	4.54
61	134	176	1.39	6.3	1.395	22	9.87	9.27	3.94
62	170	203	1.37	6.9	1.17	26	9.55	8.82	6.57
63	217	243	1.39	7.5	1.375	22	14.14	7.88	6.80
64	700	468	1.23	11	1.187	26	15.67	12.59	10.22
65	753	475	1.19	11.3	1.158	28	14.77	12.78	8.50
66	50	95	1.45	4.6	1.584	20	8.15	5.14	3.82
67	71	110	1.32	5.1	1.219	26	7.61	6.72	4.07
68	332	285	1.23	8.6	1.265	28	13.11	10.01	6.37
69	73	124	1.48	5.2	1.471	24	8.37	6.69	3.56
70	209	232	1.36	7.4	1.332	26	10.88	9.26	5.81
71	173	200	1.33	6.9	1.179	26	10.93	7.57	7.36
72	64	97	1.25	5	1.396	12	8.36	4.48	4.25
73	177	201	1.32	7	1.217	28	10.60	7.06	6.52
74	130	170	1.37	6.3	1.35	28	9.99	7.51	4.24
75	157	188	1.34	6.7	1.335	28	10.35	10.01	4.43
76	68	112	1.39	5.1	1.158	28	7.01	6.09	4.37
77	106	142	1.31	5.9	1.326	22	9.74	6.86	4.40
78	965	588	1.25	12.3	1.366	28	18.68	14.01	9.04
79	324	309	1.36	8.5	1.368	26	13.49	10.08	6.27
80	285	258	1.23	8.2	1.103	28	10.53	9.53	7.76
81	927	605	1.32	12.1	1.367	28	18.47	15.86	7.78
82	73	120	1.43	5.2	1.821	16	10.98	5.57	3.53
83	347	317	1.33	8.7	1.513	28	16.85	8.14	7.15
84	815	514	1.22	11.6	1.206	28	16.81	13.58	9.47
85	82	127	1.40	5.4	1.332	26	8.45	7.23	3.54
86	328	286	1.24	8.6	1.183	28	12.73	9.47	7.50
87	116	159	1.38	6.1	1.413	26	9.66	7.06	4.36
88	59	104	1.41	4.8	1.261	24	7.36	6.28	3.86
89	1298	830	1.44	13.5	1.695	24	23.47	21.28	6.31
90	50	94	1.43	4.6	1.676	22	8.75	4.99	3.93
91	171	198	1.33	6.9	1.202	28	10.12	7.60	7.01
92	67	109	1.37	5	1.632	20	8.69	5.06	3.79
93	3470	1537	1.39	18.8	1.722	24	36.15	21.60	10.73
94	368	327	1.32	8.9	1.629	28	16.73	9.18	5.76
95	526	415	1.32	10	1.473	28	17.11	11.88	6.64
96	651	468	1.29	10.8	1.381	28	17.36	10.57	9.63
97	1321	760	1.31	13.6	1.389	20	22.43	16.44	9.04
98	1570	818	1.25	14.4	1.157	24	21.53	16.01	14.92
99	365	328	1.33	8.9	1.45	28	14.46	10.94	6.41
100	34	69	1.37	4	1.329	24	6.70	4.50	3.22
101	267	259	1.29	8	1.323	26	12.23	9.58	6.25
102	44	83	1.39	4.4	1.62	16	7.88	4.25	3.01
103	2263	1020	1.22	16.3	1.338	22	25.54	17.60	13.42
104	1948	996	1.32	15.5	1.49	26	28.91	16.29	12.20
105	255	253	1.30	7.9	1.191	28	11.38	8.96	5.93
106	221	231	1.31	7.5	1.316	24	12.16	8.05	7.56
107	35	67	1.29	4.1	1.167	24	5.83	4.68	4.58
108	713	495	1.28	11.1	1.297	24	16.37	15.11	8.26
109	138	165	1.28	6.4	1.08	24	8.39	7.56	6.16

110	2200	984	1.20	16.1	1.17	28	22.38	19.24	15.37
111	1234	746	1.34	13.3	1.696	26	24.58	12.08	10.78
112	365	327	1.32	8.9	1.424	28	13.79	10.33	5.36
113	43	78	1.31	4.4	1.378	20	6.97	5.78	2.77
114	1241	710	1.27	13.3	1.269	20	22.53	16.17	12.31
115	126	168	1.38	6.2	1.666	16	11.44	5.97	5.26
116	132	170	1.35	6.3	1.165	24	8.99	7.01	5.66
117	92	131	1.33	5.6	1.232	28	8.23	6.53	4.36
118	128	167	1.36	6.2	1.198	26	9.10	7.40	4.75
119	651	461	1.27	10.8	1.294	24	17.87	13.12	8.76
120	575	431	1.29	10.3	1.351	28	16.71	12.89	6.19
121	234	244	1.33	7.6	1.298	26	12.19	8.45	6.28
122	93	139	1.40	5.6	1.292	24	8.85	6.49	5.17
123	103	152	1.43	5.8	1.835	16	11.73	6.41	4.50
124	122	150	1.26	6.2	1.275	20	9.08	8.62	4.46
125	245	250	1.32	7.8	1.204	28	10.76	10.05	6.80
126	102	137	1.30	5.8	1.236	22	8.51	6.60	5.23
127	229	244	1.35	7.6	1.663	28	14.06	9.81	3.72
128	515	406	1.31	9.9	1.37	28	15.44	15.27	6.06
129	294	274	1.28	8.2	1.384	20	13.89	9.23	6.53
130	227	253	1.41	7.6	1.488	22	11.71	10.67	4.42
131	1017	719	1.47	12.5	1.988	22	24.13	13.44	6.78
132	1290	658	1.15	13.5	1.073	26	17.78	15.55	13.89
133	278	276	1.34	8.1	1.232	28	12.59	9.09	6.99
134	1489	747	1.18	14.2	1.219	28	20.15	15.37	10.42
135	197	223	1.36	7.2	1.724	24	14.37	7.74	5.32
136	205	222	1.32	7.3	1.377	24	11.83	8.24	5.62
137	39	83	1.48	4.2	2.218	16	9.43	5.05	2.00
138	485	370	1.24	9.8	1.187	26	15.23	10.89	10.18
139	50	93	1.41	4.6	1.314	24	7.34	5.19	3.67
140	155	197	1.41	6.7	1.501	28	12.60	7.92	5.03
141	382	309	1.21	9	1.244	28	12.90	10.75	6.89
142	76	119	1.38	5.2	1.374	28	9.15	5.72	3.99
143	805	511	1.22	11.5	1.14	24	16.65	12.26	11.15
144	298	276	1.28	8.3	1.135	26	11.79	8.99	7.80
145	486	390	1.30	9.8	1.437	24	16.44	10.94	8.25
146	97	132	1.29	5.7	1.239	28	8.58	7.16	4.39
147	119	152	1.30	6.1	1.23	20	8.63	7.22	4.88
148	283	283	1.36	8.1	1.671	28	16.13	8.06	7.33
149	228	239	1.33	7.6	1.216	26	11.97	9.03	6.78
150	73	126	1.49	5.2	2.016	26	10.13	5.23	4.10

Table B.18 Results of the CT scans of the limestone coarse aggregate

#	Vol	SA	SA/Saeq	ESD	Tr/Treq	Max	L	W	T
1	1053	700	1.40	12.6	1.65	24	22.71	16.96	6.03
2	193	220	1.36	7.2	1.191	30	10.34	8.02	6.90
3	4784	1807	1.32	20.9	1.395	30	38.16	21.52	18.79
4	117	154	1.33	6.1	1.367	20	9.80	8.36	4.47
5	3517	1497	1.34	18.9	1.761	28	34.58	16.48	15.44

6	3016	1199	1.19	17.9	1.204	30	28.19	21.96	15.37
7	288	304	1.44	8.2	1.364	24	13.06	11.76	6.85
8	695	517	1.36	11	1.509	20	19.68	12.20	7.50
9	299	271	1.25	8.3	1.416	28	14.51	9.23	4.96
10	1356	708	1.20	13.7	1.166	26	18.99	15.32	13.71
11	3116	1219	1.18	18.1	1.188	30	27.60	18.74	14.72
12	131	158	1.26	6.3	1.209	26	9.00	7.57	5.13
13	1568	801	1.23	14.4	1.245	30	20.68	19.22	9.75
14	569	418	1.26	10.3	1.239	30	15.51	12.62	8.15
15	1826	908	1.26	15.2	1.505	30	27.15	13.49	12.23
16	31	63	1.33	3.9	1.254	14	5.51	4.39	4.39
17	325	282	1.23	8.5	1.136	30	11.29	9.65	8.49
18	461	421	1.46	9.6	1.726	30	18.44	10.15	7.24
19	2562	1085	1.20	17	1.174	14	24.05	20.03	14.15
20	5823	2001	1.28	22.3	1.484	30	41.36	23.92	15.52
21	704	499	1.30	11	1.573	30	20.82	11.44	8.04
22	197	220	1.34	7.2	1.461	22	11.54	9.66	4.15
23	137	167	1.30	6.4	1.293	26	10.01	7.78	5.41
24	53	100	1.46	4.7	1.5	24	8.35	5.13	3.61
25	230	226	1.25	7.6	1.368	24	12.85	7.88	5.93
26	97	131	1.29	5.7	1.158	22	7.97	7.26	4.91
27	13003	3313	1.24	29.2	1.29	30	44.16	33.28	23.92
28	773	502	1.23	11.4	1.236	30	18.03	12.87	8.79
29	2279	1059	1.27	16.3	1.278	30	26.81	20.37	13.27
30	362	312	1.27	8.8	1.195	26	12.88	9.95	8.91
31	718	547	1.41	11.1	1.648	24	20.61	14.75	6.40
32	316	356	1.59	8.5	1.987	24	17.79	11.94	4.18
33	192	232	1.44	7.2	1.472	24	11.67	8.70	5.78
34	393	316	1.22	9.1	1.185	24	13.59	9.79	7.10
35	756	495	1.23	11.3	1.149	30	16.43	13.18	9.51
36	1145	642	1.21	13	1.335	30	21.85	12.13	11.12
37	173	209	1.39	6.9	1.344	30	11.99	8.48	5.52
38	4001	1470	1.21	19.7	1.156	30	28.59	23.00	19.20
39	4484	1660	1.26	20.5	1.351	30	33.89	28.89	12.17
40	207	224	1.32	7.3	1.653	26	14.82	7.04	5.26
41	1408	772	1.27	13.9	1.293	30	22.70	16.29	11.12
42	3828	1481	1.25	19.4	1.324	30	30.25	24.30	14.68
43	470	381	1.30	9.6	1.371	30	16.40	11.27	6.76
44	248	272	1.43	7.8	1.672	24	14.24	9.18	4.74
45	43	76	1.28	4.3	1.436	14	7.36	4.67	2.66
46	1559	781	1.20	14.4	1.25	18	22.86	14.09	12.19
47	165	180	1.24	6.8	1.259	22	10.78	8.13	5.44
48	2433	1148	1.31	16.7	1.234	20	24.83	20.76	16.55
49	535	418	1.31	10.1	1.423	14	15.38	12.27	6.81
50	1487	851	1.35	14.2	1.675	20	29.99	13.89	12.53
51	407	336	1.27	9.2	1.24	28	15.21	9.85	9.01
52	470	356	1.22	9.6	1.416	28	17.76	8.08	8.05
53	462	394	1.36	9.6	1.739	26	19.32	9.76	6.17

54	11607	2964	1.20	28.1	1.349	14	46.89	25.95	22.57
55	238	268	1.44	7.7	1.812	28	15.82	8.68	4.41
56	5551	1805	1.19	22	1.116	16	29.63	25.68	24.76
57	377	340	1.35	9	1.386	30	13.85	12.73	5.95
58	1772	880	1.24	15	1.393	30	24.74	15.89	12.04
59	114	154	1.35	6	1.505	26	10.72	5.73	4.35
60	119	156	1.33	6.1	1.277	30	10.10	6.97	4.55
61	332	313	1.35	8.6	1.55	12	14.59	11.23	5.14
62	337	298	1.27	8.6	1.267	30	14.14	8.85	7.63
63	2372	1131	1.32	16.5	1.381	30	25.35	21.03	11.20
64	151	193	1.41	6.6	1.443	26	11.75	6.88	5.65
65	4316	1616	1.26	20.2	1.266	30	29.82	23.38	17.90
66	940	594	1.28	12.2	1.345	30	21.21	13.03	10.10
67	3273	1368	1.28	18.4	1.333	30	29.78	22.04	14.47
68	68	111	1.37	5.1	1.457	24	8.27	8.08	3.11
69	1762	792	1.12	15	1.112	30	19.84	16.20	13.28
70	245	244	1.29	7.8	1.385	28	13.01	8.49	5.31
71	686	485	1.29	10.9	1.468	28	18.04	11.64	8.55
72	1239	712	1.28	13.3	1.261	30	20.29	16.11	12.82
73	96	136	1.34	5.7	1.21	28	8.34	7.14	5.54
74	105	146	1.36	5.9	1.419	26	9.32	7.53	4.08
75	544	434	1.35	10.1	1.592	30	19.57	12.11	6.30
76	2653	1090	1.18	17.2	1.195	30	25.44	19.12	14.82
77	12015	2976	1.17	28.4	1.169	30	39.90	33.97	23.62
78	2175	973	1.20	16.1	1.192	28	22.41	17.83	15.24
79	164	197	1.36	6.8	1.341	26	11.22	8.24	5.18
80	3580	1412	1.25	19	1.344	30	29.54	21.76	12.72
81	348	304	1.27	8.7	1.235	22	12.44	10.53	7.66
82	11444	3050	1.24	28	1.286	30	42.93	38.80	19.31
83	313	276	1.24	8.4	1.261	28	12.75	9.36	6.45
84	498	370	1.22	9.8	1.293	30	15.83	9.04	7.70
85	1185	632	1.17	13.1	1.153	28	18.27	12.96	12.05
86	135	171	1.35	6.4	1.411	24	11.05	7.94	5.42
87	126	175	1.44	6.2	1.625	24	10.60	8.85	3.33
88	7813	2317	1.22	24.6	1.257	30	36.92	30.34	17.90
89	774	544	1.33	11.4	1.7	30	23.55	12.27	7.24
90	6765	2080	1.20	23.5	1.282	30	38.66	25.50	20.04
91	1742	847	1.21	14.9	1.179	30	23.32	16.01	14.99
92	378	344	1.36	9	1.511	30	16.13	10.93	6.11
93	194	216	1.33	7.2	1.151	30	10.10	8.65	6.55
94	668	454	1.23	10.8	1.227	28	16.10	12.61	8.36
95	96	136	1.34	5.7	1.255	28	8.47	7.19	5.08
96	4289	1578	1.24	20.2	1.298	30	32.28	22.32	17.72
97	701	483	1.27	11	1.287	30	17.75	12.19	8.12
98	572	468	1.40	10.3	1.631	24	18.68	13.34	6.11
99	2438	1081	1.23	16.7	1.175	30	24.57	19.06	14.04
100	271	265	1.31	8	1.192	26	11.19	10.25	7.80
101	317	302	1.34	8.5	1.418	28	14.71	10.89	6.28

102	2866	1120	1.15	17.6	1.114	22	22.75	19.51	14.52
103	2839	1249	1.29	17.6	1.499	30	31.68	19.95	13.01
104	299	291	1.35	8.3	1.474	26	13.83	10.67	4.87
105	1548	814	1.26	14.4	1.261	26	22.94	17.39	12.61
106	113	156	1.38	6	1.391	30	9.86	7.40	4.19
107	254	252	1.30	7.9	1.356	22	14.11	7.56	6.65
108	215	222	1.28	7.4	1.281	26	11.07	7.75	5.74
109	371	327	1.31	8.9	1.338	22	13.94	11.11	7.38
110	597	449	1.31	10.4	1.43	30	18.42	12.58	6.76
111	322	298	1.31	8.5	1.245	24	11.84	10.51	6.58
112	299	276	1.28	8.3	1.362	24	13.89	9.61	6.57
113	284	269	1.29	8.2	1.59	24	15.47	7.64	5.87
114	2940	1183	1.19	17.8	1.152	28	24.07	19.42	16.03
115	1342	745	1.27	13.7	1.212	28	21.02	15.80	9.97
116	295	287	1.34	8.3	1.539	30	14.71	9.16	5.38
117	262	240	1.21	7.9	1.182	26	12.00	8.68	6.65
118	6148	1832	1.13	22.7	1.14	30	32.21	24.87	18.18
119	412	342	1.28	9.2	1.199	28	12.79	10.94	8.10
120	287	263	1.25	8.2	1.128	30	11.60	8.91	7.50
121	1010	599	1.23	12.4	1.164	30	18.14	13.84	11.27
122	277	283	1.38	8.1	1.727	30	16.07	8.83	4.57
123	639	428	1.19	10.7	1.106	30	14.18	11.95	10.97
124	1091	651	1.27	12.8	1.376	30	21.92	13.59	9.14
125	210	237	1.39	7.4	1.454	20	13.04	9.48	6.07
126	371	353	1.41	8.9	1.684	26	16.45	8.32	7.37
127	281	278	1.34	8.1	1.311	30	12.82	8.69	5.54
128	432	359	1.30	9.4	1.359	28	16.54	11.19	6.66
129	690	481	1.27	11	1.351	24	18.36	11.12	9.44
130	815	544	1.29	11.6	1.345	30	17.90	13.50	7.81
131	463	372	1.29	9.6	1.268	30	14.37	12.35	7.71
132	38	73	1.34	4.2	1.262	24	6.44	4.82	3.53
133	657	465	1.27	10.8	1.217	30	16.02	12.19	10.00
134	665	447	1.21	10.8	1.205	30	16.12	12.74	8.96
135	1261	688	1.22	13.4	1.203	30	19.40	17.52	10.21
136	121	158	1.33	6.1	1.217	20	9.44	8.05	5.19
137	367	322	1.30	8.9	1.21	28	13.13	10.72	7.80
138	504	404	1.32	9.9	1.233	30	14.41	12.71	8.76
139	575	413	1.24	10.3	1.273	22	15.86	11.56	9.32
140	197	217	1.33	7.2	1.334	30	11.62	8.79	4.90